Investigating how SPLUNC1 mediates its anti-viral activity against Influenza A Viruses

Thesis submitted in accordance with the requirements of the University of Liverpool

for the degree of Doctor in Philosophy by Amy Josephine Robinson

January 2022

Abstract

Seasonal influenza is a major cause of respiratory infection and results in substantial morbidity, mortality, and economic burden every year. Short-palate lung and nasal epithelial clone 1 (SPLUNC1) is a protein which is secreted into the airways and has anti-viral activity that restricts IAV entry and viral titre in vivo. Presently, it is unclear how SPLUNC1 anti-viral effect against IAV is mediated. The work described in this thesis explores SPLUNC1 function using molecular, *in vitro*, and *in vivo* approaches.

It was investigated whether a direct interaction between SPLUNC1 and IAV was responsible for this antiviral activity utilising secreted recombinant SPLUNC1 protein and immunoprecipitation. However, no interaction between SPLUNC1 and IAV was identified indicating a direct interaction is not responsible. Therefore, to allow further investigation into how SPLUNC1 mediates it antiviral activity, a SPLUNC1 deficient cell line was generated using CRISPR-Cas9 editing technology. IAV infection of these cells demonstrated SPLUNC1 KO does not affect IAV infection and replication in vitro in HBEC3-KT cells. Finally, the SPLUNC1 region S18 has previously been identified as functionally active hence, its role during IAV infection was investigated. In vivo experiments identified S18 influenced IAV in mice. Specifically, protecting against death and weight loss during the early stages of infection.

The results discussed within this thesis provide an insight into SPLUNC1 antiviral activity against IAV and identify S18 as a crucial region involved in the hosts antiviral response against IAV infection. Future work involving S18 is vital to increase our understanding of the host response and improving vaccine effectiveness against IAV.

Contents

List of Figures

List of tables

Acknowledgements

Throughout my PhD I have met so many wonderful researchers, colleagues, and friends who I owe a great deal of thanks. First, I would like to thank my supervisors Prof James Stewart and Dr Robin Flynn. You have provided so much guidance, advice and patience over the past four years that have been invaluable in my development into an independent researcher. Also, to Prof Colin Bingle who has always been only a video call away. Your support has been paramount during the latter years of my study.

Secondly, to the MRC DiMeN DTP and Dr Emily Goodall for funding my research and providing countless opportunities and support over the past four years. The opportunities this funding has provided have been crucial to my progression as both an individual and a scientist.

I owe a special thanks to current and past members of the Stewart group especially: Jordan, Parul, Ellie, and Chloe. I'll greatly miss your company and adventures in the lab and beyond. This thanks extends to all in the IC2 office, who without my PhD would have been a much duller affair.

Finally, to my family and friends for all the love and encouragement throughout my PhD. To Andrew, for unwavering love and support through all the ups and downs and moments of madness my PhD has led me too. I could not have done this without you. To my parents and sisters, for always being there and providing unwavering advice, love, and support. To Kate, for keeping me sane and providing such wonderful company throughout lockdown.

Author's Declaration

Apart from the help and advice acknowledged, I confirm that the work in this thesis represents my own work and contain no material that has been submitted for any other degree at the University of Liverpool or other institution. This research was carried out in the Department of Infection Biology and Microbiome, Institute of Infection, Veterinary and Ecological Sciences, University of Liverpool, United Kingdom.

Amy Josephine Robinson, 2022

Abbreviations

ALI	Air Liquid Interface
BAL	Bronchoalveolar lavage
CRISPR	Clustered Regularly Interspaced Short Palindromic Repeats
DMEM	Dulbecco's Modified Eagles Medium
DMSO	Dimethyl sulfoxide
DNA	Deoxyribonucleic acid
dNTPs	Deoxyribonucleoside triphosphates
d.p.i.	Days post infection
dsRNA	Double stranded RNA
ENaC	Epithelial sodium channel
For	Forward
FBS	Fetal Bovine Serum
GFP	Green Fluorescent Protein
gDNA	Genomic deoxyribonucleic acid
HA	Hemagglutination
IAV	Influenza A Virus
IN	Intranasal
IFN	Interferon
IL	Interleukin
IP	Immunoprecipitation

ISG1	Interferon Stimulated Gene
KO	Knockout
KSFM	Keratinocyte Serum Free Media
LPS	Lipopolysaccharide
MOI	Multiplicity of Infection
NA	Neuraminidase
NK cell	Natural Killer cell
PAMP	Pattern Associated Molecular Pattern
PBS	Phosphate Buffered Saline
PRR	Pattern Recognition Receptors
Rev	Reverse
RNA	Ribonucleic acid
RV	Rhinovirus
RT	Room temperature
SA	Sialic acid
sgRNA	Single guide RNA
SpD	Surfactant protein D
SPLUNC1	Short Plate Lung Nasal Epithelial Clone 1
TGFβRI	Transforming Growth Factor β Receptor I
TGFβRII	Transforming Growth Factor β Receptor II
WT	Wildtype

W/V	Weight / Volume
x *g*	x gravity

1 Introduction

1.1 Influenza A Virus

The Influenza virus is a major cause of respiratory infection and a significant global health burden. It belongs to the *Orthomyxoviridae* family that comprises seven genera; these are *Thogotovirus*, *Salmon Isavirus* and *Quaranjavirus*, alongside four Influenza viruses. The four genera of influenza viruses are: influenza A virus (IAV), influenza B (IBV), influenza C (ICV) and influenza D (IDV). Orthomyxoviridae are negative-sense, single stranded, segmented RNA viruses (1).

IAV and IBV infections can cause severe disease and epidemics in humans whereas ICV is only associated with mild illness. Thus far no IDV infections have been reported in humans. IAV infect humans and a variety of animal species, however they are endemic in wild birds and the spill over of viruses from this viral reservoir into humans can cause pandemics. The work presented in this thesis will focus only on studies of IAV.

Influenza viruses are named according to their type e.g. A, B or C. The location from which they are isolated, isolate number, year isolated then hemagglutinin and neuraminidase subtype (2). For example, the influenza A virus with the hemagglutinin subtype 3 and neuraminidase subtype 2 isolated from London in 1993, the 27th virus isolated that year, would be named as A/London/27/93[H3N2]. The host the virus was isolated from is only included if the virus was not isolated from humans (3).

1.1.1 Structure and genome

Influenza viruses can exist in either a filamentous or spherical form (4). A viral envelope encloses the viral core and spikes project from the outer surface. Inside the viral envelope are the eight RNA segments that code for the IAV genome; each segment must be present in each virion for it to be infective (Figure 1). The coding capacity of the genome is maximised using alternative splicing mechanisms and open reading frames. Consequently, the eight segments inside the viral envelope code for the ten major proteins, with segments seven and eight each coding for two polypeptides (5-7).

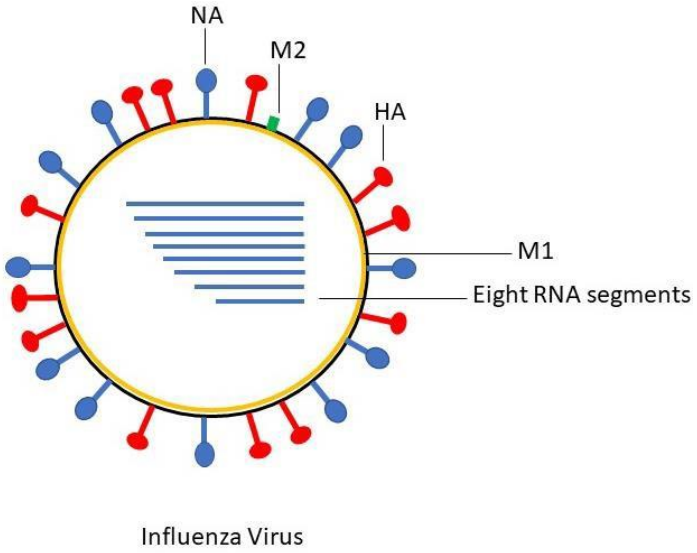

Figure 1. A diagram of IAV structure.
Viral membrane proteins HA, NA and M2 shown projecting from the viral envelope, which is supported by the M1 protein. vRNP structure is highlighted below, both vRNA ends are bound to the polymerase complex. The vRNA segment is wrapped around the NP protein.

Hemagglutinin (HA), neuraminidase (NA) and matrix-2 (M2) proteins project out from the viral envelope. The C-terminus of the HA protein is inserted in the viral membrane and the remaining portion of the molecule projects outwards. The HA protein itself

is a trimer. HA0 is the uncleaved form of the HA protein, when cleaved two proteins are produced: HA1 and HA2. This must happen for fusion to occur and influenza viruses be infectious. There are 18 different subtypes of HA which are divided into two groups based on their phylogenetic similarity. H1, H2, H5, H6, H8, H9, H11, H12, H13, H16, H17 and H18 belong to group one, the rest reside in group two (1, 8). Eleven different subtypes of NA exist. However, unlike HA1-16 and NA1-9, HA17, HA18, NA10 and NA11 do not bind to cells via sialic acid and have thus far only been identified in bats. This alters how IAV can bind and infect host cells (8).

The M2 protein is a tetrameric type III integral membrane protein. It has ion channel activity, is activated at a low pH and is highly selective for H^+ ions (9). The M2 channel protein has a crucial role during IAV infection. M2 selectively allows H^+ ions to enter the virus particle, lowing its pH. This acidification allows M1 protein to dissociation, membrane fusion to occur and the subsequent releases vRNPs into the cytoplasm. This allows virus replication to begin (10). Below the viral envelope lies the matrix (M1) protein, which also envelopes the virus core. The M1 protein has an ordered helix structure which changes at a lower pH, where it transforms into a multi-layered coil; this is accompanied virus losing its filamentous morphology and becoming spherical (11).

IAV can take a spherical and filamentous form in hosts. However, the filamentous morphology is usually only observed in nature. It is often lost *in vitro*, where the spherical morphology is predominant. This is supported by the emergence of filamentous virions following the serial passage of a spherical laboratory IAV strain in guinea pigs (12). This suggests that filamentous morphology provides an advantage in hosts that is not needed *in vitro* (11, 12). It is unclear what this advantage

specifically is however it may present an adaptation to aid IAV spread through host mucus (13).

The enveloped virus core houses the ribonucleoprotein (RNP) complex. This comprises the viral RNA segments, the nucleoprotein (NP) and the polymerase proteins: polymerase basic 1 (PB1), polymerase basic 2 (PB2) and polymerase acid (PA) (1). The RNA and NP interact to form a helical hairpin; however, this interaction has no sequence specificity and is facilitated through the negatively charged phosphate backbone of the RNA and positively charged residues of NP. This leaves the RNA bases exposed for the polymerase proteins to access (14).

The RNP complex has a very compact structure; vRNA ends have partial complementarity and form a panhandle RNA structure through Watson-Crick base pairing when bound to the polymerase proteins (Figure 1).

1.1.2 Lifecycle of Influenza A Virus

1.1.2.1 Virus entry into cells

IAV is dependent on the host cell functions for complete replication. It infects cells by binding sialic acid receptors on host cell surfaces through viral HA (Figure 2). Human IAV bind to sialic acid with an α2,6 linkage whereas avian viruses bind with a α2,3 linkage. This is reflected in the human trachea with epithelial cells containing mostly α2,6 linkages and α2,3 linkages primarily occurring in ducks, though both species do contain both linkages (15). The affinity between a HA and sialic acid receptors is low and therefore requires multiple HA proteins to bind host cells to increase the interactions strength and infect cells.

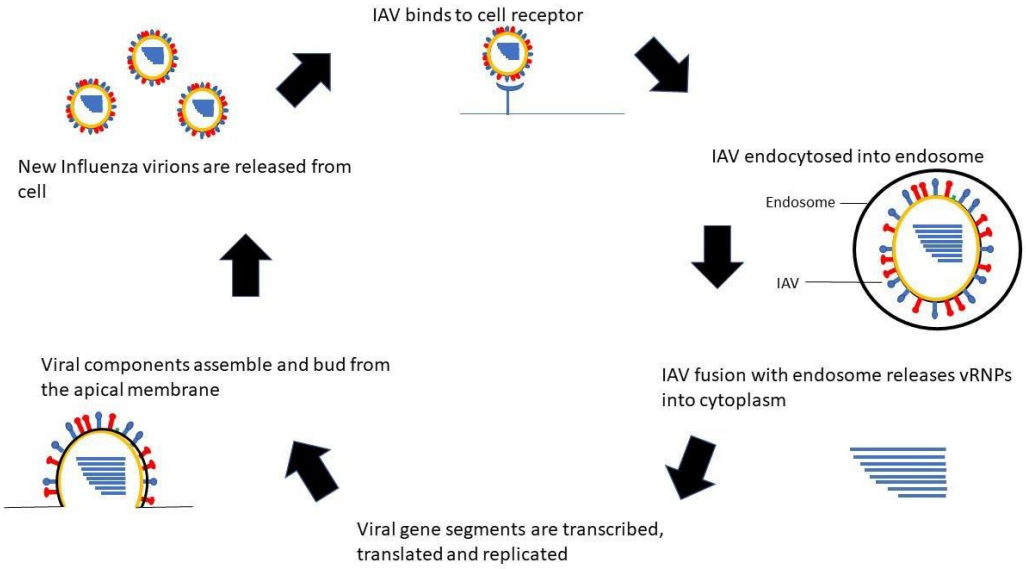

Figure 2. The influenza A virus life cycle.
IAV from binds to host cell, vRNP are, replication occurs in the nucleus and newly produced virions are released from the cell membrane through budding.

Following binding, the attached virus is transferred into the cell through receptor-mediated endocytosis in an early endosome (Figure 2). As the virus enters the endosome, endosomal acidification occurs. This then allows H^+ ions enter the virus through M2 proton channel and lower its pH (16). The early endosome then matures into a late endosome and membrane fusion occurs. This low pH causes conformational changes in M1 structure which result in the loss of its interactions with vRNPs and the viral membrane. Additionally, a conformational change in HA is triggered and exposes the fusion peptide, HA2 (17-19).

Then, NH_2-terminal of HA2 is inserted into the membrane, bringing the virus and endosome closer together (20). The presence of many bound HA molecules promotes membrane fusion through multiple conformational changes occurring simultaneously (21). These actions initiate fusion of the virus and endosome membrane forming a pore, which releases the vRNPs into the host cytoplasm (Figure

2) (22-24). The release of vRNPs into the cytoplasm signals the end of the uncoating process.

1.1.2.2 Transcription and Replication

After uncoating, all vRNPs are transported to the nucleus. vRNPs are too big to passively diffuse into the nucleus, so they are actively imported through a nuclear localisation signal (NLS) contained within each IAV polymerase protein (25, 26). A NLS present in NP can mediate the import of the RNA segments into the nucleus, via the host karyopherin import pathway (27). However, to allow entry into the nucleus M1 must also dissociate from RNPs. The evidence that M1 is essential for nuclear import is supported by the observation that amantadine, an antiviral drug which prevents IAV infection by blocking M2 ion channels and the decrease in endosomal pH. This subsequently prevents M1 dissociating vRNPs and RNP entering the nucleus (28).

During the replication cycle vRNA is transcribed into mRNA and cRNA but the control mechanism for switching between mRNA and cRNA synthesis remains unknown. The mechanisms for the initiation and termination of transcription for both vary considerably. Unlike mRNA, cRNA transcription initiation is primer independent, additionally the products are full length and do not undergo polyadenylation.

The promoter for mRNA synthesis is contained with the double stranded structure created by the 5' and 3' terminal vRNA sequences (29, 30). mRNA synthesis initiation is dependent on host cell RNA polymerase II activity. A 5'-capped primer must be 'pinched' from the host cells pre-mRNA transcripts, in a process known as 'cap-snatching' (31). The vRNA 5' end binds to PB1 to initiate the beginning of transcription (Figure 2). This induces an allosteric change that allows PB2 to bind the cap and PB1

to bind vRNA 3’ end, as the polymerases affinity for vRNA 3’ end increases (32). The polymerase complex endonuclease activity cleaves the pre-mRNA 10-14 nucleotides from the 5’ cap. A Guanine residue is added to this allowing it to bind to 3’ vRNA penultimate Cytosine, via complementary base pairing, initiating transcription (31). RNA elongation is driven by PB1’s polymerase function. During elongation, the cap detaches from the polymerase but vRNA 5’ end remains bound. The vRNA template is transcribed until a stretch of around 16 uridine bases is located at the vRNA 5’ end. This cannot be read due to steric hindrance and causes the polymerase to stutter and creates a poly(A) tail on the vRNA 3’ end (33).

1.1.2.3 Virus assembly and release

vRNP complexes are assembled in the nucleus and then exported to the cytoplasm. M1 and NS2/NEP are currently understood to be essential for the nuclear export of vRNP complexes. M1 binds to the vRNP complex in the nucleus then NS2/NEP binds to M1. This causes RNPs to dissociate from the nuclear matrix and mediates their transport out of the nucleus via nuclear pores (Figure 2) (28, 34). Nuclear export is regulated through the late expression of M1 as it allows a round of replication to take place prior to export (35).

The HA, NA and M2 proteins are synthesised on membrane bound ribosomes. They are then directed to the apical membrane, via apical sorting signals, where IAV assembles and buds (Figure 2) (36). There, HA and NA associate with lipid rafts whereas M2 does not. This could explain the low concentration of M2 in virus particles (37). It is unclear how the remaining viral proteins reach the assembly site.

Correct packaging of the 8 segments into the virus particle is required so the virus is fully infectious. The selective incorporation model states each segment acts independently and has its own packaging signal. This results in each virion possessing every segment (38). The segments are organised in a distinct pattern, with seven different length segments surrounding a central segment. This unique incorporation model and structure ensures the viral genomes structure is preserved (39).

Following the assembly of viral components at the apical plasma membrane, viruses are enveloped and bud from the host plasma membrane. Bud formation is initiated by an outer membrane curvature that itself is caused by the clustering of HA and NA at the plasma membrane. The membrane curvature continues extruding until the inner viral core is enveloped. Budding is completed when membranes fuse at the base of the bud. The virus particle is released following fission from the cell membrane (Figure 2).

Following the completion of budding all influenza virus particles need to be actively released because although they been released from the cell, they are still anchored to it as HA is bound to sialic acid receptors on its surface. NA cleaves newly budded viruses from infected cells via its sialidase activity which cleaves this HA – sialic acid interaction. This removes sialic acid from the viral glycoproteins such that virus particles do not bind themselves, allowing effective spread of the virus (40).

1.1.3 Antigenic Shift and Drift

Antigenic shift and drift are responsible for the signature antigenic variation associated with influenza viruses. All strains circulating in the human population today are previous pandemic strains, that arose from antigenic shift, and have since undergone antigenic drift. Antigenic drift is the gradual evolution of existing viral

strains over time due to mutations in HA and NA, however not all of these changes are synonymous. Antigenic shift is the creation of new viral strains with novel HA, and less frequently NA, subtypes (41). Antigenic shift creates novel virus strains that humans are immunologically naïve to therefore, the increased susceptibility and transmission that could occur among humans places a significant burden on society and may cause a pandemic (42, 43). Genetic reassortment is the primary mechanism of antigenic shift. This is enabled by the IAV segmented genome (42). A concurrent infection with two different strains can allow reassortment to occur between them and theoretically produce 254 new viral strains with a fusion of properties from both parent strains (44-46). Novel HA and NA subtypes emerge in human virus strains from the extensive influenza gene reservoir present in animals. Genetic reassortment allows the transmission of these novel IAV proteins into human circulating IAV strains (47).

Antigenic shift occurred three times in the last century: in 1918, 1957 and 1968. The 1918 Spanish influenza pandemic was caused by a strain with a HA that was most like a previously recorded avian influenza strain. The 1918 pandemic HA gene had previously crossed into humans and adapted, to allow human to human transmission, prior to the 1918 pandemic (48). The 1957 pandemic IAV strain had a novel PB1 protein of avian origin. After the pandemic this was the primary PB1 protein in circulation until 1968 (49). The 1968 pandemic strains' HA protein was previously reported in a 1963 duck IAV. Additionally, its PB1 protein was of avian origin, but distinct from 1957's PB1 protein, and its circulation novel in humans. This reaffirms that animals are reservoirs of novel HA and NA genes that could cause pandemics in human (50). Unlike the 20th century pandemics, the 2009 pandemic strain HA protein

resulted from genetic reassortment across multiple swine IAV as well as avian and human IAV (51).

Antigenic drift is due to a high mutation rate driven by IAV RNA dependent RNA polymerase, whose lack of proof reading means it is error prone (42). New human vaccines are required annually to overcome antigenic drift occurring in circulating strains (41). Due to the pressures of selection to evade the host immune response these mutations occur more frequently in the HA gene, compared to other viral proteins. However, these mutations typically only occur in specific regions such as the antigen binding site as these are the primary binding site for a host neutralising antibody (41, 52).

Reducing the efficacy of host neutralising antibodies promotes transmission among the population, is associated with greater mortality and necessitates new annual vaccines (42, 53, 54). Unlike antigenic shift which only occurs in IAV, antigenic drift can occur in IAV and IBV. The A/Fujian/411/2002 virus strain has undergone 13 amino acid mutations at two amino acid sites from the A/Panama/2007/99. However, these mutations render Panama antibodies 25% less effective at neutralising virus against the Fujian strain compared to the Panama strain (55). This underlies the importance and severe consequences antigenic drift can have. Antigenic drift is also driven by IAV evolving to evade the hosts immune response. Following IAV exposure, hosts develop immunity which decays overtime. This protects against reinfection and limits overall viral spread and growth. This in turn restricts viral diversity and encourages mutations which escape the hosts immune response (56).

1.1.4 Viral Reservoirs

IAV is a zoonotic pathogen that causes disease in many species. The primary reservoir for IAV exists in aquatic birds although other, substantial reservoirs are also present in land-based poultry, pigs, and humans (42, 53, 55, 57). Nevertheless, many other species, including horses, dogs, cats, and aquatic mammals are also susceptible to IAV. However, each species is susceptible to specific IAV subtypes (Figure 3). Virus spread is often contained within one individual species, typically with certain subtypes as the predominant strain. However, IAV virus strains can cross into other species (Figure 3). This can occur via intermediate hosts or by viral adaptive mutations (42).

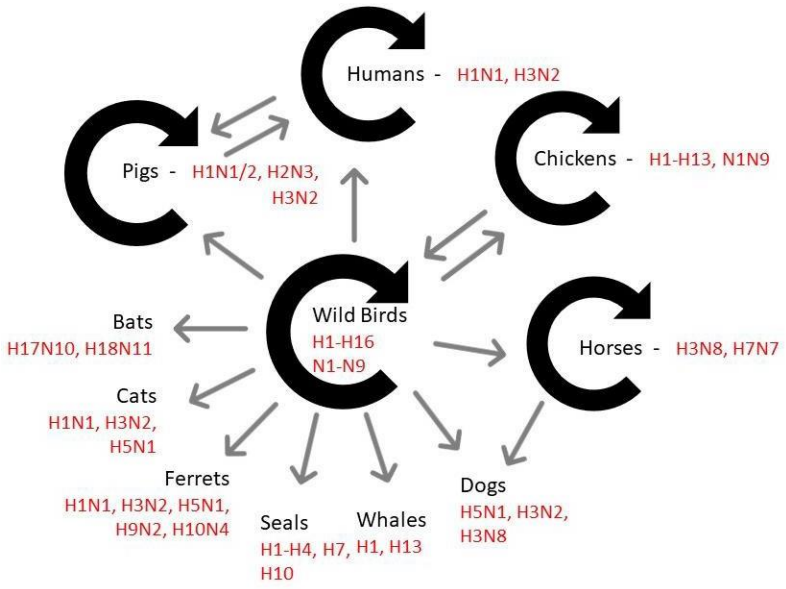

Figure 3. IAV transmission in reservoirs and across species barriers.
Influenza A Viruses circulate in wild bird, pig, and human reservoirs, black circular arrows. Transmission between species is possible, indicated by the grey arrows. The specific HA and NA subtypes each species can be infected with are labelled in red. Adapted from Long et al., (57).

Phylogenetic analysis reveals that all avian, human and swine IAV reservoirs have the same, common ancestor: an avian IAV. This is reinforced as until 1979 pigs were free of IAV infection. In 1979 a severe outbreak occurred in Europe after an avian IAV strain crossed over into the swine population (44). Following this outbreak, pigs have become viral gene reservoirs for IAV and today may act as mixing vessels for interspecies transmission between birds and humans (58). The distribution of IAV strains across the globe is affected by localisation of species, their own biological characteristics and movement. The limited intercontinental travel of pigs has led to swine lineages having a distinct geographical pattern and phylogenetic history (53). This is distinct to human and bird IAV strains, which are both capable of long-distance travel and whose phylogenetic history is much more complex.

1.1.4.1 Interspecies transmission

Avian IAV predominantly bind α-(2,3) linked sialic acid (α-2,3 - SA) unlike human IAV that predominantly bind α-2,6 – SA because avian tracheas predominantly contain α-2,3 - SA and humans α-2,6 - SA. Therefore, transmissions of strains between the two species are limited and rare but can occur. This barrier between species can be overcome, and if this occurs alongside genetic reassortment, could have devasting consequences (59, 60). Avian IAV strains can infect humans, however subsequent human to human transmission is often very limited and requires further mutations (53).

Numerous examples of this have occurred in recent years. In February 2021 seven poultry workers were infected with A/H5N8 strain of avian influenza on a farm in Russia. These are the first human infections with of this strain recorded (61). In June

2021 the first H10N3 human infection with avian IAV was reported in Zhenjiang, China (62). Neither of these avian influenza strain outbreaks in humans resulted in any human-to-human transmission, and themselves occurred due to exposure in infected poultry farms. This highlights the dangers that constantly evolving influenza viruses poses and the need for strict surveillance globally.

Although the opportunity for direct transmission of avian IAV to humans is limited it is still a distinct possibility. Pigs are crucial to the transmission of IAV between avian species and humans as unlike humans and birds they have a mix of α-2,3 - SA and α-2,6 – SA (60). This lowers the species barrier protecting pigs from cross species infections and increases their susceptibility to both avian and human IAV infection. Therefore, they can act as mixing vessels when IAV co-infection occurs, allowing strains to reassort and potentially produce a virus strain with novel HA and NA genes that could cause a pandemic (53). This is supported as human pandemics have typically started from southeast Asia, where pigs live in close contact with humans and waterfowl (44, 58, 63).

In addition to the genetic reassortment potential pigs possess, they are also reservoirs for avian-like swine virus': that can recognise human receptors. These also have the potential to be transmitted into, and crucially, between humans (60).

This is the source of the most recent pandemic in 2009, swine flu – a triple reassortment IAV strain from birds, swine, and humans. Specifically, it was derived from the reassortment of multiple swine IAV lineages in circulation in North America, Asia and Europe, and is believed to have been circulating in humans prior to the initial outbreak detected in April 2009 (51, 64, 65).

1.2 Host Response

1.2.1 Innate Immune System

1.2.1.1 Barriers

Viruses are obligate intracellular pathogens that require host cells to complete their life cycle. This leads to a within host cycle of viral invasion of cells, the synthesis of new viral proteins, virus assembly and the release of infectious progeny. The immune system utilises multiple mechanisms simultaneously to combat viruses at each of these stages. The innate and adaptive immune systems act in synergy to eradicate established infections and protect against future infections.

IAV first encounters the innate immune response which is rapid in speed of response but lacks antigen specificity. The first line of defense pathogens encounter are physical and chemical barriers. Epithelial cells are present at openings of the respiratory tract and covered are in mucus and surfactants which act to physically separate epithelia from pathogens and trap them before they can enter cells (Figure 4).

The protective mucus layer on top of respiratory epithelial cells is primarily comprised of mucins. These act to maintain airway homeostasis, disrupt pathogen aggregation, and remove cellular debris (66, 67). Other secretions such as: tears, saliva, surfactant, gastric enzymes and acid, act in similar ways as chemical barriers, to prevent pathogens cell entry or destroy them directly. Cells in the respiratory and gastric tract have cilia projections that extend outwards. In the respiratory tract these move in pulses to sweep mucus and any trapped foreign particles away from the lungs, in a process called mucociliary clearance (68).

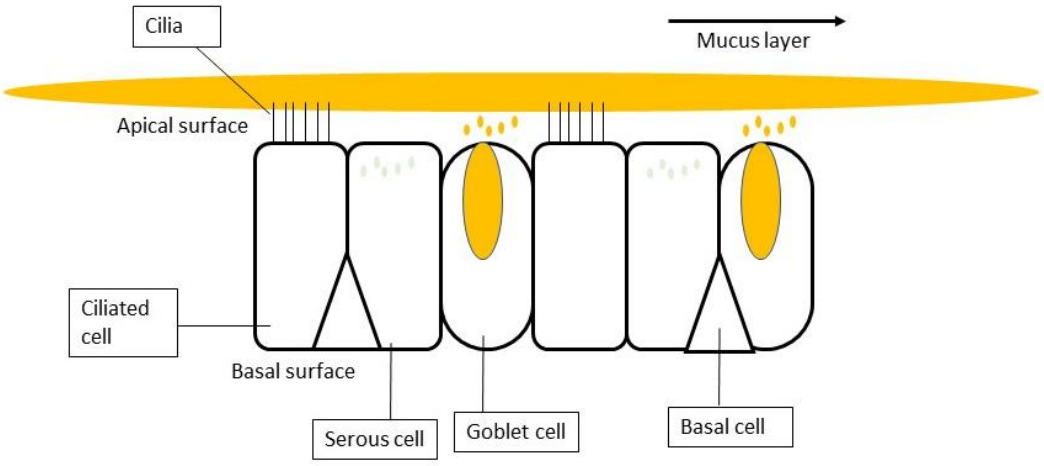

Figure 4. Respiratory epithelium from the trachea to the bronchioles.
The respiratory epithelium is lined by ciliated cells, secretory cells and submucosal glands that together form a barrier to infection. The protective mucus layer over the cells binds pathogens and other particles which are then brushed upwards by the cilia and cleared. This layer also contains host defence proteins secreted by cells that can trigger an immune response upon pathogen recognition. Tight junctions between the epithelial cells act to prevent the penetration of pathogens between cells. Adapted from Whitsett and Alenghat (67).

Pulmonary surfactant is a fluid secreted at the alveoli air-tissue interface; it is mostly composed of lipids. Palmitoyl-oleoyl-phosphatidylglycerol (POPG) and phosphatidylinositol (PI) are two lipids present in pulmonary surfactant. They can bind to the 2009 pandemic H1N1 IAV and prevent its attachment, and the therefore infection, of epithelial cells. Treatment with POPG or PI in mice infected with IAV attenuates infection, decreasing viral load, inflammatory cell infiltration and mortality (69).

Alongside lipids, surfactant is also comprised of 10% protein. The surfactant proteins A (SpA), B (SpB), C (SpC) and D (SpD) together comprise half the proteins in surfactant. Surfactant proteins A (SpA) and D (SpD) both also function as collectins: soluble, non-membrane bound pattern recognition receptors (PRR) that bind to PAMPs on the surface of pathogens. They both provide protective, antiviral activity against IAV as

the knockout (KO) of either in mice significantly increased the viral titre observed compared to wild type (WT) mice (70).

The increased lung viral titre observed in SpD KO mice is likely due to impaired viral clearance. Additionally, SpD KO mice also suffer from increased inflammation throughout infection (71).

These effects occur because SpD can bind IAV and inhibit its HA activity. Specifically, it binds mannose oligosaccharides on HA which reduce the virus' uptake into epithelial cells and causes viral aggregation. This prevents the infection of further cells and enhances IAV removal from the lung (71, 72). SpD's multimerization property allows for extensive crosslinking, further enhancing this effect (73).

SpD protection against IAV however is strain specific and often pandemic and avian IAV strains are not susceptibility to SpD. This could contribute to their virulence in humans and is likely due to less mannose oligosaccharides near the SA binding sites on HA, inhibiting its antiviral activity (74, 75). This is supported as H3 IAV isolates from post-1972 have more glycosylation sites compared to pre-1972 isolates and these later isolates are more sensitive to neutralisation by SpD, displaying lower replication rates when it is present (75).

1.2.1.2 PAMPs and PRR

Hosts detect pathogens through the recognition of conserved molecular patterns associated with pathogens, known as pathogen-associated molecular patterns (PAMPs) or damage-associated molecular patterns (DAMPs). PAMPs are molecular structures absent in the host and in the case of viruses, features of viral RNA. DAMPs are host proteins released from damaged or dying cells to initiate an immune

response (76). PAMPs and DAMPs are both recognised by pattern recognition receptors (PRR) present on immune cells. PRR activation leads to a reaction cascade which results in the induction of an immune response against the pathogen. However, host proteins, such as NLRX1, can interfere and modulate PRR during IAV infection and inhibit their host response (77).

A wide range of PRR exist; these vary in what they detect, their location and the effect they mediate. Toll-like receptors (TLR) are PRR situated in the plasma membrane of cells and endosomes. TLR 1, 2, 4 and 6 recognise microbial membrane components (78) whereas TLR 3, 7, 8 and 9 recognise nucleic acids. Specifically, TLR 9 binds viral DNA and TLR 3, 7 and 8 bind viral RNA. These differ in the forms of RNA they recognise. TLR3 bind double stranded RNA (dsRNA) whereas TLR 7 and 8 recognise single stranded RNA (ssRNA) viruses found in endosomal compartments (79-83). Once activated different TLR signal through different pathways which all contribute to establishing an anti-viral state in the host (Figure 5).

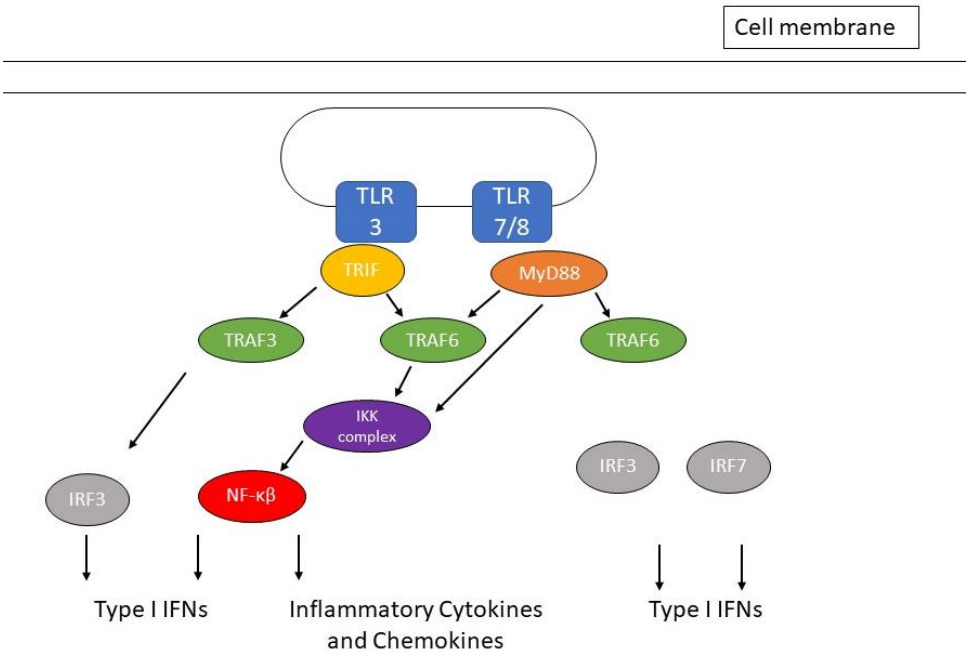

Figure 5. TLR signalling pathway following PRR activation.
Endosome expressed TLR 3, 7 and 8 are bound and activated upon RNA virus recognition. This leads to the induction of Type I IFN and the secretion of inflammatory cytokines and chemokine which ultimately result in the induction of an anti-viral state. Adapted from Makris et al., (85).

PAMPs can also be detected via cytosolic PRR such as NOD-like receptors (NLR) and RIG-I like receptors (RLR). NLR family pyrin domain containing 3 (NLRP3) and melanoma differentiated-associated gene 5 (MDA5) are NLR and RLR receptors, respectively, that detect viral RNA PAMPs (84-86). The importance of PAMP recognition and the initiation of a host immune response is demonstrated as during IAV infection NLRP3 KO mice had significantly reduced inflammatory response, viral clearance and survival rates compared to WT mice (84). RLR receptors recognise various form of viral RNA. RIG-I is activated by triphosphates at the 5' terminal of vRNA whereas MDA-5 ligands are typically longer dsRNA stretches without phosphates. However, other factors can also influence if an RNA sequence can instigate an immune response through RIG-I such as a double stranded sequence or length. These features enable the IAV vRNA promoter to act as a RIG-I ligand and

induce an interferon (IFN) response (86). During IAV infection it is primarily the RLR RIG-I, and not MDA-5, that induces the host response and the IFN mediated induction of an antiviral state (80, 87, 88).

To evade host immune responses IAV has established many strategies to evade RLR detection. First IAV transcription and replication occur in the nucleus, away from cytosolic and membrane PRRs. Therefore, PRRs cannot access vRNA present in the nucleus and trigger a host response. IAV also can evade the immune response via NS1, NS1 is the principal viral antagonist of the immune system. NS1 mediates this by binding RIG-I which prevents it activating the IFN-β promoter. Not only does this limit the RIG-I available for IAV to bind as its binding site is blocked but it also decreases the resulting anti-viral response (89). NS1 can also achieve this same effect by binding to TRIM25; this binding prevents TRIM25 ubiquitinating RIG-I CARD domains therefore suppressing signaling, IFN production and antiviral immune response (90, 91).

1.2.1.3 Interferon response

The host immune response aims to eliminate infection through a multitude of mechanisms acting in synergy to induce an antiviral state, prevent further spread and destroy pathogens, protecting neighboring, uninfected, cells from potential infection. This occurs through activating cells to secrete interferons (IFN) and other proinflammatory molecules including cytokines and chemokines. However, only some cells infected with IAV produce IFN. This acts to induce a protective, antiviral state in surrounding infected and uninfected cells (92).

Interferons are released from infected cells in response to viral infections and other

pathogens. They are divided into three classes: type I, type II and type III IFN. IFN-α and IFN-β are the predominant type I IFN (IFN-I), they bind to the IFN-α/β receptor (IFNAR). IFN-γ is a type II IFN (IFN-II) and IFN-λ is a type III IFN (IFN-III). Both IFN-I and IFN-III activate the JAK/STAT signaling pathway eliciting similar responses (93, 94). IFN-I and IFN-III can be released by all cells types but IFN-I is largely released by alveolar macrophages and IFN-III by airway epithelial cells (AEC) during IAV infection (95). These both act to limit viral infection by blocking viral RNA replication, controlling apoptosis and limiting IAV spread from the upper airway into the lungs (96, 97).

IFNs stimulate the expressions of IFN stimulated genes (ISGs). ISGs enhance pathogen detection by upregulating PRR expression; upregulating MHC class I expression; activating NK cells; and inhibiting viral replication. Subsequently this increases antigen presentation and limits virus spread (98). Protein Kinase R (PKR) is an ISG that binds dsRNA, during IAV infection it acts to limit infection and further replication (99). Specifically, during IAV infection of WT and PKR KO mice, PKR KO mice have increased IAV mRNA translation (100). However, NS1 can act to prevent this PKR mediated anti-viral response against IAV (101). This occurs through NS1 binding to PKR, inhibiting its activation and therefore antiviral activity (102).

Numerous host proteins act as ISGs and are expressed in response to IAV infection providing protection against infection; this is achieved by targeting and impairing the IAV lifecycle. ISG primarily achieve this through limiting replication or degrading IAV proteins. The host proteins IFITM3, MOV10, DDX21 and ZAPS are all examples of ISGs that impair IAV infection through limiting replication. However, each protein achieves this via a distinct mechanism. IFITM3 inhibits viral-host membrane fusion and pore

formation, MOV10 causes cytoplasmic retention of the viral NP, DDX21 prevents the polymerase complex forming and ZAPS represses translation (103-109). OAS3, TRIM32, TRIM22 and ZAPL all mediate degradation to impair IAV infection. OAS3 mediates rRNA degradation, TRIM32 binds PB1 and TRIM 22 NP to mediate their ubiquitination and subsequent degradation, ZAPL binds the polymerase proteins causing them to undergo degradation (110-113).

IFN-α inhibits IAV replication, the pre-treatment of A549 cells with IFN-α prior to infection inhibited replication as the viral genome was not able to transport into the nucleus. MxA is an ISG necessary but not solely responsible, for this effect (114). This is evidenced as IFNAR KO mice have increased mortality and morbidity due to IAV infection and greater levels of pro-inflammatory cytokines during infection, due to decreased IL-10 production (115). This demonstrates reduced IFN-α signalling leads to increased mortality through the absence of cytotoxicity and lack of regulator mechanisms downregulating IFN-γ production, supporting the previous study in A549s. IFN-β is secreted by alveolar macrophages in response to IAV infection. This causes further damage to the airway epithelial cells infected with IAV, despite IFN-β anti-viral activity (116). IFN-λ is essential during IAV infection as the KO of its receptor in mice leads to increased mortality and blunted $CD8^+$ T cell responses. This is because it impairs the migration and function of $CD103^+$ dendritic cells (DC) which require intact IFN-λ signalling to restrict IL-10 production from $CD103^+$ DC and optimally activate $CD8^+$ T cells and clear IAV infection. Therefore, IFN-λ is crucial during the response to IAV infection, provides effective T-cell immunity, and helps bridge the gap between the innate and adaptive immune systems (117).

Usually, IFNAR signalling increases IL-10 production which suppresses the release of

IFN-γ from NK cells. Therefore, IFNAR KO increases IFN-γ levels in KO mice. The depletion of NK cells in IFNAR KO mice, via a neutralising antibody, improved mice survival compared to those with intact NK cell compartments however, IFN-γ depletion did not. This indicates that NK cells are largely responsible for the acute lung injury and increased mortality observed in IFNAR KO mice during IAV infection, and demonstrates IFN-I signalling downregulates IFN-γ production (115). This also reveals not all immune responses benefit the host during infection and balance is crucial to avoiding immune mediated pulmonary injury that causes more damage than the initial infection itself (118).

An example of this is the host protein NMP4, in response to IAV it exaggerates inflammation and its absence during IAV infection is highly beneficial: reducing mortality, lung cellularity, viral titre and weight loss during IAV infection (119). This is also demonstrated when shingosine-1-phosphate receptor ($S1P_1$) activation suppresses cytokine release and the recruitment of innate cells. $S1P_1$ KO mice are protected from death during IAV infection by interfering with the signalling pathways that mediate a cytokine storm: an uncontrolled, overreaction of the innate immune system where high levels of cytokines circulate and exacerbate infection. This demonstrates that a cytokine storm is a pathological event that can cause death during influenza infection (120).

IAV itself can impact the extent of IFN response that occurs during infection. IAV strains with partial or complete deletions of NS1 are more potent IFN inducers (121). This demonstrates NS1 antagonises the IFN response during IAV infection. However, IFN antagonism can also be mediated by PB2 and PB1-F2. Both interact with the mitochondrial antiviral signalling protein (MAVS) to inhibit the promotion of IFN-β

expression and therefore the antiviral response to IAV infection (122, 123).

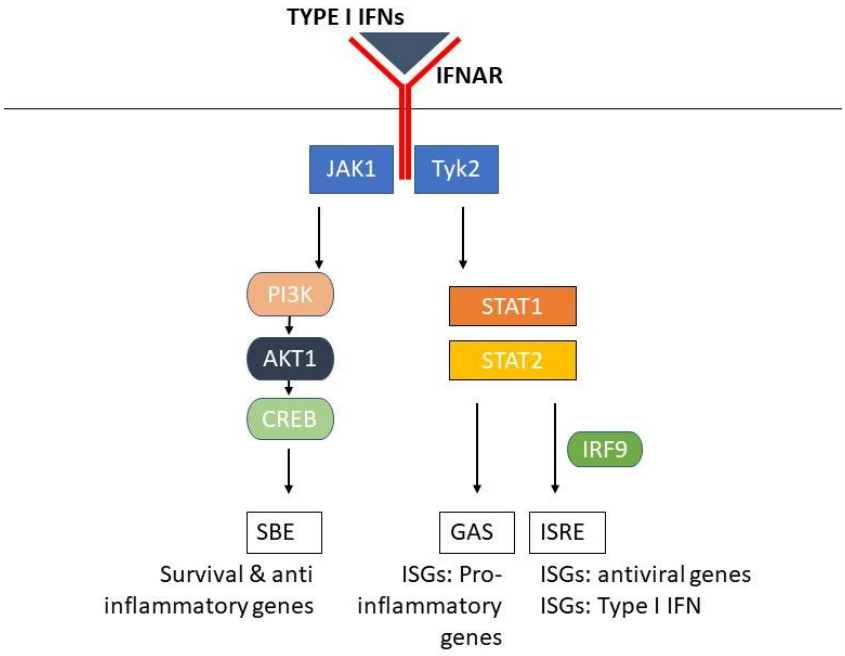

Figure 6. Type I IFN signalling pathway and mediated effects.
Following IFN-I release it binds to the IFN-α/β receptor (IFNAR) and initiates a signaling cascade which results in complex translocation to the nucleus. There it binds IFN-stimulated response elements (ISRE) on IFN stimulated gene (ISG) promotors to activate gene transcription and antiviral state induction. Adapted from Makris et al., (85).

The release of IFN and other cytokines induces an antiviral state that is mediated not only by ISG but the recruitment and activation of leukocytes. Neutrophils, macrophages, T cells and other leukocytes migrate along chemokine gradients from circulation and tissues to sites of inflammation (Figure 6). Chemokine gradients are caused by some ISGs during pathological conditions and by immune cells that are recruiting cells to sites of infection. The net result of this is enhanced phagocytosis, antigen presentation, increased complement, and NK mediated cell lysis at infection sites (124).

When neutrophils are recruited to the site of infection, they are typically refractory to infection and act to destroy pathogens. They achieve this through degranulation, the release of toxic granules from their cytoplasm and neutrophil extracellular traps

(NETs). NETs are composed from webs of chromatin fibres with these cytoplasmic granules within. These trap pathogens for degradation and prevent pathogens from spreading within the host. However, both responses can damage the host tissue and their control is essential to avoid an excessive response damaging respiratory tissues. Additionally, these recruited cells typically secrete further chemokines to recruit more cells to the infection site and amplify the immune response (118).

1.2.1.4 Natural Killer cells

NK cells are a type of innate lymphocyte that are activated in response to the secretion of IFN-α and IFN-β and promote defense against viruses. They provide a rapid response to virus infected cells by recognising the downregulation of MHC-I, a key feature of viral infected cells, and attacking them. Once active, they have many functions that together mediate an anti-viral response. In response to activation, they produce IFN-γ which primes other immune cells, promotes phagocytosis by macrophages, and supports the adaptive immune response killing infected cells (125, 126).

NK cells are the prime source of IFN during early infection, and essential for activation of the innate immune system (127, 128). Exogenous IFN-γ administration during the early stage of IAV infection protects against mortality and excess inflammation. This effect is NK cell dependant as IFN-γ administration stimulates NK cell proliferation and function therefore promoting viral clearance during infection (129).

NK cell mediated cytotoxicity occurs via the release of perforin and granzymes from cytoplasmic granules. These induce apoptosis in target cells and infected cells. However, the role of NK mediated cytotoxicity during viral infection is limited (127).

NK cells can also kill cells by other methods such as; engagement of death (FAS/CD95) receptors and antibody dependent cell-mediated cytotoxicity (ADCC) (125, 126).

During IAV infection NK cells are actively recruited and accumulate in the lungs to assist in viral clearance. NK cells were depleted using antiserum to GM1, expressed on NK cell membranes, during IAV infection; viral titres, morbidity and mortality all increased, demonstrating the protective importance of their antiviral activity (130, 131). However, NK cell activity can also increase infection induced immunopathology with NK cell depletion via a monoclonal antibody reducing mortality (132). Additionally, increased NK cell activity observed throughout pregnancy increases inflammation, infection induced pathology, morbidity and mortality during IAV infection (133). This suggests a variable role for NK cells during IAV infection that must be balanced for a protective anti-viral effect to occur. This may be mediated by dose-dependent responses as variable NK functions have been observed during *in vivo* infection using variable IAV doses (132, 134).

1.2.1.5 Priming the adaptive immune response

A key function of the innate immune system is to prime and present antigens to T- and B-cells, to activate the adaptive immune response. This antigen presentation leads to a more versatile, specific, long-lasting immune response. It occurs following the internalisation and presentation of antigens by antigen presenting cells (APC) such as dendritic cells (DC). Antigens are degraded into small peptide fragments and displayed on the cell surface in MHC complexes so they can be recognised by a T- or B-cell. It is currently unknown which specific DC subset is responsible for IAV antigen presentation (135). However, $CD103^+$ and $CD11b^+$ DC are critical APC subsets in

mediating an adaptive immune response against IAV infection. Both DC subsets present antigen to $CD4^+$ T cells but $CD103^+$ DC preferentially present to $CD8^+$ T-cells (136).

Only DC are professional APC however many other cells such as macrophages and B-cells can act as APC under certain conditions (137). It has also been postulated that neutrophils can act as APC during IAV infection. Their depletion via a monoclonal antibody significantly reduced the IFN-γ levels produced by $CD8^+$ T-cells in the lungs during infection suggesting less $CD8^+$ T-cells were activated in the absence of neutrophils and they can act as APC (138). However, other studies have observed that neutrophils are only crucial for sustaining $CD8^+$ T-cell responses at the site of infection, not for maintaining influenza antigen presentation. Therefore, neutrophils may not act as APC but their presence be crucial for effective $CD8^+$ T-cells responses and cytokine production (139).

During IAV infection, antigens are typically acquired by DC through phagocytosis or direct infection (135). However, infection does not always result in the release of infectious virions as only myeloid and not plasmacytoid DC are able to support virus replication (140). The infection of DC and APC could be a consequence of viral evolution mechanism targeting impairment of the adaptive immune response. First, through apoptosis of infected DC and secondly, by impairing the cross presentation of infected cells up to 300 times compared to uninfected cells, determined by quantitative analysis of western blot showing IAV internalised by infected and uninfected DC (140).

Following antigen presentation during the initial immune response, APC travel through the lymphatic system to the lymph nodes to present antigen to resident

adaptive immune cells. This provides an environment where APC can display their antigens to T-cells and B-cells and activate the adaptive immune response.

1.2.2 Adaptive Immune System

The adaptive immune response is comprised of cell-mediated and humoral immunity. It is a highly specific pathway that is activated upon exposure to pathogens. Unlike the innate immune system, it can create memory responses and provide lifetime protection. Cell-mediated immunity protects the host by identifying and destroying infected cells. This is primarily mediated by T-cells and is particularly effective at killing virus infected cells and stimulating other immune cells. Humoral immunity is primarily mediated by antibodies secreted from plasma cells, differentiated B-cells. Antibodies act to prime and neutralise antigens to assist with pathogen elimination.

1.2.2.1 T-cells

T-cells develop in the thymus and exit, once mature, as naïve T-cells. T-cells are comprised of two major subsets: $CD8^+$ T-cells and $CD4^+$ T-cells. These are named after the surface proteins, CD8 and CD4, they display. They travel through the blood and lymphatic systems in search of APC presenting one specific antigen via its MHC complex. Each T-cell has a unique T-Cell Receptor (TCR) that recognises one specific antigenic epitope when presented on APC by MHC, not as free extracellular antigens. To activate a T-cell and stimulate an effector immune response three signals are required. The first is antigen specific and involves the TCR and MHC-APC complex. The second occur through the interaction of co-stimulatory molecules present on the

T-cell and APC, such as those detailed in Figure 7. The third signal is mediated by polarizing cytokines that guide T-cell differentiation into effector T-cell subsets (141). If the sole signal present is between the APC and TCR then T-cell anergy or tolerance occurs and future T-cell activation in response to the same antigen is harder. Co-stimulation is therefore essential for an effective immune response to occur.

Antigens are presented on APC by either class I or class II MHC molecules; MHC class I molecules are expressed on all nucleated cells and present intracellular pathogens to $CD8^+$ T-cells. Conversely, MHC class II molecules are only expressed on professional APC and only present extracellular pathogens to $CD4^+$ T-cells. However, MHC class I molecules are also capable of presenting extracellular/exogenous antigens to $CD8^+$ T-cells via cross presentation. Cross presentation enables pathogens like viruses and tumours in the host to induce an immune response against them.

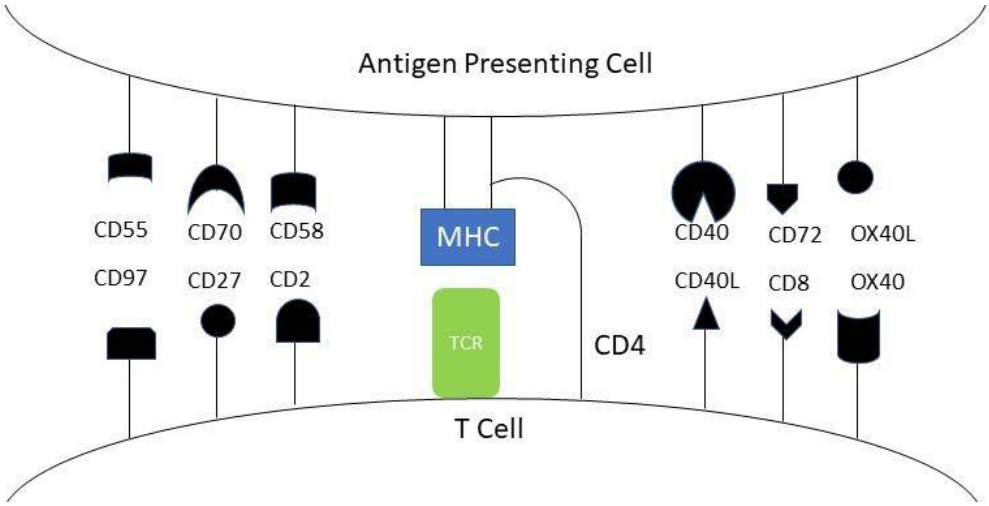

Figure 7. The interaction of co-stimulatory ligands and receptors projecting from APC and T-cells.
Co-stimulatory ligands bind receptors on T-cells alongside the antigen binding to the TCR. This co-stimulation is essential for the APC-TCR interaction resulting in T cell activation and an effector immune response. Image from Gizinski et al., 2010 (142).

$CD8^+$ T-cells are cytotoxic T-cells (CTL) and $CD4^+$ T cells helper T-cells (Th). CTL instruct infected cells to undergo programmed cell death and secrete perforins, granzymes and cytokines, such as IL-2 and IFN- γ, that amplify the innate and adaptive immune responses through recruitment of other immune cells, for example macrophages and NK cells (143). $CD4^+$ T-cells effector responses differ depending on their type: type 1, type 2, or type 17. $CD4^+$ T-cell's type is decided by specific cytokine pattern, from a common precursor cell. Type 1 Th cells amplify the cellular mediated immune response. They release IFN-γ and TNF-β and induce programmed cell death via macrophages and CTL. Type 2 Th cells amplify humoral B cell responses. They stimulate B cell proliferation, class switching and most importantly antibody production. They produce IL-4, IL-6, IL-10 and IL-13 cytokines that induce an anti-inflammatory response and inhibit type 1 Th cell response. Type 17 Th cells are distinct from type 1 and 2 Th. They typically lie at mucosal barriers and produce IL-17, inducing a pro-inflammatory response (144).

More specifically, both $CD8^+$ and $CD4^+$ T-cells are required for protection and clearance of IAV infection. Knockout mice defective in MHC I are also defective in antigen presentation and unable to activate $CD8^+$ T-cells during non-lethal IAV infections. These KO mice suffer from delayed viral clearance compared to WT mice. The clearance of infection in these mice is most likely due to $CD4^+$ T-cells, demonstrating that $CD8^+$ T-cells are not the sole mediators of protection and viral clearance against IAV (145). $CD8^+$ T-cells do however provide cross protection against heterologous virus strains. This was demonstrated via T-cell antibody-mediated depletion in mice prior to IAV vaccination (146).

$CD4^+$ T-cells are required during IAV infection for viral clearance and survival. Their depletion increased mortality, susceptibility to IAV and decreased the number of $CD8^+$ T cells recruited in bronchoalveolar lavage (BAL) during infection. This shows that $CD4^+$ T-cells promote the expansion and recruitment of $CD8^+$ T-cells during IAV infection and both are required for survival (147, 148). In addition to recruiting and mediating $CD8^+$ T-cells activation during IAV infection, $CD4^+$ T-cells also promote B-cell recruitment and activation through differentiation to Th1 cells (149).

T-cells form a crucial part of the host's immune response to IAV infection. Nude mice with no T-cells suffer from significantly increased mortality compared to WT mice during IAV infection. However, these deaths occurred significantly later than those in WT mice with infection persisting up to 28 days post infection in nude mice compared to 14 days in WT mice. Additionally, nude mice also had an increased number of pathological lesions and lower antibody titres the lung compared to WT mice during infection (150). Together this data confirms that although the innate immune response is protective during IAV infection, T-cells have a vital role in the host response and are crucial for the swift eradication of infection.

However, not all immune responses to viral infection benefit the host. During IAV infection $CD8^+$ T-cells follow neutrophil secreted chemokine trails and migrate to the infected tissue (151). IL-10 is a chemokine secreted in response to IAV viral antigens and is detectable in BAL 4 days post infection (d.p.i.). IL-10 levels increase from 4 d.p.i. peaking at day 8, this significant increase is accompanied by the recruitment of $CD8^+$ and $CD4^+$ T-cells and lung viral titre. This demonstrates IL-10 expression coincidences with the eradication of infection. The inhibition of IL-10 via a monoclonal antibody significantly increases and accelerates mortality in murine IAV infection models.

Interestingly however, this is due to increased inflammation and not a change in viral titre or clearance (152). This suggests IL-10 can modulate the immune response to avoid infection induced immunopathology and death.

A similar role is also suggested for the cytokine TRAIL. TRAIL deficiency impairs $CD8^+$ T-cell mediated immunity with IAV infected mice suffering increased mortality correlating with an increase in $CD8^+$ T cells and no change in viral load, compared to WT mice (153). This is due to the regulation of CD8 T-cells by TRAIL and controlling the magnitude of inflammation. Therefore, its deficiency in mice increases inflammation, chemokine expression, cytotoxic activity and increases the chance of infection induced immunopathology and excessive tissue damage during IAV infection (154).

1.2.2.2 B cells

Humoral immunity is mediated by B-cells. They mediate this through by acting as APC and secreting antibodies. Unlike T-cells, B-cells can recognise free circulating antigens or those attached to the surface of microbes and trigger an immune response. This typically occurs in secondary lymphoid organs which act to bring the innate and adaptive immune system together (155).

Like T-cells, B-cells receptors (BCR) have a unique variable region for each antigen fragment. BCR are composed of two structures: a membrane bound immunoglobulin and a signal transduction molecule. It is comprised from two heavy and two light chains joined by disulphide bonds. Together they form two regions: the constant region and the variable region (Figure 8). It is the variable region that contains the unique antigen binding site, the constant region determines the isotype (IgA, IgD,

IgE, IgG or IgM) of the BCR. The signal transduction molecule is an Igα/Igβ heterodimer which spans the cell membrane, close to the BCR. It mediates downstream signalling following receptor activation.

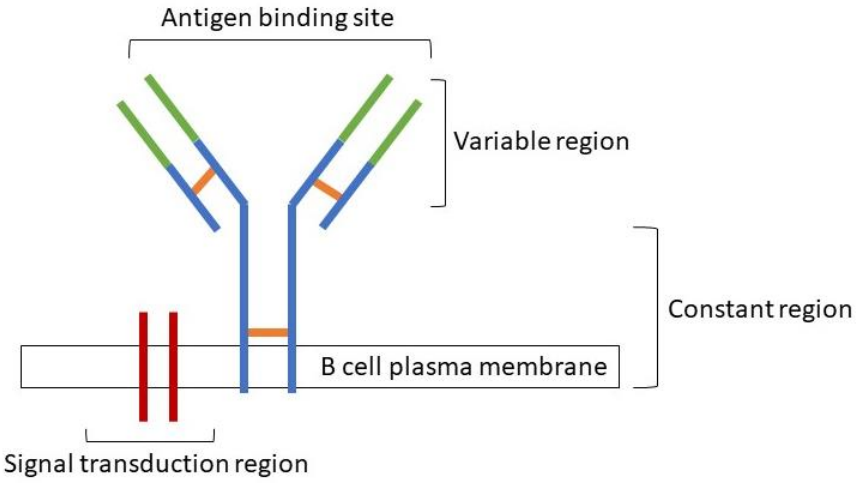

Figure 8. Structure of B cell receptor.
The BCR is comprised of a variable region which contains the antigen binding site and the constant region which determines the isotype of the receptor. The signal transduction region is connected to the membrane bound immunoglobulin via a disulphide bridge. Adapted from Chaplin (155).

The humoral immune response is primarily activated by T-cell dependent and independent mechanisms. BCR co-stimulation is essential alongside for clonal expansion to occur. This results in the production of identical daughter cells, termed plasmablasts, from the activated parent cell that can act as either effector or memory cells during the humoral immune response.

Plasmablasts differentiate following clonal expansion and act as either short-lived plasmablasts, long-lived plasma cells or memory cells. Together these mediate short- and long-term protection against encountered antigens. Individually, short-lived plasmablasts secrete antibodies that bind and neutralise pathogens, such as free virus particles. Long-lived plasma cells have undergone affinity maturation and

secrete antibodies with a greater affinity for their target antigen. Memory cells circulate throughout the body and initiate a stronger, and quicker response upon re-exposure to an antigen.

Antibodies secreted from plasma cells mediate the humoral immune response by binding their pathogen target preventing it binding to cells and causing further infection. Antigen-antibody complexes can then removed by macrophages or NK cells. Antibodies also help eradicate infection through opsonisation of pathogens, enhancing phagocytosis, activation of the complement cascade and triggering antibody dependent cell-mediated cytotoxicity (ADCC) (118).

B cells are crucial for the resolution of IAV infection in mice. B-cell KO leads to impaired viral clearance and increased mortality compared to WT mice (156, 157). B-cells are crucial for generating a neutralising antibody, which is essential as part of the hosts response to infection. Its neutralisation of progeny virus mean B-cells are as important as $CD8^+$ T-cells for the clearance of antigens and recovery of the host against IAV infection (158). This is supported by B cells importance during IAV rechallenge. Increased mortality is observed in B-cell KO mice upon rechallenge due to no neutralising antibody being in circulation. However, after vaccination increased resistance occurs following rechallenge in B-cell KO mice. This is due to the presence of a memory T-cell response which promotes recovery, indicating virus can be cleared without the humoral immune response. Though this clearance does not occur in the absence of both B cells and $CD8^+$ T cells (159). Together this data demonstrates the crucial role of humoral immunity against IAV and is reinforced by the longer lasting nature of the humoral memory response compared to T-cell memory response (156-158).

The host's immune response is primarily regulated by antigen availability. Upon clearance of an antigen a lack of signal arises and consequently immune response decreases. This leads to most effector cells involved in the immune response no longer being required. They undergo apoptosis to prevent unnecessary inflammation and tissue damage now the infection is resolved (160).

1.3 Short Palate Lung and Nasal Epithelial Clone 1 (SPLUNC1)

1.3.1 Expression and Distribution

SPLUNC1 was first identified in the lower respiratory tract, specifically the trachea and upper bronchi, and in the nasal and oral cavities in mouse embryos (161). Soon after, its expression was also identified in humans in the trachea and upper airways, nasopharyngeal epithelium and salivary glands (162). As well as humans and mice, SPLUNC1 is expressed and conserved in rats, chimpanzees, rhesus monkeys, dogs, and cattle (163, 164). Orthologs of SPLUNC1 have been identified in pigs, chinchillas, ferrets, bats, whales, gorillas, cats, pandas, rabbits, goats, sheep and numerous other species (165-168).

The human Short Palate Lung and Nasal Epithelial Clone 1 (*splunc1*) gene has 9 exons and is located on chromosome 20q11.2 (162). The translated SPLUNC1 protein is a 25 kDa monomer composed from a six-stranded antiparallel β-sheet flanked by six α-helices (169). However, multiple isoforms of SPLUNC1 have been identified in human nasal lavage samples, indicating SPLUNC1 undergoes N-linked glycosylation as well as other post-translational modifications (170). It is between the β-sheet and α-helices that the greatest structural variabilities between human and mouse SPLUNC1 occur. Although the human protein is 72% identical to the murine protein (Figure 9) (162),

exon 2 in the murine gene has an additional amino acid region present that is deleted in the human protein. This region is visible as the additional region at the N-terminus of Figure 9-C, compared to Figure 9-B. (171). These variabilities mean that SPLUNC1 may function differently in mice compared to humans (172).

```
Human     1 MFQTGGLIVFYGLLAQTMAQFGGLPVPL-----------------------DQTLPLNV 36
            MF  G L+V  GLLA + AQ  GLP+PL                        Q LPL V
Mouse     1 MFLVGSLVVLCGLLAHSTAQLAGLPLPLGQGPPLPLNQGPPLPLNQGQLLPLAQGLPLAV 60

Human 37 NPALPLSPTGL-AGSLTNALSNGLLSGGLLGILENLPLLDILKPGGGTSGGLLGGLLGKV 95
         +PALP +PT L AG  T+ALS GLLSGGLLGILEN+PLLD++K GGG S GL+GGLLGK+
Mouse 61 SPALPSNPTDLLAGKFTDALSGGLLSGGLLGILENIPLLDVIKSGGGNSNGLVGGLLGKL 120

Human  96 TSVIPGLNNIIDIKVTDPQLLELGLVQSPDGHRLYVTIPLGIKLQVNTPLVGASLLRLAV 155
          TS +P LNNI+DIK+TDPQLLELGLVQSPDGHRLYVTIPLG+ L VN P+VG SLL+LAV
Mouse 121 TSSVPLLNNILDIKITDPQLLELGLVQSPDGHRLYVTIPLGLTLNVNMPVVG-SLLQLAV 179

Human 156  KLDITAEILAVRDKQERIHLVLGDCTHSPGSLQISLLDGLGPLPIQGLLDSLTGILNKVL 215
           KL+ITAE+LAV+D Q RIHLVLGDCTHSPGSL+ISLL+G+   P+Q  LD+LTGIL KVL
Mouse 180  KLNITAEVLAVKDNQGRIHLVLGDCTHSPGSLKISLLNGVT--PVQSFLDNLTGILTKVL 237

Human 216 PELVQGNVCPLVNEVLRGLDITLVHDIVNMLIHGLQFVIKV 256
          PEL+QG VCPLVN +L GLD+TLVH+I  +LIHGLQFVIKV
Mouse 238 PELIQGKVCPLVNGILSGLDVTLVHNIAELLIHGLQFVIKV 278
```

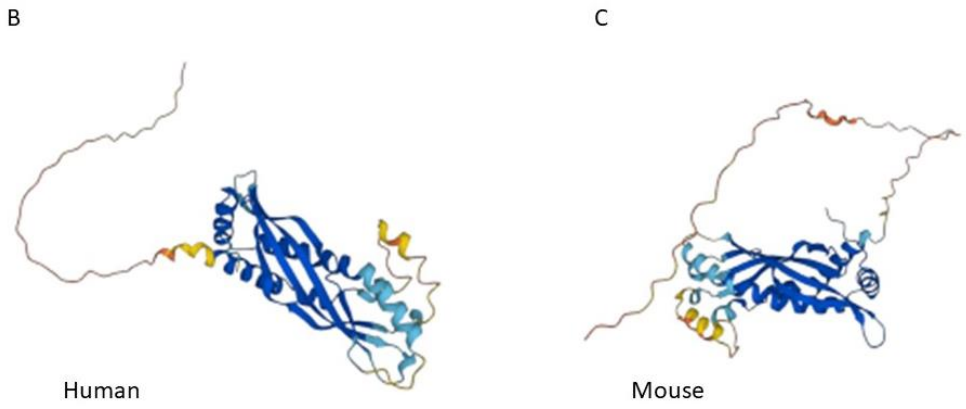

Figure 9. Alignment of Human and Mouse SPLUNC1 amino acid sequence
(A) Human SPLUNC1 (NP_001230122.1) and Mouse SPLUNC1 (NP_035256.2) sequences are aligned in top and bottom rows, respectively. The middle row details the amino acids conserved between species. The S18 sequence utilised in this thesis is highlighted in yellow. (B) shows the protein structure of human SPLUNC1 and (C) the protein structure of murine SPLUNC1. (B) and (C) were produced using Alpha Fold (273).

In addition to the respiratory tract and nasal and oral cavities, SPLUNC1 is also

expressed in humans in saliva and the lining fluids of the airways and nasal regions (173-177). In the respiratory tract SPLUNC1 expression changes throughout with expression greatest in the trachea, decreasing throughout until the bronchi. Expression stops in the bronchioles and is absent in the peripheral lung (175, 178, 179).

In the respiratory tract SPLUNC1 is expressed in the upper respiratory epithelium by ciliated cells and in submucosal ducts and glands by columnar, squamous, ciliated, and serous cells (175, 177, 178, 180, 181). It is also expressed in mucosal glands in the nasal cavity, parotid and submandibular glands, saliva, nasopharyngeal secretions and tears (175, 177, 178). As well as its expression in stomach mucosa and epithelium, glands in eyelid tissue and in mice in non-ciliated cells in the respiratory epithelium, ducts and luminal of larynx, and weakly in larynx gland serous and mucus cells (182).

However, SPLUNC1 expression does vary between models. In mice strains, expression in the BAL of 6 week old mice is two-fold higher in BALB/c mice compared to C57BL/6 mice (183). Interestingly, differential expression has also been observed depending on sex. Expression of SPLUNC1 in female mice was significantly lower than that in male mice (184). In cell culture SPLUNC1 expression is dependent on the differentiation status of cells, and is greater when human nasal epithelial cells have differentiated (180, 185). In addition, SPLUNC1 expression also varies with age. SPLUNC1 expression is primarily postnatal not pre-natal and is typically detected in the trachea or bronchi a few days after birth (171). This is supported with the observation that SPLUNC1 expression is greater in the saliva of full term, compared to premature, babies at birth (186). SPLUNC1 expression and intensity decreases with

age in both humans and mice (183, 184).

SPLUNC1 is also known as bactericidal/permeability-increasing fold-containing family A 1 (BPIFA1) because its N-terminal domain is similar to bactericidal/permeability-increasing (BPI). This similarity meant that SPLUNC1 was hypothesised to have innate antimicrobial activity like BPI does (169, 187, 188).

1.3.2 Biological functions

1.3.2.1 Anti-bacterial

The SPLUNC1 analogue, BPI, has innate antimicrobial activity; meaning that SPLUNC1 was suspected of also having innate antimicrobial activity upon its discovery (188). Subsequently, SPLUNC1 has been observed to have anti-bacterial activity against many bacteria. It inhibits the growth of *Pseudomonas aeruginosa* colonies through bacteriostatic properties, forming small pores in bacteria wall which increase their permeability and restrict growth (189, 190). SPLUNC1 also inhibits the formation of biofilms in *in vitro* models of *Pseudomonas aeruginosa* infection (191). The antibacterial activity of SPLUNC1 is supported as its overexpression is essential for survival during *Pseudomonas aeruginosa* infection and its knockout in mice leads to increased biofilm formation, inflammation and changes to the epithelial secretions including decreased expression of MUC5A, MUC5B and Clara cell secretory protein (CCSP) (192, 193).

Klebsiella pneumoniae is another gram-negative bacterium, like *P. aeruginosa*, whose infection is affected by SPLUNC1. During *K. pneumoniae* infection, SPLUNC1 was found to inhibit biofilm formation, alongside decreasing susceptibility and severity of infection (194). The importance of SPLUNC1's antibacterial activity is further suggested as SPLUNC1 expression increases throughout *K. pneumoniae* infection, peaking 24 hours later (194). SPLUNC1 also has bacteriostatic and antibiofilm activity against *Burkholderia Cepacia Complex,* another gram-negative bacterium (195). Furthermore, SPLUNC1 expression is modulated, but significantly reduced, in the

bronchioalveolar lavage (BAL) of mice with pneumonia induced by the bacteria S*treptococcus* and *P. aeruginosa* (179).

SPLUNC1 also has antibacterial effects against *Mycoplasma pneumonia*, an atypical bacterium which is neither gram positive nor negative. SPLUNC1 reduces its growth in both mice and humans by decreasing *M. pneumonia* adhesion and promoting bacterial clearance (196). During infection in mice increased SPLUNC1 expression was observed 4 hours post-infection, triggered by TLR2 stimulation and the NK-κβ signalling pathway (197, 198).

SPLUNC1 binds lipopolysaccharides found in the outer membrane of gram-negative bacteria. This interaction contributes to its surfactant, bacteriostatic and antimicrobial activity against gram-negative bacterium (170, 176, 189, 199). However, SPLUNC1 anti-biofilm activity is not due to its surfactant activity but its α4 helix, as its deletion removes anti-biofilm activity (199, 200). SPLUNC1 antibacterial activity is supported by its overexpression in transgenic mice resulting in enhanced bacterial clearance and death of many bacteria (192, 201). SPLUNC1 overexpression also decreased neutrophil infiltration and proinflammatory cytokine expression, SPLUNC1 KO reversed these (192, 202). Furthermore, SPLUNC1 KO mice have infections with an increased severity (202).

1.3.2.2 Immunomodulation and Regulation

SPLUNC1 assists the immune system clearing pathogens via multiple mechanisms. It can act as a chemoattractant and recruit neutrophils and macrophages to remove pathogens (190, 201, 203). During acute inflammation it can control neutrophil recruitment through IFN-γ and IFN-λ regulation of CXCL10 production (203).

Additionally, in these neutrophils SPLUNC1 is present in their granules, there its expression is linked to neutrophil activation, degranulation and stimulating neutrophil elastase activity (196, 204). Despite this however, neutrophil elastase is capable of degrading recombinant SPLUNC1 protein. Prevention of this degranulation helps to decrease the bacterial load observed during murine infections (205, 206).

SPLUNC1 anti-inflammatory activity is also observed in mice where it can inhibit eosinophilic inflammation (207). Furthermore, SPLUNC1 expression is reduced in patients with oral lichen planus, chronic inflammation of oral mucus membranes, compared to controls (208). However, inflammation and initiation of the adaptive immune response in turn can also inhibit SPLUNC1 expression (183). Inflammation is also known to be greater in those with type 2 diabetes mellitus (DM) and expression of SPLUNC1 is also lower in type 2 DM patients compared to non-DM sufferers (209). Additionally, SPLUNC1 is associated with pro-Th1 and anti-Th2 activity. Th2 cytokines, such as IL-13, decrease SPLUNC1 expression and bacterial clearance. This may underlie the occurrence of persistent bacterial infections in allergic airways or simply reflect where SPLUNC1 is expressed and is not directly involved in host responses to pathogens (210, 211).

SPLUNC1 expression is regulated via a multitude of mechanisms and modulates during infection. SPLUNC1 is dose dependently down regulated by IL-13 in cell culture (185). IL-13 also inhibits the SPLUNC1 expression induced by LPS and in those with eosinophilic chronic rhinosinusitis with nasal polyps and bacterial infection (212). In alveolar macrophages SPLUNC1 is down regulated by chloride channel accessory 1 (CLCA1) (213). In lung epithelial cells expression is regulated by NOGO-B and induced following TLR2 activation (212, 214, 215). Finally, its expression is also regulated by

genotype. The SPLUNC1 rs750064 CC genotype results in significantly less mRNA expressed in epithelial cells from asthmatic and non-asthmatic patients, compared to the CT and TT genotypes. The CC genotype had a 33% incidence rate, an impact on baseline lung function in asthmatic patients and correlates with greater eosinophilic inflammation (216).

1.3.2.3 Anti-viral effects

Antiviral activity by SPLUNC1 has been observed against Epstein-Barr virus (EBV) in multiple models. SPLUNC1 addition to EBV transformed B-cell cell lines results in apoptosis and decreased EBV replication (189, 217). SPLUNC1 also inhibited the infection of human peripheral lymphocytes with EBV (217). SPLUNC1 can also reduce inflammation associated with EBV infection. The infection of nasopharyngeal carcinoma (NPC) cells with EBV induces the release of inflammatory cytokines however SPLUNC1 expression reverses this EBV induced inflammation (218).

SPLUNC1's antiviral activity however is not limited to EBV as SPLUNC1 KO mice support higher levels of human rhinovirus replication, compared to WT mice (219). Interestingly, SPLUNC1 expression is modulated in multiple viral infection including IAV, murine γ-herpesvirus 68 (MHV-68) and EBV. Specifically, MHV-68 infection modulates SPLUNC1 expression in the trachea, bronchi, and bronchioles. At seven d.p.i. there was a significant decrease in the expression area and intensity in the bronchioles. However, at 14 d.p.i. SPLUNC1 expression had been reversed and was greater in infected compared to non-infected mice in the trachea, bronchi, and bronchioles. The expression levels observed at 14 d.p.i. correlated with club cells differentiation into mucus secreting cells (220). This suggests SPLUNC1 could have

antiviral activity against multiple viruses and is involved in host mediated viral clearance. However SPLUNC1 expression did not change in human immunodeficiency virus (HIV) infection (221) suggesting this antiviral activity is not universal.

1.3.2.3.1 Antiviral activity of SPLUNC1 against IAV

In collaboration with Prof Colin Bingle at the University of Sheffield, our lab further investigated the possibility of SPLUNC1 having an antiviral role against IAV. During the infection of female CD57/B6L wildtype mice with IAV, SPLUNC1 expression significantly changes. It was significantly lower at 5 and 7 d.p.i. but by 14 d.p.i. expression had recovered to pre-infection levels (Figure 10). The decrease in expression observed at 7 d.p.i. primarily occurred in the trachea and bronchi. In the bronchioles the only expression change observed during infection was the significant increase in staining area and intensity at 14 d.p.i. (222). These findings are supported as a significant decrease in SPLUNC1 expression has been previously observed during IAV. However, this only occurs after an initial significant upregulation a few hours after infection (183, 223).

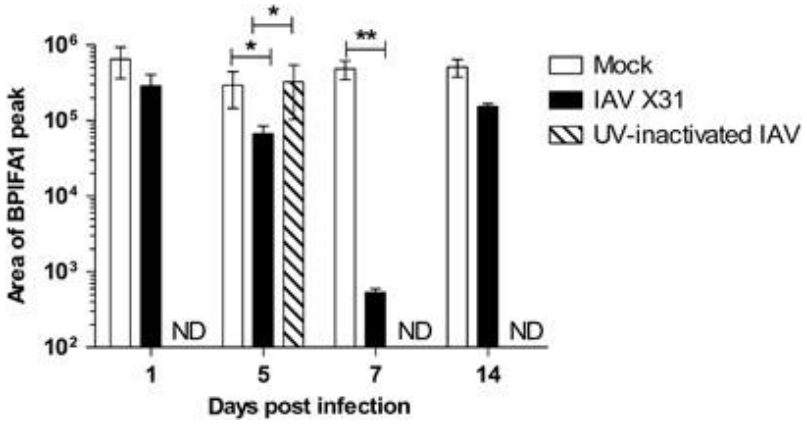

Figure 10. SPLUNC1 expression decreased throughout IAV infection in mice.
Mice (n=4 per group) were intranasally infected with 10^3 pfu IAV X-31. Protein levels were determined from bronchoalveolar lavage samples. Statistics used were one-way analysis of variance (ANOVA) with Tukey post-hoc test. Reproduced with permission from (222).

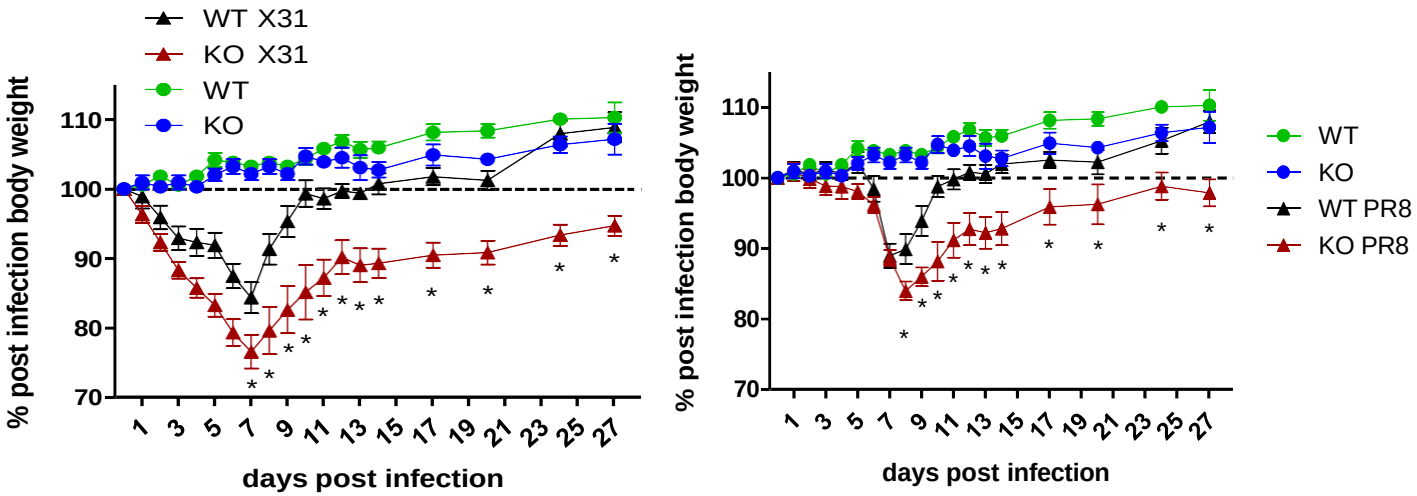

Figure 11. SPLUNC1 KO mice lose significantly more weight during IAV compared to WT mice.
Wildtype and SPLUNC1 KO mice (n=6 per group) were intranasally infected with 10^3 pfu IAV X-31. Mice were weighed daily and represented as a percentage of the starting weight. Data represents the mean value ±s.e.m. and asterisks indicate statistical difference (two-way analysis of variance (ANOVA) with Bonferroni post-hoc test. Unpublished data from Stewart Group, reproduced with permission.

During IAV infections, SPLUNC1 KO mice lost significantly more weight throughout IAV infection with PR8 and X31 strains compared to wild type mice (Figure 11); furthermore, SPLUNC1 KO recorded significantly higher IAV virus titres at 1, 3, 5 and 7 d.p.i. (Figure 12). Therefore, the absence of SPLUNC1 enabled IAV to be more pathogenic and lethal throughout infection (Figure 13) (222).

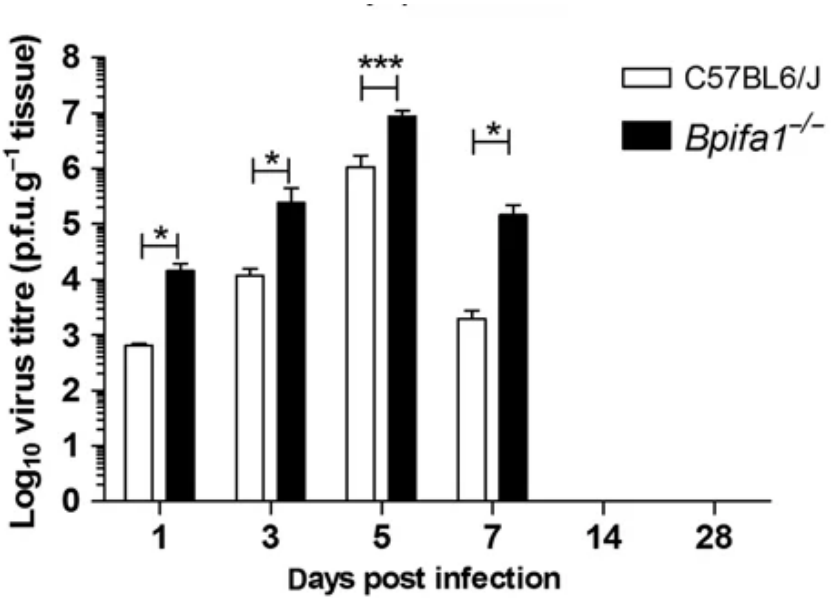

Figure 12. Virus titres in lung tissues after infection with IAV X-31.
C57BL6/J and SPLUNC1 KO mice were infected with 10^3 p.f.u. IAV X-31 intranasally. Lung tissue samples were taken at multiple timepoint post infection. Virus titres were determined by plaque assay. Statistics used were two-way ANOVA with Bonferroni post test, *P<0.05, ***P<0.001. Reproduced with permission from (222).

Additionally, IAV infection spread and reached the distal bronchioles and alveoli earlier in SPLUNC1 KO mice compared to WT mice, at one day post infection (Figure 14) (222). This supports the conclusion that SPLUNC1 absence encourages IAV infection. SPLUNC1 also limited the infection of epithelial cells. Mouse tracheal epithelial cells (mTEC) derived from WT and SPLUNC1 KO mice were grown at air-liquid interface (ALI) in culture then infected with IAV. The SPLUNC1 KO mice derived mTEC ALI cultures had an increased number of infected cells with IAV RNP complexes

compared with those from WT mice, a 2-fold higher intracellular IAV NP load and a higher IAV titre in apical wash fluid. The shows that SPLUNC1 limits IAV infection by preventing the infection of epithelial cells. Furthermore, in WT mTEC ALI cultures IAV bound predominantly to SPLUNC1-negative cells; demonstrating SPLUNC1 can decrease IAV binding and consequently the infection of cells (222).

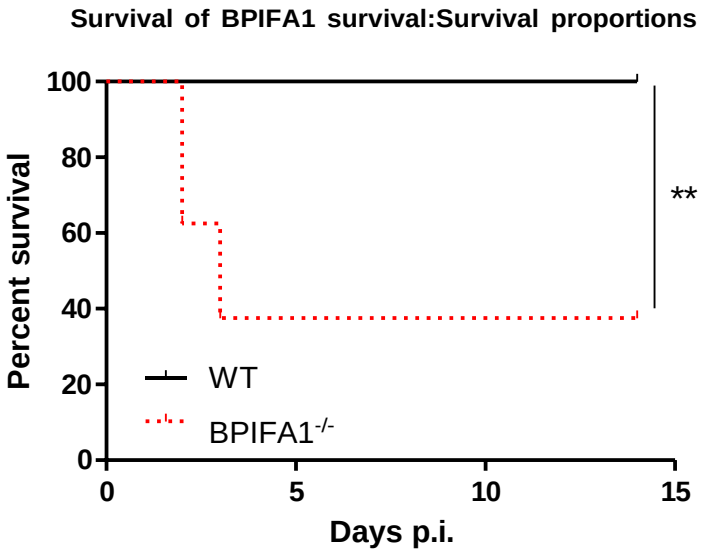

Figure 13. SPLUNC1 KO mice have decreased survival compared to WT mice following IAV infection.
Wildtype C57BL6/J and SPLUNC1 KO mice were infected with 10^3 p.f.u. IAV X-31 intranasally. Survival was determined by 20% weight loss from starting weight or high severity health score. Unpublished data from Stewart lab, reproduced with permission.

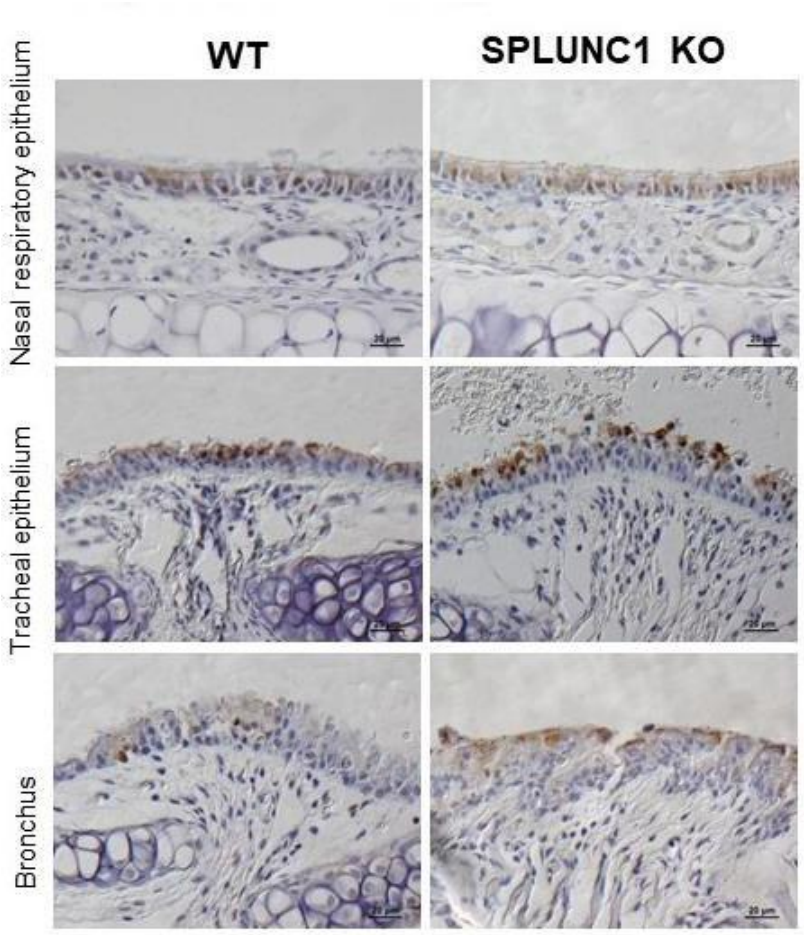

Figure 14. IAV spreads quicker in the absence of SPLUNC1.
WT (C57BL/6J) and SPLUNC1$^{-/-}$ mice were intranasally infected with 10^3 pfu. IAV X-31. Lung tissue was collected at 1-day post infection and IAV antigen detected by immunohistology using goat anti-IAV. Reproduced with permission from (222).

1.3.3 Involvement in disease

1.3.3.1 Cystic Fibrosis and other pulmonary diseases

SPLUNC1 can regulate the epithelial sodium channel (ENaC) by binding extracellularly to its subunits ENaC α, β and γ. ENaC is particularly important in cystic fibrosis (CF) patients as its activity increases in the absence of Cystic Fibrosis Transmembrane conductance Regulator (CFTR), which causes Airway Surface Liquid (ASL) dehydration and reduced mucociliary clearance. SPLUNC1 binding to ENaC causes ENaC internalisation, changing the of ENaC density in the plasma membrane (224). In turn

this reduces Na^+ and ASL absorption, by reducing ENaC cleavage and activation. It is through this interaction that ASL volume is controlled (225, 226).

SPLUNC1 expression varies in cystic fibrosis patients compared to those who do not suffer the disease. SPLUNC1 expression is increased in the bronchiolar epithelium and in inflammatory mucus plugs. The increased expression observed is in respiratory epithelial not inflammatory cells (227). Due to SPLUNC1's antimicrobial and anti-inflammatory activity its increased expression could be advantageous to CF patients. However, SPLUNC1 expression is not always greater in CF patients and some studies have identified a significantly reduction in protein levels in the sputum of CF patients. Neutrophil elastase present in CF sputum can degrade SPLUNC1. This correlates with the decreased expression of SPLUNC1 and increased expression of ENaC subunits in the bronchi of some CF. Therefore, this decreased SPLUNC1 expression is encouraging increased ENaC activity and ASL dehydration (225).

Human SPLUNC1 has an 18 amino acid region at the beginning of the N terminus, which is not present in its tertiary protein structure, named S18 (169, 228-230). S18 itself does not possess any antimicrobial or anti-biofilm activity associated with SPLUNC1 (231). However, it can inhibit the ENaC channel therefore increasing ASL height and reverse the ASL dehydration seen in CF patients. It achieves this by binding to the ENaC β subunit and inhibiting absorption but not secretion (230, 231). However, S18 is degraded by proteases in CF sputum. Therefore, an optimised version of S18, SPX- 101, was created. SPX-101 increases ASL height, regulates ENaC surface density and mucus transport. Furthermore, SPX-101 increased the weight, a known indicator of overall mouse health, and survival of β-ENaC transgenic mice. Furthermore, it is not degraded by CF sputum (229, 232). The human S18 sequence

is partially conserved in mice but is interrupted in murine SPLUNC1 with an extra region contained in exon 2 (Figure 9-A). S18 is present at the N-terminus of SPLUNC1 and is free of tertiary protein structure in humans and mice (Figure 9-B & C). SPLUNC1 can also regulate ASL volume by changing the of ENaC density in the plasma membrane (224). In addition, SPLUNC1 ENaC activity is pH dependent. This is due to two salt bridges present in SPLUNC1 protein. Acidic ASL cause SPLUNC1 to become inactive. CF ASL is acidic, this renders SPLUNC1 inactive and ENaC and ASL regulation does not occur in CF airways (233). This is supported by the increased ENaC and cleaved ENaC protein identified in CF bronchi (225). SPLUNC1 antibacterial activity is also pH sensitive. SPLUNC1 inactivity in acidic CF airways therefore could also contribute to the increased bacteria growth observed in CF patients (234).

In addition to CF, SPLUNC1 has also been linked with an involvement in other pulmonary diseases. In both Chronic Obstructive Pulmonary Disease (COPD) and pulmonary fibrosis SPLUNC1 expression differs with disease severity. SPLUNC1 expression is significantly greater in severe COPD sufferers compared to mild and non-sufferers, and in progressive vs stable idiopathic pulmonary fibrosis (235, 236). In COPD, expression inversely correlated to lung function and positively correlated with goblet cell hyperplasia (235). The modulation of expression during the progression of pulmonary disease could suggest SPLUNC1 involvement in this process.

1.3.3.2 Airway Irritants and Allergy

Recently, SPLUNC1 has been identified as an epithelial derived smooth muscle relaxing factor that can regulate airway contraction. SPLUNC1 expression is reduced

in asthmatic patients, this correlates with airway smooth muscle contraction (ASMC), this effect was mimicked in SPLUNC1 knockout mice (237, 238). This occurs because SPLUNC1 α6 helix inhibits Ca^{2+} entry during ASMC, this decreases myosin light chain phosphorylation and consequently ASMC (237).

SPLUNC1 expression and activity also differs in smokers. Expression in nasal lavage fluid and airway epithelium is reduced in smokers (239, 240). Exposure to cigars and cigarettes inhibits SPLUNC1 antimicrobial activity as well as its ability to bind human bronchiolar epithelial cells and regulate ASL height (241, 242). Additionally, expression of a particular SPLUNC1 isoform, molecular weight of 28.1 kDa, was notably increased proportionally in smokers, indicating possible inflammatory activity (243).

SPLUNC1 expression is reduced in numerous other situations including: airway symptoms relating to metalwork exposure at work (244), seasonal allergic rhinitis during the pollen season (239, 245) and in chronic rhinosinusitis sufferers with nasal polyps (CRSwNP) (181, 211, 239, 244, 245). Decreased expression in those with CRSwNP is due to decreased glands in those with nasal polyps (181). Interestingly SPLUNC1 expression was further decreased in CRSwNP patients with eosinophil presence, indicating inflammation at their site (211).

1.3.3.3 Cancer

SPLUNC1 involvement has been implicated and connected in numerous types of cancer. Its expression is significantly greater in those with lung cancer compared to benign lung diseases (246). In addition, it has been identified as a potential biomarker for the diagnosis and grading of numerous cancers, including the lung, colon, salivary

glands and stomach (184, 247-249). SPLUNC1 has already been identified as a marker for non-small cell lung cancer (NSCLC) diagnosis and staging (250). Its expression is enhanced in 81% NSCLC tumour tissue and 25% of lung cancer biopsies overall (251, 252). SPLUNC1 was the most upregulated gene in NSCLC patient peripheral blood samples with expression also upregulated in pleural fluid and saliva micro-vesicles (250, 253, 254). Furthermore, SPLUNC1 presence in lymph nodes in non-small cell lung cancer (NSCLC) indicated micro-metastasis (255). However this had no relationship with patient progression in early stage NSCLC (256).

SPLUNC1 is also known to contribute to the growth and development of nasopharyngeal carcinoma (NPC). SPLUNC1 expression is upregulated in the initial growth stages but is downregulated and lost during NPC progression and the later, aggressive stages of tumour growth (217, 257, 258). Its initial upregulation suggests SPLUNC1 contributes to the initial resistance of NPC growth. However, its later downregulation demonstrates the resistance developed to this mechanism as NPC growth progresses (252, 259).

SPLUNC1 is likely involved in a gene network associated with NPC carcinogenesis. SPLUNC1 transcription can be stimulated by All Trans Retinoic Acid (ATRA) but itself can decrease known oncogenes expression. ATRA inhibits the growth of NPC cells (258). This is partly achieved through increased SPLUNC1 expression as SPLUNC1 decreases oncogene expression and inhibits the oncogenicity of EBV in the respiratory epithelium (189). Therefore, increased SPLUNC1 expression during initial NPC development tries to inhibit the growth of NPC cells (189, 258).

1.4 Aims

SPLUNC1 is a host protein with known antiviral activity against IAV, a pathogen that causes significant illness and places a substantial burden on society. However, little is known about SPLUNC1 antiviral role in the immune response and the mechanism of action for this antiviral activity has not yet been elucidated. Therefore, the overall aim of this project was to elucidate whether SPLUNC1 antiviral activity was due to a direct interaction with IAV, further explore SPLUNC1 effect on IAV infection and produce SPLUNC1 KO cell line using CRISPR-Cas9 technology to aid these studies. Finally, SPLUNC1 S18 region will also be investigated to identify if it is responsible for SPLUNC1 antiviral activity and if it could act as an adjuvant and enhance protection against IAV infection.

2 Methods

2.1 Mammalian Culture techniques

2.1.1 Cell passaging and maintenance

Cells were cultured in 25, 75 or 175 cm^2 vented tissue culture flasks (Corning) at 37°C in humidified incubators with 5% CO_2. Cells were routinely passaged at 90% confluence. Media was removed, cells washed twice in D-PBS-0.01% EDTA (v/v) and trypsin-EDTA (0.25%) (Thermo Fisher) added. Cells were incubated for 5 min to break up the cell monolayer then collected in media and cells pelleted at 1,500 x *g* for 5 min. Cells were resuspended in fresh media and spilt 1:10 into a fresh flask. Cells were routinely tested for mycoplasma every two months. The cell lines used are identified below in 2.1.2 and Table 1.

2.1.2 Cell lines

Table 1 – Details of cell lines used and their culture medium.

Cell line	ATCC Code	Media
HEK 293T	CRL-3216	Dulbecco's Modified Eagle's Medium (DMEM) high glucose (Sigma) supplemented with 10% (v/v) fetal bovine serum (FBS) (Gibco), 2mM L-glutamine (Sigma), 100 U/ml penicillin (Sigma) and 100 µg/ml streptomycin (Sigma).
A549	CCL-185	DMEM with 10% FBS (Gibco), 2mM L-glutamine (Sigma), 100 U/ml penicillin (Sigma) and 100 µg/ml streptomycin (Sigma).
MDCK	CCL-34	DMEM with 10% FBS (Gibco), 2mM L-glutamine (Sigma), 100 U/ml penicillin (Sigma) and 100 µg/ml streptomycin (Sigma).
MDCK-SIAT1	Provided by Prof.	DMEM with 10% FBS (Gibco), 2mM L-glutamine (Sigma), 100 U/ml penicillin (Sigma),100 µg/ml

	Paul Digard	streptomycin (Sigma) and 50µg/ml geneticin (G418) (Sigma).
BHK-21	CCL-10	DMEM with 10% FBS (Gibco), 2mM L-glutamine (Sigma), 10 U/ml penicillin (Sigma) and 100 µg/ml streptomycin (Sigma).
Jurkat	TIB-152	Roswell Park Memorial Institute (RPMI) 1640 Medium (Sigma) supplemented with 10% (v/v) FBS (Gibco), 2mM L-glutamine (Sigma), 100 U/ml penicillin (Sigma) and 100 µg/ml streptomycin (Sigma).
HBEC3-KT	CRL-4051	Keratinocyte Serum Free Media (KSFM) (Thermo Fisher) supplemented with 5 ng/ml recombinant Epidermal Growth Factor (rEGF), 50 µg/ml Bovine Pituitary Extract (BPE) and 50 µg/ml gentamicin (Sigma). Or PneumaCult Ex Plus basal media (Stem Cell) supplemented with 50X PneumaCult Ex Plus supplement, 96 ng/ml hydrocortisone (Stem Cell) and 50 µg/ml gentamicin (Sigma). Or PneumaCult-ALI basal medium (Stem Cell) supplemented with PneumaCult-ALI 10X supplement, 480 ng/ml hydrocortisone (Stem Cell), 4 µg/ml heparin (Stem Cell) and 50 µg/ml gentamicin (Sigma).

2.1.3 Thawing

Vials of frozen cells were warmed to 37^{o}C in a water bath. Media was added slowly, dropwise to the thawed cells to dilute the DMSO (Sigma). One drop of media was added every 10 s for the first ml, 2 drops for the second ml. This continued till the total volume was 7 ml. Cells were pelleted at 1500 x *g* for 5 min then the pellet re-suspended in fresh media and placed in a T25 flask (Corning).

2.1.4 Freezing

Cells were pelleted at 1500 x *g* for 5 min. The pellet was re-suspended in half the desired final volume pre-chilled freezing media 1 (40% FBS and 60% complete media). Then pre-chilled freezing media 2 (20% DMSO, 50% complete media and 30% FBS) was added dropwise to the cells. Cells were then placed in a MrFrosty Freezing Container (Thermo Fisher) overnight at -80^{o}C and transferred to liquid nitrogen the following day. Note, HBEC3-KT cells were frozen without FBS present.

2.1.5 Transfection of cell lines

Transfections were performed with HEK 293T cells in a variety of plates and flasks (Corning). HEK 293T cells were plated at 6x10^{4} cells/cm^{2} 24 h prior to transfection to achieve 70% confluence at the point of transfection. Cells were then transfected with either calcium phosphate or TransIT-LT1 (MirusBio).

2.1.5.1 Calcium Phosphate

For 6 well plates, 15 µl 2.5M $CaCl_2$ and 1 µg plasmid was made to a total volume of 75 µl with ddH_2O. This was added dropwise using a Pasteur pipette (StarLab) to an equal volume of 2x HEPES solution (Sigma), which was slowly having air bubbled through. This solution was incubated at room temperature (RT) for 30 min, thereafter the mixture was added dropwise to confluent cells. Cells were then incubated for 24 h at 37^{o}C in a humidified CO_2 incubator then supernatant collected, and cells harvested, as required, for downstream processing.

2.1.5.2 TransIT-LT1

For 6 well plates, 2.5 µg plasmid was mixed with 250 µl OptiMEM (ThermoFisher) and 7.5 µl TransIT-LT1 (Mirus Bio). This mixture was incubated at RT for 30 min before being added to the media of each well dropwise. Twenty four hours later, supernatant was collected, and cells harvested or lysed, as required, for downstream processes.

2.1.6 Air Liquid Interface (ALI) cell culture

HBEC3-KT cells grown routinely in PneumaCult Ex Plus complete media were plated at $1x10^4$ cells/well onto 0.4 µM Thincert inserts (Greiner) in 12 well plates (Greiner) with both the well and insert containing PneumaCult Ex Plus complete media. When cells were confluent, the media was removed from the well and replaced with PneumaCult-ALI complete media; the insert media was removed entirely. During ALI culture, media was changed throughout every two days. Once cells were confluent, the apical insert was washed weekly with D-PBS to remove excess mucus. KT cells in PneumaCult-ALI complete media were grown at ALI for 3 weeks before use in downstream experiments. HBEC3-KT cells grown on ALI scaffolds will be referred to as HBEC3-ALI cells in this thesis.

2.1.7 Supernatant Concentration

Supernatants collected from transfections and cell debris were pelleted at 1500 x *g* for 5 min then the supernatant concentrated using Amicon Ultra Centrifugal filters (10k) (Merck) following manufacturer's instructions. When using 0.5 ml filters 20x

concentration was performed at 14,000 x *g* for 15 min and 15 ml filters 30x concentration at 4,000 x *g* for 20 min.

2.1.8 Viral strains

A variety of IAV strains were used during IAV infections and experiments during this study. Details of these strains, their subtype and isolation are detailed below in Table 2.

Table 2 - Details of the Influenza A Virus strains utilised in this thesis.

Strain	**Subtype**	**Origin**
A/Puerto Rico/8/34 (PR8)	H1N1	A/Puerto Rico/8/34, (260)
MCherry PR8	H1N1	A/Puerto Rico/8/34, (260)
GFP PR8	H1N1	A/Puerto Rico/8/34, (260)
A/X31	H3N2	Kilbourne, 1969. (261)
Eng195	H1N1	Human, A/England/195/2009

2.1.9 Virus growth and preparation

All PR8 strains and X31 were grown in the allantoic cavity of 9-day old embryonated chicken eggs (PDRC). Eggs were incubated in an egg incubator at 37^{o}C and viability assessed by candling eggs. Eggs were inoculated using an 18 G needle and syringe with 150 µl of IAV diluted at 1:1000 or 1:10000 in PBS. Eggs were then incubated for 48-72 hours at 35^{o}C for human strains and 37^{o}C for avian strains, the eggs viability was assessed again 24 h post inoculation and eggs containing dead embryos were

discarded. Upon completion of incubation the eggs were chilled overnight at 4°C to euthanise the embryos. The allanotoic fluid containing IAV was harvested separately from each egg then stored at -80°C prior to use.

H1N1 Eng195 IAV was grown in MDCK-SIAT1 cells. Virus was incubated with 50% confluent MDCK-SIAT1 cells, plated 24 h previously, for 30 min. After inoculation, media supplemented with 50 µg/ml TPCK Trypsin but without FBS and G418 was added to cells. Four days later, the supernatant containing virus was collected. Both were titred by plaque assay, detailed in 2.1.11.

2.1.10 Viral Infections

Twenty-four hours before the time of infection, cells were plated to achieve 75% confluence the following day. After 24 h media was removed and in cases where FBS was present cells were washed once with D-PBS. Media was then replaced with IAV diluted in the appropriate amount of serum free media supplemented with 1 µg/ml TPCK trypsin (Thermo Fisher), to cleave HA0 as not all cell lines produce this endogenously, then incubated for 1 h at 37°C with 5% CO_2. After 1 h, the virus mix was removed and replaced with fresh serum free media and incubated for up to 72 h. MDCK cells were most frequently used for IAV infection as their high susceptibility to various IAV strains and has established them as the standard cell line for *in vitro* culture.

2.1.11 Plaque assays

Plaque assays were performed on 100% confluent MDCK cell plated 24 h earlier at $1x10^6$ cells/well in a 12 well plate. Virus dilutions were performed in a 96 well plate containing 270 µl DMEM supplemented with 0.1% TPCK trypsin. Thirty µl sample was

added to the first well and 10-fold serial dilution performed until 10^{-7} dilution.

Supernatant samples from *in vitro* cell infections were prepared by debris being removed by pelleting at 1500 x *g* for 5 min.

Tissue samples were homogenised using a Tissue Lyser LT. Twenty-five mg tissue was added to a 1.5ml micro-centrifuge tube containing 1 stainless steel bead and 500 µl DMEM. The tissue samples were homogenised at 30 Hz for 2 min, and repeated up to three times if the tissue was not completely homogenised. Tissue debris was pelleted at 2000 x *g* for 5 min at 4°C and the supernatant used as the virus sample in plaque assays.

Media was removed from the confluent plate of MDCK's and the cells washed once with D-PBS. The virus dilution sample, 270 µl, was added to its corresponding well and incubated at 37°C with 5% CO_2 for one h. Then, the virus dilution was replaced with 1:1 mix of 2.4% Avicel and overlay media (20% 10X DMEM, 2% P/S and L-glutamine, and 3% HEPES and $NaHCO_3$). Cells were incubated for up to 72h then fixed with 4:3 Acetone:Methanol and stained with 0.04% crystal violet. Plaques were counted manually by eye and the viral titre calculated using the equation:

$$Virus\ titre\ (PFU/ml) = \frac{pfu}{ml} = \frac{Number\ of\ plaques}{volume\ x\ dilution}$$

Where volume is ml of virus dilution sample and the serial fold dilution of the well the plaques were counted from.

2.1.12 Hemagglutination Assays

A 96-well round bottom plate was filled with 50 µl D-PBS. Column one was filled with 50 µl sample, mixed and then serially diluted 1:1 across the plate. After mixing in column 11, 50 µl was discarded; column 12 was left as a negative control. Then 0.5% of washed chicken red blood cells (Generon) were added to each well at a 1:1 dilution.

The plate was mixed by gentle tapping, then incubated at room temperature for 1 hour. After this time, a button pinprick indicates a negative result and a halo or hazy well that hemagglutination has occurred and virus is present. Each sample was run in duplicate during each assay.

2.1.13 MTS assay

MTS assays were performed to determine the number of viable cells in cytotoxicity assays. Cells were plated in a 96 well flat-bottom plate 24 h prior to peptide addition, to achieve 70% confluence 24 h later. Each peptide was added at desired concentrations and incubated for 72 h. The MTS assay was performed with CellTitre 96 AQ_{ueous} One Solution Cell Proliferation Assay (Promega). Twenty µl CellTitre 96 AQ_{ueous} One Solution reagent was added to each well of the plate then incubated at 37^{o}C in a humidified, 5% CO_2 incubator for 3h. Absorbance was then measured at 490 nm with an Infinite F50 plate reader (Tecan).

2.1.14 Sorting and maintenance of HBEC3-KT CRISPR edited cells

2.1.14.1 Sorting via flow cytometry

HBEC3-KT cells transfected 48 h earlier with sgRNA-Cas9 GFP plasmids were sorted using BD FACSAria II in a level 2 biosafety cabinet. Cells were collected via trypsin and resuspended in flow buffer (1x D-PBS, 0.5% BSA and 2mM EDTA) prior to sorting. First, live cells were selected by side scatter (SSC) SSC-A and forward side scatter (FSC) FSC-A, then doublets were excluded using a FSC-H and FSC-A gate. Transfected cells were identified as GFP positive and sorted using high GFP FITC-A into complete KSFM

media. This was completed at Liverpool School of Tropical Medicine facilities with the assistance of Dr Jesús Reiné.

2.1.14.2 Maintenance

After GFP sorting, cells were subject to limiting dilution in a 96-well plate to produce one cell per well in complete KSFM media. Cells incubated in a 37°C in a humidified 5% CO_2 incubator until confluent and the media changed every 2 to 3 days. Cells were passaged into a 24 well plate and maintained with 1:5 passaging twice a week whilst undergoing genotyping. Cells were subsequently re-sorted, as necessary to achieve a 100% pure edited population, through serial dilution to one cell per well in a 96-well plate.

2.2 Cloning

2.2.1 PCR amplification

PCR amplification was utilised to insert 6x His tag and Kozak consensus sequence onto the desired DNA fragment for downstream cloning processes. The templates used for PCR amplification of human SPLUNC1 (NM_016583), human surfactant protein D (SpD) (BC022318), mouse Transforming Growth Factor β receptor I (TGFβRI) (NM_001312868), mouse Transforming Growth Factor β receptor II (TGFβRII) (NM_009371) and human TGFβRII (NM_001024847) were human DNA, plasmid, bovine serum cDNA and plasmid, mouse cDNA and plasmid (Addgene #11766) respectively. The sequences for the desired DNA fragments were identified from GenBank. Cystatin-SpD (Figure 15) and Cystatin-TGFβRII (Figure 16 bookmark59) sequences were synthesised by GeneArt Gene Synthesis (ThermoFisher). PCR

amplification was performed using either KOD polymerase (Merck) (Table 3 and Table 4) or Phusion (New England BioLabs) (Table 5 and Table 6). The conditions and reagents used are detailed below. Annealing temperatures used in PCR reactions varied and are detailed in 2.2.9. The primers utilised in these PCR reactions are detailed in Table 7. Geneious Prime software was used throughout to annotate sequences and primers, aid sequencing results analysis, and produce vector and sequence maps.

Table 3 – Reagents and volume required for 50 µl PCR reaction using KOD polymerase.

Component	**50 µl Reaction**
10x buffer #1 for KOD DNA Polymerase	5 µl
10 mM $MgCl_2$	5 µl
2 mM dNTPs	5 µl
Forward Primer	1 µM
Reverse Primer	1 µM
Template DNA	1 µg
KOD DNA Polymerase	0.4 µl
PCR grade Water	To 50 µl

Table 4 – PCR cycling conditions for PC reactions using KOD polymerase.

PCR reaction stage	Conditions	Number of cycles
Initial denaturing	95°C, 1 min	-
Denaturing	94°C, 30 s	35
Annealing	61-77°C, 30 s	
Elongation	72°C, 2 min	
Final elongation	72°C, 5 min	-
Hold	4°C, ∞	-

Table 5 - Reagents and volume required for 50 µl PCR reaction using Phusion.

Component	**20 µl Reaction**
5X Phusion HF buffer	4 µl
10mM dNTPs	0.4 µl
Forward Primer	1 µM
Reverse Primer	1 µM
Template DNA	1 µg
Phusion DNA Polymerase	0.2 µl
Nuclease-free water	To 20 µl

Table 6 - PCR cycling conditions for PC reactions using Phusion.

PCR reaction stage	Conditions	Number of cycles
Initial denaturing	98°C, 30 s	-
Denaturing	98°C, 10 s	35
Annealing	55-72°C, 30 s	
Elongation	72°C, 30 min	
Final elongation	72°C, 10 min	-
Hold	4 °C	

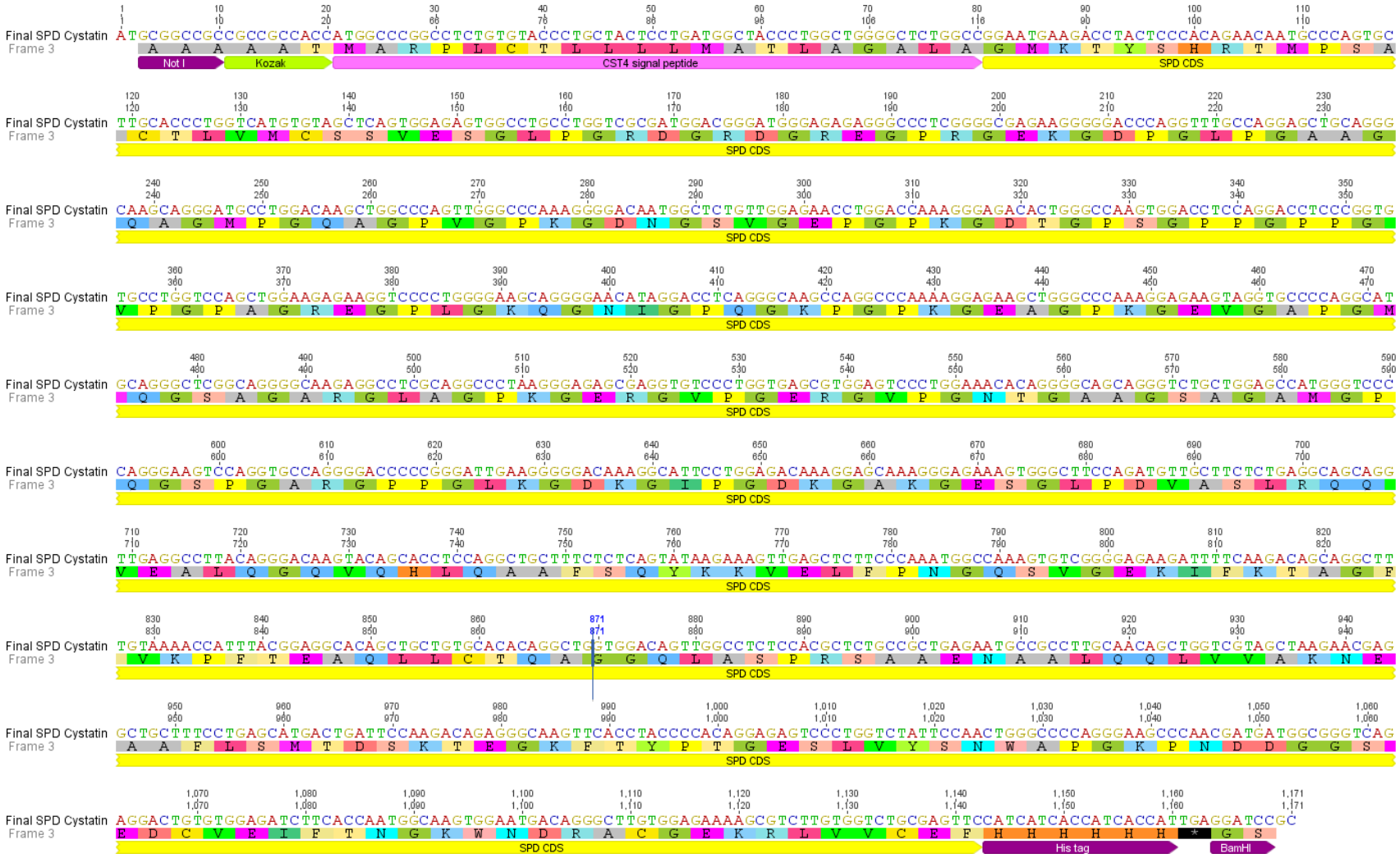

Figure 15. Diagram of Cystatin secretion signal-SpD sequence synthesised by GeneArt Gene Synthesis (Thermo Fisher).

Figure 16. Diagram of Cystatin secretion signal-TGFβRII sequence synthesised by GeneArt Gene Synthesis (Thermo Fisher).

2.2.2 Agarose gel electrophoresis

1% (w/v) agarose (Sigma) gel was prepared with 1x TAE buffer (40 mM Tris base, 20 mM Acetic acid, 1 mM EDTA) and SYBR safe (Invitrogen). Samples were diluted with 6x gel loading dye (NEB) then loaded onto the gel alongside GeneRuler 1kb or 100bp Plus DNA ladder (ThermoFisher). The gel was run for 45 min at 100V to separate products by weight then visualised using ChemiDoc imaging system (BioRad).

2.2.3 Gel purification

Following PCR amplification of inserts for cloning, PCR reactions were subject to gel electrophoresis and the desired band was excised and gel purified to extract the desired amplified fragment. The desired gel band was excised using a scalpel and gel purification performed using QIAquick Gel Extraction Kit (QIAgen) following the manufacturer's instructions.

2.2.4 PCR product purification

Where PCR products were purified directly from the reaction purification was used to remove nucleotides, primers and enzymes from the PCR reaction product. It was performed with QIAquick PCR purification kit (QIAgen) using the manufacturer's instructions.

2.2.5 Sticky-end restriction enzyme cloning

Restriction enzyme cloning was used to ligate the PCR amplified fragments and expression vector together, pVR1255 (Figure 17), producing the desired plasmid. pVR1255 was used as it contains a hCMV Intron A region that increases translation efficiency. Both the PCR amplified fragment and the expression vector, pVR1255 (260) (Figure 17), were digested with restriction enzymes. One µg DNA was used in the reaction with NEB3.1 buffer (New England BioLabs) and respective restriction enzymes (New England BioLabs). The reactions were incubated at 37°C for 2 h and the vector subsequently dephosphorylated using calf intestinal alkaline phosphatase (CIAP) (Invitrogen). For a 20 µl restriction enzyme reaction 2 µl 10X dephosphorylation buffer and 1 µl CIAP were added then incubated at 37°C for 20 min. This was to dephosphorylate the linearised vectors 5'-phosphate groups and allow the DNA insert to be ligated with the plasmid.

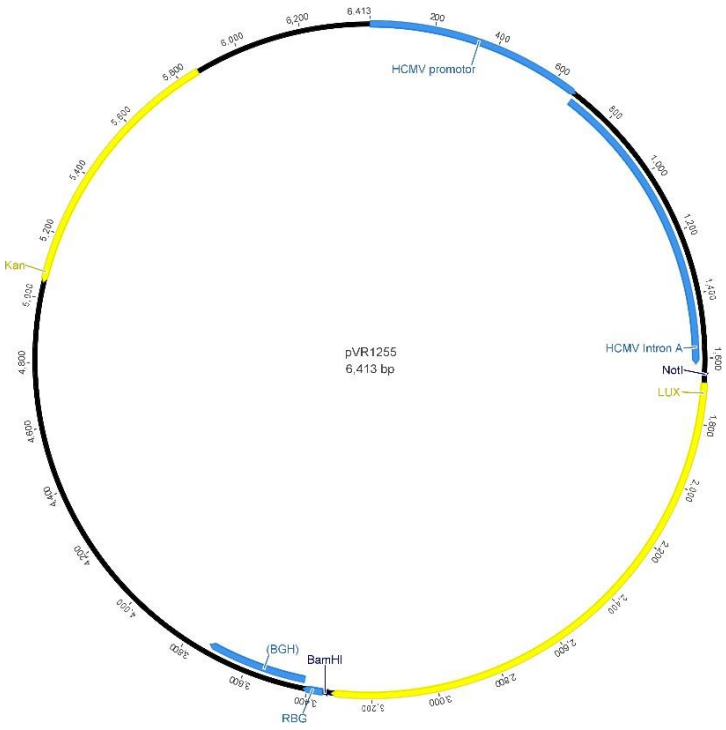

Figure 17. pVR1255 vector map produced in Geneious.

2.2.6 CRISPR

IDT online CRIPSR design tool was used to identify possible sgRNA sequences directly upstream of PAM sites (5'-NGG) in SPLUNC1 gDNA (NM130852.3). These were screened for possible off target effects and those gRNA excluded. sgRNA were annealed using 10 µM forward and reverse sgRNA with 10x T4 ligation buffer in a thermocycler at 37^{o}C for 30 min, 95^{o}C for 5 min then the temperature decreased to 25^{o}C at 5^{o}C min^{-1}. Annealed sgRNA were diluted 1:200 and ligated into pSpCas9(BB)-2A-GFP (PX458) kindly gifted from Feng Zhang (Addgene plasmid # 48138; http://n2t.net/addgene:48138; RRID:Addgene_48138). Ligation and subsequent transformation reactions were performed as described in 2.2.7.

2.2.7 Ligation & Transformation

Ligation of the PCR amplified fragment into linearised pVR1255 was performed using T4 DNA ligase (10X) (ThermoFisher) overnight at 4^{o}C with 1 unit of T4 DNA ligase. The following day, OneShot Top10 Chemically Competent *E. coli* (Invitrogen) were used to transfer plasmids into bacteria. pVR1255 plasmid (2 µl) was mixed with 50 µl competent bacteria in a 1.5 ml eppendorf and incubated on ice for 30 min. Cells were heat shocked at 42^{o}C for 30 s before returning to ice for 2 min. This mixture was supplemented with 350 µl of warmed SOC medium (Invitrogen) then incubated at 37^{o}C in a shaking incubator at 180 rpm for 1 h. After, 50 µl of the mix was plated onto LB agar plates supplemented with appropriate antibiotic. This was to select for the growth of bacteria containing the transformed plasmid only, which contained an antibiotic resistance gene. Kanamycin (Sigma) was used at 50 µg/ml with pVR1255

and ampicillin (Sigma) at 100 µg/ml with pSpCas9(BB)-2A-GFP. The plates were incubated overnight at 37°C.

2.2.8 Selection of bacterial colonies and plasmid DNA extraction from bacteria

After overnight incubation, 10 individual bacterial colonies were picked using a pipette tip and inoculated into 5 ml of LB broth (Sigma) supplemented with the respective antibiotic. These were incubated at 37°C, shaking at 180 x *g* for 20 h. Bacteria were pelleted from cultures at 5000 x *g* for 10 min and plasmid DNA was extracted using QIAgen Spin Miniprep Kit (Qiagen) as per manufacturer's instructions. Plasmid DNA was eluted in 30 µl TE buffer.

Selected colonies were screened using PCR and RE digest. PCR reactions were set up with the primers used to generate the DNA fragment via PCR amplification. PCR was performed using KOD polymerase detailed in 2.2.1. Restriction enzyme digestion was performed using the conditions detailed in 2.2.5. PCR and RE digest products were separated using gel electrophoresis (2.2.2) with positive colonies identified through expected molecular weights. Confirmation of the plasmid sequence was obtained via Sanger sequencing (Source BioScience), with the forward PCR amplification primer.

Once a positive colony was confirmed a QIAgen EndoFree Plasmid Maxi Kit (QIAgen) was used to prepare plasmid stocks for future use and plasmid stored aliquoted at -20°C.

Plasmid DNA was extracted from bacteria on a larger scale using a QIAgen EndoFree Plasmid Maxi Kit (QIAgen). Positive bacterial colonies were inoculated into 250 ml LB

broth supplemented with kanamycin (50 µg/ml) or ampicillin (100 µg/ml). These were incubated at 37°C in shaking incubators at 200 x *g* for 17 h. DNA was pelleted at 6000 x *g* for 15 min at 4°C and plasmid DNA extracted using manufacturer's instructions. Plasmids were eluted in 500 µl TE buffer. The quality and quantity of the plasmid DNA was determined using a NanoDrop One spectrophotometer (Thermo Scientific), with >250 µg DNA with an A260/280 >1.8 as the minimum limit accepted. Plasmids were then sent for sequencing (Source BioScience), from the forward PCR amplification primer.

2.2.9 Primers

Table 7 - List of primers used in PCR amplification and colony screening experiments

Name	Sequence (5'-3')	Annealing temperature (°C)
BPIFA1 Forward	ATGCGGCCGCCGCCGCCACCATGTTTCAAACTGGAGGCCTC	77
BPIFA1 Reverse	GCAGATCTTTAATGGTGATGGTGATGATGGACCTTGATGACAAACTGTAGTC	
SpD Forward	ATGCGGCCGCCGCCGCCACCATGCTGCTCTTCCTCCTCTCT	67
SpD Reverse	GCGGATCCTCAATGGTGATGGTGATGATGGAACTCGCAGACCACAAGACG	
SpD Sequencing Forward	GGGACCCCCGGGATTGAAGG	-
SpD Sequencing Reverse	CCTTCAATCCCGCTGGTCCC	
Murine TGFβRII Forward	ATGCGGCCGCCGCCGCCACCGGCCCGCATCCTGAGA	61
Murine TGFβRII Reverse	GCGGATCCTCAATGGTGATGGTGATGATGCGCACCGCCATTGTCGCT	
VR1255 Forward	AATAGCTGACAGACTAACAGACTG	-
VR1255 Reverse	GAGTGAGCTGATACCGCTC	
TGFβRI Forward	ATGCGGCCGCCGCCGCCACCGGCCCGCATCCTGAGA	72
TGFβRI Reverse	GCGCATCCTCAATGGTGATGGTGATGATGTATTCTTCTGAGAAGATGA	
Human TGFβRII Forward	ATGCGGCCHCCGCCGCCACCATGCAACTGTGTAAATTTTGTGATG	67
Human TGFβRII Reverse	GCGGATCCTCAATGGTGATGGTGATGATGCGCACCGCCA	
Cystatin S Sequence	ATGGGCTCTCACCCTCCTCTCCTGCAG	-
Cystatin Forward	AGATATCATGCGGCCGCCGCCGCCACCATGGCCCG	70
Cystatin Reverse	TGGGAGTAGGTCTTCATTTCGGCCAGAGCCCCAGCCAGGG	
Cystatin InFusion Forward	TGTGATCAGATATCGCGGCCCGCCGCCACCATGGCCCG	65
Cystatin-SpD Forward	ATGCGGCCGCCGCCGCGGCCACCATGGCC	65
SpD InFusion Forward	CCCTGGCTGGGGCTCTGGCCGAAATGAAGACCTACTCCCA	65
SpD InFusion Reverse	TTGAGGATCCGGATCCTCAATGGTGATGGTGATGATGGAACTC	

Cystatin-TGFβ Forward	GGCTCTGGCCCAACTGTGTAAATTTTGTGATGTGA	72
Cystatin-TGFβ Reverse	TACACAGTTGGGCCAGACCAGCAGCCAGG	-
TGFβ InFusion Reverse	GCCAGAAGTAGATCTGGATCTCAATGGTGATGGTGATGATGT	-
U6 F (CRISPR)	GAGGGCCTATTTCCCATGATTCC	-

2.3 RNA analysis

2.3.1 RNA extraction from cell pellets

RNA extraction from cells was carried out using TRIzol reagent (Thermo Fisher). Cell culture media was removed, cells washed twice with D-PBS and 1 ml TRIzol reagent added to the cell monolayer. The flask was incubated for 5 min before the samples were collected.

Each sample was supplemented with 200 µl chloroform, mixed then separated at 12,000 x *g* for 15 min at 4°C. The sample was separated into three layers: an upper aqueous phase containing RNA, an interphase, and a lower phase containing DNA. The 500 µl upper phase was removed and transferred into a fresh 1.5 ml Eppendorf and 500 µl isopropanol added. The samples were incubated for 10 min at room temperature prior pelleting the RNA at 12,000 x *g* for 10 min at 4°C. The supernatant was removed and the pellet washed with 1 ml 70% ethanol. The RNA was pelleted again at 7,500 x *g* for 5 min at 4°C, the supernatant removed and the pellet air dried for 5-10 min. The RNA was resuspended in 50 µl nuclease free water and quantified using a NanoDrop (Thermo Fisher).

2.3.2 RNA extraction from tissue samples

Tissue samples were homogenised using a Tissue Lyser LT and 25 mg tissue added to a 1.5ml micro-centrifuge tube containing ceramic beads and 1 ml LS TRIzol. The tissue samples were homogenised at 30 Hz for 2 min, and repeated up to three times if the tissue was not completely homogenised. Tissue debris was pelleted at 2000 x *g* for 5 min at 4^{o}C and the supernatant underwent RNA extraction as described in 2.3.1.

2.3.3 RNA extraction from swabs

Throat swabs taken from mice described in 2.5.2 were placed in 500 µl DMEM and underwent one freeze thaw cycle to improve RNA yield. The swab was removed and the DMEM mixed with 1ml LS TRIzol. This mix incubated at RT for 5 min and then the RNA extracted as described in 2.3.1.

2.3.4 DNase treatment

RNA was treated with TURBO DNase kit (Thermo Fisher) to remove any residual DNA present in the extracted samples. Samples were diluted to 200 ng/µl with nuclease free water. 5 µl 10x TURBO DNase buffer and 1µl TURBO DNase was added to 50 µl RNA. The reaction was incubated at 37^{o}C for 21 min. TURBO DNase was inactivated with EDTA to a final concentration of 15 mM and incubation at 75^{o}C for 10 min.

2.3.5 cDNA synthesis

cDNA was synthesised from DNase treated RNA using SuperScript IV (SSIV) (Invitrogen). The first strand was synthesised from a reaction comprised of: 50 µM

random primers, 10 mM each dNTP, 500 ng RNA were mixed to a volume of 13 µl with nuclease free water. The mix was heated at 65°C for 5 min then one minute on ice to anneal primers to the RNA. Meanwhile the reverse transcription (RT) reaction mix was assembled with 4 µl SSIV 5x buffer, 1 µl DTT, 1µl RNase inhibitor and 1 µl SSIV per reaction. This was mixed, 7 µl added to each primer annealed RNA reaction and then incubated at 55°C for 10 min. The reaction was then inactivated with an 80°C incubation for 10 min.

2.3.6 PCR

For PCR, Phusion DNA Polymerase (Thermo Fisher) was used as described in 2.2.1 (Table 5 and Table 6 bookmark57). Annealing temperature was varied according to primers used and extension time to PCR product length. PCR products were visualised using agarose gel electrophoresis described in 2.2.2.

2.3.7 RT-qPCR

2.3.7.1 SYBR Green

RT-qPCR for SPLUNC1 was performed with SYBR green using SYBR green master mix (ThermoFisher). SPLUNC1 was quantified using 10mM of each primer detailed in 2.3.8 and the standard curve constructed from a 10-fold serial dilution of SPLUNC1-pVR1255 plasmid from 10^9 to 10^3 copies/reaction. All samples were run as duplicates with 100ng RNA quantified sample. Total reaction volume was 25µl per sample. The thermal cycling conditions were: 1 cycle of 50°C for 10 minutes and 1 cycle of 95°C for 5 minutes, followed by 35 cycles of 95°C for 10 secs and 60°C for 30 secs. A melt

curve was performed at the end of each assay to ensure each qPCR amplicon only had one distinct length; this is represented as a single discrete peak on a melt curve (Table 9).

2.3.7.2 TaqMan

qPCR experiments were performed for 18s and IAV on DNase treated RNA using GoTaq 1-Step RT-qPCR System (Promega) to quantify IAV viral loads. IAV viral load was quantified using the IAV primers and probe published with CDC IAV detection kit (20403211). The standard curve was constructed using the IAV reverse genetics M plasmid. 18s standard curve was generated using PCR amplification of murine 18S cDNA fragment using the primers F: ACCTGGTTGATCCTGCCAGGTAGC and R: GCATGCCAGAGTCTCGTTCG. Both 18s and IAV standards were diluted 10-fold from 10^9 to 10^3 copies/reaction to produce the standard curve. The S18 primers and probe were utilised at 400 nM and 200 nM respectively. Each sample was quantified from 100 ng RNA using the conditions below (Table 8) and run-in duplicate. The primers utilised in these reactions are detailed in Table 10. Total reaction volume was 25µl per sample.

Table 8 – RT-qPCR cycling conditions using Taqman.

Reaction stage	Conditions	Number of cycles
RT	45°C, 15 min	-
RT inactivation	95°C, 2 min	-
Denature	95°C, 3 s	40 cycles
Anneal/Extension	60°C, 30 s	

2.3.7.3 Gene quantification

Following RT-qPCR, data was analysed using relative standard curve method. The starting quantity of RNA in each reaction (in ng) was calculated using the standard curve and cycle threshold from each sample. As each sample was run in duplicate, first the mean starting quantity for each sample was calculated. It then converted to copies per µg of RNA in each sample. The expression of the target gene, for example SPLUNC1, was then normalised to the house keeping gene for each sample, 18s. To achieve this, 18s expression was normalised with the copies of 18s/µg in each sample divided by the mean 18s copies/µg from all samples. This normalised 18s value was then multiplied by the copies of SPLUNC1/µg for each sample and the expression of SPLUNC1/µg normalised to 18s calculated.

2.3.7.4 Melt Curve

Melt curve steps were performed at the end of each SYBR green RT-qPCR, as detailed in 2.3.7.1. Melt curve peak temperatures for SPLUNC1 and 18s are detailed below in Table 9.

Table 9 - Melt Curve temperatures for SYBR green RT-qPCR assays.

Primer	Sample	Peak 1 (°C)	Peak 2 (°C)
SPLUNC1	Positive	85.50	None
SPLUNC1	Negative	None	None
18s	Positive	80.50	None
18s	Negative	None	None

2.3.7.5 Standard Curves

RT—qPCR data was analysed using the relative standard curve method detailed in 2.3.7.3. Standard curves were constructed as detailed in 2.3.7.1 and 2.3.7.2.

Standard curves from each assay are included below (Figure 18, Figure 19 and Figure 20).

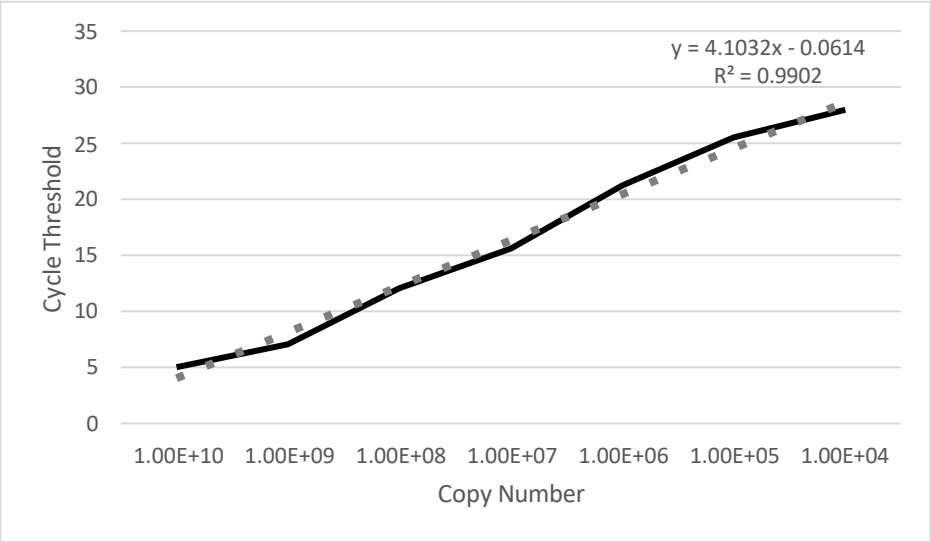

Figure 18. SPLUNC1 RT-qPCR standard curve.
Standard curve was constructed from 10-fold serial dilution of SPLUNC1-pVR1255 plasmid from 10^9 to 10^3 copies/reaction. Data points present are an average from sample run in duplicate and presented in black. Standard curve line of best fit is present in grey.

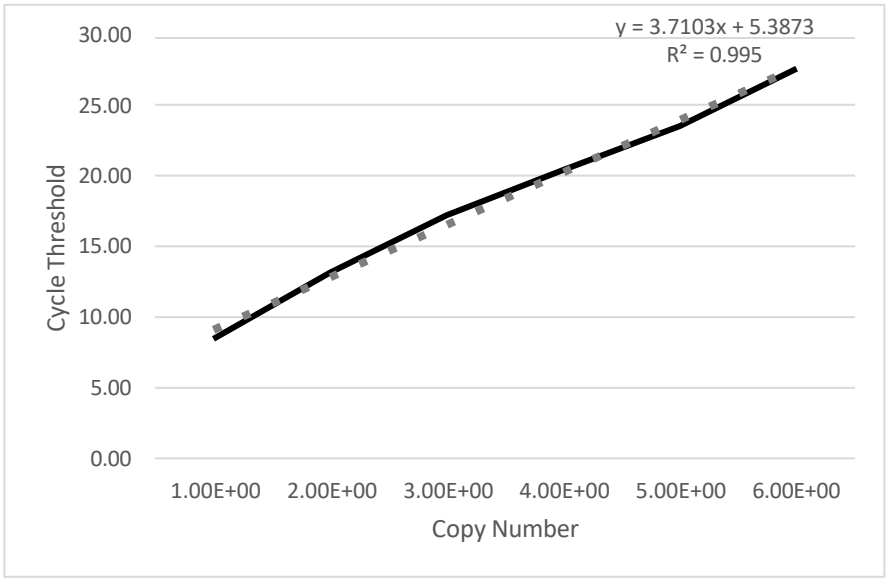

Figure 19. IAV RT-qPCR standard curve.
Standard curve was constructed from 10-fold serial dilution of IAV M plasmid from 10^9 to 10^3 copies/reaction. Data points present are an average from sample run in duplicate and presented in black. Standard curve line of best fit is present in grey.

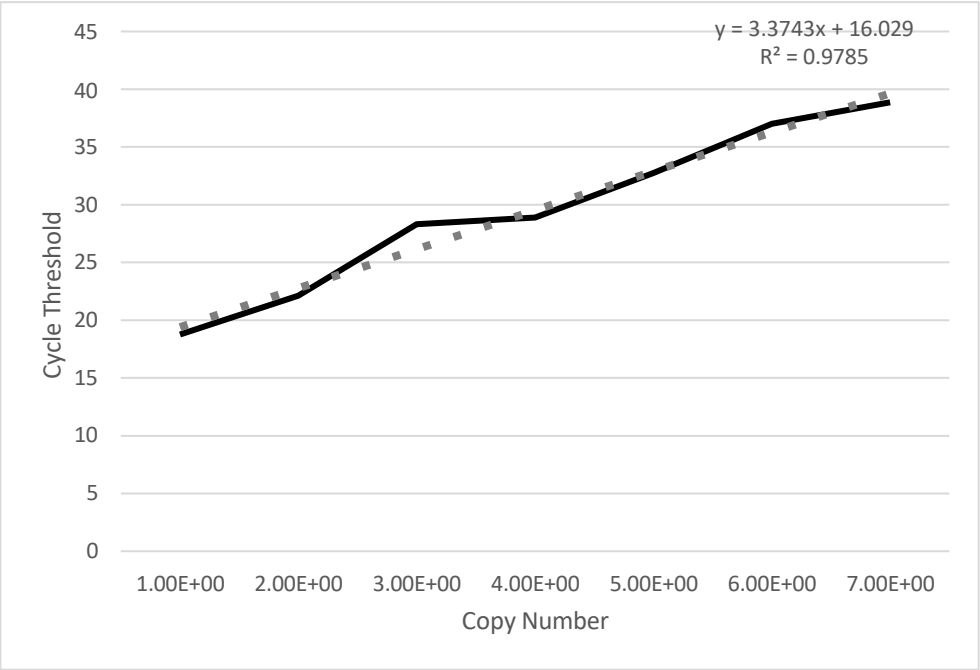

Figure 20. 18s RT-qPCR standard curve.
Standard curve was constructed from 10-fold serial dilution of Murine 18s cDNA fragment from 10^9 to 10^3 copies/reaction. Data points present are an average from sample run in duplicate and presented in black. Standard curve line of best fit is present in grey.

2.3.8 Primers

Table 10 – Primers used in qPCR reactions

Name	**SYBR green or Taqman RT-qPCR**	**Sequence (5'-3')**	**Annealing temperature (°C)**
SPLUNC1-F qPCR	SYBR green	ATGCCCTCAGCAATGGCCTGCT	60
SPLUNC1-R qPCR		GTGAGGCTGTCCAGAAGACC	
GAPDH F	-	GCACCGTCAAGGCTGAGAAC	65
GAPDH R	-	TGGTGAAGACGCCAGTGGA	
Intron F	-	TACCCATGCCATGTTGGACTT	65
Intron R	-	CCCTGGTGGAGATCAAAGCTC	
Tectin Forward	-	TGGAGCTGTGTCGTGATGTC	65
Tectin Reverse	-	GCATACACAGCACTTCGTCG	
IAV M F	Taqman	GACCAATCCTGTCACCTCTGAC	60
IAV M R		AGGGCATTTTGGACAAAGCGTCTA	
IAV M probe		56-FAM CGTGCCCAGTGAGCAAGGACTGCA 3IABkFQ	

18s F	Taqman	ACCTGGTTGATCCTGCCAGGTAGC	60
18s R		AGCCATTCGCACTTTCACTGTAC	
18s Probe		5-HEX TCAAAGATTAAGCCATGCATGTCTAAGT ACGCAC 3IABkFQ	

2.4 Protein analysis

2.4.1 Sample preparation

Cell monolayers were washed three times with D-PBS-0.01%EDTA (Sigma) then lysed using 2x sample buffer (4% SDS, 20% glycerol, 0.004% bromophenol blue, 0.125 M Tris). Supernatant samples were prepared by adding an equal volume of 2X sample buffer (4% SDS, 20% glycerol and 120 mM Tris-Cl pH 6.8). Each sample was supplemented with 5% 2-mercaptoethanol (v/v) (Sigma) then boiled at 95^{o}C for 10 min.

2.4.2 SDS-PAGE

2.4.2.1 Tris glycine

Proteins were separated by molecular weight using 12% acrylamide resolving gels (33% 1.5M Tris pH 8.8, 12% acrylamide, 25.8% dH_2O, 0.1% SDS, 0.05% APS and 0.2%

TEMED) topped with stacking gel (11.6% 0.5M Tris pH 6.8, 5% acrylamide, 70% dH_2O, 0.1% SDS, 0.09% APS and 0.1% TEMED). Each well was loaded with 15 µl of each sample alongside 10 µl Spectra multicolour broad range protein ladder (Thermo Fisher). The SDS-PAGE gel electrophoresis was performed at 120 V for 1.5 h in 1x running buffer (25 mM Tris, 190 mM glycine and 0.1% SDS).

2.4.2.2 Tris Tricine

Tris tricine gels were used in SDS PAGE to visual proteins under 20kDa. Tris Tricine gels were 12% and comprised of a separating and stacking phase. Separating gels were comprised of 36.4% 29:1 acrylamide, 33.3% 3M Tris-CL/SDS at pH8.4, 30% water, 10% glycerol, 0.2% 10% APS and 0.1% TEMED. When the separating gel had set, the stacking gel was constructed on top with 10% 29:1 acrylamide, 25% 3M Tris-CL/SDS at pH8.4, 64% water, 8% 10% APS and 2% TEMED. Each well was loaded with 30 µl of sample alongside 10 µl Spectra multicolour broad low range protein ladder (Thermo Fisher). The gel tank was submerged in 1x anode buffer (0.2 M Tris-Cl, pH8.9), which covered the main apparatus, and 1x cathode buffer (0.1 M Tris, 0.1 M Tricine and 0.1% SDS) on the top of the gel wells. The SDS-PAGE gel electrophoresis was performed with the assembled, submerged gel tank at 110V for 30 min then 150 V for 75 min.

2.4.3 SDS-PAGE staining

2.4.3.1 Coomassie blue staining

Following protein separation by SDS-PAGE, proteins were visualised using coomassie staining. Gels were submerged in coomassie staining solution (40% methanol, 10%

glacial acetic acid and 0.025% coomassie brilliant blue), heated for 1 min in a microwave then incubated with agitation for 1 h at RT. Gels were washed three times for five min in ultra-pure water prior to incubation in the destaining solution (40% methanol and 10% glacial acetic acid). Gels were heated in a microwave for one minute prior to incubation at RT with rotation for 30 min. Gels were washed three times for five min in ultra-pure water then imaged using a ChemiDoc Imager System (BioRad).

2.4.3.2 Silver staining

Alternatively, silver staining was used to visualise lower concentration proteins due to its greater sensitivity. This was performed with Pierce Silver Stain Kit (Thermo Fisher) as per manufacturer's instructions. Following protein separation by SDS-PAGE, gels were washed 2 x 5 min in ultra-pure water, fixed in 30% ethanol:10% acetic acid solution for 2 x 15 min and then washed in 10% ethanol and ultra-pure water twice each for 5 min. Gels were sensitised for 1 min with sensitiser working solution then incubated with stain working solution, both supplied with the kit, for up to 30 min. Gels were washed briefly twice with ultra-pure water prior to incubation with the developer working solution, supplied with the kit, for 2-3 min, until the desired balance of protein bands and background was reached. This reaction was stopped with incubation in 5% acetic acid for 10 min. All steps were completed with agitation. Gels were imaged using a ChemiDoc Imaging Systems (BioRad).

2.4.4 Western blot

Following, SDS-PAGE gel electrophoresis. Proteins were transferred onto a 0.45 µm nitrocellulose membrane (Merck) via wet transfer using a Mini Trans-Blot cell (BioRad) and transfer buffer (25 mM Tris, 190 mM glycine and 20% methanol) at 100 V for 1 h.

Following this, membranes were blocked in 5% milk powder (w/v) in Tris Buffered Saline supplemented with 0.1% Tween-20 (TBS-T) at RT for 1 h, with rotation. The membranes were then incubated in the primary antibody (Table 11) diluted in 5% milk TBS-T at RT for 1 h. Membranes were then washed three times for 5 min in TBS-T. Secondary antibodies (Table 11) diluted in 5% milk TBST were incubated for 1 h with membranes at room temperature under agitation. Membranes were then washed three times in TBST for 5 min prior to visualisation with Clarity Western ECL Substrate (BioRad), as per manufacturer's instructions, and ChemiDoc Imaging Systems (BioRad).

2.4.5 Antibodies

Table 11 - List of all antibodies used in all experiments

Antibody	**Species**	**Company**	**Dilution**	**Clone Number / Product Number**
Monoclonal anti-polyhistidine	Mouse	Sigma	1 in 3000	HIS-1
Monoclonal SPLUNC1 antibody	Mouse	R&D	1 in 500	251512

Monoclonal anti-Surfactant protein D	Mouse	Abcam	1 in 2000	10B2
Polyclonal Human TGFβR2 Isoform 2 antibody	Goat	R&D	1 in 2000	AF1003
Monoclonal anti- TGFβRII ectodomain antibody	Mouse	Abcam	1 in 2000	MM0056-4F14
Mouse SPLUNC1 A	Rabbit	-	1/1000	Made against peptide
Mouse SPLUNC1 B	Rabbit	-	1/1000	Made against peptide
Human SPLUNC1	Rabbit	-	1/1000	Made against peptide
Anti-Influenza A virus antibody	Goat	Meridian	1 in 500	B655311G-1
Goat anti mouse peroxidase IgG	Goat	Sigma	1 in 10,000	A4416
Rabbit anti-Goat	Rabbit	Deko	1 in 2,000	P044901-2

2.4.6 Protein purification

Recombinant proteins were purified from supernatant of transfected cells, 24 h post transfection with expression plasmid, performed as detailed in 2.1.5. Purification was performed with 1 g of Ni-IDA resin (ThermoFisher), with a 1 ml bed volume, per 20mg protein. Disposable plastic resin columns were equilibrated with 4 bed volumes of Lysis-Equilibration-Wash (LEW) buffer (50 mM monosodium phosphate and 300 mM sodium chloride at pH 8.0). Supernatant was applied to bind the resin column using gravity flow prior to being washed twice with LEW buffer. The protein was eluted with equilibration buffer (50 mM monosodium phosphate, 300 mM sodium chloride and 250 mM imidazole at pH 8.0) in three separate fractions.

2.4.7 Immunoprecipitation

Immunoprecipitation was performed using Amicon Ultra-15 centrifugal filter (Thermo Fisher) concentrated supernatant collected 6 days post-transfection of HEK293T cells with SPLUNC1 or Cystatin S – SpD plasmids. In the cases where murine SPLUNC1 was investigated, 10 µg protein from bronchioalveolar lavage (BAL) samples from 10-week-old wildtype C57BL/6 mice were used as the antigen sample, detailed in 2.5.4. These samples incubated with $3.4x10^4$ pfu X31 IAV, 10 µl/ml HALT protease inhibitors and 50 ng/µl TPCK trypsin for 1.5h at 37^oC to form the preparation for immunoprecipitation.

2.4.7.1 Crosslinking

Crosslinking was completed with either 4% paraformaldehyde (PFA) (Sigma) or DSS (Thermo Fisher). 4% PFA (v/v) was added to samples and mixed for 10 min at RT with agitation prior to quenching with glycine to a final concentration of 125 mM for 5 min. DSS was added to samples to a final concentration of 3 mM then incubated for 30 min at RT and quenched with 20 mM EDTA for 15 min.

2.4.7.2 Immunoprecipitation

Immunoprecipitation of human SPLUNC1 was performed with Ni-IDA resin and immunoprecipitation of SpD or murine SPLUNC1 with protein A Sepharose and the respective antibody. Protein lo-bind tubes (Eppendorf) were used throughout. All samples underwent crosslinking prior to immunoprecipitation apart from SpD.

2.4.7.2.1 Using Ni-IDA resin

Human SPLUNC1-IAV preparation and activated Ni-IDA resin were mixed and incubated at RT for 30 min with resuspension every five min. Samples were pelleted at 1000 x *g* for 1 minute. Supernatant was removed and pellet washed twice with RIPA buffer with the resin transferred to a fresh tube at the final wash. Resin pellets were re-suspended in 50 µl 2x sample buffer and prepared as described in sample preparation; 1.4.1.

2.4.7.2.2 Immunoprecipitation via Protein A Sepharose

SpD or murine SPLUNC1 - IAV preparations were immunoprecipitated by their respective antibody detailed in 2.4.5 and bound to Protein A Sepharose. Antigen and antibody samples were incubated for 1 h at RT on a HulaMixer (Thermo Fisher) prior

to the addition of Protein A Sepharose in D-PBS. This was incubated for 1.5 h at RT on a HulaMixer. Samples were pelleted at 4,000 x *g* for 1 minute then supernatant removed and the pellet washed in TBS with 1% NP40. Wash steps were repeated twice with bead mixture transferred to a fresh tube at the final wash. Resin pellets were re-suspended in 50 µl 2x sample buffer and prepared as described in sample preparation; 1.4.1.

2.4.8 Bradford Protein Assay

Pierce BCA Protein Assay Kit (Thermo Fisher) was utilised to determine the concentration of protein. BSA protein standards with a concentration range of 0-2000 µg/ml were prepared and 25 µl loaded into a flat bottom 96 well plate in triplicate. Then 25 µl of each unknown sample was loaded in triplicate, followed by 200 µl Pierce BCA Protein Assay working reagent was added to each well, and the plate mixed thoroughly on a shaker for 30 s then incubated at 37^{o}C for 30 min. The plate was cooled to RT and measured at 562 nm on an Infinite F50 plate reader (Tecan).

To calculate the protein concentrations, a standard curve was constructed from the BSA standards and then utilised to determine the concentration of each unknown sample.

2.4.9 Peptides

2.4.9.1 Synthesis

S18 (**GGLPVPLDQTLPLNVNPA**), S18 scrambled control (S18sc) (**NLQVPPTVPLLNGPDLAN**) and SPX101 (**aaLPIPLDQTaa**) peptides were synthesised by Severn Biotech (Kidderminster, UK). Peptides were deemed >85%, >75% and >95% pure by HPLC, respectively.

2.4.9.2 Formulation

3 mg lyophilised S18 peptide was resuspended in hydrogel then prepared in the Bio-Courier formulation which will enhance S18 stability and delivery intranasally. S18 was prepared with a 1:4 Peptide:Biocourier ratio and stored at 4^{o}C prior to use.

2.4.10 Immunofluorescence

KT cells were plated at 1.5x10^{5} cells/well in a 12 well plate with each well containing a 13 mm spherical coverslip (Thermo Fisher). Cell culture media was removed 24 h later and cells washed once with D-PBS then fixed with 4% PFA for 30 min at RT. Samples were blocked in blocking buffer (1x D-PBS, 3% BSA and 0.5% Triton) overnight at 4^{o}C with rotation. The following day, cells were stained with Maackia amurensis I+II (MAA) or Sambucus Nigra (SNA) biotinylated lectins (2BScientific) diluted 1:200 in blocking buffer for 1 h at RT. Samples were washed three times with D-PBS prior to incubation with Alexa Fluor 568 Streptavidin (Thermo Fisher) diluted 1:1000 in blocking buffer for 1 h at RT. Samples were then washed 6 times in D-PBS and attached to the microscope slides with 10 µl VECTASHIELD HardSet Antifade

mounting media containing DAPI (2BScientific). Samples were visualised with a LSM confocal microscope by Dr Thomas Waring at the CCI Liverpool.

2.5 Animal work

2.5.1 Mice

All murine experiments were approved by the University of Liverpool Animal Welfare Committee and performed under UK Home Office Project Licences I2EF4E56C and 70/8599. Mice were kept in individually ventilated cages (Techniplat, GM500) under barrier and 12 h light/dark conditions. Food and water were provided *ad libitum*. Transgenic SPLUNC1 $^{-/-}$ mice were bred at the University of Liverpool under UK Home Office Project Licence 70/8378. Wildtype sex, age and background matched control mice were purchased Charles River (Margate, UK).

2.5.2 Influenza A Virus infection of mice

BALB/C Mice were assigned randomly into each group and inoculated intranasally with a 10 µl dose of IAV containing $1x10^3$ pfu diluted in sterile PBS. This was performed under light anesthesia with ketamine (Zoetis, Ketavet) by intramuscular infection. Mice were euthanised by cervical dislocation 5 d.p.i.. Lung and nasal tissue samples were removed for downstream analysis. Mice underwent a throat swab everyday post infection to monitor viral load. This was performed under light anaesthesia with isoflurane by inhalation.

2.5.3 Peptide administration in mice

Mice were administered with 40 µg S18 peptide in formulation at 1 µg/µl, 40 µg S18 peptide in PBS at 1 µg/µl, vehicle formulation control or PBS control under light anaesthesia with isoflurane by inhalation. This was performed 1 d and 2 h prior to infection as well as everyday post infection until mice were euthanised.

2.5.4 BAL collection

Wildtype C57BL/6L and SPLUNC1$^{-/-}$ mice, that were 10 weeks old, were euthanised by cervical dislocation. Bronchioalveolar lavage samples were taken immediately with D-PBS.

2.6 Statistical analysis

Data was analysed using Prism 9 software (GraphPad) and presented as individual data points and mean ± standard error of the mean (SEM). Statistical significance was determined using a variety of tests, detailed below. Mann-Whitney U tests were used compare the difference between two independent groups. Kruskal Wallis was used to determine if the data was statistically significant when one independent variable was present and not normally distributed in three or more groups. Two-way Analysis of Variance (ANOVA) was used when two independent variables were present. Bonferroni post hoc test was used following two-way ANOVA to determine exactly where the statistical differences occurred between the groups. Log rank test was used to determine if survival was different between group in *in* vivo experiments. P values <0.05 were considered significant.

3 Investigation of a direct interaction between SPLUNC1 and IAV

3.1 Introduction

SPLUNC1 has been reported to have antiviral activity against multiple viruses in human and murine models. Although this antiviral activity by SPLUNC1 has been observed against numerous viruses, such as EBV, RV and IAV this effect is not universal. An important limitation thus far is that murine models have been used to identify antiviral activity against EBV, RV and IAV (183, 218-220, 222, 223). Antiviral activity of SPLUNC1 in humans has only been reported against EBV (189, 217). No antiviral activity against IAV in humans has been studied or reported at the time of writing.

The exact mechanism by which SPLUNC1 contributes to the host's antiviral response is unclear; it is associated with host cell apoptosis, decreased viral replication, inhibition of viral infection of host cells, and modulation of the innate cytokine response (189, 217-219). Specific regions of SPLUNC1 have been identified as mediating its antibacterial activity but the role of these regions in SPLUNC1 antiviral effects has not been investigated (199, 200, 258).

3.2 Aims

The aim of this chapter was to investigate if there is a direct physical mechanism SPLUNC1 utilizes to restrict IAV infection. Firstly, by generating recombinant human SPLUNC1 protein via the construction and use of SPLUNC1 expression plasmids. Then, purifying this recombinant protein to produce a purified source of recombinant

SPLUNC1 to utilize in downstream assays. Finally, by investigating if a direct interaction is occurring between SPLUNC1 and IAV.

3.3 Results

3.3.1 Cloning of expression plasmids

Human SPLUNC1, referred to as SPLUNC1 onwards, was cloned into the expression vector pVR1255 (Figure 17) to facilitate the expression of recombinant SPLUNC1 protein. A 770bp DNA fragment corresponding to SPLUNC1 was amplified by PCR using primers that added a Kozak sequence and NotI and BglII restriction enzyme sites to the 5' and 3' ends respectively, to facilitate cloning into the expression vector, pVR1255, using restriction enzymes, as described in 2.2.5. The amplified PCR product was separated and visualized on a 1% agarose gel to confirm its size. pVR1255 was digested with NotI and BamHI and the PCR amplified SPLUNC1 fragment was digested prior to cloning into pVR1255 (Figure 21). BglII was used instead of BamHI as the hSPLUNC1 DNA sequence contains a BamHI restriction enzyme site rendering it unsuitable for BamHI digest. Digest via BglII instead produces complementary sticky ends suitable for cloning. These products were visualized via gel electrophoresis to confirm correct digestion prior to ligation (Figure 21). The digested SPLUNC1 and pVR1255 were ligated with T4 DNA ligase to produce a new vector, hSPLUNC1-VR1255. This product was transformed in OneShot Top10 Chemically Competent *E. coli* and colonies containing the correct insert were selected for growth using kanamycin, as described in 2.2.7. DNA was extracted from single bacterial colonies by miniprep extraction and screened for hSPLUNC1 insert by colony PCR. Products

were separated by gel electrophoresis to confirm the molecular size. Colonies 2-6 were of the correct size and commercially sequenced to confirm SPLUNC1 sequence insertion (Figure 21).

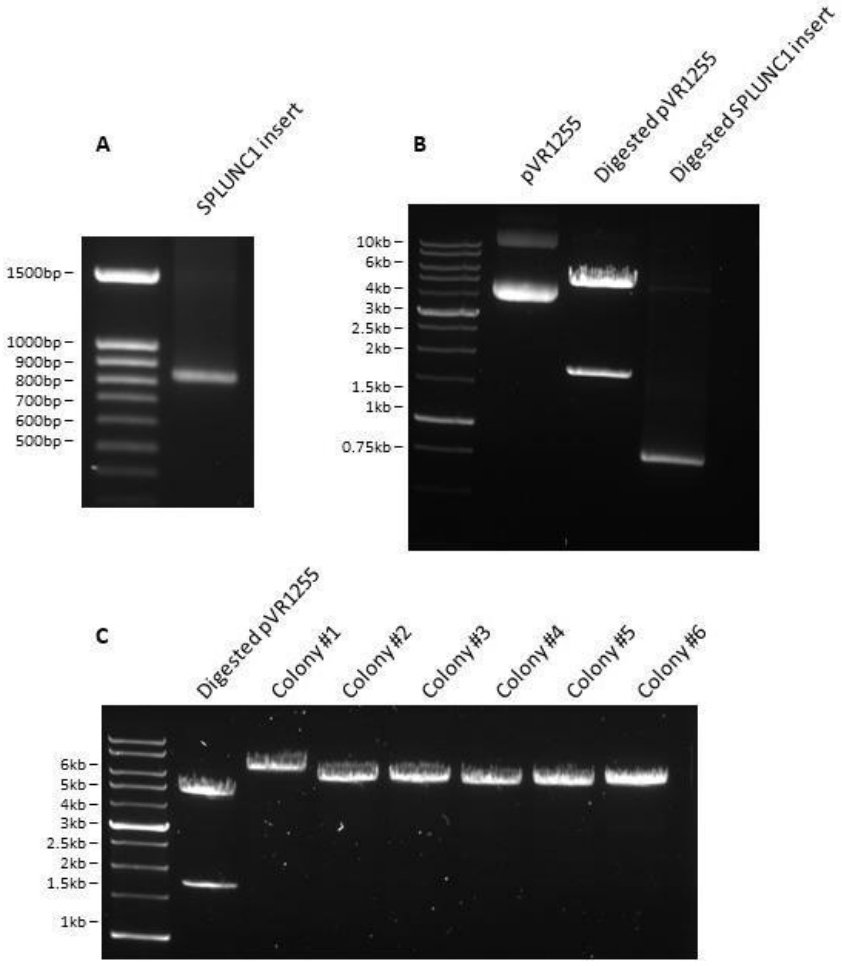

Figure 21. SPLUNC1-pVR1255 expression plasmid construction.
(A) Gel electrophoresis was used to visualize the SPLUNC1 insert produced via PCR amplification from the human DNA template. (B) Undigested pVR1255, pVR1255 digested with NotI and BamHI, and SPLUNC1 insert digested with NotI and BglII products were visualized using gel electrophoresis to confirm the product's molecular size prior to ligation. (C) Six colonies from transformation underwent miniprep. These were then digested with NotI and visualized using gel electrophoresis to identify if the SPLUNC1 insert had been successfully ligated into pVR1255.

Surfactant protein D (SpD) was chosen as a positive control for IAV binding as it is known to interact with IAV (72). It was also cloned into the expression plasmid

pVR1255 so recombinant SpD protein could be produced and used in downstream experiments. The human SpD, here on referred to as SpD, DNA sequence was PCR amplified from human cDNA, then restriction digested with BamHI and NotI prior to insertion into pVR1255 using restriction digest cloning (Figure 18). DNA was extracted from colonies via miniprep, digested with BamHI then separated and visualized using gel electrophoresis to establish SpD has been successfully inserted into pVR1255 (Figure 22). Where successful cloning was suggested in colonies 3 and 6, commercial Sanger sequencing was used to confirm the identity of colonies.

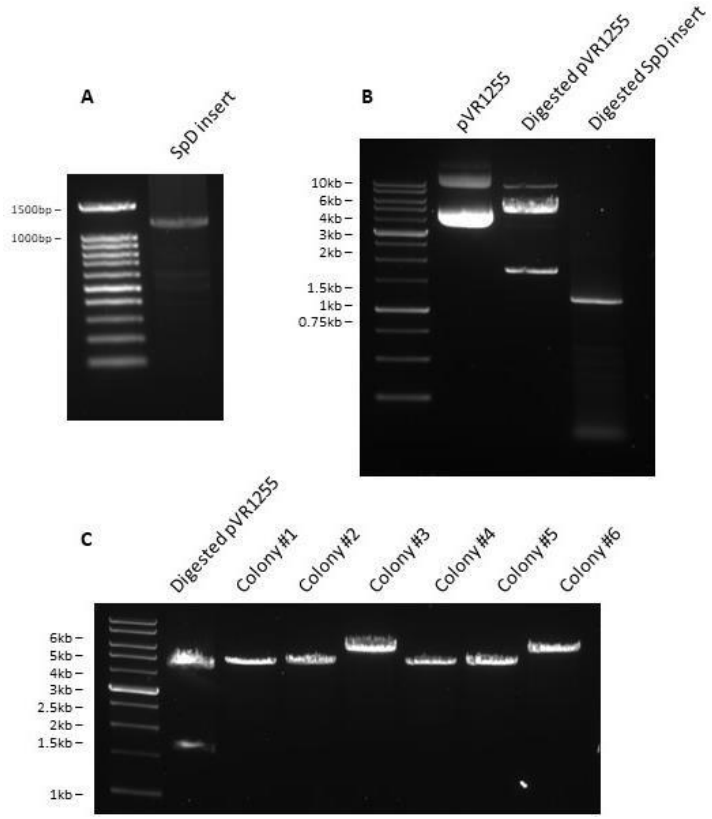

Figure 22. SpD-pVR1255 expression plasmid construction.
(A) Gel electrophoresis was used to visualise SpD insert produced via PCR amplification from human template DNA. (B) pVR1255, digested pVR1255 and digested SpD insert, both digested with NotI and BamHI, were visualised using gel electrophoresis to confirm the products molecular size prior to cloning. (C) Six colonies produced from transformation underwent miniprep and were subsequently digested with NotI. Gel electrophoresis used to visualise these products and identify if the SpD insert had been successfully ligated into pVR1255.

Murine transforming growth factor β receptor I (TGFβRI) was selected as a negative control for SPLUNC1 IAV interaction experiments. Specifically, its ectodomain was cloned into pVR1255 because it is ubiquitously expressed, extracellular and does not bind IAV. TGFβRI PCR amplification was attempted from a plasmid, generously donated by Dr Flynn, and bovine cDNA however, both were unsuccessful templates (Figure 19). Following this, a NotI restriction enzyme site was identified in TGFβRI rendering it unsuitable for this cloning method. Instead, murine transforming growth factor β receptor II (TGFβRII) ectodomain was selected. PCR amplification of TGFβRII ectodomain was initially attempted, but unsuccessful, from mouse cDNA. TGFβRII was eventually successfully PCR amplified from a plasmid template, pCMV5B-TGFbeta receptor II wt kindly gifted by Joan Massaque & Jeff Wrana (Addgene #11766) (Figure 23). This template was human and chosen so all plasmids and proteins used in these experiments were from the same species. The amplified insert was cloned into pVR1255 using restriction enzyme cloning with NotI and BamHI. DNA was extracted from the colonies, digested with BamHI then separated and visualized using gel electrophoresis (Figure 24). Again, where successful cloning was indicated, commercial sequencing confirmed this.

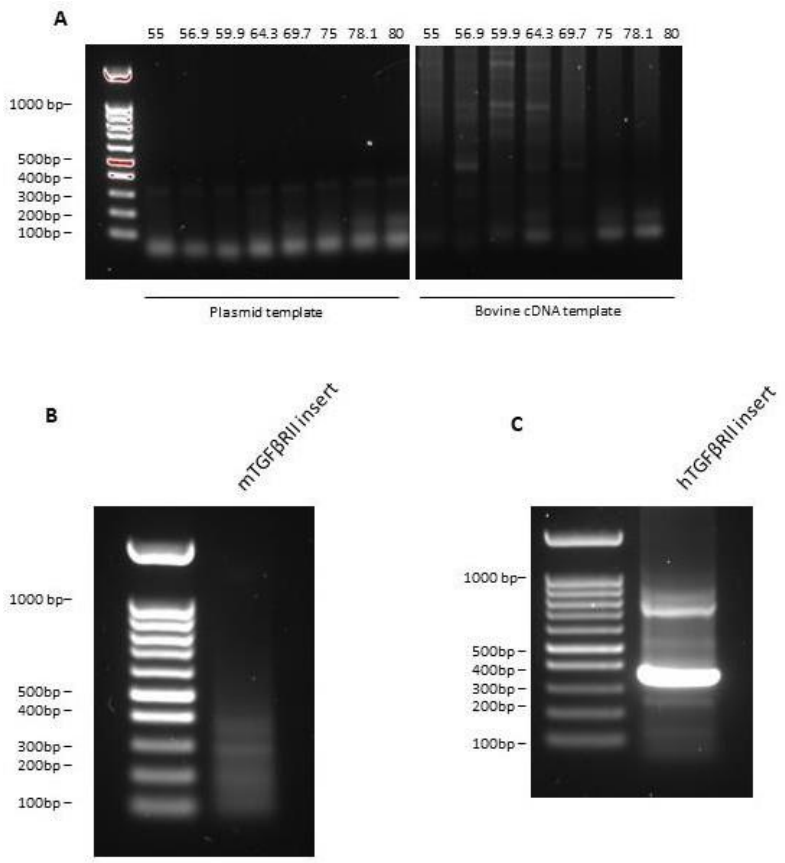

Figure 23. Transforming Growth Factor β Receptor I (TGFβRI) and Receptor II (TGFβRII) amplification attempts from different templates.

(A) Gel electrophoresis was used to visualise PCR amplification of mTGFβRI performed with an annealing temperature gradient from plasmid and bovine cDNA. (B) Gel electrophoresis was used to visualise mTGFβRII ectodomain PCR amplification from mouse cDNA. (C) Gel electrophoresis was used to visualise hTGFβRII ectodomain PCR amplification from a plasmid template (Addgene #11766).

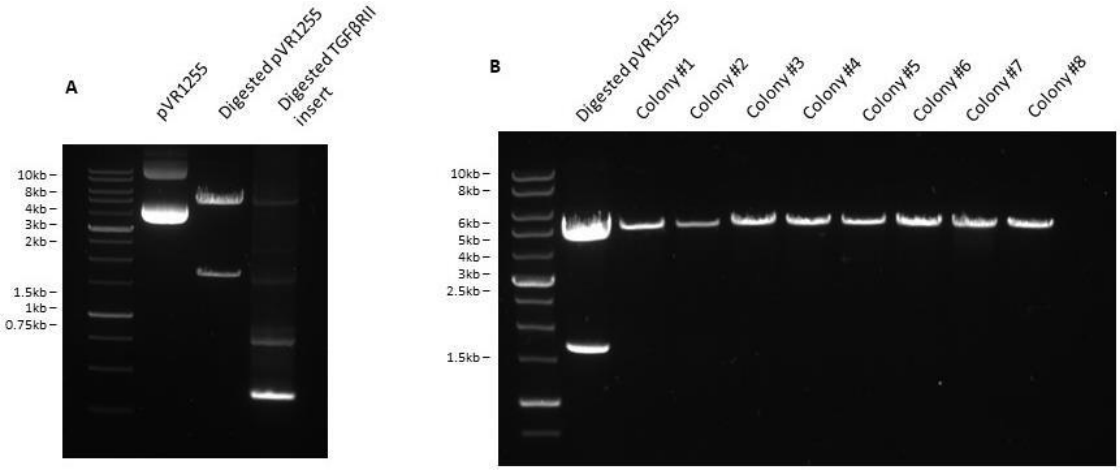

Figure 24. TGFβRII-pVR1255 expression plasmid construction.
(A) pVR1255, digested pVR1255 and digested TGFβRII insert, both digested with NotI and BamHI, were visualized using gel electrophoresis to confirm the products molecular size prior to cloning. (B) Eight colonies were selected to undergo miniprep and genotyping after transformation. These were digested with BamHI and visualized using gel electrophoresis to identify if the TGFβRII insert had been successfully ligated into pVR1255.

3.3.2 Protein expression from expression plasmids

3.3.2.1 Optimization of transfection in HEK293T cells

Prior to transfecting expression plasmids, the protocol for transfection into HEK293T cells was optimized using a GFP plasmid to assess transfection efficiency. A calcium phosphate transfection protocol was performed with one element altered sequentially to assess its affect compared to the original, standard protocol, described in 2.1.5. Seven aspects of the protocol were altered in total with four having positive impacts on transfection efficiency: changing media to DMEM only 1 hour before and 6 hours after the transfection, increased particle density and a glycerol shock (Figure 25). However, a glycerol shock was not used in the final,

optimized protocol due to its cytotoxicity outweighing its overall benefits; all other adjustments were included in the final protocol. Replacing the media with complete media 1-hour pre-transfection and incubation of the transfection mix at 37°C, not room temperature, did not increase transfection efficiency and were not used in this protocol again. Following this, the quantity of DNA transfected was optimized. The standard quantity of DNA transfected was 1 µg/6 well-plate well and this was increased to 2, 4 or 8 µg/well. However, increasing the quantity of DNA transfected did not increase the transfection's efficiency and was not altered (Figure 26).

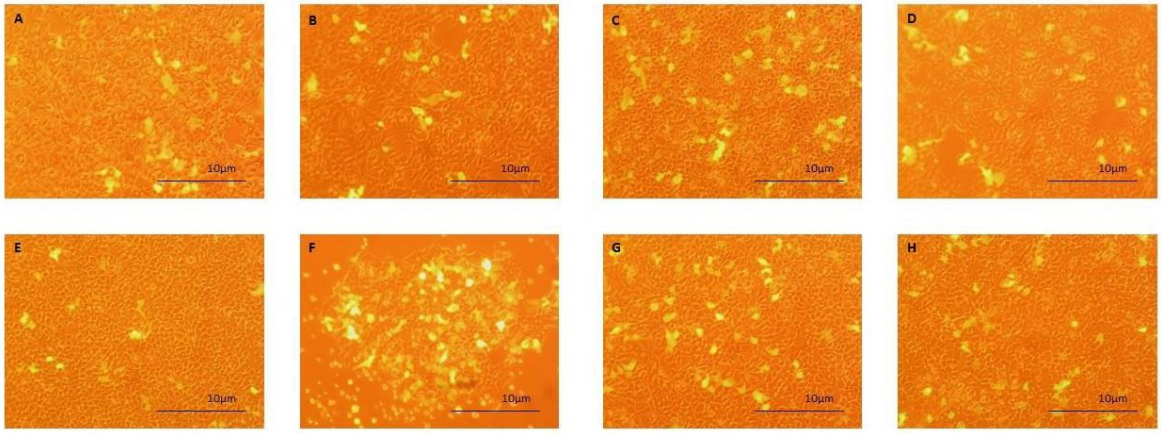

Figure 25. Calcium phosphate transfection protocol optimization.
The efficiency of the calcium phosphate transfection protocol into HEK293T cells was assessed using a green fluorescent protein (GFP) plasmid to estimate transfection efficiency. (A) shows the standard protocol and (B-H) the results when one element altered individually to assess how it affected transfection efficiency. HEK293T cells were plated 24 hours before transfection. The individual elements altered were (B) Media replaced one hour pre transfection with complete DMEM (+10% FBS, 1% P/S and 1% L-Glutamine). (C) Media changed one hour pre transfection to DMEM only. (D) Media changed six hours post transfection to DMEM only. (E) Incubation of the transfection mix for 30 minutes at 37°C, instead of RT. (F) Glycerol shock utilized at the point of transfection. (G) Different particle density of transfection solution, 200µl/2ml instead of 120µl/2ml. (H) Different particle density of 400µl/2ml for transfection solutions

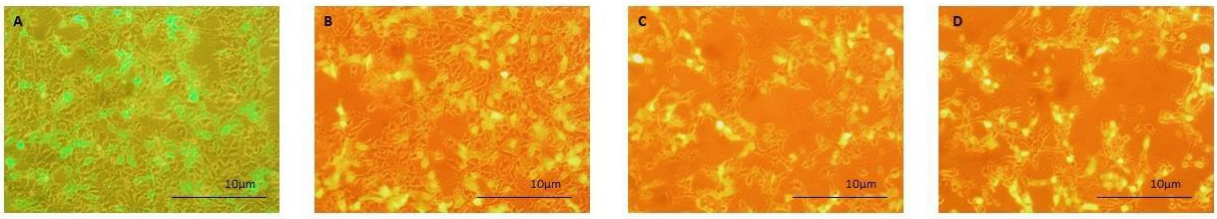

Figure 26. Optimising the DNA quantity used in calcium phosphate transfections.

1µg of DNA was used as standard (A) throughout optimisation calcium phosphate transfections in six well plates. This was varied to 2µg (B), 4µg (C) or 8µg (D) DNA/well to identify the optimal quantity. This was assessed using a green fluorescent protein (GFP) plasmid to estimate transfection efficiency.

Following optimization of calcium phosphate transfection protocol, its transfection rate was compared against other reagents to ensure the optimal method was used. Lipofectamine 3000, TransIT LT1 and PEI were compared using efficiency indicated by a GFP plasmid. Lipofectamine 3000 and TransIT LT1 both had increased efficiencies compared to calcium phosphate 24 hours post transfection (Figure 27). However, although lipofectamine 3000 gave an increased efficiency it was more cytotoxic to cells and therefore not used further. PEI efficiency was only greater 48 hours post transfection, leaving TransIT LT1 as the only alternative to the calcium phosphate protocol. TransIT LT1 was used from this point onwards in this study, unless stated otherwise.

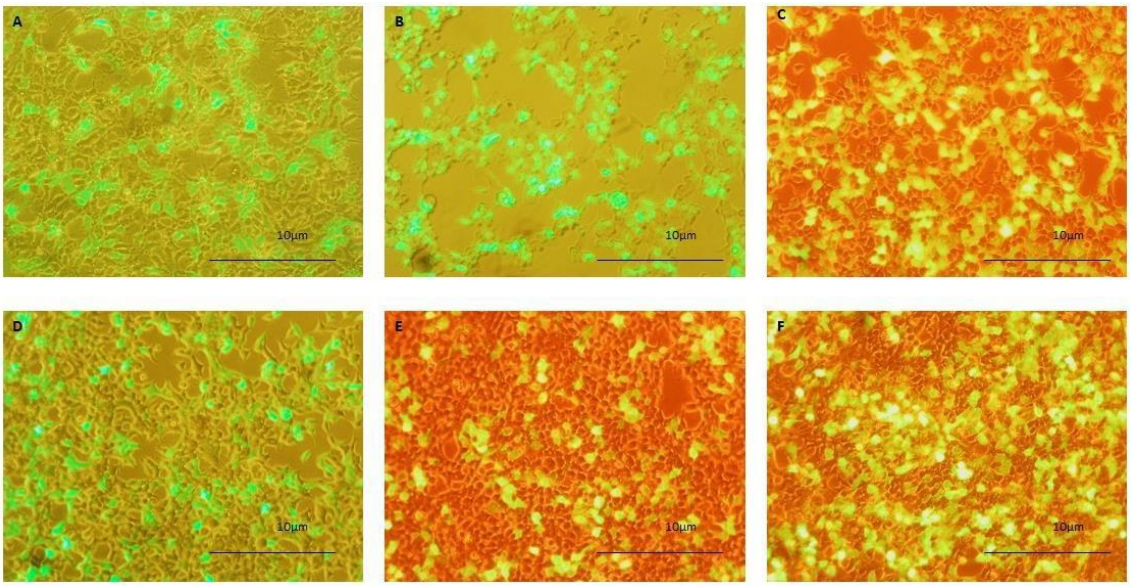

Figure 27. Comparison of transfection efficiencies from various methods and reagents.

The efficiency of the optimized calcium phosphate transfection protocol was assessed against other transfection reagents to ensure the best method was identified. HEK293T cells were transfected with a GFP plasmid to assess the efficiency 24 hours post transfection. (A) Calcium phosphate method, (B) lipofectamine 3000, (C) TransIT LT1, (D) TransIT LT2020, (E) PEI and (F) PEI 48 hours post transfection.

3.3.2.2 Protein expression following expression plasmid transfection

Following transfection optimization, the expression plasmids were transfected into HEK293T cells. This was to confirm that plasmid transfection resulted in transient protein intracellular expression and extracellular secretion that can be used downstream to produce purified recombinant protein. First, SPLUNC1-VR1255 was transfected into HEK293T cells using calcium phosphate, described as 2.1.5.1. Subsequent expression and secretion of SPLUNC1 was expected as the plasmid contains SPLUNC1's secretion signal and SPLUNC1 is secreted in humans. Cell lysate and supernatant were collected 24 hours post transfection and probed for SPLUNC1 protein expression via western blot with SPLUNC1 and His tag antibodies, described as 2.4.4. SPLUNC1 protein expression and secretion was identified 24 hours post

transfection using a SPLUNC1 antibody. However, neither was detected by the His antibody despite its presence in the SPLUNC1-VR1255 DNA sequence (Figure 28). This is likely due to steric hindrance or specificity issues related to the antibody. Therefore, use of anti-His detection was discontinued.

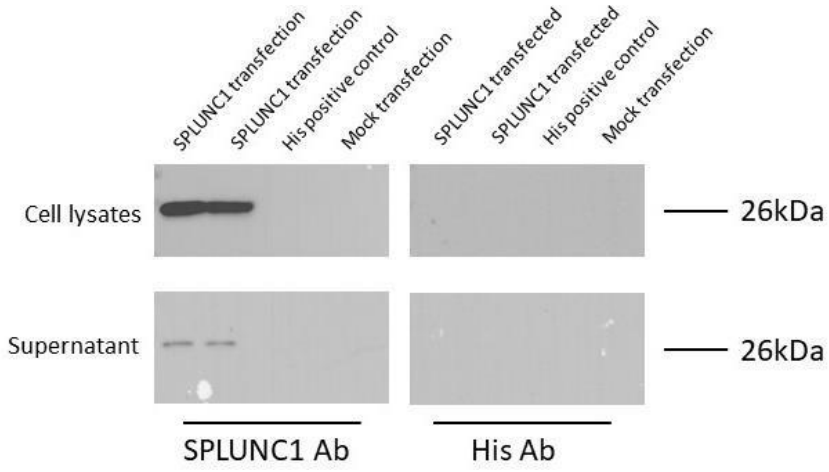

Figure 28. SPLUNC1 is expressed and secreted by HEK293T cells
HEK293T cells were transfected with SPLUNC1 plasmid and incubated for 24 hours. Cell were lysed using SDS then cell lysate and supernatant samples collected and probed for SPLUNC1 and His via western blotting. SPLUNC1 sample lanes are duplicates. His positive control is outer membrane vesicles (OMV) cell extract. Cell lysate membranes were exposed for 10 seconds and the supernatant membrane for 300 seconds.

Following SPLUNC1 expression, detection of SpD was attempted. SpD-VR1255 was transfected into HEK293T cells and incubated for 24, 48 or 72 hours. Intracellular SpD expression was detected in cell lysate at each timepoint however, no SpD secretion was detected at all (Figure 29). Although, SpD has a molecular weight of 40kDa it was identified throughout with a double band at 40kDa. This is due to some SpD protein undergoing post-translational modification. To identify whether this was due to a low concentration of SpD present in the supernatant, supernatant collected 24 hours post transfection was concentrated using a 10 kDa centrifugal filters then probed via

western blot for SpD protein secretion, described as 2.4.4. However, no secreted SpD was detected in concentrated supernatant either (Figure 29).

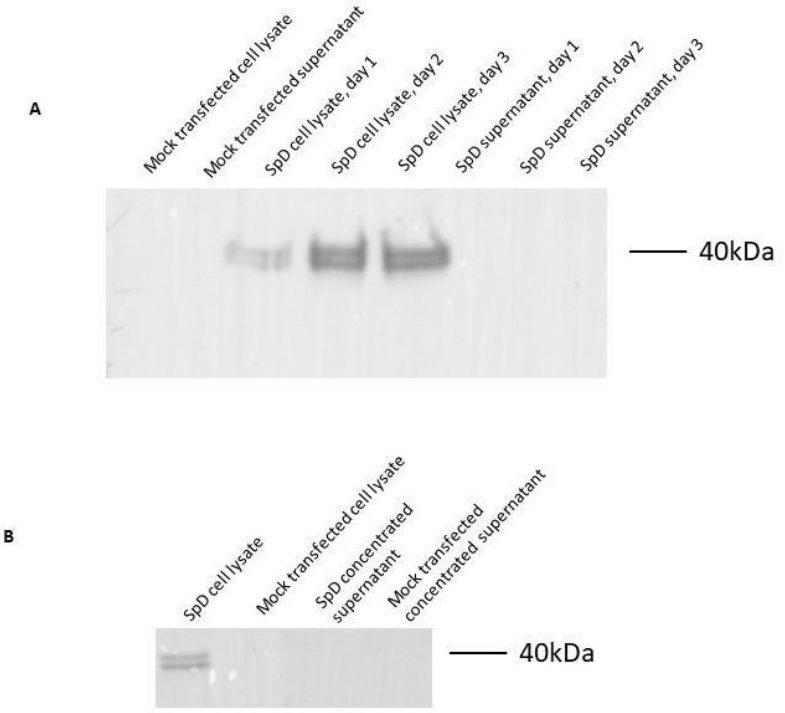

Figure 29. SpD is only expressed intracellularly and is not secreted extracellularly by HEK293T cells.
(A) HEK293T cells were transfected with SpD plasmid and left for 24-72 hours. Cell were lysed using SDS then cell lysate and supernatant samples were collected and probed for SpD via western blotting. Membrane was exposed for 210 seconds. (B) HEK293T cells were transfected with SpD plasmid and left for 24 hours. Cell were lysed using SDS then cell lysate and supernatant samples were collected. Supernatant samples were concentrated using centricon 10 kDa centrifugal filter at 14000rpm for 10 minutes. All samples were probed for SpD via western blotting and the membranes were exposed for 180 seconds.

3.3.2.3 Troubleshooting SpD secretion pathway

The absence of SpD secretion post-transfection was investigated as it is required to produce purified recombinant protein for downstream assays. SignalP was used to identify and calculate the strengthen of SpD secretion signal. This uncovered that although SpD secretion signal was identified by SignalP's algorithm, its strength was

relatively weak at 0.694 (Figure 30). Extracellular SpD secretion following transient plasmid transfection has been observed previously however, a Cystatin S secretion signal was used in this system as opposed to the native SpD secretion signal (261). Cystatin S secretion signal and strength was identified by SignalP at 0.918 (Figure 30). Therefore, the SpD-VR1255 was re-cloned with Cystatin S replacing SpD's secretion signal.

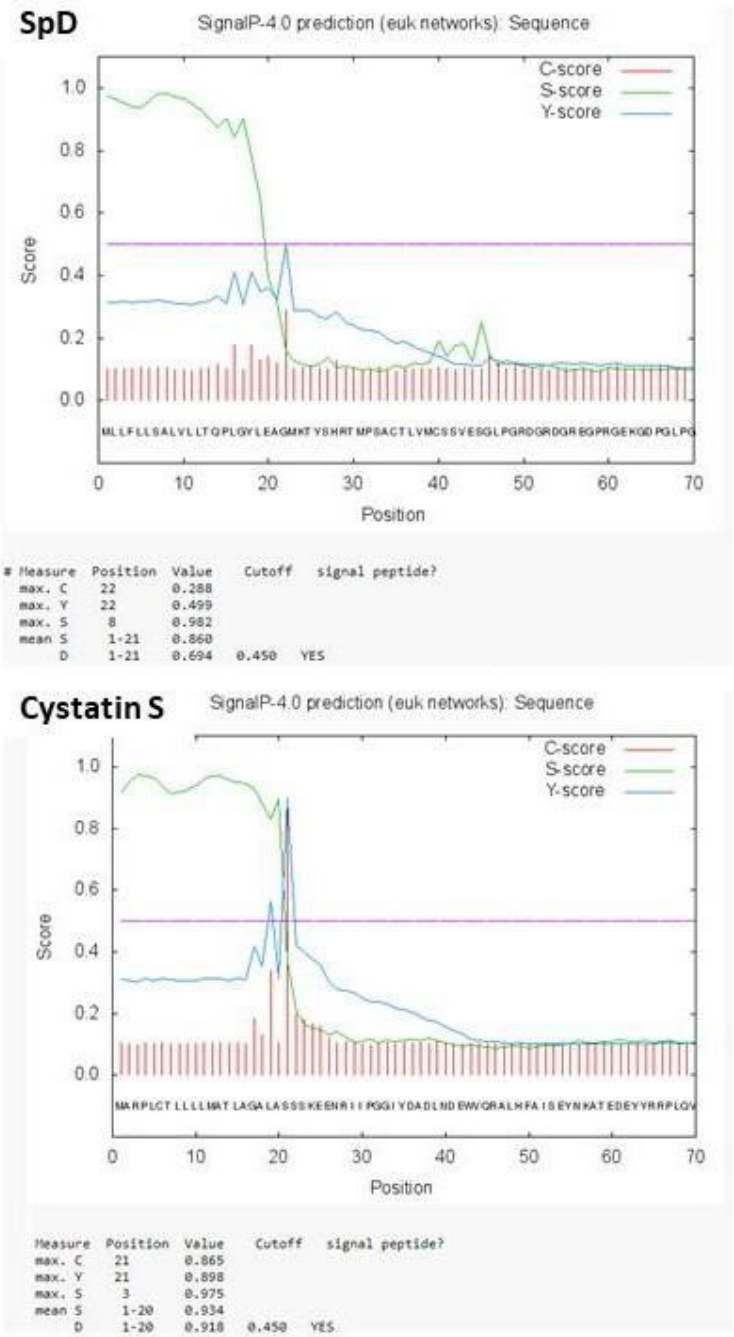

Figure 30. Secretion signal strengths of SpD and Cystatin S calculated by Signal P

Signal P algorithm was used to identify the presence and strength of secretion signals in SpD and Cystatin S DNA sequences. The S-score reports whether each amino acid is part of signal peptide with a high score indicating it is. C-score identifies the secretion signals cleavage site score and the start of the mature protein. The Y-score is a derivative of the C- and S- scores and used to identify the signal peptide cleavage site when more than one C-score peak occurs.

SpD-VR1255 re-cloning was attempted using InFusion cloning methodology. Cystatin

S secretion signal was PCR amplified on an annealing temperature gradient from an

oligonucleotide of Cystatin S full secretion signal (Figure 31). The SpD cDNA sequence insert, excluding the secretion signal, was also PCR amplified (Figure 31). The correct respective bands were gel extracted and cloned into the linearized pVR1255 using Takara InFusion cloning kit. Following transformation, the resulting colonies underwent DNA extraction and were PCR screened for Cystatin S. However, none of

the colonies successfully incorporated the Cystatin S signal secretion sequence (Figure 27). To overcome this issue, a Cystatin S secretion signal – SpD coding sequence DNA construct, with a kozak sequence, 6x His tag and restriction enzyme cloning sites included, was synthesized by GeneArt ThermoFisher (Figure 15).

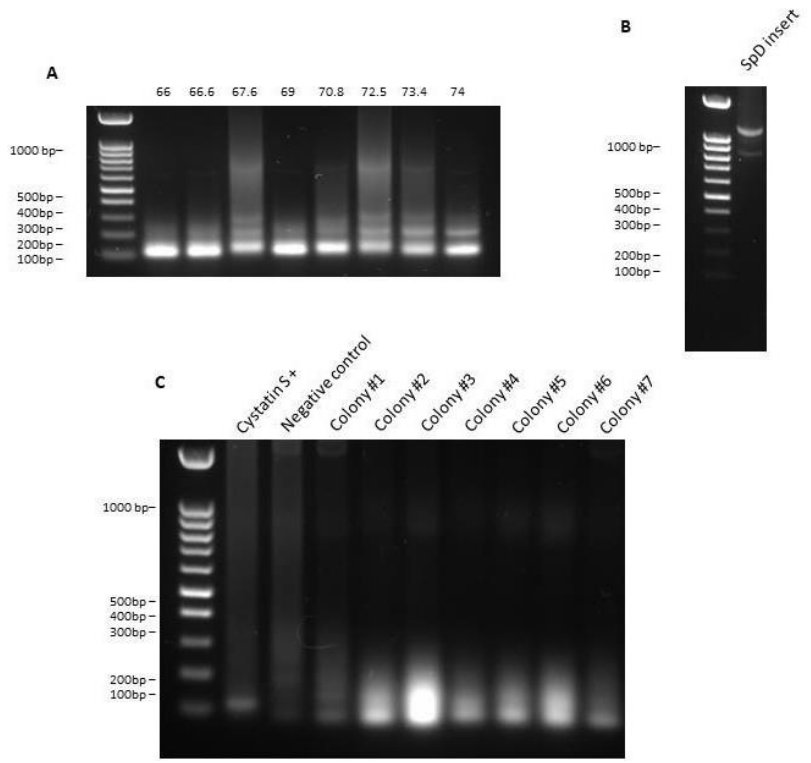

Figure 31. Cystatin S:SpD InFusion cloning and colony screening
(A) Gel electrophoresis was used to visualise the Cystatin S insert produced via PCR amplification with an annealing temperature gradient. (B) Gel electrophoresis was used to visualise the SpD insert produced via PCR amplification from a plasmid template. (C) Seven colonies observed after transformation underwent miniprep and PCR amplication for Cystatin S. Gel electrophoresis used to visualise these products and identify if the Cystatin S insert had been successfully ligated into pVR1255.

The synthesized Cystatin S:SpD fragment was PCR amplified and then digested, alongside the expression vector pVR1255, with the restriction enzymes NotI and BamHI. These products were visualized via gel electrophoresis to check the digested fragments size prior to ligation into pVR1255 (Figure 32), described as 2.2.5. After transformation, DNA was extracted from the colonies, screened for Cystatin S:SpD fragment using BamHI restriction enzyme digest and visualized using gel electrophoresis. This showed five of the six colonies had Cystatin S - SpD correctly inserted and was subsequently confirmed via sequencing (Figure 32).

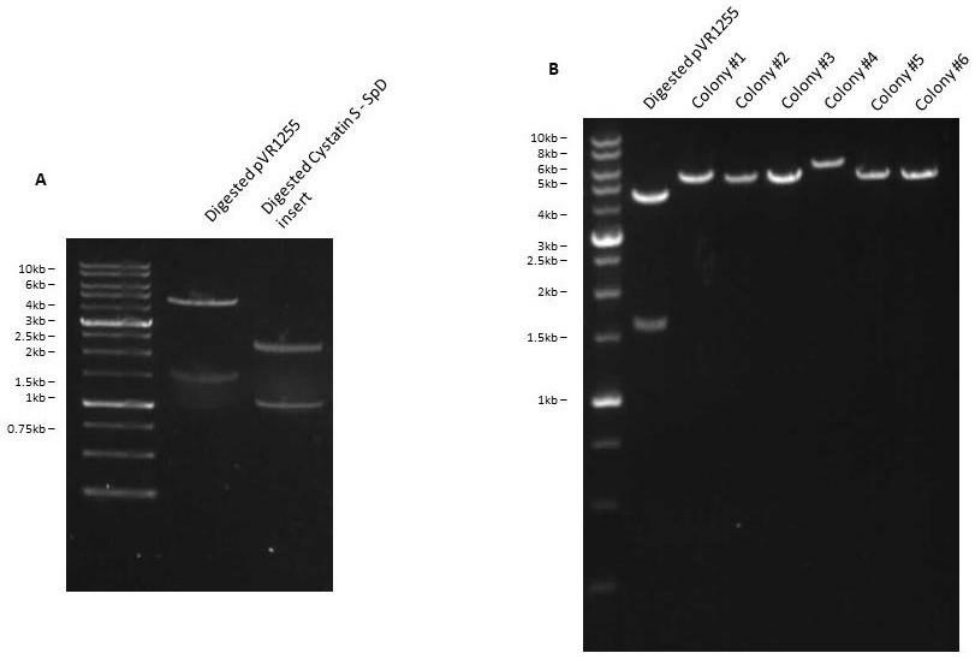

Figure 32. Cloning Cystatin S:SpD fragment into the expression vector pVR1255
(A) Gel electrophoresis was used to visualise the pVR1255 and Cystatin S:SpD insert digested with NotI and BamHI and confirm their molecular size prior to ligation. (B) Six colonies observed after transformation underwent miniprep then were digested with NotI. Gel electrophoresis used to visualise these products and identify if the Cystatin S:SpD insert had been successfully ligated into pVR1255.

Resequencing of the TGFβRII-pVR1255 plasmid showed it had been constructed without a secretion signal so a Cystatin S:TGFβRII fragment was also synthesized by GeneArt (Figure 16). TGFβRII-pVR1255 was then reconstructed via restriction enzyme

cloning with the enzymes NotI and BamHI and the Cystatin S:TGFβRII fragment, as described in 2.2.5 (Figure 33). Colonies underwent DNA extraction via miniprep and were screened for Cystatin S – TGFβRII insertion via NotI digest. Digest products were visualized by gel electrophoresis and where Cystatin S:TGFβRII insertion was indicated, in colonies 2 and 6, sequencing was used to confirm (Figure 33).

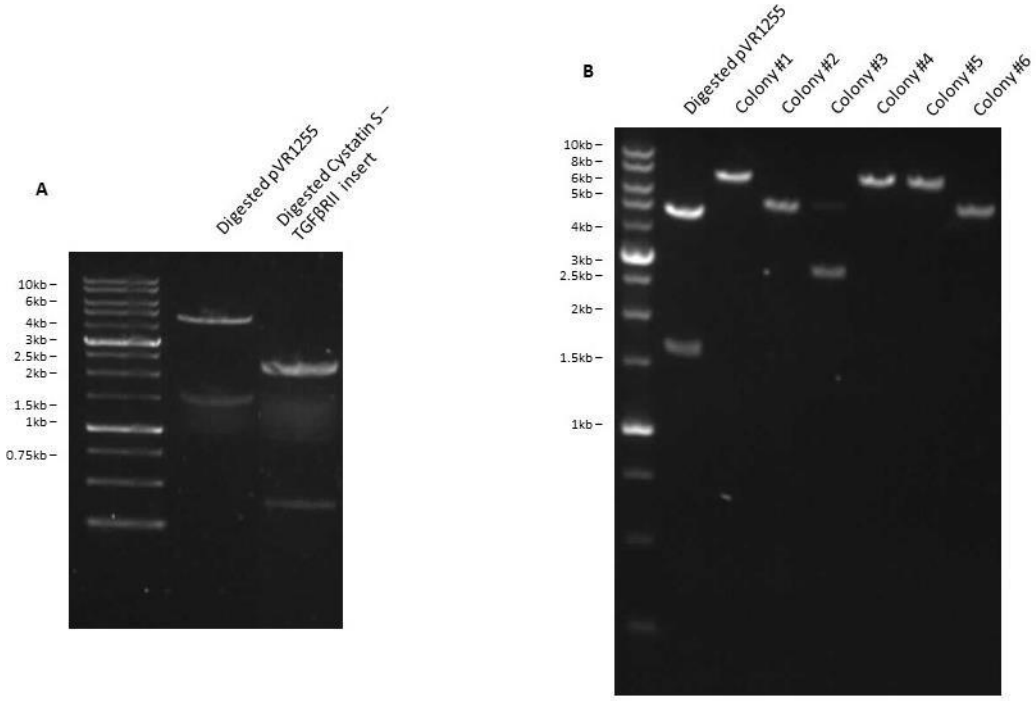

Figure 33. Cloning Cystatin S:TGFβRII fragment into the expression vector pVR1255 (A) Gel electrophoresis was used to visualise pVR1255 and Cystatin S:TGFβRII digested with NotI and BamHI to confirm the products molecular weights after restriction enzyme digest. (B) Six colonies observed after transformation underwent miniprep and were digested with NotI. Gel electrophoresis was used to visualise the products and identify if the Cystatin S:TGFβRII insert had been successfully ligated into pVR1255.

Cystatin S:SpD - VR1255 expression plasmid was transfected into HEK293T cells to establish if a stronger secretion signal resulted in SpD protein secretion. Transfected cells were left for 24 or 72 hours and then cell lysate and supernatant collected. These were probed with SpD antibody by western blot, described as 2.4.4. However, SpD

was still only expressed intracellularly by HEK293T cells and not secreted extracellularly, even 72 hours post transfection (Figure 34).

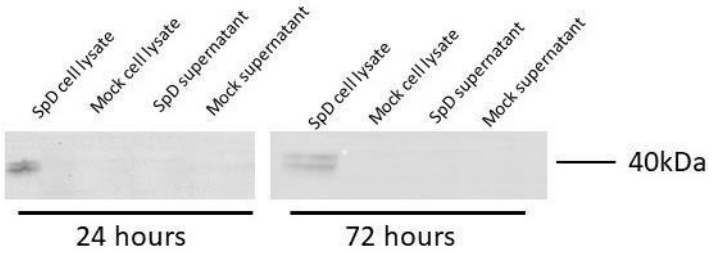

Figure 34. SpD is only expressed and not secreted by HEK293T cells
HEK293T cells were transfected with Cystatin S:SpD plasmid and left for 24 or 72 hours. Cell were lysed using SDS then cell lysates and supernatant samples collected and probed for SpD via western blotting. Membrane were exposed for 270 seconds.

To rule out this being a compatibility problem between the cloning plasmids and HEK293T cells, Cystatin S:SpD – VR1255 expression plasmid was transfected into three different cell lines using calcium phosphate, described as 2.1.5.1. These cell lines were BHK, Jurkat, A549 cells and A549s cells grown in Hams F12 media with an alveolar type II phenotype. 24 hours later, cell lysate and supernatant were collected and probed for SpD secretion however only BHK and A549 cells expressed SpD intracellularly and no SpD extracellular secretion was observed in any cell line (Figure 35).

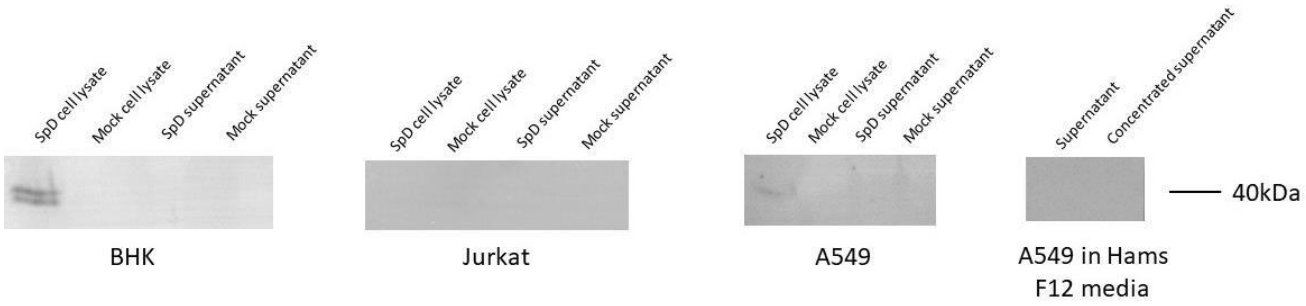

Figure 35. SpD is not secreted by other cell lines
BHK, Jurkat and A549 cell lines were transfected with Cystatin S - SpD plasmid and incubated for 24 hours before cell lysate and supernatant samples were collected and probed for SpD via western blotting. A549 cells were also grown in Hams F12 nutrient mix media for 3 weeks then supernatant samples taken and concentrated using centricon 10 kDa centrifugal filter. These were also probed for SpD via western blotting. All membranes were exposed for up to 420 seconds.

Lastly, HEK293T cells were transfected with SpD-VR1255 and Cystatin S:SpD - VR1255 plasmids and incubated for 6 days, to ensure that sufficient time was allowed for protein expression and proteins with a low concentration in supernatant to be observed. Afterwards, cell lysate, supernatant and 20-fold concentrated supernatant samples were probed for SpD protein expression and secretion, described as 2.4.1. The transfection of both SpD plasmids resulted in SpD protein expression and secretion, although this is only detected in the concentrated supernatant sample (Figure 36).

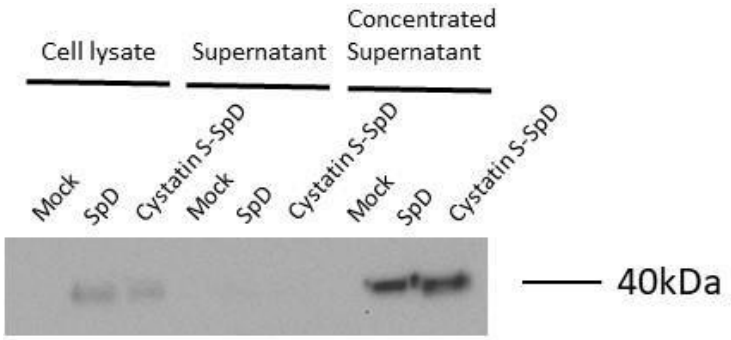

Figure 36. SpD can be detected in supernatant when incubated for six days and concentrated 20-fold.
HEK293T cells were transfected with SpD or Cystatin S-SpD plasmids and left for six days. Cells were lysed using SDS then cell lysate and supernatant samples collected. Supernatant samples were concentrated using centricon 10 kDa centrifugal filters by 20-fold via centrifugation at 14000rpm for 10 minutes. All samples were probed for SpD via western blotting and membranes exposed for 210 seconds.

Following this, SPLUNC1-VR1255 and Cystatin S:SpD – VR1255 were transfected into HEK293T cells and left for 6 days prior to probing for protein expression in cell lysate, supernatant and concentrated supernatant. This is to ensure that both SPLUNC1 and SpD proteins can be secreted in identical settings to allow their use in parallel, downstream applications. The secretion of SPLUNC1 and SpD is observed in concentrated supernatant from days 3-6 after transfection (Figure 37).

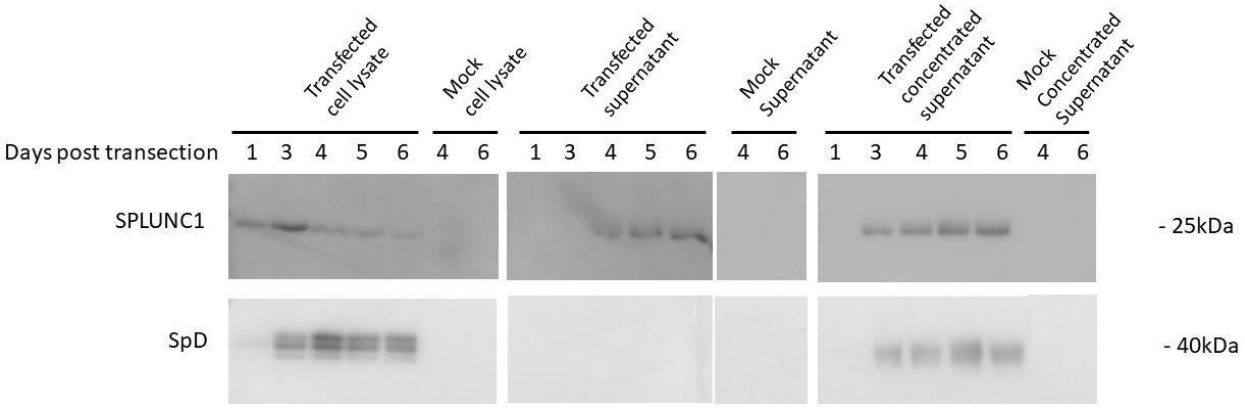

Figure 37. SPLUNC1 and SpD expression 1, 3, 4, 5 and 6 days after transfection

HEK93T cells were transfected with SPLUNC1 and Cystatin-SpD plasmids and incubated for 6 days. Supernatant samples were concentrated 20-fold using centricon 10 kDa centrifugal and centrifugation at 14000rpm for 10 minutes. All samples were probed for SPLUNC1 or SpD via western blotting and membranes exposed up to 180 seconds**.**

3.3.2.4 TGFβRII expression

Following the construction of Cystatin S:TGFβRII expression plasmid, it was investigated whether transfection resulted in protein expression. This is so purified recombinant TGFβRII ectodomain can be produced and used as a negative control for downstream SPLUNC1 binding experiments. The Cystatin S – TGFβRII plasmid was transfected into HEK293T cells using calcium phosphate, described as 2.1.5.1. 24 hours later cell lysate and supernatant samples were prepared and probed for TGFβRII via western blotting, described as 2.4.4. However, no TGFβRII protein expression was detected (Figure 38).

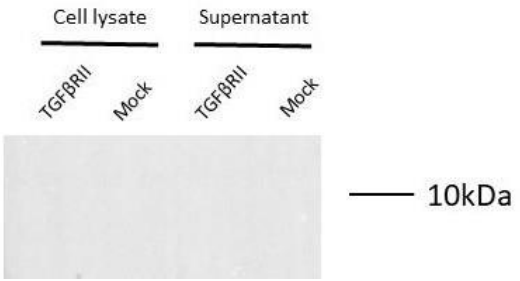

Figure 38. No TGFβRII expression or secretion was detected following transfection. Cystatin S:TGFβRII ectodomain plasmid was transfected into HEK293T cells. 24 hours later cells were lysed using SDS then cell lysate and supernatant samples collected and probed for TGFβRII (AF1003) via western blot. Membranes were exposed for 500 seconds.

Western blotting was then performed on TGFβRII positive controls samples, A549 and NK92 cell lysates, and Cystatin S:TGFβRII – pVR1255 plasmid transfected cell lysates to establish an effective, accurate protocol. Western blotting was performed with two antibodies, each with three concentrations and blocking buffers to identify TGFβRII expression. However, none of these antibodies or conditions detected TGFβRII expression in positive controls or test samples (Figure 39). Therefore, it was decided to use the empty pVR1255 vector as a negative control.

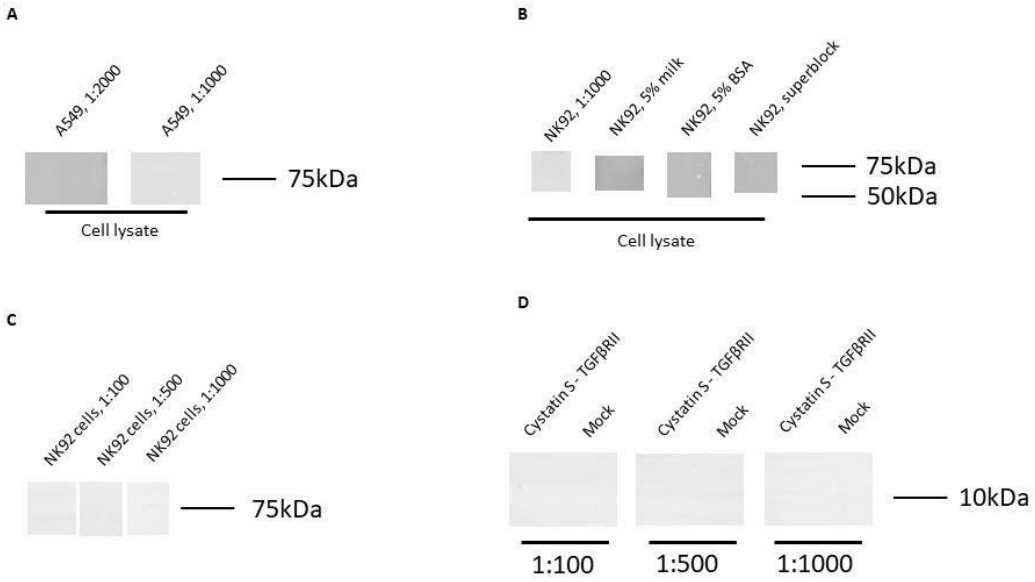

Figure 39. TGFβRII expression was not identified any positive control or test sample

TGFβRII expression was not detected from A549 or NK92 cell lysate or Cystatin S:TGFβRII expression plasmid transfection. (A) A549 cell lysate samples were probed for TGFβRII (AF1003) via western blot with two antibody dilutions; 1:2000 or 1:100, 1:2000 was utilised elsewhere unless stated otherwise. (B) NK92 cell lysate was probed for TGFβRII (AF1003) via western blot with one of three blocking buffers: 5% milk in Tris Buffered saline with 1% tween-20 (TBS-T), 5% BSA in TBS-T or superblock. 5% milk in TBS-T was used unless stated otherwise. (C) NK92 cell lysate samples were probed for TGFβRII (AB78419 – clone number: MM0056-4F14) via western blot with one of three antibody dilutions: 1:100, 1:500 or 1:1000. (D) Cell lysates from HEK293T cells transfected with Cystatin S:TGFβRII plasmid were probed for TGFβRII (AB78419 – clone number: MM0056-4F14) via western blot. All membranes were exposed for 500 seconds.

3.3.3 Human SPLUNC1 is not N-glycosylated

It has been shown previously that mouse SPLUNC1 is N-glycosylated however it is unknown whether human SPLUNC1 protein is also N-glycosylated. To establish this SPLUNC1-VR1255 was transfected into HEK293T cells alongside a mouse SPLUNC1 plasmid with or without the presence of tunicamycin, which inhibits N-glycosylation (262). 24 hours later cells were lysed with SDS and visualized with human and mouse SPLUNC1 antibodies, respectively, via western blotting, described as 2.4.4. Treatment

with tunicamycin at 5 µg/ml confirmed that mouse SPLUNC1 is indeed N-glycosylated but human SPLUNC1 is not (Figure 40).

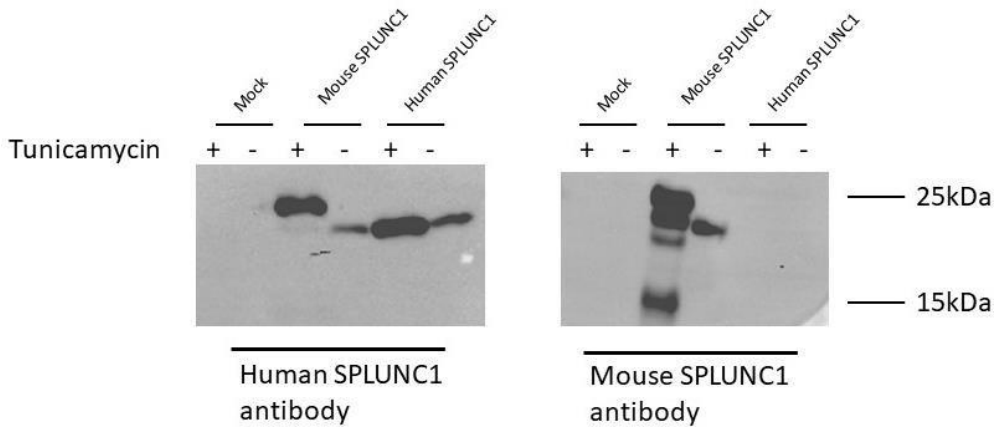

Figure 40. Human SPLUNC1 is not N-glycosylated
Human or mouse SPLUNC1 plasmids were transfected into HEK293T cells and incubated with or without 5 µg/ml tunicamycin, which inhibits N-glycosylation, for 24 hours. Cells were lysed using SDS then cell lysate samples collected and probed with human or mouse SPLUNC1 antibodies via western blot. Membranes were exposed for 300 seconds.

To establish if other isoforms of human SPLUNC1 protein are consistently expressed or undergoing N-glycosylation, human SPLUNC1 plasmid was transfected into HEK293T cells cultured in either complete DMEM supplemented with 10% FBS, 1% P/S and 1% L-glutamine or DMEM only and in the presence of either tunicamycin at 0.5 or 5 µg/ml. 6 days later, cell lysate and supernatant samples at neat, 10 fold or 45 fold concentrations were probed for SPLUNC1. No N-glycosylation or other SPLUNC1 isoforms were detected under any condition, in any sample (Figure 41).

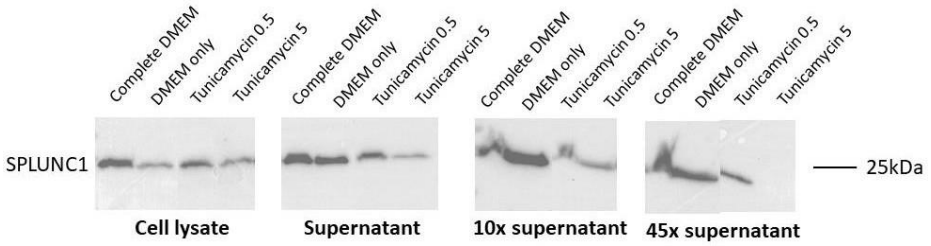

Figure 41. Human SPLUNC1 is not N-glycosylated or secreted in other isoforms
SPLUNC1-VR1255 plasmid was transfected into HEK293T cells and incubated for 6 days in various conditions: complete DMEM media (DMEM supplemented with FBS, P/S and L-glutamine), DMEM only, and the addition of 0.5 or 5 µg/ml tunicamycin. Cells were lysed using SDS, supernatant collected and concentrated using Centricon Ultra-15 10 kDa filters. These samples were probed with human SPLUNC1 antibodies via western blot. Membranes were exposed for up to 180 seconds.

3.3.4 SPLUNC1 protein purification

Expression plasmids used in these experiments were constructed with a 6x His tag located at the 3' end of the cDNA sequence. This was to enable protein purification via immobilized metal ion affinity chromatography (IMAC) using Ni-IDA resin. Ni-IDA resin contains immobilized Ni^{2+} ions that are usually bound by water but are displaced by histidine residues, enabling purification. Ni-IDA resin was selected to purify recombinant protein as it is silica based and preferred to an agarose-based resin that encourages non-specific binding.

This was first trialed with SPLUNC1-VR1255 plasmid on a small scale to establish proof of concept. Supernatant was collected 24 hours post transfection of HEK293T cells using calcium phosphate and purified using Ni-IDA resin, described as 2.4.6. Transfections were completed in a serum-free media to prevent non-specific binding of fetal bovine serum to Ni-IDA resin during purification. Purified protein was eluted in three separate fractions using 250 mM imidazole, then separated by weight via SDS-PAGE and stained with coomassie and silver stains to visualize proteins.

Coomassie staining is known to be less sensitive than silver staining and it was unable to detect any protein in the eluted fractions at 25 kDa, the molecular weight of SPLUNC1 (Figure 42). Proteins at 25 kDa were detected in the elution fractions using silver staining, demonstrating the increased sensitivity of silver staining is required to visualize the proteins present in eluent fractions following protein purification (Figure 42).

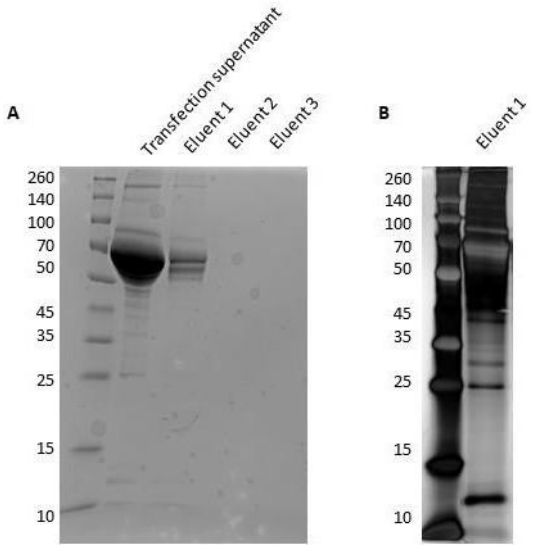

Figure 42. Silver staining is needed to visualise proteins present in the eluent fractions. HEK293T cells were transfected with SPLUNC1 plasmid. Supernatant was collected 24 hours post transfection and purified using Ni-IDA resin. SPLUNC1 was eluted from Ni-IDA resin in 3 fractions using 250 mM imidazole. The eluent fractions collected from purification were ran on SD-PAGE gels alongside the input supernatant. (A) Coomassie staining was used to visualise the proteins present in the fractions following purification. (B) Eluent 1 visualised with silver staining, instead of coomassie.

The initial pilot of SPLUNC1 purification was performed with the flow through collected from each purification stage to identify if recombinant SPLUNC1 protein was successfully bound to Ni-IDA, the washes were removing any bound protein and

if SPLUNC1 was being eluted. These fractions were visualized using western blotting with a SPLUNC1, described as 2.4.4. Western blotting indicated that SPLUNC1 was only present in the initial input and first eluent fraction confirming proof of principle and that Ni-IDA can be used to purify SPLUNC1 protein from transfected supernatant (Figure 43). However, silver staining of the first eluent demonstrates the low purity of this fraction and the need for further optimization to produce purified recombinant SPLUNC1 protein (Figure 43).

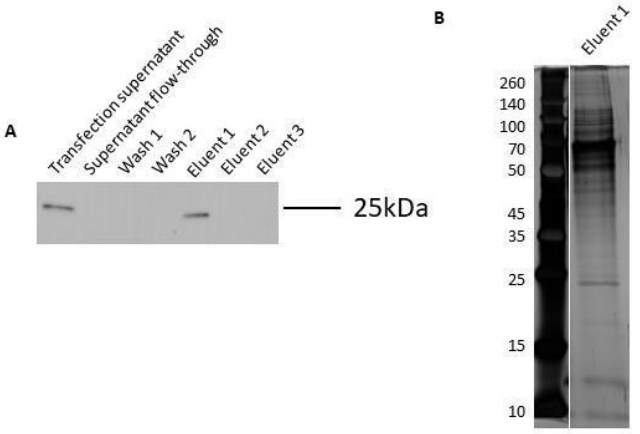

Figure 43. SPLUNC1 can be purified and eluted using Ni-IDA resin
HEK293T cells were transfected with SPLUNC1 plasmid. 24 hours later supernatant was collected and purified using Ni-IDA resin. (A) All fractions from purification were collected and underwent western blotting. The membrane was exposed for 210 seconds (A). (B) Silver staining was used to visualise the proteins present in eluent fraction 1 following purification.

To ensure that all SPLUNC1 protein was eluted from the Ni-IDA resin after purification Ni-IDA resin was mixed with 2x sample buffer to remove any remaining, separated by SDS-PAGE then probed for SPLUNC1 protein via western blotting, described as 2.4.4. This identified that SPLUNC1 was still present following purification and not all protein was eluted in the three fractions (Figure 44). Therefore, purification was

repeated with this Ni-IDA resin to remove all the SPLUNC1 protein however, SPLUNC1 was still present after repurification demonstrating a harsher buffer is required for SPLUNC1 elution (Figure 44).

Figure 44. SPLUNC1 protein remains bound to Ni-IDA resin after the purification protocol.
(A) After purification Ni-IDA resin was mixed with 2x sample buffer then separated by SDS-PAGE gel and underwent western blotting. (B) The resin was re-purified after discovering SPLUNC1 remains stuck to Ni-IDA resin following purification. Afterwards this sample was mixed with 2x sample buffer, separated by SDS-PAGE gel then underwent western blotting. Both membranes were exposed for 240 seconds.

To ensure complete elution of SPLUNC1 protein from Ni-IDA resin, the elution buffer was modified and re-purification of used Ni-IDA resin completed with increasing concentrations of imidazole with and without the presence of CHAPS. CHAPS was selected as a zwitterionic detergent that has no charge, it does not denature proteins and can be removed by dialysis. The first eluent fraction and resin post re-purification were probed for SPLUNC1 protein by western blot to identified if the alternative elution buffers removed the remaining SPLUNC1 protein. SPLUNC1 was only completely removed from Ni-IDA resin by 1M imidazole or with an elution buffer containing 2% CHAPS and 250 mM imidazole (Figure 45). This was determined as even though SPLUNC1 is not present in any eluent fractions it was no longer present

on the resin after re-purification. It is likely it was not detected in the eluents as it was at too low a concentration or lost during the procedure to non-specific binding.

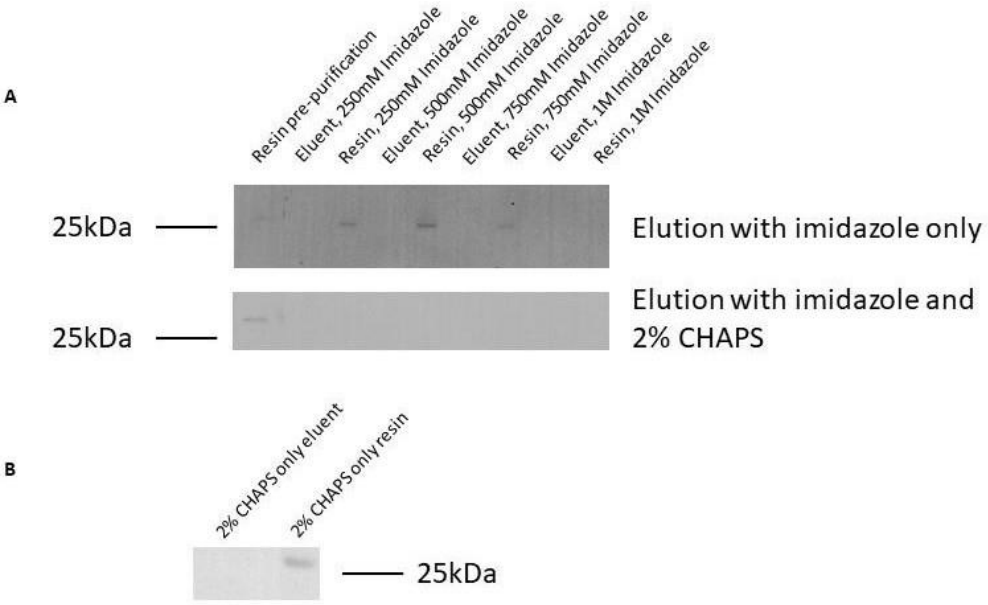

Figure 45. SPLUNC1 protein is only removed from NI-IDA resin by an elution buffer containing imidazole and CHAPS or high concentration imidazole
(A) Resin used in previous purification attempts was re-purified with various imidazole concentrations (250 mM – 1 M) with and without 2% CHAPS present. All eluent and resin samples were collected and subsequently underwent western blotting. (B) Resin used in previous purification attempts was re-purified with only 2% CHAPS. Samples were collected and subsequently probed for SPLUNC1 via western blotting. Both membranes were exposed for 210 seconds.

Although the elution of SPLUNC1 protein has been optimized the eluent fractions still contain numerous contaminating proteins. To combat this, the washing steps used increased in size and frequency. Silver staining showed the positive impact of these changes on eluent purity (Figure 46). Therefore, these washing changes were kept in the protocol for protein purification from transfected supernatant. Yet overall, the low purity of SPLUNC1 protein yielded meant the transfection and concentration of secreted SPLUNC1 protein was used instead generating purified recombinant

SPLUNC1 protein to use in downstream experiments, despite optimization of the protocol.

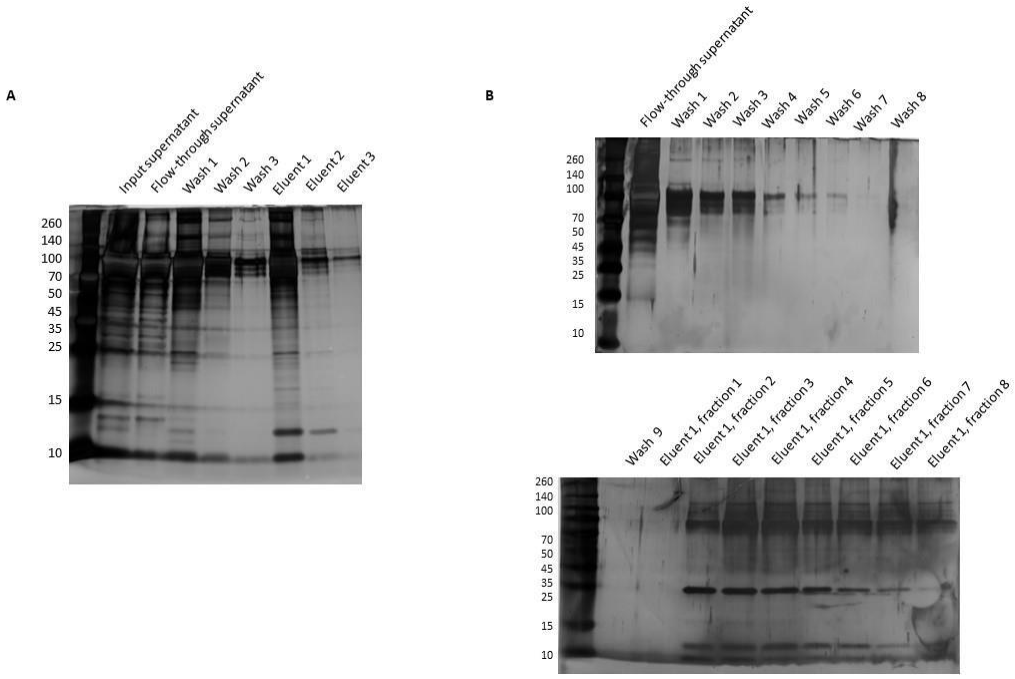

Figure 46. Extra washes improve the purity of eluent fractions
HEK293T cells were transfected with SPLUNC1 plasmid. 24 hours later supernatant was collected and purified using Ni-IDA resin. All fraction from purification were collected, ran on a SDS-PAGE gel and visualised using silver staining. (A) Purification protocol involved three wash steps whereas (B) involved ten wash steps.

3.3.5 SPLUNC1 does not interact with IAV

3.3.5.1 Human SPLUNC1

It was originally planned to use purified recombinant protein to investigate whether SPLUNC1 directly interacts with an Influenza A Virus (IAV) and mediates SPLUNC1 antiviral activity during infection. Due to the above findings, concentrated supernatant collected 6 days post-transfection was used as an alternative. Alongside the SPLUNC1 investigation SpD was used as a positive control because it has been

shown previously to interacts with IAV (74). The empty pVR1255 plasmid was the negative control for these experiments.

First, SPLUNC1 pulldown was optimized, to do so SPLUNC1-VR1255 was transfected into HEK293T cells and the supernatant collected 6 days later then concentrated using Amicon centrifugal filters. The concentrated SPLUNC1 supernatant was then mixed with Ni-IDA resin under various conditions for up to 30 minutes to identify the optimum conditions for binding. Once complete, Ni-IDA was mixed with sample buffer to elute bound protein. These were separated using SDS-PAGE then visualized by western blotting, described as 2.4.4. This identified that SPLUNC1 bound to Ni-IDA resin best under resuspension for 30 minutes (Figure 47).

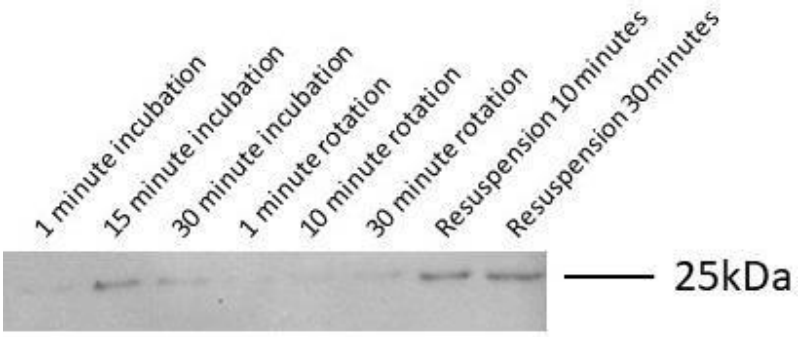

Figure 47. Optimising the SPLUNC1-Ni-IDA resin interaction for immunoprecipitation experiments.
SPLUNC1 transfected supernatant was incubated with Ni-IDA resin under different conditions to identify the optimum conditions for SPLUNC1 pulldown. The supernatant was mixed with Ni-IDA resin and either: incubated for 1-30 minutes, mixed in suspension for 1-30 minutes or incubated for 10-30 minutes with repeated resuspension every 5 minutes. Samples were separated via SDS-page electrophoresis then underwent western blotting. Membranes were probed for SPLUNC1 and exposed for 60 seconds.

After SPLUNC1 precipitation was optimized, the most effective crosslinking method was investigated. This was to ensure that any weak or labile protein-protein interactions were preserved and would be detected. Formaldehyde and DSS were

both evaluated as crosslinking agents at various concentrations using IAV X31 to identify which is superior and best to use as a crosslinking agent during immunoprecipitation. IAV X31 subsequently underwent western blotting with samples prepared under reducing and non-reducing conditions, described in 2.4.1. This revealed that although formaldehyde is an effective crosslinking reagent, indicated by the absence of lower, 25 kDa, molecular weight bands as its concentration increases, DSS is a more effective at both 3 and 5 mM (Figure 48). 3 mM DSS was selected to use during immunoprecipitation experiments as increasing the concentration further to 5 mM does not increase its activity.

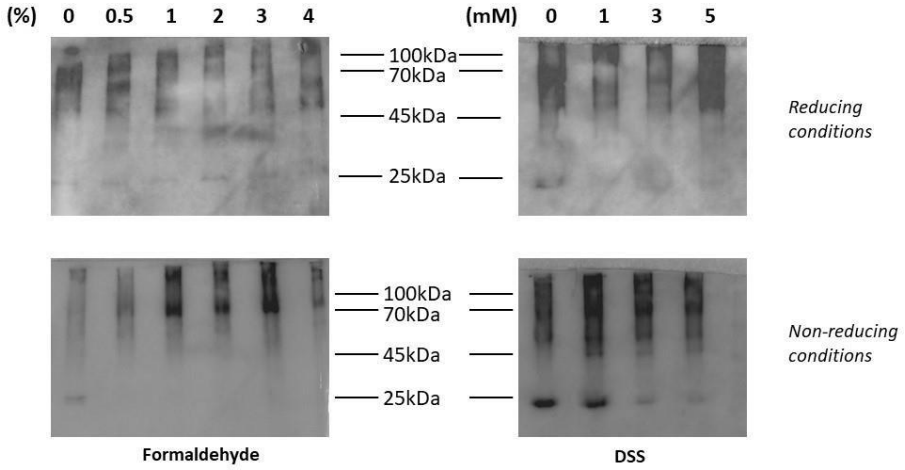

Figure 48. Evaluation of cross-linking reagents using IAV-X31.
IAV X-31 was crosslinked with various concentrations of formaldehyde (0-4%) or DSS at room temperature. Reactions were quenched with 125 mM and 20 mM glycine respectively. Samples were separated via SDS-page electrophoresis then underwent western blotting with anti-SPLUNC1.

Experiments to investigate if SPLUNC1 bound IAV were completed in parallel with SPLUNC1-VR1255 and mock, empty pVR1255, concentrated supernatant collected 6 days after transfection. Experiments were performed on concentrated supernatant spiked with IAV X31, in the presence and absence of TPCK trypsin. SPLUNC1 was

immunoprecipitated with Ni-IDA resin, washed, then eluted with SDS. These samples were then separated by weight using SDS-PAGE and probed with SPLUNC1 and IAV (H3N2) antibodies to establish if SPLUNC1 was successfully precipitated and if IAV was pulled down with SPLUNC1, indicating an interaction was occurring. No IAV proteins were detected following SPLUNC1 immunoprecipitation, indicating an interaction is not occurring and this result was reproduced in three independent experiments (Figure 49).

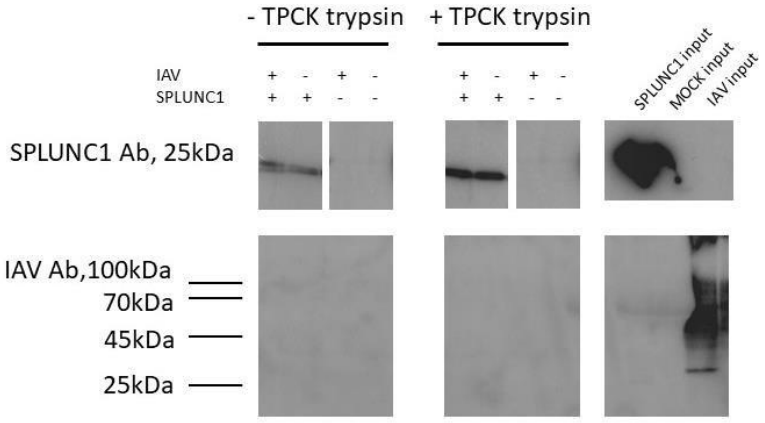

Figure 49. No interaction between SPLUNC1 and IAV is indicated.
An immunoprecipitation reaction was performed on supernatant collected from HEK293T cells 6 days after transfection with SPLUNC1-VR1255 plasmid and concentrated using Amicon Ultra-15 10 kDa filters. Samples were mixed with X31 IAV for 1.5 hours at 37^{o}C, crosslinked with DSS then immunoprecipitation using Ni-IDA resin. Washes were performed with RIPA buffer. SPLUNC1 was eluted from the Ni-IDA after the immunoprecipitation using SDS. These samples underwent western blotting with anti-SPLUNC1 and anti-IAV. Membranes were exposed for up to 180 seconds. This immunoprecipitation was performed with and without the presence of TPCK trypsin. This experiment has been performed three separate times.

SpD immunoprecipitation was completed alongside the above experiment as a positive control to demonstrate our approach can detect protein-protein interactions involving IAV. Again, concentrated supernatant collected 6 days post transfection was used alongside pVR1255 plasmid mock as a negative control. First, the

immunoprecipitation of SpD itself was attempted using both Ni-IDA resin and a SpD antibody bound to protein A Sepharose (Ab-Sepharose). Immunoprecipitation experiments were performed and the flow through collected from each step alongside the eluents and original input. This was performed under varying conditions to identify those which were optimal. All samples collected were prepared and then probed for SpD via western blot. This identified that SpD is not eluted following its immunoprecipitation using Ni-IDA resin, however the Ab-Sepharose system does successfully pull down SpD and allow its elution for downstream analysis (Figure 50). Therefore Ab-Sepharose was used to immunoprecipitate SpD for further experiments with an antibody dilution of 1:200.

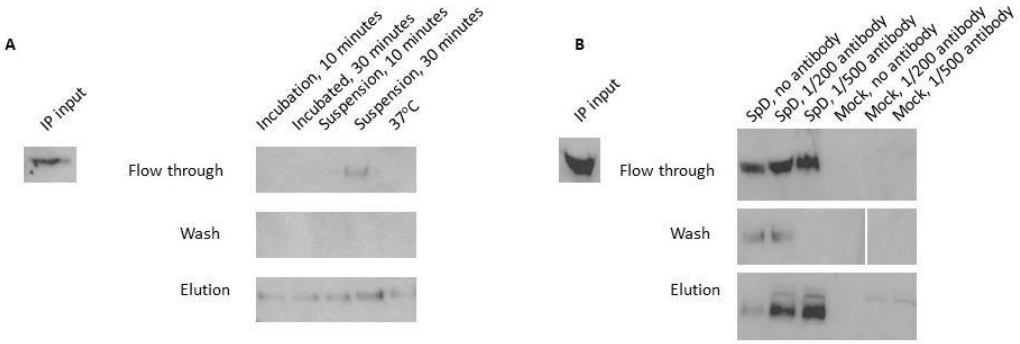

Figure 50. Optimization of SpD immunoprecipiation
Cystatin S:SpD plasmid was transfected into HEK293T cells and left for 6 days. Then the transfected supernatant was collected and concentrated using Amicon Ultra-15 filters. This was used to optimize SpD immunoprecipitation with (A) Ni-IDA resin and (B) Protein A Sepharose and SpD antibody.

SpD concentrated supernatant was spiked with IAV X31 then immunoprecipitated with identical crosslinking, washes and elution conditions as SPLUNC1. However, SpD is only immunoprecipitated when crosslinking with DSS does not take place (Figure 51). Therefore, the experiment was repeated without crosslinking. This identified

that SpD does interact with an IAV protein at 50 kDa, which corresponds to the molecular weight of HA1, in the presence of TPCK trypsin (Figure 52).

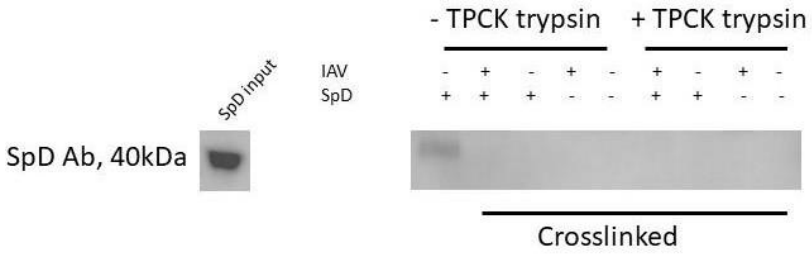

Figure 51. SpD is only immunoprecipitation experiments if no cross linking occurs.

SpD immunoprecipitation was performed with concentrated supernatant, collected 6 days after transfection with Cystatin S:SpD plasmid. It was mixed with X31 IAV for 1.5 hours at 37°C then crosslinked with DSS prior to SpD immunoprecipitation by protein A Sepharose and anti-SpD. Washes were performed with RIPA buffer. SpD was eluted from the Sepharose after immunoprecipitation using SDS. These samples then underwent western blotting with SpD antibody. Membranes were exposed for up to 180 seconds. This immunoprecipitation was performed with SpD concentrated supernatant and IAV X-31 incubated with and without the presence of TPCK trypsin.

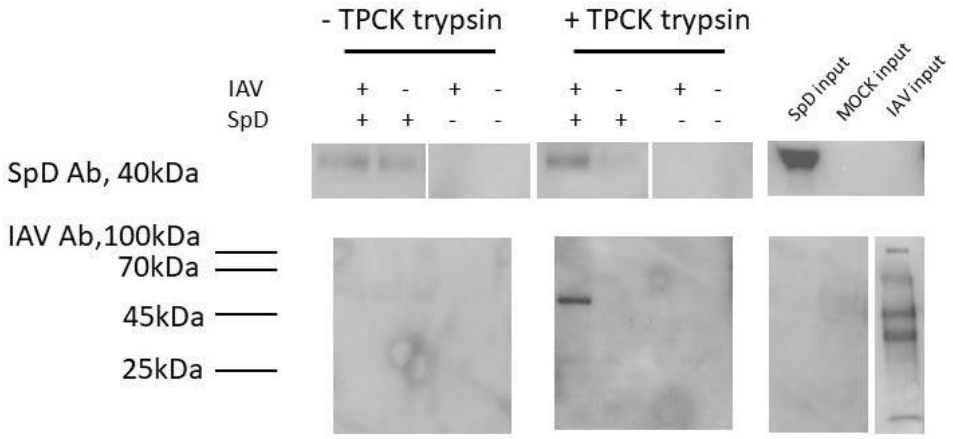

Figure 52. SpD interaction with IAV

An immunoprecipitation reaction was performed on concentrated supernatant, collected from HEK293T cells 6 days after transfection with Cystatin S-SpD plasmid and concentrated using Amicon Ultra-15 10 kDa filters, which had been mixed with X31 IAV for 1.5 hours at 37°C. This was performed with and without the presence of TPCK trypsin. SpD was then immunoprecipitation by protein A Sepharose and SpD antibody. Washes were performed with RIPA buffer. SpD was eluted from the Sepharose after the immunoprecipitation using SDS. These samples then underwent western blotting with SpD and IAV antibodies. Membranes were exposed for up to 180 seconds.

3.3.5.2 Using murine SPLUNC1

To confirm that the conditions used to test *in vitro* interactions of SPLUNC1 and IAV were not masking *in vivo* conditions, BAL fluid containing murine SPLUNC1 (mSPLUNC1) was obtained as an input for immunoprecipitation. Immunoprecipitation of mSPLUNC1 from bronchoalveolar lavage (BAL) samples was attempted using two different anti-murine SPLUNC1 antibodies bound to protein A Sepharose alongside a no antibody control. Flow through samples were collected from each stage alongside the final eluent to identify if any mSPLUNC1 is lost during the experiment. mSPLUNC1 immunoprecipitation was best with antibody A however, this requires further optimization due to loss of protein during washing and not all mSPLUNC1 being immunoprecipitated initially (Figure 53).

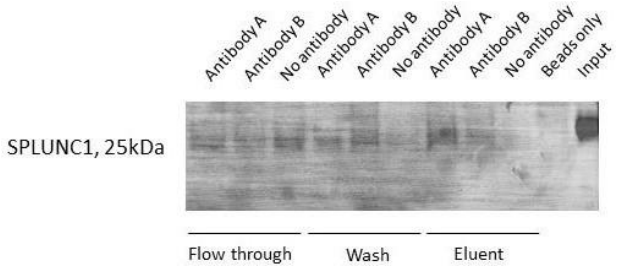

Figure 53. Optimization of mSPLUNC1 immunoprecipitation from WT BAL.
Immunoprecipitation of mSPLUNC1 from WT BAL was completed with protein A Sepharose and mouse SPLUNC1 antibodies A or B. Samples were washed once with RIPA buffer and mSPLUNC1 eluted using SDS in 2x sample buffer. In addition to the eluent, flow through and wash samples were collected and underwent western blotting with SPLUNC1 antibodies. Membranes were exposed for up to 40 seconds.

Further optimization of mSPLUNC1 immunoprecipitation was completed with various conditions altered including temperature, antibody concentrations, wash buffer, incubation times and a free antibody pulldown approach. Again, flow through

samples were collected at each stage and visualized, after being separated by weight using SDS-page, by either silver staining or western blotting, described as 2.4.4. This revealed that mSPLUNC1 immunoprecipitation was only improved when performed with longer incubation times (Figure 54).

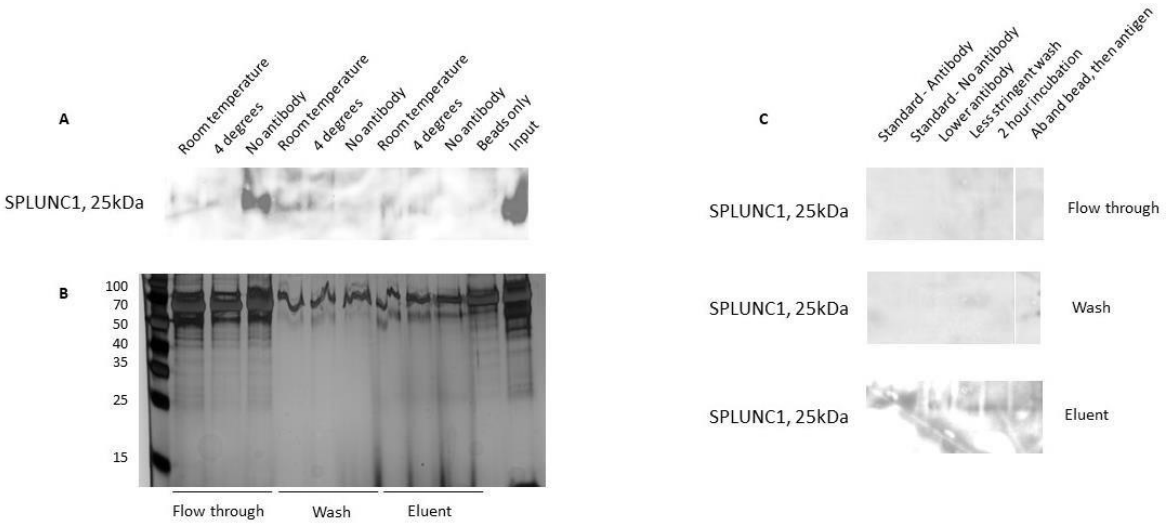

Figure 54. Optimization of mSPLUNC1 immunoprecipitation from WT BAL
(A and B) mSPLUNC1 was immunoprecipitated from WT BAL by protein A Sepharose and mouse SPLUNC1 antibody A at either room temperature for 1 hour or overnight at 4 degrees. Samples were washed once with RIPA buffer. mSPLUNC1 was eluted from the Sepharose after the immunoprecipitation using SDS in 2x sample buffer. Eluent, flow through and wash samples were collected and underwent (A) western blotting with SPLUNC1 antibodies or (B) silver staining. (C) mSPLUNC1 was immunoprecipitated under various conditions. Eluent, flow through and wash samples were collected and visualised via western blotting. All membranes were exposed for up to 40 seconds.

Mouse BAL was primed with IAV X31 then incubated at 37^{o}C for one hour prior to immunoprecipitation and visualization via western blot. This was performed in the presence and absence of TPCK trypsin and revealed that mSPLUNC1 does not interact with IAV when other co-factors or native proteins are present (Figure 55).

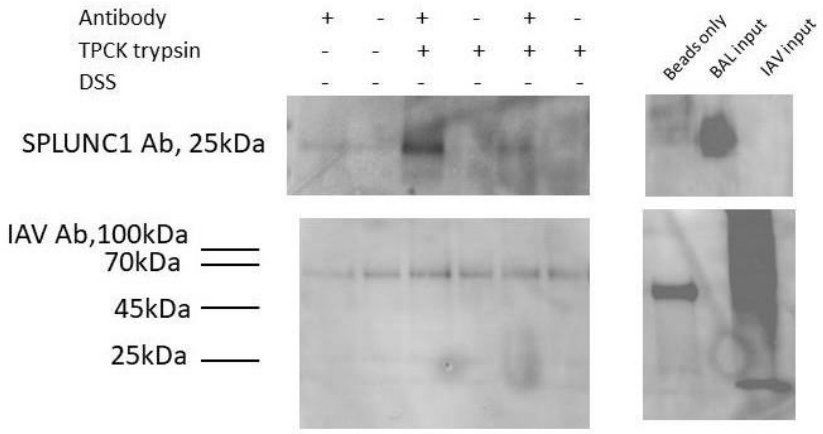

Figure 55. mSPLUNC1 does not interact with an IAV protein in the presence of co-factors

A mSPLUNC1 immunoprecipitation was performed on WT BAL mixed with X31 IAV for 1.5 hours at 37^{o}C. This was performed with and without the presence of TPCK trypsin. SPLUNC1 was then immunoprecipitated by protein A Sepharose and SPLUNC1 antibody. Washes were performed with RIPA buffer. SPLUNC1 was eluted from the Sepharose following immunoprecipitation using SDS. These samples then underwent western blotting with SPLUNC1 and IAV antibodies. Membranes were exposed for up to 60 seconds. Figure is representative of three independent experiments.

3.4 Discussion

This chapter set out to establish whether SPLUNC1 antiviral effect is mediated by a direct interaction between itself and an IAV protein. First, recombinant SPLUNC1 was characterized prior to its use in downstream assays. This demonstrates that human SPLUNC1 does not undergo N-glycosylation, unlike murine SPLUNC1. This is observed even though human SPLUNC1 contains N-glycosylation sequons which are evenly interspersed throughout its length (170, 263). Although human SPLUNC1 can be glycosylated is does not occur in the main isoform present in humans. Together, this suggests that SPLUNC1 function could differ across species and that N-glycosylation might be key to mediating this (170). This suggestion is further supported as murine SPLUNC1 contains an additional amino acid region in exon 2, compared to human SPLUNC1, and the two species only share 66% amino acid similarity (172). The role of the species-specific sequences in SPLUNC1 is currently unclear however, glycosylation is known to be important for human SpD antiviral activity against IAV therefore these species difference could be crucial to how SPLUNC1 functions (74).

Meanwhile the purification of SPLUNC1 revealed CHAPS was required for the complete elution of SPLUNC1 from Ni-IDA resin. CHAPS is a zwitterionic detergent that preserves the native state of proteins and is often used to solubilize proteins that are insoluble due to their hydrophobicity. It is necessary for the elution of SPLUNC1 from Ni-IDA resin as SPLUNC1 has a hydrophobic core and 44% of its total amino acids are hydrophobic (166, 199, 230). This means SPLUNC1 is not very soluble in water and often binds non-specifically to other proteins, particularly lipids. This ability of

SPLUNC1 to bind lipids could be decreasing the availability of the expressed SPLUNC1 protein for purification, due to it already being involved in other interactions or SPLUNC1 binding site itself being occupied. Also, it is likely to partly responsible for the poor purity observed following purification in this thesis and in previously recorded attempts, as these non-specific interactions are purified alongside SPLUNC1 and consequently decrease the overall purity recorded (264). Both these facts contribute to why SPLUNC1 purification, with respect to the aim of producing purified recombinant protein, was unsuccessful in this thesis and other sources were ultimately utilised. However, these factors could influence SPLUNC1 function positively, meaning it acts as a surfactant or via non-specific binding capacity.

Finally, immunoprecipitation experiments with human and murine SPLUNC1 revealed that neither interact with IAV. The fact this result was also observed when BAL was the sample means that other cofactors or proteins that could be needed for an interaction were present. This suggests a direct interaction is likely not responsible for SPLUNC1's antiviral activity during IAV infection and another mechanism is responsible. Nonetheless, there are a few aspects of this experiment that must be considered and could impact these results. Firstly, it is possible the 6x His tag present at SPLUNC1's N-terminus impacts protein folding, and therefore its structure and function. Secondly, SPLUNC1's could already be binding with something else, and its binding site occupied. This would limit the number of other interactions that could occur and ultimately be detected. Finally, a protein or cofactor that mediates mSPLUNC1's interaction with IAV might only be upregulated during IAV infection. Therefore, investigations for this interaction would be more reliable and robust experiment using BAL from an IAV infected mouse.

It is possible that human and murine SPLUNC1 act via distinct mechanisms because only murine SPLUNC1 is N-glycosylated and other species-specific differences. However, this study found that SPLUNC1 from neither species interacted with IAV directly. This means that in the context of its antiviral activity against IAV it is likely that N-glycosylation does not influence SPLUNC1 mechanism of function and is in fact unrelated, given that it does not function via the same mechanism as human SpD. Since SPLUNC1 is not acting via a direct interaction it must be involved in the hosts antiviral response via an alternative mechanism. It is possible that SPLUNC1 is binding itself non-specifically or to other hydrophobic proteins and acting in complex with other proteins or as part of a larger signaling pathway which mediate its effect. Alternatively, its hydrophobicity could reflect its ability to act as a surfactant and this surfactant activity could be crucial to mediating its antiviral activity (199). It is more likely that SPLUNC1 is involved in a larger, overriding immune response pathway or mechanism during IAV and mediating its anti-viral effect. This could be mediated by IL-13. SPLUNC1 expression is down regulated by IL-13 *in vitro* and *in vivo* during human disease (185, 212). It is possible that SPLUNC1 is being modulated by IL-13 during IAV infection as part of a larger signalling pathway or immune complex, that is involved in the hosts antiviral response. To establish this, an *in vivo* experiment should be performed with WT and SPLUNC1 KO mice infected with IAV, and a subset administered with an IL-13 monoclonal antibody. If IL-13 is mediating SPLUNC1 anti-viral activity, then IL-13 antibody administration could lead to IAV infected WT mice having a SPLUNC1 KO phenotype.

Finally, modulation of SPLUNC1 expression has been observed to associate with the timing of IAV infection with expression significantly lower at 5 and 7 d.p.i. before

recovery by day 14 (222). This also occurs during infection with EBV, RV, MHV-68 and *Pseudomonas aeruginosa*. Therefore, this repeating expression pattern may hold clues to SPLUNC1 antiviral function and should be further investigated to establish its role during IAV infection, alongside IL-13. It is possible that IL-13 and SPLUNC1 are both being modulated by the same factor but are affected in opposite ways.

In summary, SPLUNC1 is an antiviral peptide during IAV infection however, a direct interaction between an IAV protein and human or murine SPLUNC1 is not likely responsible for mediating its antiviral effect. Understanding how SPLUNC1 mediates this function is crucial to progressing IAV research and treatment options as it continues to have a significant burden on health globally. Further experiments are needed, such as investigating the roles of IL-13 and variable SPLUNC1 expression during IAV infection, to elucidate how SPLUNC1 mediates its antiviral activity during infection.

4 Engineering an *in vitro* SPLUNC1 deficient cell line

4.1 Introduction

Based on previous data (Chapter 3) and as evident from the published literature, the mechanism by which SPLUNC1 elucidates its antiviral activity during IAV infection is unknown. However, we have established this is not due to a direct interaction with IAV. Therefore, to investigate this an *in vitro* model was established to explore this anti-viral activity and allow comparison between the effect on IAV infection on WT and SPLUNC1 KO cells. SPLUNC1 KO mice have a very distinct, reproducible phenotype and the generation of an *in vitro* SPLUNC1 KO model would be invaluable when investigating how SPLUNC1 functions. CRISPR-Cas9 allows more accurate gene editing with a large degree of control over the specificity and nature of the mutations, compared to other editing tools (265). It can be used to decrease gene expression to knockout levels and identify host factors required for IAV replication and infection. A CRISPR-Cas9 SPLUNC1 KO cell model would help establish whether SPLUNC1 modulates the host response or influenza itself during infection (266). Furthermore, this *in vitro* model would allow the completion of complementation experiments that could be crucial when elucidating exactly how SPLUNC1 operates. This exploration into how SPLUNC1 modulates IAV infection is crucial to advancing research and knowledge into the hosts response to IAV and reducing the burden influenza places on society.

4.2 Aims

The overall aim for this chapter was to use CRISPR-Cas9 gene editing technology to engineer a knockout cell line that was deficient in SPLUNC1 protein and to then utilize it to investigate SPLUNC1's function during IAV infection. Firstly, HBEC3-KT cells were characterized to confirm they were a suitable model for this study. Secondly, CRISPR-Cas9 gene editing technology was applied to KO *splunc1* from HBEC3-KT cells. Finally, the resulting cell line was used to explore the effect of SPLUNC1 KO has on IAV infection.

4.3 Results

4.3.1 Characterization of HBEC3-KT cells

Human bronchiolar epithelial cells immortalized with CDK4 and hTERT, HBEC3-KT cells, were chosen as model to investigate SPLUNC1 role during influenza A Virus (IAV) infection as they are representative of the setting of this antiviral activity *in vivo.* In this thesis these cells will be referred to as KT cells. First, KT cells were characterized when grown in submerged culture in either Keratinocyte Serum Free Media (KT-KSFM), PneumaCult-ExPlus (KT-ExPlus) or PneumaCult-ALI (KT-ALI) medias, described as 2.1.2. KT cells are usually grown in submerged culture with an epithelial-like morphology that is distinct in each media (Figure 56). KT-KSFM cells grow with an elongated polygonal shape. KT-ExPlus cells grow with a similar but more elongated polygonal shape like KT-KSFM cells, however they grow in distinct patches unlike the singular nature of KT-KSFM cells. KT-ALI cells have a polygonal, cobblestone-like morphology without any cell elongation. KT cells can also be cultured and

differentiated to form 3D cell culture models with Air Liquid Interface (ALI) scaffolds in PneumaCult ExPlus and ALI medias.

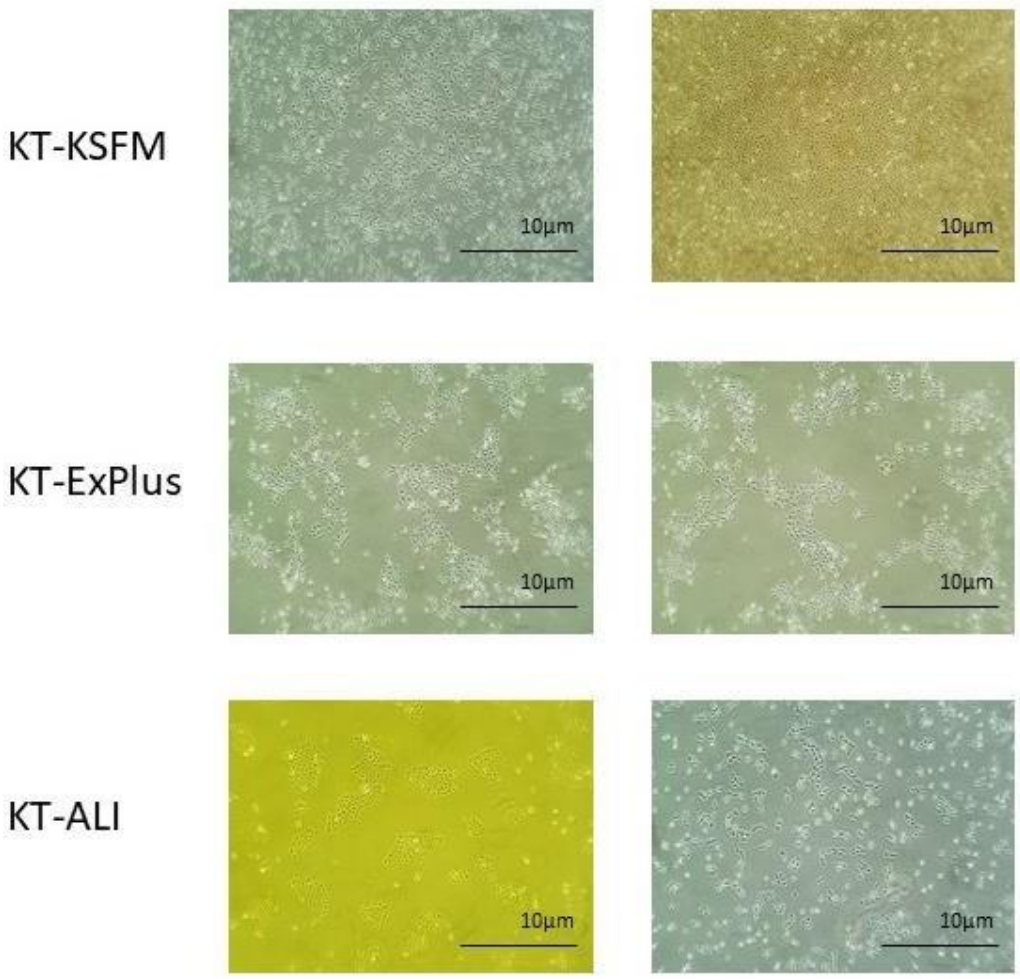

Figure 56. KT cells morphology in different medias
KT cells were grown in submerged culture in either Keratinocyte Serum Free Media (KT-KSFM), PneumaCult ExPlus (KT-ExPlus) or PneumaCult ALI (KT-ALI). Images are duplicated to show cell morphology at different stages of confluence.

SPLUNC1 expression in KT cells was then characterized to establish whether they could be used as a model to investigate SPLUNC1 anti-viral role during IAV infection. SPLUNC1 RNA expression is upregulated in both KT-ExPlus and KT-ALI cells, compared to KT-KSFM (Figure 57). SPLUNC1 protein expression is subsequently observed in

both KT-ExPlus and KT-ALI cells but not KT-KSFM cells (Figure 57). This demonstrates KT cells differentiate in ExPlus and ALI medias to have a secretory morphology.

A

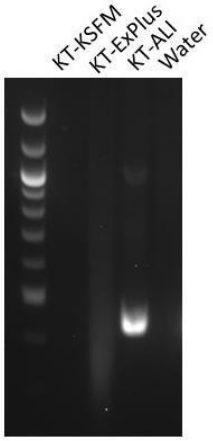

B

Sample	SPLUNC1/µg RNA normalized to 18S
KT-KSFM	$2.04x10^{1}$
KT-ExPlus	$3.37x10^{4}$
KT-ALI	$1.11x10^{4}$

C

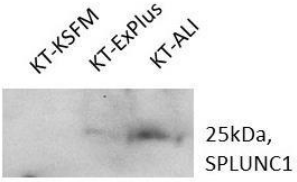

Figure 57. SPLUNC1 expression in KT cells.
KT cells were grown routinely in KSFM, ExPlus and ALI media as independent cultures. (A) cDNA was synthesized from extracted RNA then subject to standard PCR with SPLUNC1 primers. Subsequent products were separated on an 1% agarose gel. (B) qPCR was performed on KT cells grown in submerged culture in KSFM, ExPlus and ALI media. Samples underwent qPCR with SPLUNC1 and 18S primers. Afterwards, SPLUNC1 expression was normalized to 18S. (C) KT cells grown in submerged culture in KSFM, ExPlus and ALI media then lysed with SDS and probed for SPLUNC1 via western blot.

4.3.2 Culture of HBEC3-KT cells at Air Liquid Interface (ALI)

HBEC3-KT cells were grown and differentiated on Air Liquid Interface (ALI) scaffolds to form an epithelial monolayer with ciliated and secretory cells that model those found in human airways *in vivo*. KT cells were plated on ALI scaffolds and cultured for up to 24 days, described in 2.1.6. In this thesis HBEC3-KT cells cultured on ALI scaffold will be referred to as HBEC-ALI cells. During this period changes in cell morphology and the initiation of mucosal secretions were visible, this occurs from 7 days with cells also becoming more spherical (Figure 58).

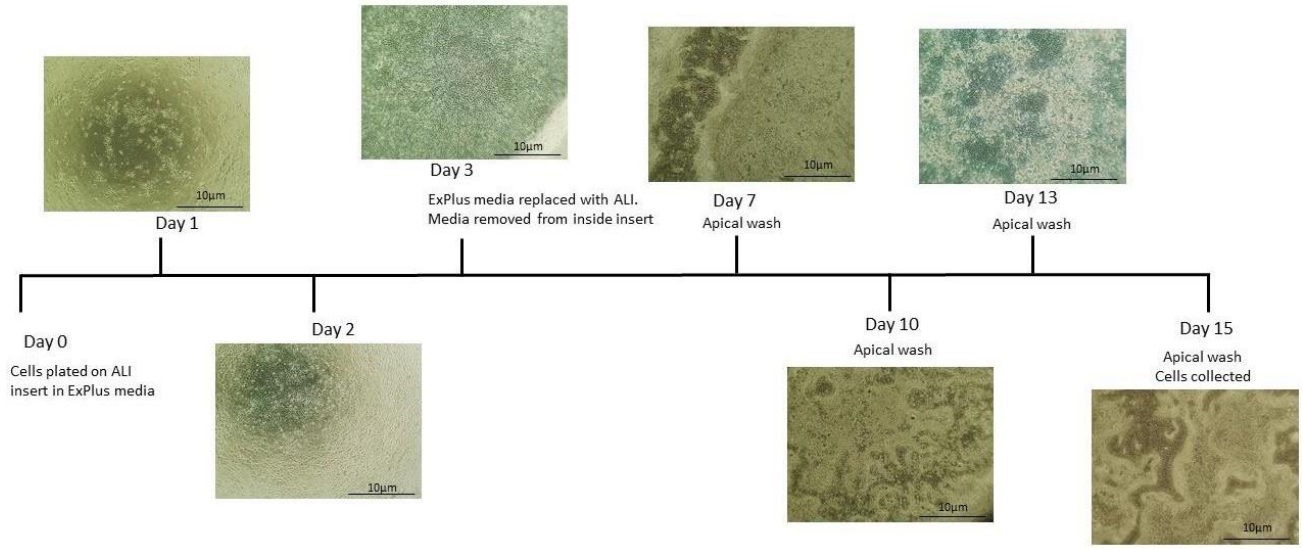

Figure 58. HBEC3-ALI cells were grown and differentiated on Air Liquid Interface (ALI) scaffolds.
KT-ExPlus cells were plated on ALI scaffolds and both the well and insert submerged in ExPlus media. When the cells reached confluence the ExPlus media was replaced with ALI media and media removed from the insert entirely. HBEC3-ALI cells underwent an apical wash with PBS weekly to remove excess mucus. Media was replaced every two days throughout. Images were captured using Ucam Plus on a light microscope and are presented with a 10 µm scale bar.

This was initially performed with two different plating densities of cells per insert: $1x10^4$ and $3x10^4$. After 15 days of culture, RNA was extracted from the HBEC3-ALI cells and probed for secretary and cilia markers, SPLUNC1 and TEKTIN1 respectively. RT-PCR, described as 2.3.7, revealed that the RNA expression of both SPLUNC1 and TEKTIN1 was upregulated following differentiation at ALI, but this was greater when cells were plated at a lower starting density (Figure 59). ALI cultures were also probed for the SPLUNC1 secretion onto the apical surface. This is observed *in vivo* and would be expected to occur following the upregulation of RNA expression. Apical washes were taken once a week with 100 µl PBS gently drained down the side of the insert scaffold. These revealed SPLUNC1 secretion began between 13-16 days of culture (Figure 59).

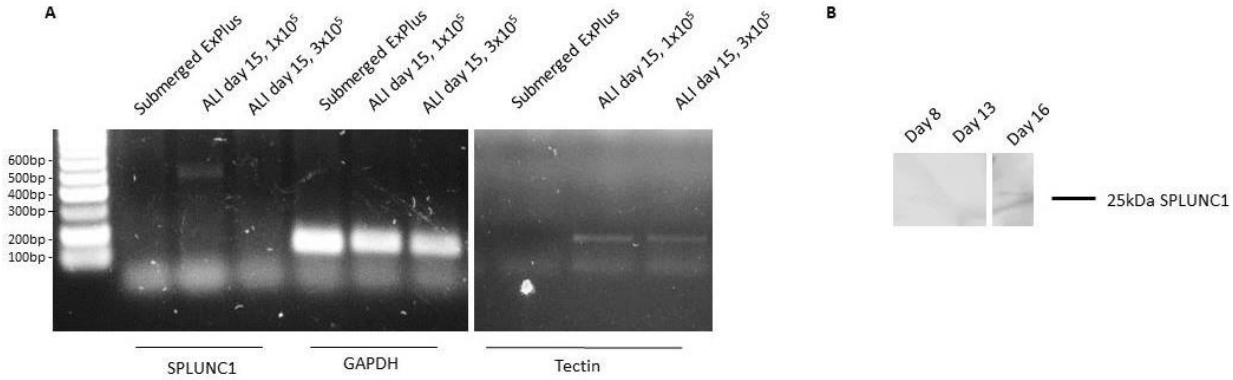

Figure 59. HBEC3-ALI cells have secretory and ciliated morphology.
KT cell culture on ALI scaffold was performed with two different starting cell densities: $1x10^4$ and $3x10^4$. (A) On day 15 HBEC3-ALI cells were harvested in TRIzol, RNA extracted, then DNase treated. RNA was used to synthesise cDNA which was the template for PCR reactions. cDNA underwent PCR reaction for SPLUNC1 a secretory cell marker (550bp), GAPDH as a housekeeping gene (200bp) and TEKTIN1 as a cilia marker (200bp). This was also performed on a sample of KT cells from submerged culture in ExPlus media. (B) Apical washes were taken from ALI inserts with 100 µl PBS at various timepoints following culture with PneumaCult ALI media. Apical wash samples were mixed with 2x sample buffer then probed for SPLUNC1 via western blotting.

4.3.3 Infection of HBEC3-KT cells with Influenza A Viruses

KT cells susceptibility to IAV infection was investigated using a GFP tagged PR8 IAV strain. This was performed with and without TPCK trypsin present because it was unknown whether KT cells could cleave HA0 endogenously. IAV infection is confirmed by the visual presence of green fluorescence under microscope, following infection. KT-KSFM cells are susceptible to IAV infection in the presence and absence of TPCK trypsin, although KT-KSFM cells were more susceptible when TPCK trypsin was present, as judged by the degree of fluorescence in the transfected cultures (Figure 60). KT-ExPlus are also susceptible to IAV with and without TPCK trypsin, however it does not greatly change the proportion of cells infected 24 hours post infection

(Figure 60). Conversely, KT-ALI cells were not susceptible to infection under either condition when an MOI of 1 was used.

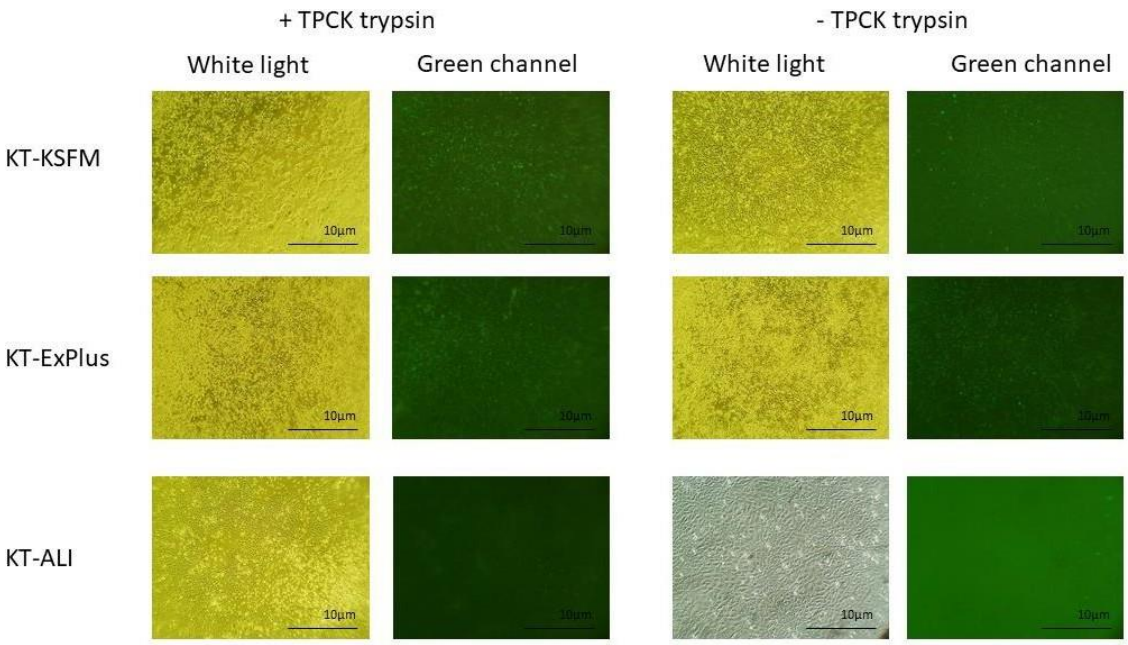

Figure 60. IAV Infection of KT cells with GFP-PR8.
KT cells in KSFM, PneumaCult ExPlus or PneumaCult ALI were plated 24 hours prior to infection. These were infected with GFP-PR8 IAV at an MOI of 0.1. This was completed with and without the presence of TPCK trypsin. Images were taken on a light microscope 72 hours post infection. MDCK cells were infected alongside as a positive control, as they are the standard cell line used for IAV infections *in vitro* cell culture.

To establish if this was due to a low virus concentration, KT-ALI cells were infected with RFP-PR8 IAV strain at an MOI of 2.5 and incubated for 72 hours. However, KT-ALI cells were still not susceptible to IAV infection (Figure 61). To identify if this lack of susceptibility to infection was a strain specific, human KT-ALI cells were infected with a human H1N1 strain isolated during the 2009 swine IAV pandemic, Eng195. A human H1N1 strain was utilized after the previous use of PR8, H1N1, as this was the only human IAV strain available. However, after inoculation at two different MOI with and without the presence of TPCK trypsin did not lead to IAV infection and no

cell death was observed (Figure 61). KT cells susceptibility to IAV was also assessed when cultured at an ALI. HBEC3-ALI cells were cultured for three weeks prior to infection with GFP-PR8 IAV at numerous MOI and with TPCK trypsin present. However, none of these conditions led to IAV infection (Figure 62).

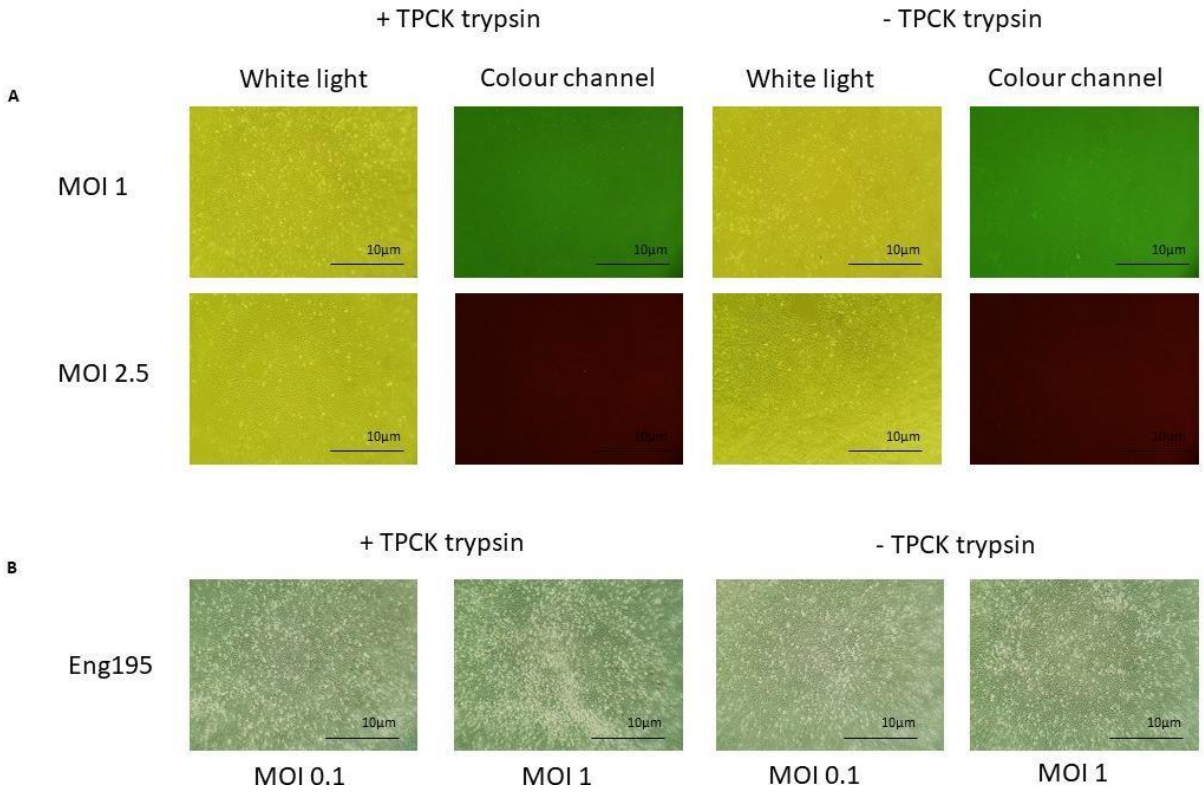

Figure 61. Infection of KT-ALI cells with various IAV strains.
KT-ALI cells were plated 24 hours prior to infection then infected with either (A) GFP-PR8 IAV at an MOI of 1, RFP-PR8 at an MOI of 2.5 or (B) human H1N1 Eng195 pandemic IAV at an MOI of 0.1 or 1. This was completed with and without the presence of TPCK trypsin. Images were taken 72 hours post infection on a light microscope. MDCK cells were infected alongside as a positive control, as they are the standard cell line used for IAV infections *in vitro* cell culture. N=3, two independent experiments.

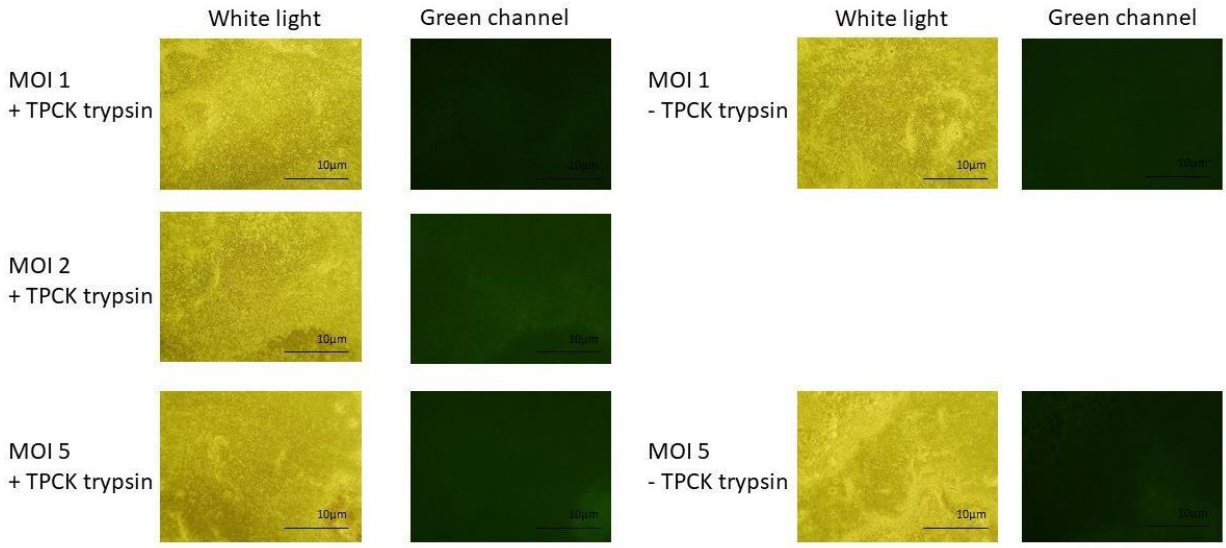

Figure 62. HBEC3-ALI cells are not susceptible to IAV infection
HBEC3-ALI cells were cultured for 24 days prior to infection with GFP-PR8 IAV. Cells were infected for 1 hour then incubated for 72 hours prior to visualization under microscope. Two independent experiments.

4.3.4 Expression of sialic acid receptors on HBEC3-KT cells

IAV bind sialic acid (SA) receptors on glycans on host cell membranes for cell entry, specifically α2,3 and α2,6 linked SA. Avian IAV preferentially bind α2,3 linked SA residues whereas human and swine IAV bind α2,6 linked SA residues. This mirrors the expression of predominantly α2,6 linked SA in human airways and α2,3 linked SA in birds. KT cells grown in submerged culture in each media were stained for α2,3 - and α2,6 - linked SA using *Maackia amurensis* agglutinin (MAA) and *Sambucus nigra* agglutinin (SNA) lectins, respectively, to evaluate their expression and distribution in these cells qualitatively.

Immunofluorescence analysis of KT-KSFM cells reveals widespread expression of both MAA and SNA on all epithelial cells (Figure 63). SNA staining suggests the expression of α2,6 - linked SA appears greater in KT-KSFM cells than α2,3 - linked SA.

KT-ExPlus cells also have widespread distribution of MAA and SNA staining on epithelial cells. SNA staining appears greater than MAA expression in KT-ExPlus cells and SNA expression in KT-KSFM cells, this suggests KT-ExPlus cells may expression more α2,6 - linked SA (Figure 64). KT-ALI cells also have widespread MAA and SNA distribution in all cells although SNA expression is more diffuse in KT-ALI cells compared to KT-KSFM and KT-ExPlus cells (Figure 65). Interestingly, MAA staining appears strongest in KT-ALI cells where it also might be greater than SNA expression.

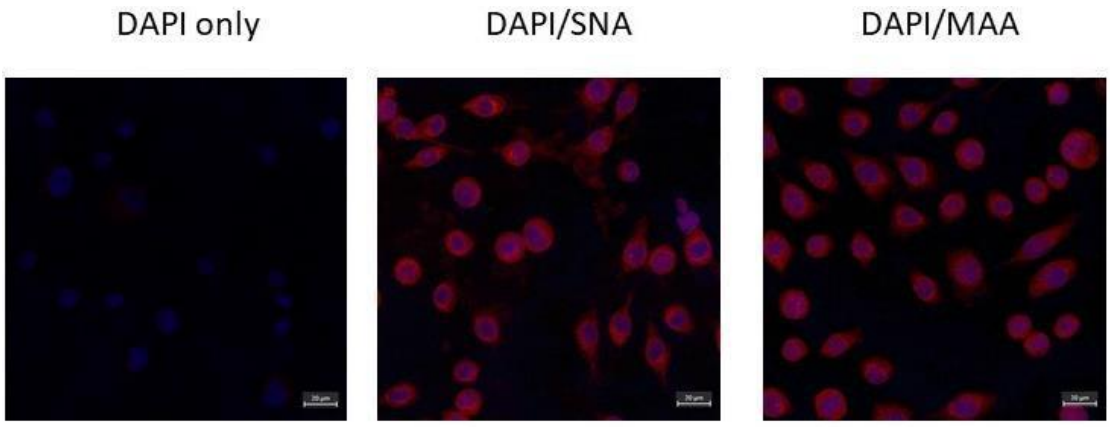

Figure 63. KT-KSFM cells have strong α2,3-linked and α2,6-linked sialic acid expression. KT-KSFM cells were grown in submerged culture on coverslips for 24 hours at 37°C then fixed in 4% PFA, stained with biotinylated Sambucus Nigra Lection (SNA) or biotinylated Maackia Amurensis (MAA), then Streptavidin Alexa Fluor 568 conjugate and counterstained with 4',6-diamidino-2-phenylindole (DAPI). Slides were imaged with a LSM 780 confocal microscope at 561 and 405nm. Images present with a 20 µm scale bar.

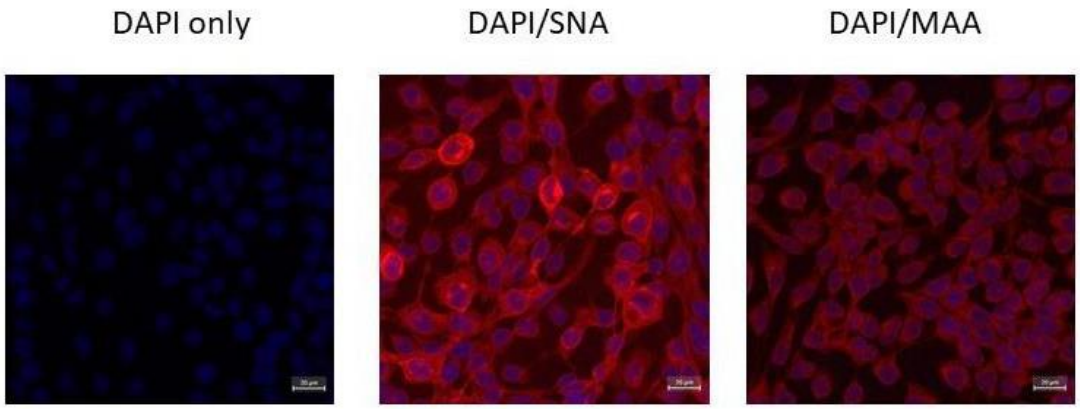

Figure 64. KT-ExPlus cells have strong α2,3-linked and α2,6-linked sialic acid expression. KT-ExPlus cells were grown in submerged culture on coverslips for 24 hours at 37°C then fixed in 4% PFA, stained with biotinylated Sambucus Nigra Lection (SNA) or biotinylated Maackia Amurensis (MAA), then Streptavidin Alexa Fluor 568 conjugate and counterstained with 4',6-diamidino-2-phenylindole (DAPI). Slides were imaged with a LSM 780 confocal microscope at 561 and 405nm. Images present with a 20 µm scale bar.

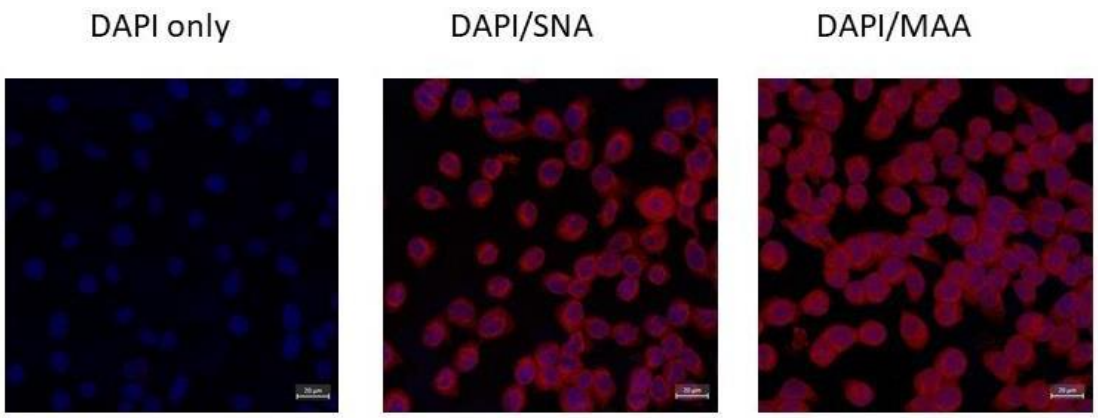

Figure 65. KT-ALI cells have strong α2,3-linked and α2,6-linked sialic acid expression. KT-ALI cells were grown in submerged culture on coverslips for 24 hours at 37°C then fixed in 4% PFA, stained with biotinylated Sambucus Nigra Lection (SNA) or biotinylated Maackia Amurensis (MAA), then Streptavidin Alexa Fluor 568 conjugate and counterstained with 4',6-diamidino-2-phenylindole (DAPI). Slides were imaged with a LSM 780 confocal microscope at 561 and 405nm. Images present with a 20 µm scale bar.

4.3.5 SPLUNC1 KO in HBEC3-KT cells

SPLUNC1 KO in KT-KSFM cells was attempted with CRISPR-Cas9 technology. This was to create an *in vitro* model to investigate its anti-viral role during IAV infection. Single guide RNA (sgRNA) sequences that were 20 nucleotides long and upstream of PAM sites, NGG, were selected to target Cas9 to SPLUNC1 gDNA. There Cas9 can interrupt and cleave the sequence, inducing a double stranded break in the DNA. This is repaired by cell DNA repair pathways and introduces mutations into gDNA.

Figure 66. sgRNA target SPLNUC1 gDNA in exon 2 to disrupt SPLUNC1 secretion signal and N terminus.
SPLUNC1 gDNA annotated showing where the four CRISPR-Cas9 SPLUNC1 sgRNA sequences bind and target Cas9. The sgRNA sequences are annotated: For33, For53, Rev 97 and Rev 18. Genotyping primers are also annotated. Image was produced using Geneious.

sgRNA sequences were designed and selected using IDT's online CRISPR design tool which excludes gRNA with possible off target effects. Four sgRNAs were designed to targeting exon 2 of SPLUNC1 gDNA because this is where the SPLUNC1 start codon

and secretion signal are located. Therefore, a mutation is likely to have a larger impact resulting in the loss of protein secretion (Figure 66). The sgRNA sequences were cloned into Cas9-GFP plasmid as described in 2.2.6. sgRNA - Cas9-GFP plasmids were confirmed by commercial sequencing prior to their use (Figure 67).

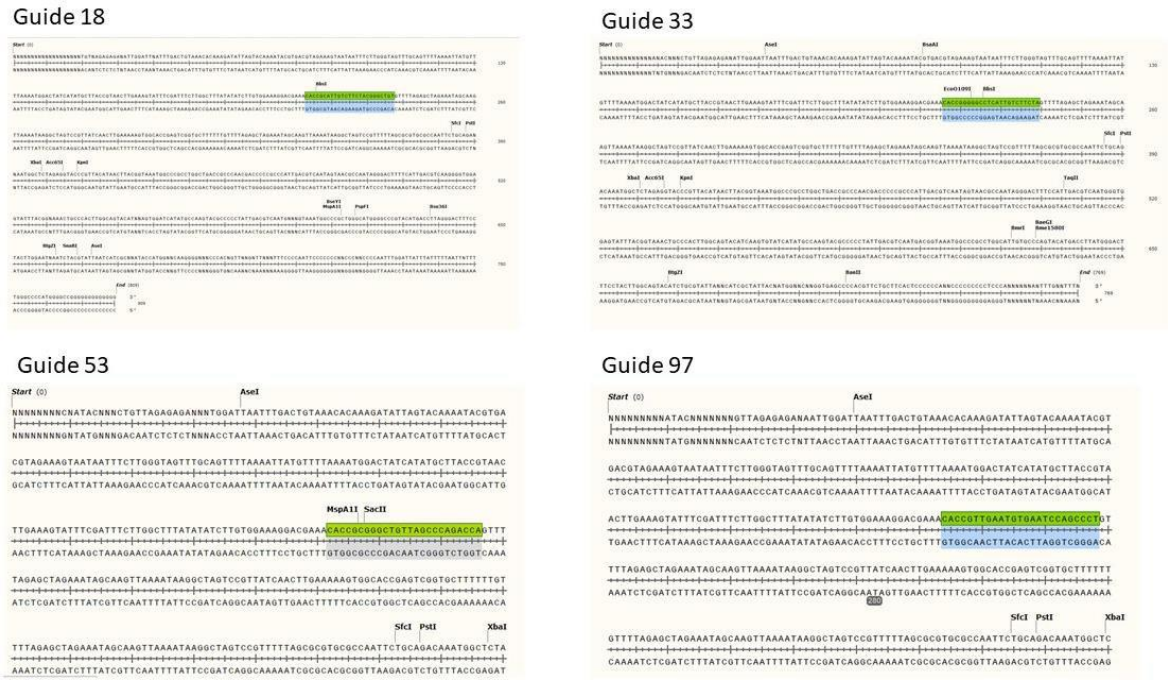

Figure 67. Sanger sequencing confirms the insertion of sgRNAs into the Cas9-GFP plasmid.
Following cloning the sgRNA sequence into the Cas9 GFP plasmid, plasmids underwent sanger sequencing to confirm the plasmid sequence was correct. Guide RNA sequences identified in green.

Prior to the transfection of sgRNA – Cas9-GFP plasmids, the ability to transfect KT cells was assessed with a GFP plasmid. KT cells were transfected as described in 2.1.5.2 and observed 24 hours later. Both KT-KSFM and KT-ExPlus cells were responsive to transfection with a good efficiency rate. However, KT-ALI cells could not be transfected with TransIT LT1 but with lipofectamine 3000 (Figure 68). This

confirms KT cells are susceptible to transfection and therefore can undergo gene editing with sgRNA - Cas9-GFP plasmids.

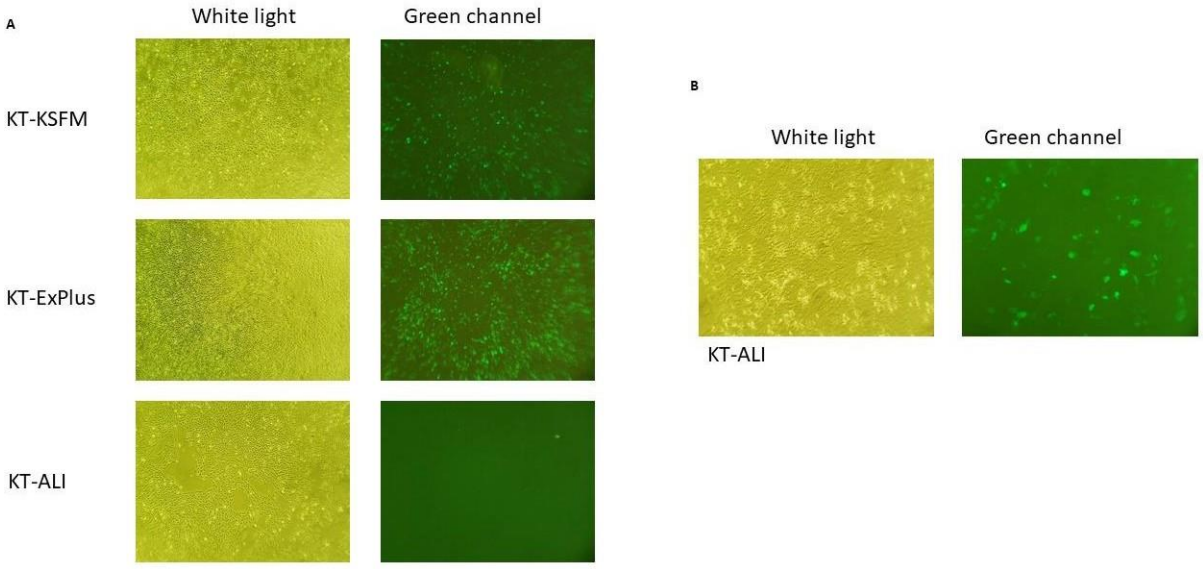

Figure 68. Optimizing the transfection of KT cells
KT cells grown in submerged culture were transfected with GFP plasmid using (A) TransIT LT1 or (B) Lipofectamine 3000 to assess transfection efficiency. Cells were incubated for 24 hours prior to imaging on a light microscope.

SPLUNC1 sgRNA - Cas9-GFP plasmids were transfected into KT-KSFM cells in pairs because this will introduce two separate dsDNA breaks in the gDNA. This increases the likelihood of a larger sized DNA mutation occurring compared to the transfection of one sgRNA and therefore, also the probability that the SPLUNC1 protein is KO of the KT-KSFM cell line. The SPLUNC1 sgRNA - Cas9-GFP plasmids were transfected in four combinations, with both forward and reverse sgRNA paired together. The entire CRISPR-Cas9 editing process used to edit KT-KSFM cells is outlined in Figure 69.

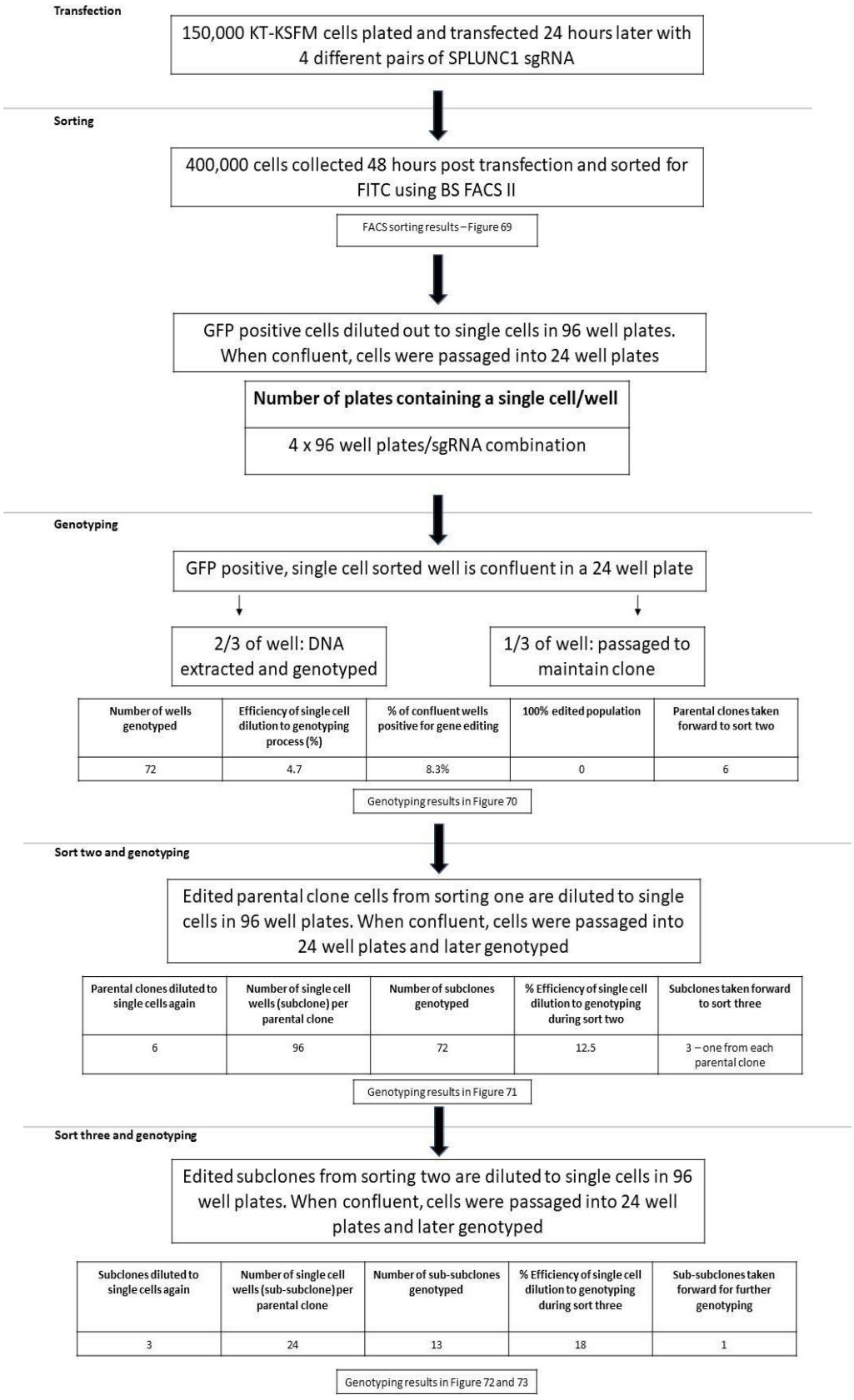

Figure 69. Flow diagram illustrating the transfection, sorting, and genotyping pathway taken to establish a SPLUNC1 deficient KT-KSFM cell line.

SPLUNC1 gRNA - Cas9-GFP plasmids were transfected into KT-KSFM cells and left for 48 hours prior to FACS sorting for GFP positive cells. Each gRNA combination had different levels of transfection efficiency, indicated by green, fluorescent cells post transfection (Figure 70). This shows all four sgRNA combinations were successfully transfected into KT-KSFM cells, but it is unclear whether the cells have been transfected by one or both sgRNA. Although the transfection efficiency appears greater at 24 hours post transfection compared to 48 hours, cells were sorted for GFP 48 hours post transfection as the transfection optimization experiment demonstrated this in fact was superior (Figure 68). Cells were collected 48 hours post transfection and live, single cells sorted for FITC GFP and isolated as single cells in 96 well plates as described in 2.1.14.1. The number of cells recovered, and those positive for FITC GFP, during FACS sorting is stated in Figure 67. Cells were then incubated and allowed to expand then passaged and genotyped once confluent as described in 2.1.14.2 (Figure 69).

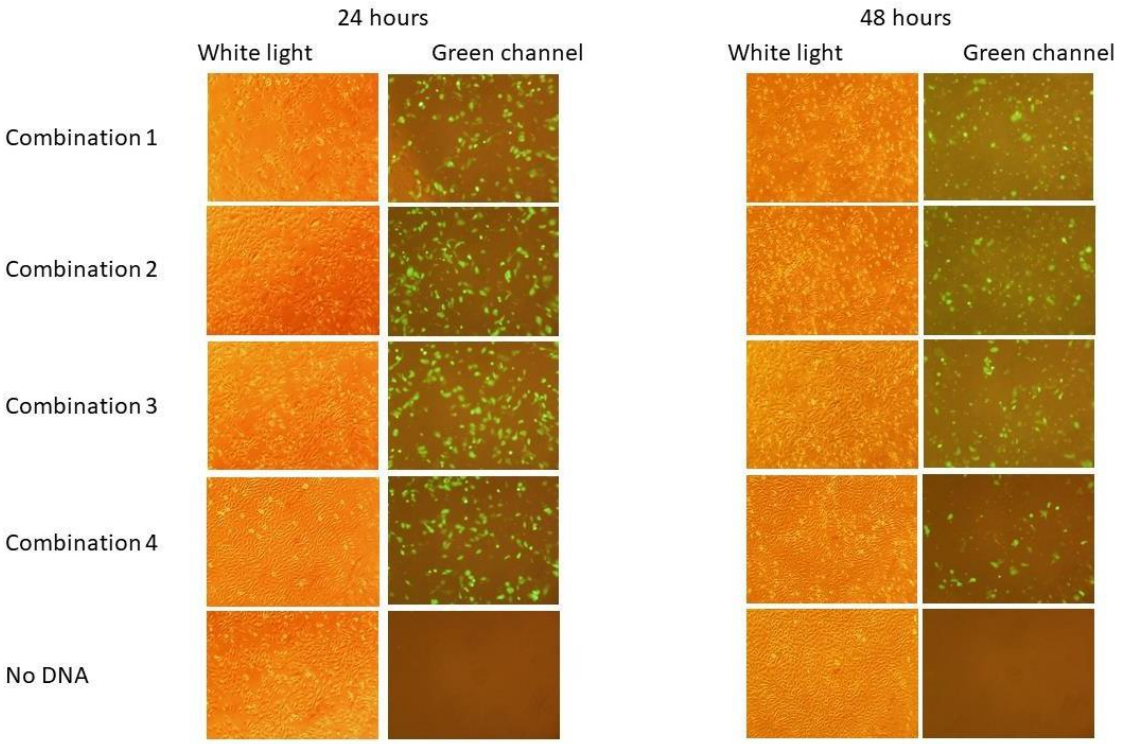

Figure 70. Efficiency of double sgRNA transfection into KT-KSFM cells.
KT-KSFM cells were transfected with four different sgRNA combinations – combination 1: For33 & Rev18, combination 2: For33 & Rev97, combination 3: For53 & Rev18, combination 4: For53 & Rev97 – using TransIT LT1. Cells were imaged at 24 and 48 hours post transfection with a light microscope to assess efficiency. Each combination was transfected in triplicate. At 48 hours post transfection cells were collected via trypsination, triplicates pooled and prepared for FACS sorting.

sgRNA plasmids transfected	Input number of cells for cell sorting	Number of GFP positive cells recovered from sorting	Percentage of GFP positive cells from transfection (%)
Combination 1	117896	28681	24.2
Combination 2	209348	37333	17.8
Combination 3	189433	17349	9.2
Combination 4	357591	15059	4.2

Figure 71. FITC GFP positive cells were isolated during FACS sorting.
FACS sorting was performed a BD FACSAria II for FITC GFP on KT-KSFM cells transfected 48 hours earlier with sgRNA Cas9-GFP plasmids. This quantified the number of cells sorted, the number of those positive for FITC GFP and overall transfection efficiency.

Following expansions, KT-KSFM clones were genotyped to identify whether any SPLUNC1 gDNA modifications had occurring following CRISPR-Cas9 editing. This was performed using PCR with the primers identified above (Figure 67), GAPDH was also used as a positive control. Unedited SPLUNC1 gDNA genotyping PCR had a product of 592bp, the presence of bands with different sizes indicates gene editing has occurred. Genotyping revealed three clones had undergone editing: 2, 11 and 36 (

Figure 72). Clone 36 had undergone a large 440bp deletion, smaller deletions 50bp have occurred in clones 2 and 11. However, none of these colonies have a 100% edited population so they were resorted, as described in 2.1.14.2, to establish a 100% edited population. Clones 7, 9 and 23 have no product from the SPLUNC1 genotyping PCR but do for GAPDH. This shows the gDNA sample for the genotyping PCR was not problematic but that editing may have occurred to the extent that a PCR product cannot be formed anymore. Therefore, these clones were also expanded (Figure 69). These six clones were expanded as they were the only cells that showed evidence of gDNA editing upon genotyping. For the rest of this study clone 2 will be known as S1, clone 11 - S2, clone 36 - S6, clone 7 - S4, clone 9 - S5 and clone 23 – S6.

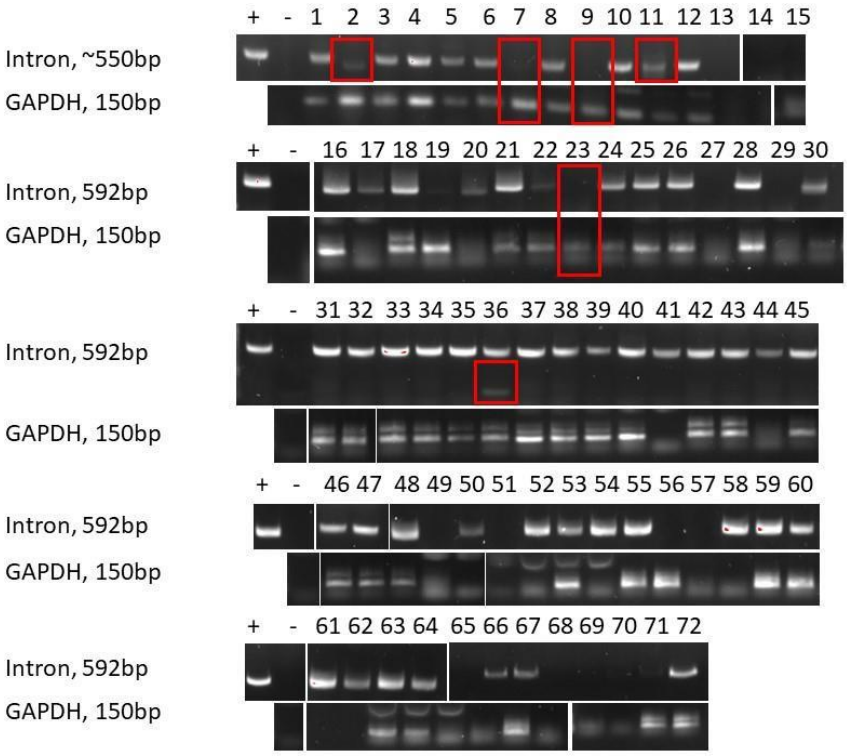

Figure 72. Genotyping for SPLUNC1 deletion and GAPDH in the selected KT-KSFM cells. The sgRNA transfected KT-KSFM cells were sorted for GFP, collected, and grown from single cells for further analysis. When confluent, DNA was extracted, and cells screened for SPLUNC1 editing and GAPDH as a housekeeping gene/positive control. Unedited cells should produce a band of 592bp and 150bp bands, respectively. Edited clones highlighted in red.

Once the edited parental clones identified during sort one had been resorted, the newly sorted subclone single cells were allowed to expand so they could undergo genotyping once confluent (Figure 69). Genotyping following sort two sorting was completed for SPLUNC1 only. None of the expanded edited clones had a 100% edited population following the second sort (Figure 73). Therefore, a third sort to single cells was required to establish this. Clone S3 was expanded from sample 25 as this cell population had smallest quantity of unedited gDNA. Clones S1 and S2 were resorted from samples 3 and 13 respectively. Genotyping also revealed that clones S4, S5 and

S6 had no undergone editing, and they were not further used in these experiments (Figure 73).

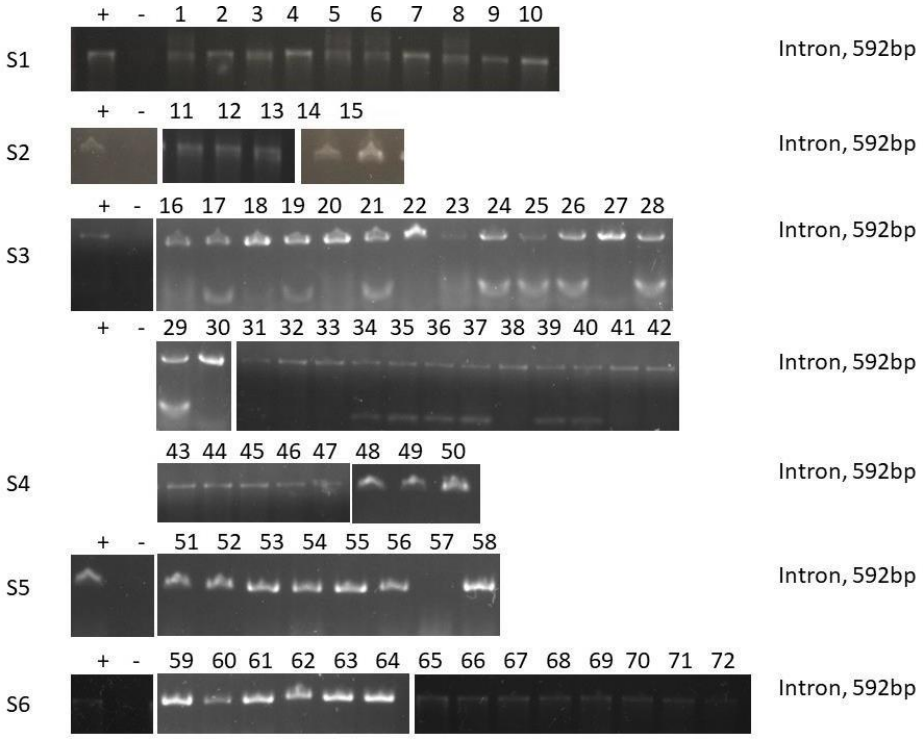

Figure 73. Genotyping of selected CRISPR edited SPLUNC1 clones following sort two Selected edited colonies were resorted to single cells following initial genotyping. When confluent, DNA was extracted from these cells and screened for SPLUNC1 editing. Unedited cells should produce a band of 592bp PCR product.

Genotyping following sort three identified that a 100% edited cell population from clone S3 had been established (Figure 74). This underwent further genotyping via western blotting, described in 2.4.4, to identify if this gDNA deletion resulted in the knockout SPLUNC1 protein. Western blotting revealed that the 440bp gDNA deletion does knockout the SPLUNC1 protein in KT cells (Figure 75). Sequencing of the edited PCR product revealed a 472bp deletion: from midway in exon 2 encompassing all of exon 3 (Figure 75). PCR genotyping revealed a 100% population had still not been established for clones S1 and S2 after sort three (Figure 69). As a SPLUNC1 KO cell line had already been established these clones were not used further in this study.

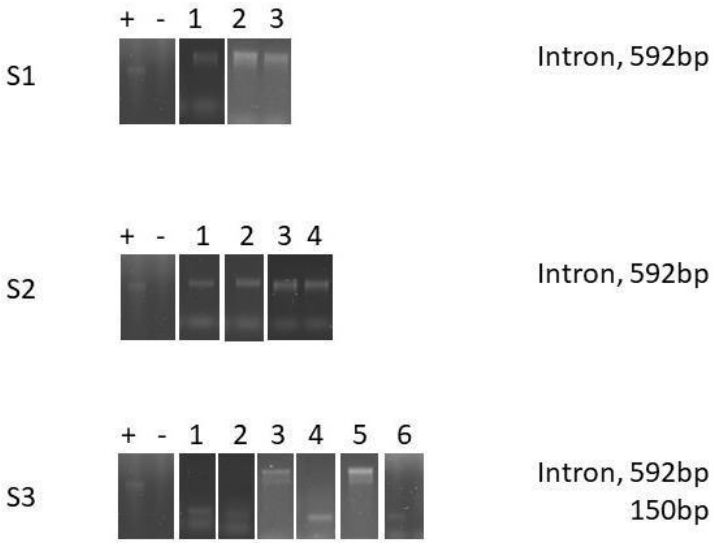

Figure 74. Genotyping following third sort of CRIPSR edited SPLUNC1 colonies identifies 100% edited population

Selected colonies were resorted to single cells following sort two. When confluent, DNA was extracted from these cells and screened for SPLUNC1 editing via PCR. Unedited cells produce a band of 592bp PCR product.

Figure 75. SPLUNC1 KO in KT cells is confirmed and sequenced
(A) Colonies where a 100% edited population was indicated were grown in KT-ALI media for one week then harvested, lysed in SDS and probed for SPLUNC1 via western blotting. (B) PCR product of 100% edited SPLUNC1 KO clone was sequenced using commercial sanger sequencing to identify the exact deletion. SPLUNC1 KO gDNA sequence is aligned against wildtype unedited gDNA and annotated in yellow using Geneious.

4.3.6 SPLUNC1 role during IAV infection *in vitro*

SPLUNC1 role during IAV infection was investigated by determining if the viral titre recorded following IAV infection differed in SPLUNC1 KO KT cells compared to unedited cells. KT cells were infected with PR8 IAV at an MOI of 1 in the presence of TPCK trypsin, incubated for 48 hours and the secreted Influenza viral titre established by plaque assay from the supernatant, both as described in 2.1.11. This revealed that SPLUNC1 KO did not significantly increase IAV titre following infection in KT cells. SPLUNC1 KO in fact reduced the viral titre observed in KT-KSFM and KT-ExPlus cells, however this was not statistically significant with p=0.1 for both KT-KSFM and KT-ExPlus cells. SPLUNC1 KO in KT-ALI cells did not alter viral titre following IAV infection, p>0.99 (Figure 76).

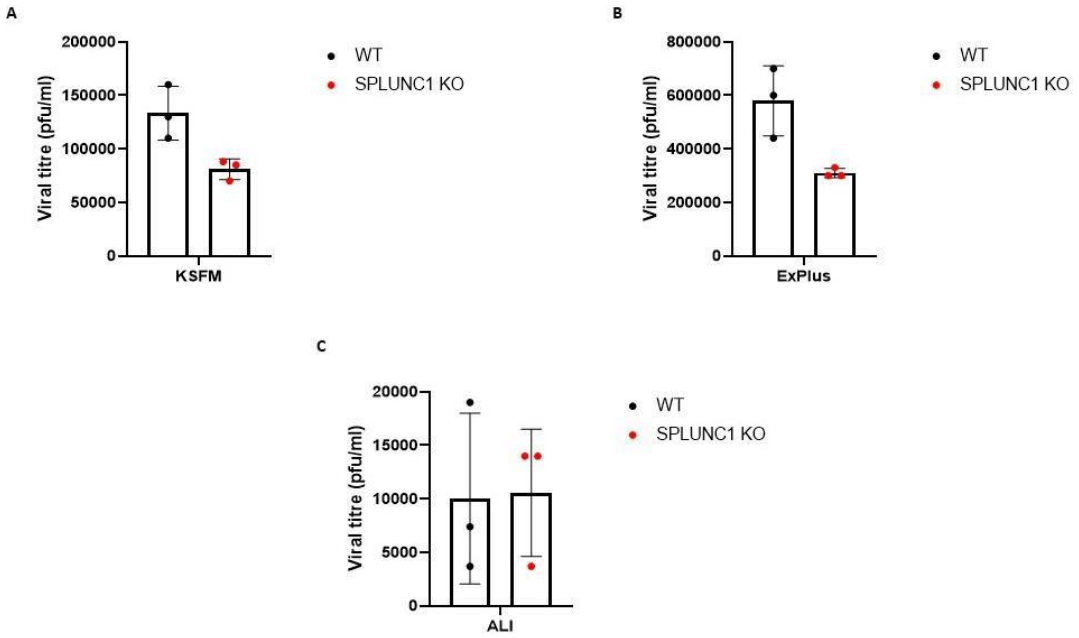

Figure 76. SPLUNC1 KO does not have a significant effect on viral titre in IAV infected KT cells.
KT cells in KSFM, ExPlus and ALI media were plated 24 hours prior to infection with GFP-PR8 at an MOI of 1. 72 hours later, supernatant was collected and IAV virus titre quantified by plaque assay. Data presented with error bars as S.E.M. (N=3), one independent experiment. Statistical analysis was performed with Mann-Whitney U test.

The effect of SPLUNC1 KO *in vitro* was also investigated with an IAV infection at an MOI of 0.1 for 24 hours using KT-ExPlus and KT-ALI cells. This was performed in addition to the infection above as these conditions were used in the IAV infection of mTEC cultures from WT and SPLUNC1 KO mice and a significant difference in viral titre subsequently observed (222). Viral titre was quantified using plaque assay (described in 2.1.11). This revealed that SPLUNC1 KO in KT-ExPlus did not significantly increase the viral titre recorded from IAV infection compared to WT KT-ExPlus cells (Figure 77), p=0.457. KT-ALI cells were also infected with IAV under these conditions however, plaque assay did not identify any IAV.

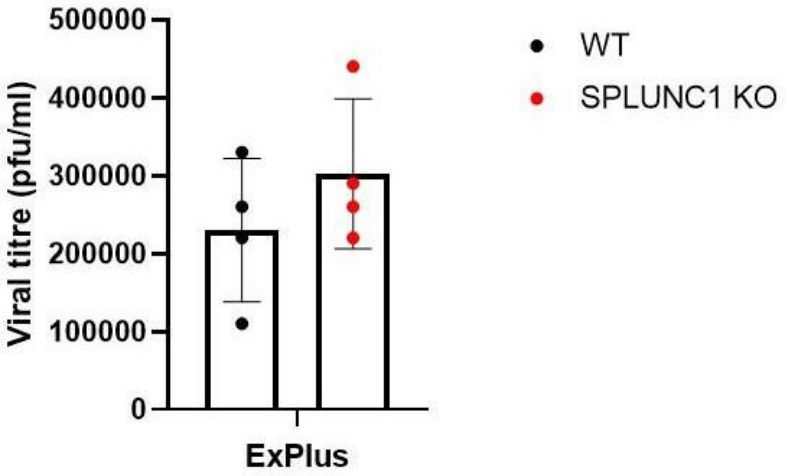

Figure 77. SPLUNC1 KO does not have a significant effect in KT-ExPlus cells
KT-ExPlus cells were plated 24 hours prior to infection with PR8 at an MOI of 0.1. 24 hours later the supernatant was collected and IAV virus titre quantified by plaque assay. Data presented with error bars as S.E.M. (N=4), one independent experiment. Statistical analysis was performed with Mann-Whitney U test.

4.4 Discussion

This chapter describes the characterization of HBEC-KT cells, the generation of an *in vitro* SPLUNC1 deficient cell line and established that *in vitro* SPLUNC1 KO does not affect viral titres following *in vitro* IAV infection. First, KT cells were characterized to assess their suitability as an *in vitro* respiratory model for IAV infection. KT cells are a human bronchiolar epithelial cell line that can mimic those seen *in vivo*. Their culture in PneumaCult ExPlus and ALI media led to differentiation and subsequent SPLUNC1 RNA and protein expression *in vitro*. Although SPLUNC1 RNA expression/µg is greater in KT-ExPlus cells compared to KT-ALI cells in Figure 53-B, this is not reflected in Figure 53-A. This is due to the higher cDNA content in the KT-ExPlus sample appearing as a smear in the PCR product instead of a defined product. Overall, this demonstrates that KT cells are a suitable cell line to use to manipulate SPLUNC1 expression and explore its mechanism of activity during IAV infection. KT cells susceptibility to IAV infection was also assessed during their characterization. KT-KSFM and KT-ExPlus cells are susceptible to infection. However, KT-ALI cells susceptibility to infection is unpredictable and not robust. In section 4.3.3, KT-ALI cells were not susceptible to two strains of IAV however in section 4.3.6, KT-ALI cells were susceptible to IAV infection. In 4.3.3 the presence of infection was indicated by GFP, due to the use of GFP tagged PR8 virus strain, and visual presence of cell death however, neither were visible following the infection of KT-ALI cells under any condition. In 4.3.6, IAV infection and viral titres were confirmed and established using plaque assays. The absence of consistency with regards to KT-ALI cells susceptibility to IAV suggests an experimental issue, such as a mixed population of GFP-PR8 and PR8, or another, external interfering factor. Although it is currently unclear what the identity of this

external factor is and why KT-ALI cells are not always robustly susceptible to IAV infection, this data shows SPLUNC1 is not the cause of this issue as IAV infection has been recorded, and is not statistically different, in both WT and SPLUNC1 KO KT-ALI cells. Additionally, a low density of receptors that allows IAV to enter cells (Figure 61), α2,6 linked SA receptors, is not responsible for KT-ALI cells not being consistently susceptible to IAV infection. However, the strength of this statement could be improved through quantitative analysis and counting of the expression of α2,3 and α2,6 linked SA receptors, in addition to the qualitative analysis in this thesis.

Finally, the infection of KT cells with IAV also revealed that whilst the addition of TPCK trypsin was necessary and enhanced IAV infection in KT-KSFM cells it was not needed for KT-ExPlus cells. This reveals that when cultured in PneumaCult ExPlus media KT cells endogenously produce sufficient proteases, such as transmembrane serine protease 2 (TMPRSS2), that cleave HA and allow influenza to infect cells.

In this chapter a SPLUNC1 deficient *in vitro* cell line was generated in human bronchiolar epithelial cells. This was achieved using CRISPR-Cas9 editing technology through the deletion of half of exon 2 and the entirety of exon three. Despite SPLUNC1 protein no longer being expressed other regions of SPLUNC1 gDNA are still present. It is unknown whether these regions of SPLUNC1 from exon 4-8 are important for SPLUNC1 antiviral activity.

Following the generation of SPLUNC1 KO KT cells, IAV infections were performed using the recovered clones alongside WT KT cells to identify if this targeted SPLUNC1 deficiency effected IAV infection or replication. However, the IAV infections performed at two MOI and time periods saw no statistically significant difference in the terminal viral titres achieved. Interestingly SPLUNC1 KO *in vitro* in

Figure 76 trended towards being protective against IAV infection, the opposite of what would be expected. Although this was not a statistically significant difference it is not clear why this occurred, or the implications of it. It is possibly due to the *in vitro* conditions not being able to suitably reflect SPLUNC1's function, or SPLUNC1's primary function as is protective 24 hours post infection, but these titres were taken at 48 hours post infection. The IAV infections performed in Figure 76 saw different viral titres recorded in unedited KT cells in KSFM, ExPlus and ALI media because the number of cells present in each well was not consistent across the three media. Additionally, KT cells grow at different rates in each media and the cells are infected by IAV with a different efficiency in each media. Overall, this data shows that human SPLUNC1 deficiency does not affect IAV infection and replication in an *in vitro* human bronchiolar epithelial cell line. However, other experiments should be performed to identify if SPLUNC1 deficiency affects other aspects of IAV infection. First, it should be investigated to see if SPLUNC1 affects the binding and entry of IAV into cells at the point of infection using immunofluorescence. This would establish the timing of SPLUNC1's role during infection, as previously SPLUNC1 has been shown to limit IAV entry into murine models at 24 hours post infection (222). Secondly, IAV infections should be performed in WT and SPLUNC1 KO KT cells in each media and RNA-seq performed. This would enable the identification of differences between the host response to IAV infection when SPLUNC1 is absent. Both these experiments would provide crucial data for further exploration into how SPLUNC1 elucidates is antiviral activity.

The *in vitro* SPLUNC1 deficient model generated in this chapter did not demonstrate any antiviral activity by SPLUNC1 against IAV unlike the SPLUNC1 KO mice model

utilized *in vivo*. This could be due to *in vitro* models not including all the complexes and interactions that SPLUNC1 has *in vivo.* However, the performance of other additional experiments is necessary before it can be stated no antiviral activity is shown by SPLUNC1 in the *in vitro* model. Particularly, the completion of RNA-seq to identify any transcriptome disparities during IAV infection when SPLUNC1 knockout as this data would be invaluable with the aim of further understanding how SPLUNC1 functions. It is possible that no antiviral activity from SPLUNC1 was identified in this *in vitro* model due to the species difference between it and the murine *in vivo* model. To date, there has been no evidence that human SPLUNC1 also has anti-viral activity against IAV like murine SPLUNC1. Therefore, this may explain the absence of a difference during SPLUNC1 deficiency *in vitro* during IAV infection. A murine SPLUNC1 KO *in vitro* model might be more suitable when trying to elucidate how SPLUNC1 mediates its antiviral activity in future experiments.

In summary, this chapter has described the engineering of an *in vitro* human bronchiolar SPLUNC1 deficient cell line and used it to investigate the effect of SPLUNC1 deficiency during IAV infection. However, no statistically significant difference was observed in the viral titres obtained following infection therefore, the mechanism which SPLUNC1 mediates its antiviral activity could not be elucidated. Further experiments need to be performed to investigate how SPLUNC1 functions and establish whether human SPLUNC1 does protects against IAV.

5 SPLUNC1 peptide S18 influences IAV infection *in vivo*

5.1 Introduction

From the data presented thus far, it is still unclear how SPLUNC1 mediates its antiviral activity during IAV infection. Therefore, SPLUNC1 involvement and its role was further investigated in this chapter. Multiple approaches have been used to identify and validate the role of SPLUNC1 during IAV infection. These have been used in this chapter to investigate how SPLUNC1 functions, if complementary experiments produce mirror phenotypes, and whether, when combined, all results indicate a single mechanism is occurring.

Previously, a specific region of hSPLUNC1, S18, has been identified as functionally active in the respiratory airway of humans and mice. The S18 sequence originates from human SPLUNC1. It is partially conserved in mice, but the sequence is interrupted (Figure 9). S18 binds and activates epithelial sodium channels (ENaC) and reverses airway surface liquid (ASL) dehydration observed in cystic fibrosis patients however, it has yet to be investigated for an antiviral role. Therefore, S18 and its optimised version, SPX101, with greater stability and delivery via nebulisation to the lung will be investigated in this study alongside a negative control, a scrambled S18 peptide (S18sc) to establish if these regions of SPLUNC1 are involved in modulating IAV infection (267). The S18 peptide will be administered *in vivo* with my industrial collaborator, SiSaf, novel delivery formulation which provides greater stability and retention. This is to establish if it can act as an adjuvant and increase S18 ability to provoke an immune response or improve its potency like other vaccine adjuvants have been used previously, such as alum (268).

5.2 Aims

The aims for this chapter were to further explore SPLUNC1's function and role in the context of IAV infections. Firstly, through establishing an *in vitro* assay that reflect the effect of SPLUNC1 KO *in vivo* and therefore allows investigation into its mechanism of activity. Secondly, by examining the role of the SPLUNC1 peptides during IAV infection *in vitro* and *in vivo.* Finally, by administering S18 with SiSaf's novel delivery formulation to aid retention in the nasal and respiratory tract and assess whether this impacts infection *in vivo.*

5.3 Results

5.3.1 *In vitro* experiments with SPLUNC1 and IAV

5.3.1.1 Recombinant SPLUNC1 protein does not inhibit hemagglutination

Hemagglutination, or the binding of IAV to RBC, and hemagglutination assays are used to quantify the amount of IAV in a sample. Hemagglutination assays were performed, as described in 2.1.12, with the lowest concentration of IAV that caused hemagglutination in the presence of RBC only and mock (VR1255 plasmid) and recombinant SPLUNC1 (pVR1255-SPLUNC1) protein were added in equal concentrations to identify if SPLUNC1 affected IAV hemagglutination. However, SPLUNC1 did not enhance hemagglutination compared to the mock, negative control (Table 12).

Table 12 – Recombinant SPLUNC1 protein does not inhibit hemagglutination

VR1255 and SPLUNC1-VR1255 plasmids were transfected into HEK293T cells, supernatant collected six days later and used as recombinant SPLUNC1 or mock protein, respectively. Hemagglutination assays were performed with a total of 17µg protein that was serially diluted to with a factor of 10, 0.5% chicken red blood cells and IAV PR8 mCherry at $5.6x10^3$ pfu. Each assay was repeated three times independently with similar results.

Sample	Greatest dilution that inhibited hemagglutination
Mock	1/8
SPLUNC1	1/8

5.3.1.2 SPLUNC1 protein does not affect viral titre following IAV infection.

SPLUNC1 protein was used to treat MDCK cells prior to infection with IAV to investigate whether this had a protective effect on IAV infection. SPLUNC1 protein was introduced into cells via transfection or added as secreted recombinant protein. First, cells were transfected with the empty VR1255 plasmid or VR1255-SPLUNC1 plasmid, 24 hours prior to infection with IAV. Viral titre was determined after a 72-hour incubation period by plaque assay, performed described as 2.1.11. SPLUNC1 transfection did not affect or reduce the IAV infection viral titre, with p=0.4 (Figure 78). To establish if this was due to a low concentration of protein present, recombinant SPLUNC1 or mock protein was mixed with IAV virus for one hour and added to cells at the time of infection with IAV for 1 hour at three different concentrations, then viral titre determined by plaque assay. However, the addition of recombinant SPLUNC1 protein at any concentration also did not affect IAV infection viral titre with p=0.133 (Figure 79). The presence of SPLUNC1 in each supernatant dilution was confirmed by western blotting prior to completing these experiments.

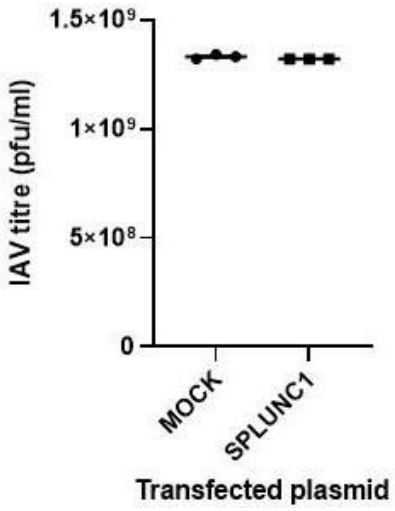

Figure 78. SPLUNC1 transfection does not affect IAV infection titre.
MDCK cells were transfected with VR1255 (mock) and SPLUNC1-VR1255 plasmids, 24 hours later infected with IAV PR8 at MOI of 1 for 1 hour and the viral titre from the supernatant of the infected cells determined by plaque assay. Data represented by individual data points from independent experiments and mean ±SEM. N=3, one independent experiment. Statistical analysis was performed using Mann-Whitney *U*-test.

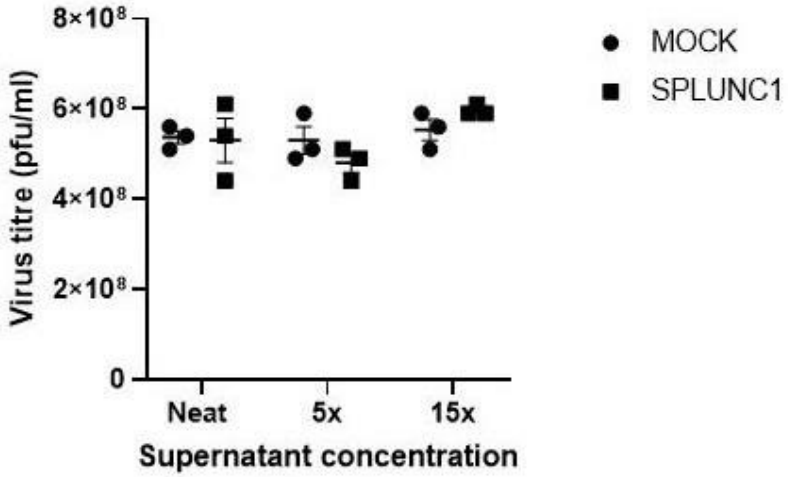

Figure 79. SPLUNC1 protein does not affect IAV titre observed after infection.

HEK293T cells were transfected with SPLUNC1-VR1255 and VR1255 (mock) plasmids, supernatant was collected and concentrated. MDCK cells were infected with MOI of 1 IAV PR8 that had been preincubated with 5 (Neat), 25 (5x) or 75 µg (15x) SPLUNC1 protein for 1 hour. Cells were incubated for 48 hours, and viral titre of the infected cells was determined by plaque assay. Data represented by individual data points from independent experiments and mean ±SEM. Statistical analysis was performed with two-way ANOVA.

5.3.1.3 Murine SPLUNC1 KO BAL from naïve mice does not protect IAV infection *in vitro*

Due to the previously observed *in vivo* phenotype of SPLUNC1 KO mice, it was hypothesized that BAL from WT mice would be more protective against IAV infection compared to SPLUNC1 KO BAL. Therefore, BAL was collected post-mortem and pooled from four 8-10 week old WT and KO mice then incubated with IAV for 1 hour prior to infection. An MOI of 0.01 was used for this IAV infection due to the low concentration of protein present in the BAL dilutions. MDCK cells were infected with the BAL-IAV mix, incubated for 48 hours and the supernatant viral titre determined subsequently by plaque assay and cell viral load by qPCR, described as 2.3.7. This was performed with BAL used at a variety of dilutions to ensure the optimal concentration was assessed.

Plaque assays showed there was no difference in IAV infections completed with pre-treatment of WT or SPLUNC1 KO BAL. There was no statistically significant difference in the viral titre obtained from the supernatant following infection at each dilution with p=0.6 (Figure 76). Cell viral load was determined after IAV infection by qPCR. This also determined that there was no statistically significant difference in the copies of IAV/µg RNA from the WT BAL IAV infection compared to SPLUNC1 KO BAL with p=0.0667 (Figure 80). Together, this data demonstrates WT BAL is not more protective during IAV infection than SPLUNC1 KO BAL.

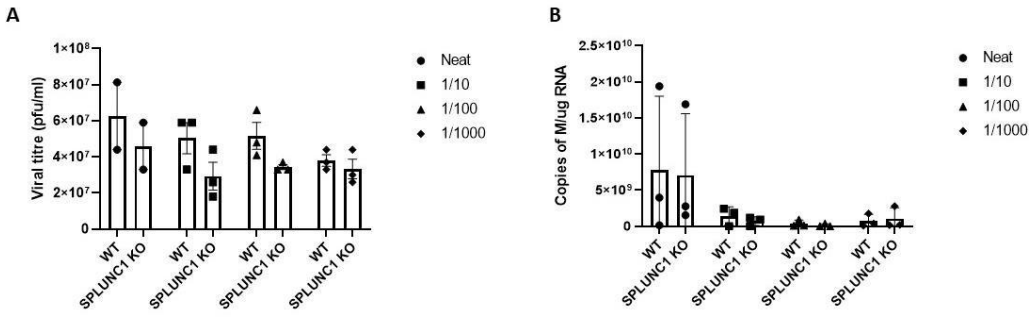

Figure 80. WT BAL does not offer increased protection against IAV infection than SPLUNC1 KO BAL

BAL samples were taken from 8-10 weeks old wildtype (WT) and SPLUNC1 KO C57/BL6 mice and the samples from four mice pooled. MDCK cells were infected with an IAV PR8 at an MOI of 0.01 for 1 hour in the presence 10 µg WT or KO BAL/well. BAL was used at concentration of neat, 1/10, 1/100 or 1/1000. Cells were then incubated for 48 hours, supernatants collected, and viral titre determined by plaque assay. Performed with biological replicates, n=3. (A). Data represented by individual data points and mean ±sem. Statistical analysis was performed (Mann-Whitney *U*-test, $p<0.05$). (B) Infected cells RNA viral titre was determined by qPCR and presented as M IAV protein normalized to 18S/µg. Data represented by individual data points from one independent experiment and mean ±sem. Statistical analysis was performed with two-way ANOVA.

5.3.2 Assessment of SPLUNC1 peptides stability and cytotoxicity *in vitro*

The S18 sequence of SPLUNC1 lies at the N terminus (Figure 9) and is free of a tertiary protein structure. It has been identified and described in the literature as a functionally active region of SPLUNC1 that binds the ENaC and mediates its activity. It has also been shown it reverses the ASL dehydration that characterizes CF however, this peptide has never been investigated to establish whether it is responsible for the antiviral activity SPLUNC1 exhibits against IAV (226).

A

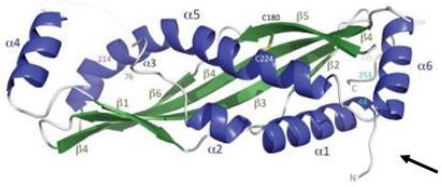

B

1 MFQTGGLIVF YGLLAQTMA FGGLPVPLDQ TLPLNVNPAL PLSPTGLAGS LTNALSNGLL
61 SGGLLGILEN LPLLDILKPG GGTSGGLLGG LLGKVTSVIP GLNNIIDIKV TDPQLLELGL
121 VQSPDGHRLY VTIPLGIKLQ VNTPLVGASL LRLAVKLDIT AEILAVRDKQ ERIHLVLGDC
181 THSPGSLQIS LLDGLGPLPI QGLLDSLTGI LNKVLPELVQ GNVCPLVNEV LRGLDITLVH
241 DIVNMLIHGL QFVIKV

Figure 81. S18 peptide is contained in N-terminus of SPLUNC1 and not present in SPLUNC1's protein structure

(A) Protein structure of SPLUNC1. S18 is present in the N-terminus, indicated by arrow. (B) Amino acid sequence of SPLUNC1. Grey highlights indicate secretion signal and yellow S18 sequence. Part A adapted from (199).

5.3.2.1 Stability assessments with the SPLUNC1 peptides

The stability of the SPLUNC2 peptide S18 was evaluated against a scrambled S18 (S18sc) negative control and delivery optimised S18 sequence, SPX-101. Each SPLUNC1 peptide was assessed in a range of conditions prior to use in *in vitro* and *in vivo* experiments. The stability of each peptide was assessed for up to four weeks at a variety of temperatures. Due to the small molecular weight of the peptides, they were run and separated on Tris-Tricine SDS-PAGE gels, described as 2.4.2.2. This is because they are superior at separating proteins with molecular weights below 20 kDa and the peptides have molecular weights of 1-2 kDa. Following SDS-PAGE, proteins were visualized using silver staining, described as 2.4.3.2.

Time and temperature stability trials with the S18 peptide revealed it does not degrade or aggregate over time when stored for up to four weeks at RT, 4^{o}C or -20^{o}C (Figure 82). No degradation or aggregation was also observed with the SPX101 peptide when stored at these temperatures for up to four weeks (Figure 83). The S18sc peptide was stable at RT and -20^{o}C however, aggregation was observed when

it was stored at 4°C, particularly following storage for two weeks (Figure 84). Therefore, the peptides were all stored at -20°C over prolonged periods of time.

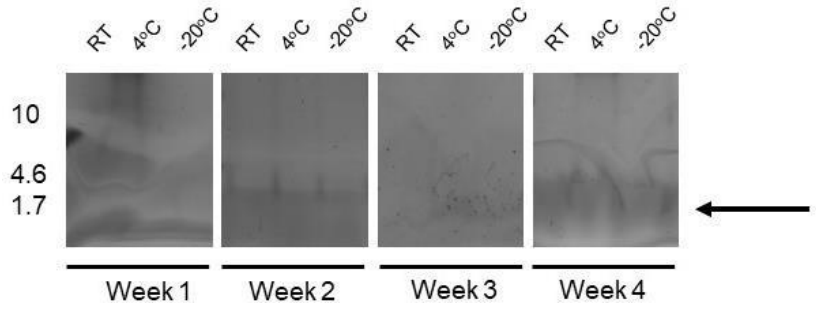

Figure 82. S18 peptide is stable across a range of times and temperatures.
S18 peptide was incubated at either room temperature, 4 degrees or -20 degrees for up to 4 weeks. Following incubation samples were separated by molecular weight on a Tris-Tricine SDS-PAGE gel and visualized using silver staining.

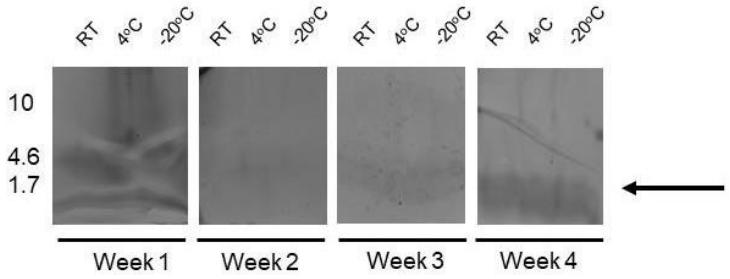

Figure 83. SPX101 peptide is stable across a range of times and temperatures.
SPX101 peptide was incubated at either room temperature, 4 degrees or -20 degrees for up to 4 weeks. Following incubation samples were separated by molecular weight on a Tris-Tricine SDS-PAGE gel and visualized using silver staining.

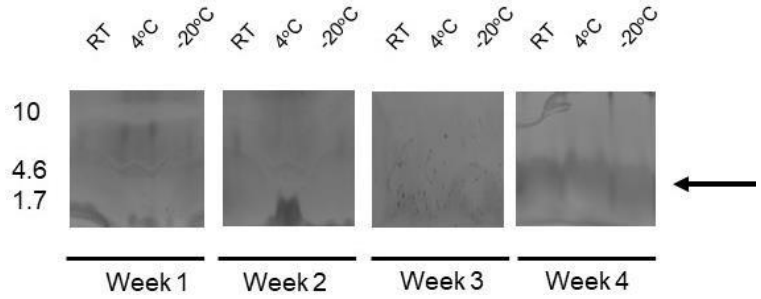

Figure 84. S18sc peptide aggregates when stored at 4 degrees.
S18sc peptide was incubated at either room temperature, 4 degrees or -20 degrees for up to 4 weeks. Following incubation samples were separated by molecular weight on a Tris-Tricine SDS-PAGE gel and visualized using silver staining.

Stability of each peptide was also assessed at a range of pH's and in biological samples. First, the stability of each peptide was assessed in water at pH 5, 6, 7 or 8 at RT for up to six hours prior to separation and visualisation by Tris Tricine SDS-PAGE, described as 2.4.2.2. The stability of the S18 and SPX101 peptides was not affected by pH but aggregation was observed in the S18sc peptide at pH 7 and 8 (Figure 85).

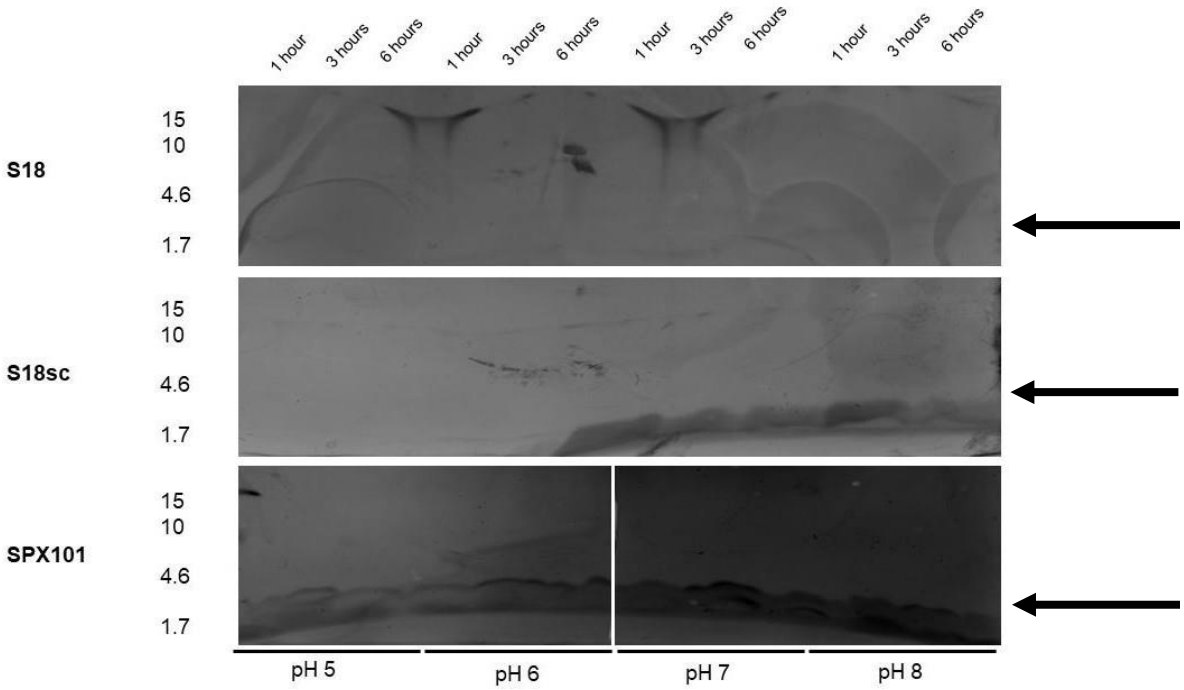

Figure 85. SPLUNC1 peptides are relatively stable at a range of pH's.
S18, S18sc, SPX101 peptides were incubated at pH 5, 6, 7, or 8 at room temperature for up to 6 hours. Following incubation samples were separated by molecular weight on a Tris-Tricine SDS-PAGE gel and visualized using silver staining.

The stability of the peptides in a natural biological matrix was assessed using BAL and serum obtained from 8 - 10 week old C57BL/6J mice. This was to establish how long the peptides might be present in the respiratory tract during *in vivo* experiments and whether they would be stable. None of the peptides are stable in BAL with both degradation and aggregation occurring. All three peptides are degraded overtime whereas only SPX101 aggregates after incubation with BAL for six hours. All three of the peptides are more stable in serum with no degradation or aggregation visible following six-hour incubation (Figure 86).

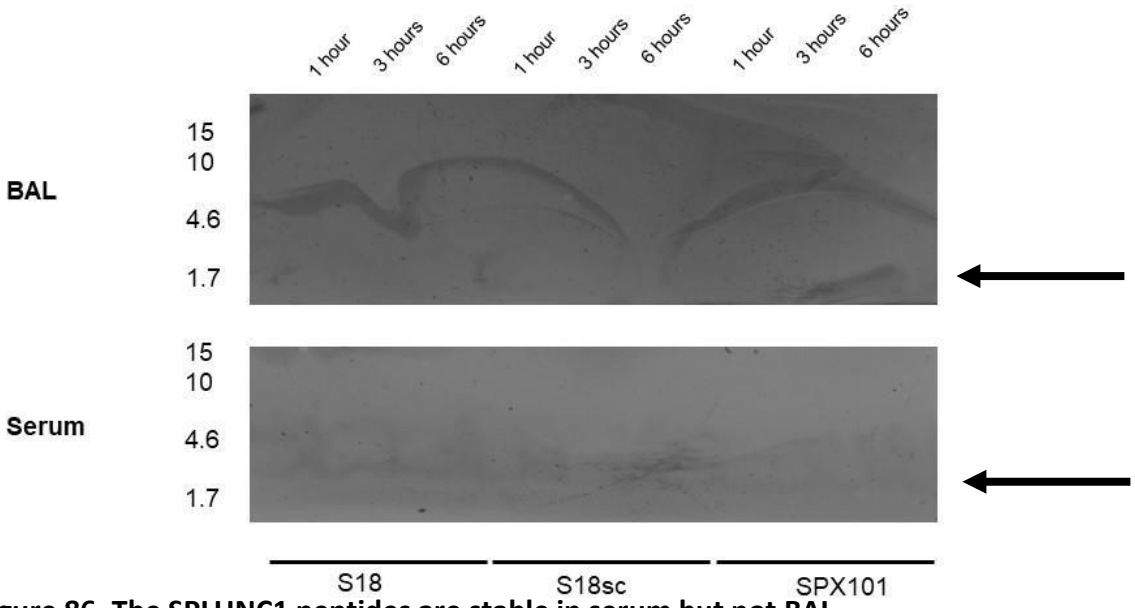

Figure 86. The SPLUNC1 peptides are stable in serum but not BAL.
S18, S18sc, SPX101 peptides were incubated at room temperature for up to 6 hours in murine serum or BAL. Following incubation samples were separated by molecular weight on a Tris-Tricine SDS-PAGE gel and visualized using silver staining.

5.3.2.2 SPLUNC1 peptides cytotoxicity *in vitro*

The cytotoxicity of the SPLUNC1 peptides S18, S18sc and SPX101 was assessed prior to their use *in vitro* in four different cell lines using MTS assays. The cytotoxicity of each peptide was assessed at a range of therapeutic concentrations (1 mM – 0.01 µM) following the incubation of cells and peptide for 72 hours using a Promega Cell Viability kit, described in 2.1.13. The four cell lines used to assess cytotoxicity were lung epithelial cell lines: KT-KSFM, KT-ExPlus, KT-ALI and A549. S18, S18sc or SPX-101 were not cytotoxic to any cell line at any concentration (Figure 87, Figure 88 and Figure 89).

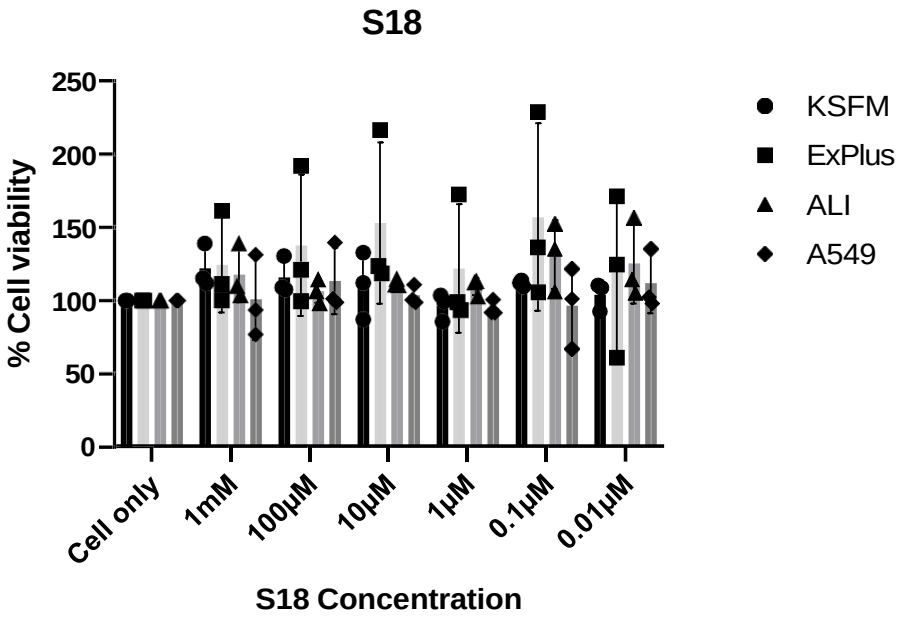

Figure 87. S18 peptide is not toxic to cells at any concentration.
KT-KSFM, KT-ExPlus, KT-ALI and A549 cells were incubated for 24 hours prior to the addition of S18 peptide. The S18 peptide was added to a final concentration from 1 mM – 0.01 µm, incubated for 3 days and cell viability assessed using Promega cell proliferation assay. Performed with technical replicates of n=3, one independent experiment.

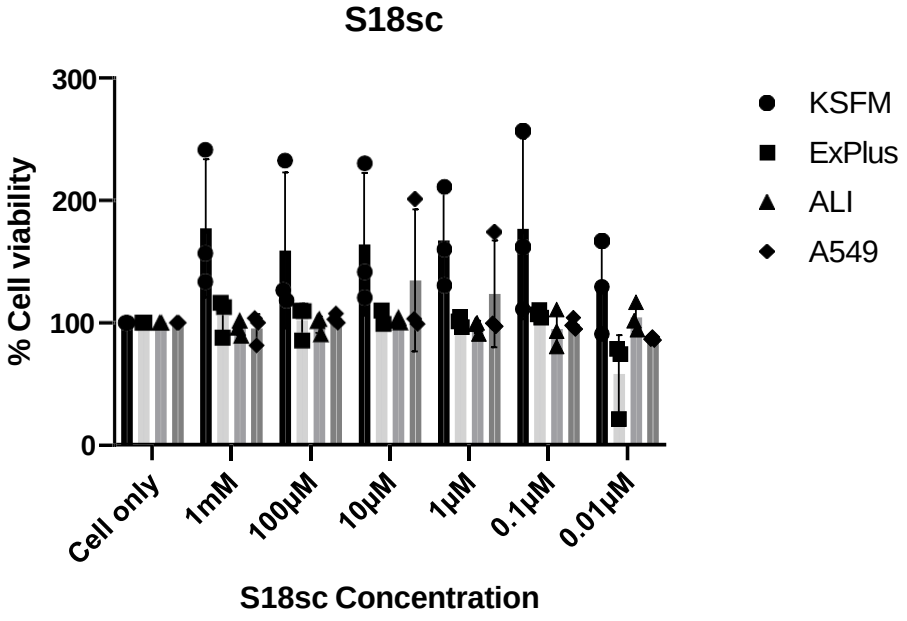

Figure 88. S18sc peptide is not toxic to cells at any concentration.
KT-KSFM, KT-ExPlus, KT-ALI and A549 cells were incubated for 24 hours prior to the addition of S18sc peptide. The S18sc peptide was added to a final concentration from 1 mM – 0.01 µm, incubated for 3 days and cell viability assessed using Promega cell proliferation assay. Performed with technical replicates of n=3, one independent experiment.

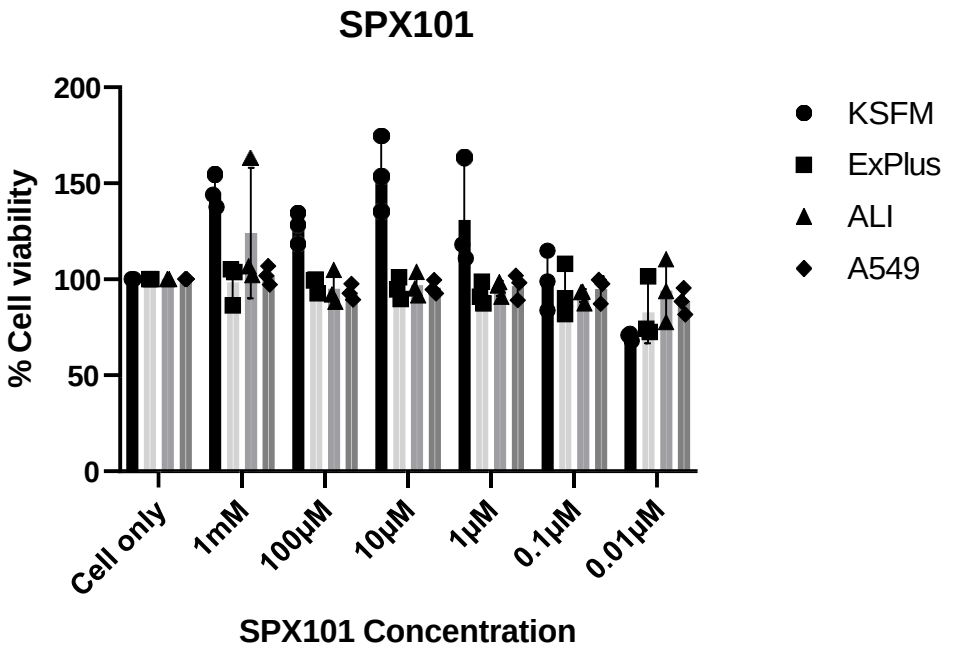

Figure 89. SPX101 peptide is not toxic to cells at any concentration.
KT-KSFM, KT-ExPlus, KT-ALI and A549 cells were incubated for 24 hours prior to the addition of SPX101 peptide. The SPX101 peptide was added to a final concentration from 1 mM – 0.01 µm, incubated for 3 days and cell viability assessed using Promega cell proliferation assay. Performed with technical replicates of n=3, one independent experiment.

5.3.3 Establishing the effect of the SPLUNC1 peptides on IAV *in vitro*

The S18 and SPX101 SPLUNC1 peptides were used alongside their negative control peptide, S18sc, to investigate whether they are involved in the mechanism that mediates SPLUNC1 anti-viral activity. It is unclear how SPLUNC1 functions and these peptides have been previously identified as functionally active in the respiratory tract (226). Additionally, they are regions not mapped on SPLUNC1 tertiary structure, this free structure could enable binding to other host proteins or co-factors and mediate this antiviral activity.

S18 and SPX101 were investigated during the infection of four cell lines with IAV, described as 2.1.10. MDCK, A549, KT-KSFM and KT-ExPlus cells were infected with

PR8 IAV in the presence of 10 mM or 100 mM peptide, as the peptides have been used therapeutically at these concentrations previously *in vitro* (226). The peptides could not be used at these concentrations in the cytotoxicity assays in 5.3.2.2 due to the quantity of peptide required and limited amount available. However, it has been shown previously that they are not cytotoxic at these concentrations *in vitro* (226). IAV and the indicated peptide were pre-incubated for 1 hour prior to the infection of cells. Cells were infected for 1 hour, then incubated for 48 hours to allow virus replication. Viral titre of infected supernatant was subsequently determined by plaque assay, described as 2.1.11. The addition of the S18 and SPX-101 SPLUNC1 peptides did not decrease viral titres significantly in MDCK cells compared to the S18sc negative control peptide. The S18 and SPX-101 peptides did not decrease IAV viral titres at all in A549 cells. The addition of S18 and SPX-101 to KT cells in KSFM or ExPlus media also did not decrease viral titres. Viral titres were below the limit of detection in KSFM and ExPlus media with certain peptides and are therefore represented with 0. In fact, the addition of 10µM SPX-101 to KT-KSFM or KT-ExPlus cells, and both S18 and SPX-101 at 100µM to KT-ExPlus increased IAV viral titres observed following infection, but not with statistical significance. Overall, no antiviral activity was detected by use of either S18 or SPX101 as the addition of either did not decrease the viral titre observed following infection (Figure 90). The difference in viral titres observed between the cell lines in Figure 86 is due to the different efficiency of each cell line has with IAV.

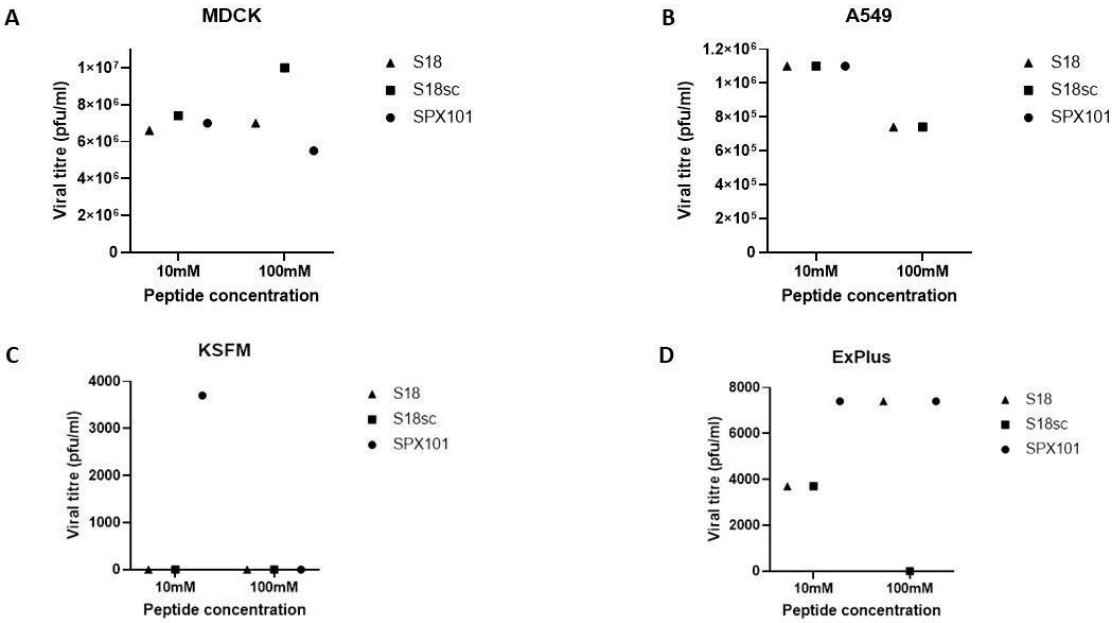

Figure 90. SPLUNC1 peptides do not have an anti-viral activity against IAV infection *in vitro*.

MDCK (A), A549 (B), KT-KSFM (C) and KT-ExPlus (D) cells were infected with an MOI of 1 of IAV PR8 in the presence of 10 mM or 100 mM S18, S18sc or SPX101 peptide, respectively, for 1 hour. 48 hours later supernatant was collected, and viral titre determined by plaque assay, n=1. Y-axis changes across parts (A) through to (D).

The SPLUNC1 peptides S18 and SPX101 were then assessed for their ability to bind and affect hemagglutination. Hemagglutination is the binding of IAV to red blood cells and establishing if these peptides impact hemagglutination could provide vital indications to how SPLUNC1 is functioning against IAV. However, the SPLUNC1 peptides did not inhibit hemagglutination at 100Mm, or any lower concentration (Table 13).

Table 13 - SPLUNC1 peptides does not inhibit hemagglutination
Hemagglutaination assay was performed on 100 mM peptide, serially diluted by a factor of 10, with 0.5% chicken red blood cells and IAV PR8 mCherry at $5.625_{x10}{}^{3}$. Each sample was repeated three separate times, alongside IAV and PBS containing positive and negative control wells respectively.

Sample	Greatest dilution that inhibited hemagglutination
S18	0
S18sc	0
SPX101	0

5.3.4 SPLUNC1 peptide S18 administration on IAV infection *in vivo*

The effect of the SPLUNC1 peptide S18 on IAV infection was first assessed *in vivo* using BALB/C wildtype mice to investigate whether they were protective against IAV infection. Mice were infected with $1x10^3$ pfu IAV X31 intranasally and treated with intranasal S18 peptide or respective control one day prior to infection and each day subsequently until 5 d.p.i. when the experiment was ceased. The S18 peptide was administered solely or in combination with a novel delivery formulation (described in 2.4.9.2), produced by SiSaf, to prolong retention in the nasal and respiratory tract. PBS and formulation only groups were also performed to allow full comparison and assessment of the effects of S18 itself and the formulation delivery on IAV infection.

Mice body weight was measured daily throughout the experiment as a measure of animal health and presented as a % of starting body weight on Day 0. Mice weighing 20% less than their starting weight had to be culled for welfare reasons. All mice in the PBS, formulation only groups, one mouse in the S18 + formulation, and two in the S18 only group had to be euthanised 4 d.p.i. due to >20% weight loss or adverse health scoring. At 5 d.p.i. one further mouse in the S18 only group had lost >20% body weight. The administration of S18 peptide during IAV infection, alone or in

combination with SiSaf stability formulation, significantly increased survival compared to the PBS and formulation only control groups. S18 combined with SiSaf's stability formulation increased survival with a p value of 0.0051 compared to PBS and formulation only groups. Administration S18 alone increased survival to p=0.0190 (Figure 91-A). The SiSaf formulation delivery did not significantly increase survival compared to S18 alone with p=0.2552. At 1 d.p.i. weight loss did not differ significantly between the groups. At 2 d.p.i. the S18 + formulation group did record less weight loss compared the other three groups however this difference was only statistically significant between PBS and S18 + formulation groups with p=0.0213. Through 3 and 4 d.p.i. the non S18 treated groups continued to lose more weight, but this difference was not significant (Figure 91-B).

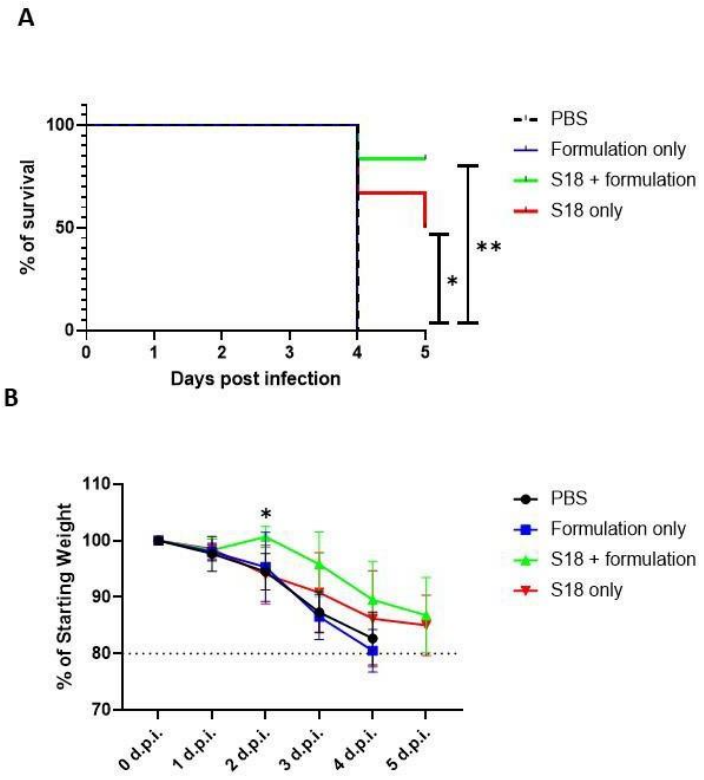

Figure 91. S18 administration influenced IAV infection in mice.
BALB/C mice were infected intranasally with $1x10^3$ pfu IAV X31 and treated with either 40 µl PBS, formulation only, S18 + formulation or S18 only at 1 µg/µl daily (n=6 per group, one dependent experiment). (A) Survival curve was constructed with endpoint determined with mice culled at 20% weight loss from starting weight or high severity health score. Statistical analysis was performed with log rank test. (B) Mice were weighed daily, and the data presented as a percentage of the starting weight. Data represents mean ±S.E.M. Statistical analysis was performed with two-way ANOVA with Bonferroni post hoc test, * indicates p value <0.05 and ** p<0.01.

Throughout the experiment daily oral throat swabs were taken to allow monitoring of viral load during the progression of infection, in addition to those assessed when the experiment was terminated. This would provide a greater insight into S18 impact on IAV infection. Swabs reveal that the viral load observed across the four groups starts to differ from 2 d.p.i. and this continues until the experiment concludes (Figure 92). At 2 d.p.i. the formulation only IAV load spikes in comparison to the remaining three groups, but decreases down to a more comparable level 3 d.p.i.. The disparity

in swab viral load between the groups is most clearly displayed 4 d.p.i. where it is greatest in the formulation only group and decreases through the PBS, S18 + formulation and S18 only group, where it is lowest. Throughout the later stages of infection, the viral load is higher in the S18 + formulation group compared to S18 only. However, at no stage during infection there was a statistically significant difference between the IAV copies/µg RNA in each group on a given day post infection. Although at 2 d.p.i. the statistical difference between formulation only and S18 + formulation was p=0.0743 and the formulation only versus S18 only was p=0.0973. IAV lung titres were determined upon experiment cessation by plaque assay described in 2.1.11. IAV lung viral titre was greatest in the PBS only group, but there was no statistically significant difference between any group following IAV infection, p=0.4690 (Figure 93).

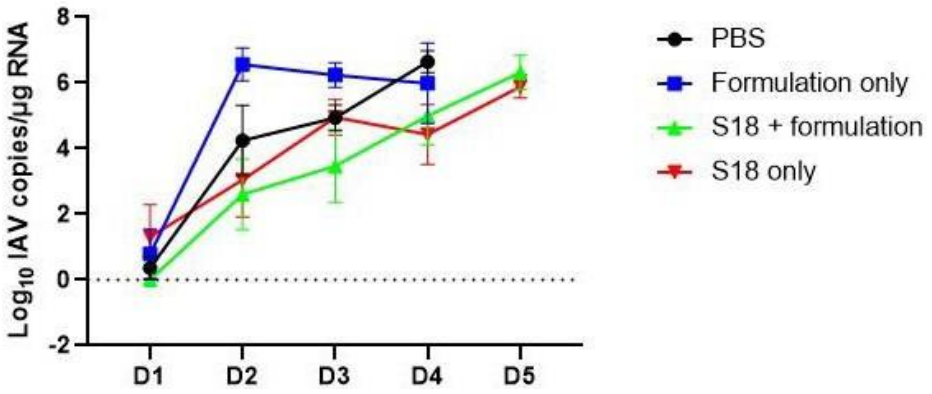

Figure 92. S18 does not affect the oral IAV viral load throughout infection.
Following IAV X31 infection, mice were swabbed daily to determine their IAV viral load. RNA was extracted from swabs and IAV copies/µg RNA determined by qPCR. Data represented by Mean ±SEM and statistical analysis was performed with two-way ANOVA and Bonferroni post-hoc test for IAV copies at each timepoint. Each group n=6, one independent experiment.

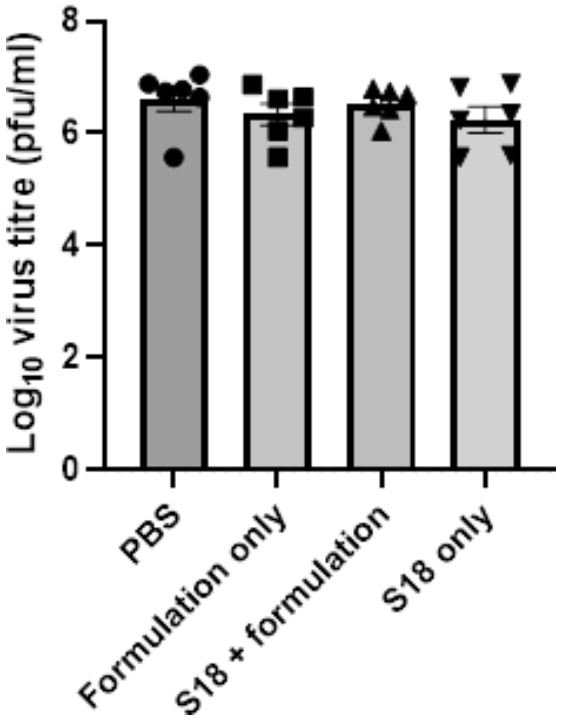

Figure 93. S18 does not affect lung viral titres during IAV infection.
Following IAV X31 infection, two lower right lung lobes were homogenized, and viral titre determined by plaque assay. Represented as individual data points and mean ±SEM and statistical analysis was performed with Kruskal-Wallis test. Each group n=6, one independent experiment.

5.4 Discussion

This chapter has described multiple approaches to investigate how SPLUNC1 functions during IAV infection. Firstly, hemagglutination assays revealed SPLUNC1 protein does not affect IAV hemagglutination. This means that SPLUNC1 does not interfere or prevent virus particles binding RBC and a lattice RBC structure forming. Therefore, SPLUNC1 protein does not inhibit or prevent IAV binding during infection, and this does not cause the antiviral activity seen against IAV.

To further study the impact of SPLUNC1 on IAV infection, *in vitro* IAV infections were performed with the addition and absence of SPLUNC1 protein, respectively. These results would be expected to mirror each other, with SPLUNC1 addition providing a protective, antiviral effect and SPLUNC1 depletion the opposite. However, neither the addition nor KO of SPLUNC1 from BAL had any effect on IAV infection. Specifically, SPLUNC1 did not affect IAV replication, infection, or viral titres *in vitro*. It is possible this does not mimic the *in vivo* results and differences seen between wildtype and SPLUNC1 KO mice previously (222) because these BAL samples were taken from uninfected mice where no immune response to IAV was present. This supports the results concluded from the hemagglutination experiment and suggests human SPLUNC1 protein does not meditate antiviral activity during IAV infection.

Two SPLUNC1 peptides have been identified as functionally active regions that mediate biological effects (230, 231). These were selected to investigate if they are involved in mediating the previously observed SPLUNC1 antiviral activity. These two peptides, S18 and SPX101, are both from one specific region of hSPLUNC1 that does not form part of SPLUNC1 3D protein structure (230, 233). The two peptides and their

scrambled negative control are stable in various conditions and not cytotoxic enabling them to be used in *in vitro* and *in vivo* experiments. However, they were not stable in BAL and therefore were administered in combination with SiSaf's formulation which is designed to aid retention in the respiratory tract and lung. This was to establish if delivery using the formulation impacted the activity of these peptide *in vivo*, where they may not be stable and easily degraded. However, there was not a significant difference in any result when the S18 peptide was administered *in vivo* using SiSaf's formulation or solely. Therefore, this delivery method did not increase S18 peptide activity or impact IAV infection during this study.

The effect of these SPLUNC1 peptides on *in vitro* IAV infection was assessed using four different cell lines. However, no statistically significant effect on infection was observed in any of these cell lines. It is possible this occurred due to a suboptimal concentration of peptide or due to the species difference between murine and human SPLUNC1 (172), as the KT cells are human and an antiviral role has not been described for human SPLUNC1, unlike its murine counterpart. Additionally, these peptides did not inhibit hemagglutination demonstrating they do not directly affect IAV binding or infection.

Converse to *in vitro* SPLUNC1 and IAV infection models, the administration of the SPLUNC1 peptide S18 *in vivo* to an acute IAV infection model did impact infection. It significantly increased the survival of mice during IAV infection and S18 treated mice lost less weight throughout infection, while this was only significant at certain timepoints. This demonstrates that the S18 peptide does influence IAV infection in mice and it could be the active region of SPLUNC1 that mediates its antiviral effect.

Interestingly, S18 peptide did not increase the survival of BALB/C mice by reducing IAV viral titre. There was no difference in viral titre determined by oral throat swabs throughout infection or in the lung titres determined at 5 d.p.i.. This suggests that S18 improves survival during IAV infection through an alternative mechanism such as immune modulation. To further investigate the impact of S18 on IAV infection a series of further experiments should be performed. This includes infecting mice with a lower IAV X31 dose to allow the effect of the peptide treatment on the later stages of infection and recovery to be analyzed. Additionally, cytokine levels should be studied to determine whether S18 is modulating these and the increase in survival observed is due to the prevention of a cytokine storm and an excessive immune response (120). These studies with S18 will provide important, further insights into how SPLUNC1 functions and whether its antiviral activity is due to the modulation of cytokine levels during IAV infection.

Together, this chapter has identified a possible mechanism that explains how SPLUNC1 mediates its previously observed antiviral activity against IAV virus. S18 influences the infection of mice, increasing their survival rate and reducing weight loss during infection. However, it does not alter viral titre throughout infection, unlike the phenotype seen in SPLUNC1 KO mice (222). Therefore, although an active region of SPLUNC1 that affects IAV infection has been identified further experiments are needed to investigate if S18 also mediates the lower viral titres observed in SPLUNC1 KO mice. Future experiments that should be performed include administering SPLUNC1 KO mice with the S18 peptide during IAV infection and analysing whether this reverses SPLUNC1 KO mice phenotype, or just impacts their survival and weight loss. Additionally, the creation of an S18 deficient mouse strain would isolate the

effect of S18 and allow a direct comparison between its phenotype during IAV infection and that of SPLUNC1 KO mice. The absence of SPLUNC1 protein having any noticeable effect on IAV in this chapter reaffirms that an alternative mechanism, such as S18 is likely responsible for meditating SPLUNC1 antiviral activity. Finally, S18 demonstrated an affect during IAV infection *in vivo* and not *in vitro*, this may be explained as follows: firstly, *in vivo* models study the infection within a whole living organism which allow the examination of more experimental endpoints that *in vitro* experiment don't allow, such as weight loss (269). Therefore, they might be a superior model for studying certain aspects of IAV infection and explain the different results these models have produced; also the *in vitro* experiments were mostly performed in human cell lines and human SPLUNC1 has not yet been associated with antiviral activity, unlike murine SPLUNC1 (172). However, this species differences between murine and human SPLUNC1 may not be responsible for this *in* vitro result as S18 originates from the human SPLUNC1 sequence. This sequence is partially conserved in mice, but is interrupted with the extra exon 2 region that is contained within murine SPLUNC1. Therefore, it could be that part of this S18 fragment mediates its *in vivo* activity and the extra murine region does not impact its activity. Alternatively the extra fragment in mSPLUNC1 could mediate other function as well, such as the modulation of viral titres during IAV infection in SPLUNC1 KO mice previously.

In summary, this chapter has identified that the hSPLUNC1 peptide S18 influences IAV infection and significantly decreases mortality. It also established that SPLUNC1 protein does not impact IAV infection *in vitro* and that S18 is the likely active region of SPLUNC1 that mediates its antiviral activity against IAV infection. However, further

investigation is needed to establish exactly how S18 functions and determine whether it modulates viral titres as well during IAV infection.

6 Final Discussion

The work presented in this thesis explored how SPLUNC1 mediates its antiviral activity against IAV. It is revealed that this activity is not due to a direct interaction between SPLUNC1 and IAV but is instead mediated, indirectly by the S18 peptide region of SPLUNC1, located near its N-terminus. S18 administration *in vivo* during IAV infection significantly increased survival and reduced weight loss, demonstrating it is an active of region of SPLUNC1 that modulates the hosts response during infection. Numerous methods have been used to explore how SPLUNC1 functions and mediates its antiviral activity against IAV. Together this data suggests an active region of SPLUNC1 mediates the host's response to infection. A multipronged approach was used to evaluate this thoroughly. Chapter 3 established that a direct interaction between SPLUNC1 and IAV does not occur, and direct interactions are not responsible for SPLUNC1 antiviral activity. The role of other endogenous biological co-factors was ruled out by supplementing murine BAL in the experiments, providing an environment more representative of what occurs *in vivo* where this antiviral activity is detected. Chapters 4 and 5 detailed IAV infections where SPLUNC1 was depleted and added back to establish how these differing conditions affected IAV infection. These experiments were performed *in vitro* to ascertain if these conditions mirrored the phenotypes expected following *in vivo* IAV infection of the SPLUNC1 KO model (222). Chapter 4 described the engineering of a SPLUNC1 KO cell line using CRISPR-Cas9 technology however, we demonstrate that SPLUNC1 deletion did not impact IAV infection. This observation was consistent, with infections performed with multiple biological replicates, at two different MOI, for 24 and 72 hours. This indicates SPLUNC1 protein does not affect IAV infection and replication, however this was

performed with human SPLUNC1 which has not yet been identified as antiviral unlike murine SPLUNC1 (222). Chapter 5 described the effect of SPLUNC1 addition during IAV infection and the impact of SPLUNC1 depletion of IAV infection in the presence of BAL. Like the depletion experiments performed in chapter 2, the addition of SPLUNC1 did not have an impact IAV infection. Additionally, the effect of SPLUNC1 depletion was assessed again when IAV infections were performed in the presence of WT and mSPLUNC1 KO BAL. However, there was no statistical difference in the cellular or supernatant viral titres was following infection either. Therefore, the SPLUNC1 addition and depletion experiments, where a mirror phenotype could be expected, suggests SPLUNC1 protein is not directly involved in modulating IAV infection and must be mediated by another mechanism, unlike other antiviral proteins such as ZAPS (113, 270). Chapter 5 additionally investigated specific derived SPLUNC1 peptides and their antiviral role during IAV. S18 *in vivo* experiments suggest S18 is involved in SPLUNC1 antiviral activity and modulates IAV infection. S18 significantly increases survival and decreases weight loss during IAV infection but does not achieve this through altering viral titre. The finding that only one antiviral mechanism is indicated from this thesis, and numerous others have been ruled out, supports the conclusion that S18 is a crucial, functional region of SPLUNC1 that can mediate antiviral activity against IAV.

Although data in this thesis demonstrates S18 is an antiviral, active region of SPLUNC1 this was only observed *in vivo*, not *in vitro*. This reaffirms the importance of *in vivo* models and exploring infection in the whole organism model, in the context of other systems not just cells (269). Despite *in vivo* models being superior in this aspect of modelling infection there are disadvantages of murine IAV models and how these

replicate natural IAV infection. Mice are only able to be infected with mouse adapted IAV strains which limits the study of specific strains. Additionally, they do not display all the clinical symptoms of IAV as mice typically get hypothermia, unlike humans who suffer from hyperthermia, and virus replication typically occurs in the lower respiratory tract, unlike humans where it occurs in the upper respiratory tract. Finally, they are not the most suitable small mammals for transmission experiments, ferrets are used more frequently as they mimic IAV respiratory symptoms and viral spread better. Therefore, caution should be taken when drawing conclusions from murine IAV infection experiments as they are not a natural IAV hosts and in certain experiments, other species might be more relevant hosts.

It is currently unclear how S18 functions and increases survival during IAV infection as it does not affect influenza viral titres. It is possible that S18 functions by modulating the cytokine response and decreases the excessive inflammation associated with increased weight loss and mortality during IAV infection (120). To investigate these mechanisms, serum and BAL should be analyzed to determine cytokine levels and whether they are modulated between the treatment groups. This could explain why mortality is lower in the treated groups but does not explain why viral titres are unchanged in the S18 treated groups but SPLUNC1 KO mice have decreased lung viral titres during IAV infection (222). This is because SPLUNC1 presence during the infection of NPC cells with EBV decreases the level of inflammatory cytokines such as TNF-α and weaken the inflammatory response to infection (218). TNF-α production is known to increase weight loss and can contribute to the severity of IAV infection (271, 272). Therefore, S18 may modulate TNF-α levels and contribute to the significant decrease in weight loss and mortality in the

treatment groups. Furthermore, SPLUNC1 could have two active regions that together modulate its antiviral activity. To establish whether S18 is solely responsible for the effect SPLUNC1 KO has on mice during IAV infection WT and SPLUNC1 KO mice should be inoculated with IAV and treated with S18 only and truncated SPLUNC1, without S18, to distinguish the elements of SPLUNC1 responsible for its antiviral activity. The reversal of the SPLUNC1 KO mice phenotype when S18 is administered would identify if S18 alone is responsible for the antiviral activity seen during IAV infection, however it is likely other elements of the host response are necessary for this antiviral activity to be mediated. Additionally, the impact of S18 treatment during IAV infection should be explored further with an experiment where mice are inoculated with a non-lethal dose of IAV and mice treated daily till 14 d.p.i., when mice have recovered to pre-infection weight and all virus has been cleared. This would allow the effect of S18 on the later stages of infection and recovery to be assessed. This is particularly important as weight loss in SPLUNC1 KO mice during IAV is statistically significant during these later phases and in recovery, not the first 5 days as studied in this experiment (222). Together, these two experiments would provide vital data that could massively increase our knowledge of how S18 modulates IAV infection and the host response. This data could enable S18 to be investigated as a potential adjuvant or therapy for IAV infection, which could revolutionize treatment for a virus that has a massive health, social and economic burden annually.

In this thesis both human and murine SPLUNC1 have been investigated in the context of IAV infections. To date only murine SPLUNC1 has been described in the literature as having antiviral activity against IAV, and other viruses (217, 218, 220). Therefore, the use of human SPLUNC1 in some experiments and its KO in KT cells using CRISPR-

Cas9 editing technology could be a limitation of the study and may have affected the results, if human SPLUNC1 does not also have antiviral activity. Future studies investigating whether human SPLUNC1 is antiviral would be beneficial and could have a massive impact on possible future infection inventions. This is particularly important because of the structural differences between murine and human SPLUNC1; murine SPLUNC1 includes an additional amino acid region in exon 2 and undergoes N-glycosylation (162, 171, 172). This use of mouse cell lines for CRIPSR-Cas9 editing or *in vitro* peptide IAV infection models would help establish whether the benefits of *in vivo* models is responsible for the lack of difference detected in the *in vitro* experiments in this thesis or if it is due to human SPLUNC1 being used.

S18 has already been described and proven an active region of SPLUNC1 that mediates antiviral activity however, there are still other characteristics SPLUNC1 has during IAV infection that need to be investigated to completely understand how SPLUNC1 functions (230-232). This particularly involves exploring the modulation of SPLUNC1 expression during IAV and IL - 13 role in this. IL-13 is known to downregulate SPLUNC1 expression and during the initial stages of IAV infection SPLUNC1 expression decreases, converse to what you might expect from an antiviral protein (185). Therefore, the further study of these two elements during IAV infection, and whether S18 impacts them, is worth establishing and could unpin key elements into SPLUNC1 mechanism of action. Additionally, although the SPLUNC1 KO KT cell line did not have significantly different viral titres following infection it could still contain vital information detailing the impact SPLUNC1 has on infection. Especially as S18 is included in the deleted SPLUNC1 gDNA region in this cell line. Analysis of the transcriptome of WT and SPLUNC1 KO IAV infected cell will identify alterations in

gene expression and highlight the differences that occur when SPLUNC1 is depleted (117). Combined with the future experiments suggested *in vivo* with S18 and *in vitro* in mouse cell line this could decipher exactly how SPLUNC1 mediates it antiviral activity against IAV.

In summary, the specific active region that mediates SPLUNC1 antiviral activity against IAV has been identified. S18 administration decreases mortality and morbidity during IAV infection *in vivo* but does not achieve this through altering viral titre. The recognition that the S18 region is responsible for antiviral activity means it can be investigated as a possible adjuvant or therapy against IAV and reduce the burden this disease places on society.

7 References

1. P. Palese MS. Orthomyxoviridae. DM. Knipe PH, editor. Philadelphia: Lippincott Williams & Wilkins; 2013.
2. Organisation WH. Influenza (Seasonal) - Fact Sheet 2018 [Available from: https://www.who.int/news-room/fact-sheets/detail/influenza-(seasonal).
3. Memorandums M-LJBoWHO. A revision of the system of nomenclature for influenza viruses: a WHO memorandum. 1980;58(4):585-91.
4. Chu C, Dawson I, Elford W. Filamentous forms associated with newly isolated influenza virus. Lancet. 1949:602-3.
5. Lamb RA, Choppin PW. Segment 8 of the influenza virus genome is unique in coding for two polypeptides. Proceedings of the National Academy of Sciences. 1979;76(10):4908-12.
6. Allen H, McCauley J, Waterfield M, Gething M-J. Influenza virus RNA segment 7 has the coding capacity for two polypeptides. Virology. 1980;107(2):548-51.
7. Porter AG, Smith JC, Emtage JS. Nucleotide sequence of influenza virus RNA segment 8 indicates that coding regions for NS1 and NS2 proteins overlap. Proceedings of the National Academy of Sciences. 1980;77(9):5074-8.
8. Tong S, Zhu X, Li Y, Shi M, Zhang J, Bourgeois M, et al. New world bats harbor diverse influenza A viruses. PLoS pathogens. 2013;9(10):e1003657.
9. Chizhmakov I, Geraghty F, Ogden D, Hayhurst A, Antoniou M, Hay A. Selective proton permeability and pH regulation of the influenza virus M2 channel expressed in mouse erythroleukaemia cells. The Journal of physiology. 1996;494(2):329-36.
10. Ciampor F, Bayley P, Nermut M, Hirst E, Sugrue R, Hay A. Evidence that the amantadine-induced, M2-mediated conversion of influenza A virus hemagglutinin to the low pH conformation occurs in an acidic trans Golgi compartment. Virology. 1992;188(1):14-24.
11. Calder LJ, Wasilewski S, Berriman JA, Rosenthal PB. Structural organization of a filamentous influenza A virus. Proceedings of the National Academy of Sciences. 2010;107(23):10685-90.
12. Seladi-Schulman J, Steel J, Lowen AC. Spherical influenza viruses have a fitness advantage in embryonated eggs, while filament-producing strains are selected in vivo. Journal of virology. 2013:JVI. 02004-13.
13. Dadonaite B, Vijayakrishnan S, Fodor E, Bhella D, Hutchinson ECJTJogv. Filamentous influenza viruses. 2016;97(8):1755.
14. Baudin F, Bach C, Cusack S, Ruigrok R. Structure of influenza virus RNP. I. Influenza virus nucleoprotein melts secondary structure in panhandle RNA and exposes the bases to the solvent. The EMBO journal. 1994;13(13):3158-65.
15. Gottschalk A. On the mechanism underlying initiation of influenza virus infection. Ergebnisse der Mikrobiologie Immunitätsforschung und Experimentellen Therapie: Springer; 1959. p. 1-22.
16. Wharton S, Belshe R, Skehel J, Hay A. Role of virion M2 protein in influenza virus uncoating: specific reduction in the rate of membrane fusion between virus and liposomes by amantadine. Journal of general virology. 1994;75(4):945-8.
17. Skehel J, Bayley P, Brown E, Martin S, Waterfield M, White J, et al. Changes in the conformation of influenza virus hemagglutinin at the pH optimum of virus-mediated membrane fusion. Proceedings of the National Academy of Sciences. 1982;79(4):968-72.
18. Bullough PA, Hughson FM, Skehel JJ, Wiley DC. Structure of influenza haemagglutinin at the pH of membrane fusion. Nature. 1994;371(6492):37.

19. Weber T, Paesold G, Galli C, Mischler R, Semenza G, Brunner J. Evidence for H (+)-induced insertion of influenza hemagglutinin HA2 N-terminal segment into viral membrane. Journal of Biological Chemistry. 1994;269(28):18353-8.
20. Durrer P, Galli C, Hoenke S, Corti C, Glück R, Vorherr T, et al. H+-induced membrane insertion of influenza virus hemagglutinin involves the HA2 amino-terminal fusion peptide but not the coiled coil region. Journal of Biological Chemistry. 1996;271(23):13417-21.
21. Markovic I, Leikina E, Zhukovsky M, Zimmerberg J, Chernomordik LV. Synchronized activation and refolding of influenza hemagglutinin in multimeric fusion machines. J Cell Biol. 2001;155(5):833-44.
22. Zhirnov O. Solubilization of matrix protein M1/M from virions occurs at different pH for orthomyxo-and paramyxoviruses. Virology. 1990;176(1):274-9.
23. Li S, Sieben C, Ludwig K, Höfer CT, Chiantia S, Herrmann A, et al. pH-Controlled two-step uncoating of influenza virus. Biophysical journal. 2014;106(7):1447-56.
24. Matlin KS, Reggio H, Helenius A, Simons K. Infectious entry pathway of influenza virus in a canine kidney cell line. J Cell Biol. 1981;91(3):601-13.
25. Jones IM, Reay PA, Philpott K. Nuclear location of all three influenza polymerase proteins and a nuclear signal in polymerase PB2. The EMBO journal. 1986;5(9):2371-6.
26. Akkina R, Chambers T, Londo D, Nayak D. Intracellular localization of the viral polymerase proteins in cells infected with influenza virus and cells expressing PB1 protein from cloned cDNA. Journal of virology. 1987;61(7):2217-24.
27. O'Neill RE, Jaskunas R, Blobel G, Palese P, Moroianu J. Nuclear import of influenza virus RNA can be mediated by viral nucleoprotein and transport factors required for protein import. Journal of Biological Chemistry. 1995;270(39):22701-4.
28. Martin K, Heleniust A. Nuclear transport of influenza virus ribonucleoproteins: the viral matrix protein (M1) promotes export and inhibits import. Cell. 1991;67(1):117-30.
29. Klumpp K, Ruigrok RW, Baudin F. Roles of the influenza virus polymerase and nucleoprotein in forming a functional RNP structure. The EMBO journal. 1997;16(6):1248-57.
30. Noble E, Mathews DH, Chen JL, Turner DH, Takimoto T, Kim B. Biophysical analysis of influenza A virus RNA promoter at physiological temperatures. Journal of Biological Chemistry. 2011:jbc. M111. 239509.
31. Plotch SJ, Bouloy M, Ulmanen I, Krug RM. A unique cap (m7GpppXm)-dependent influenza virion endonuclease cleaves capped RNAs to generate the primers that initiate viral RNA transcription. Cell. 1981;23(3):847-58.
32. Li ML, Ramirez BC, Krug RM. RNA-dependent activation of primer RNA production by influenza virus polymerase: different regions of the same protein subunit constitute the two required RNA-binding sites. The EMBO journal. 1998;17(19):5844-52.
33. Robertson JS, Schubert M, Lazzarini RA. Polyadenylation sites for influenza virus mRNA. Journal of virology. 1981;38(1):157-63.
34. O'Neill RE, Talon J, Palese P. The influenza virus NEP (NS2 protein) mediates the nuclear export of viral ribonucleoproteins. The EMBO journal. 1998;17(1):288-96.
35. Bui M, Wills EG, Helenius A, Whittaker GRJJov. Role of the influenza virus M1 protein in nuclear export of viral ribonucleoproteins. 2000;74(4):1781-6.
36. Boulan ER, Sabatini DD. Asymmetric budding of viruses in epithelial monlayers: a model system for study of epithelial polarity. Proceedings of the National Academy of Sciences. 1978;75(10):5071-5.
37. Leser GP, Lamb RA. Influenza virus assembly and budding in raft-derived microdomains: a quantitative analysis of the surface distribution of HA, NA and M2 proteins. Virology. 2005;342(2):215-27.
38. Fujii Y, Goto H, Watanabe T, Yoshida T, Kawaoka Y. Selective incorporation of influenza virus RNA segments into virions. Proceedings of the National Academy of Sciences. 2003;100(4):2002-7.

39. Noda T, Sagara H, Yen A, Takada A, Kida H, Cheng RH, et al. Architecture of ribonucleoprotein complexes in influenza A virus particles. Nature. 2006;439(7075):490.
40. Palese P, Tobita K, Ueda M, Compans RW. Characterization of temperature sensitive influenza virus mutants defective in neuraminidase. Virology. 1974;61(2):397-410.
41. Both GW, Sleigh M, Cox N, Kendal AJJov. Antigenic drift in influenza virus H3 hemagglutinin from 1968 to 1980: multiple evolutionary pathways and sequential amino acid changes at key antigenic sites. The Influenza Viruses. 1983;48(1):52-60.
42. Bouvier NM, Palese PJV. The biology of influenza viruses. Vaccine. 2008;26:D49-D53.
43. Kim H, Webster RG, Webby RJJVi. Influenza virus: dealing with a drifting and shifting pathogen. Viral Immunology. 2018;31(2):174-83.
44. Scholtissek CJVg. Molecular evolution of influenza viruses. Virus Genes. 1995;11(2):209-15.
45. Burnet F, Lind PJM. A Genetic Approach to Variation in Influenza Viruses: 3. Recombination of Characters in Influenza Virus Strains Used in Mixed Infections. Microbiology. 1951;5(1):59-66.
46. Hirst GK, Gotlieb TJTJoem. The experimental production of combination forms of virus: I. Occurrence of combination forms after simultaneous inoculation of the allantoic sac with two distinct strains of influenza virus. The Journal of Experimental Medicine. 1953;98(1):41-52.
47. Cox NJ, Subbarao KJArom. Global epidemiology of influenza: past and present. Annual Review of Medicine. 2000;51(1):407-21.
48. Reid AH, Fanning TG, Hultin JV, Taubenberger JKJPotNAoS. Origin and evolution of the 1918 “Spanish” influenza virus hemagglutinin gene. Proceedings of the National Academy of Sciences. 1999;96(4):1651-6.
49. Kawaoka Y, Krauss S, Webster RGJJov. Avian-to-human transmission of the PB1 gene of influenza A viruses in the 1957 and 1968 pandemics. Journal of Virology. 1989;63(11):4603-8.
50. Fang R, Jou WM, Huylebroeck D, Devos R, Fiers WJC. Complete structure of A/duck/Ukraine/63 influenza hemagglutinin gene: animal virus as progenitor of human H3 Hong Kong 1968 influenza hemagglutinin. Cell. 1981;25(2):315-23.
51. Garten RJ, Davis CT, Russell CA, Shu B, Lindstrom S, Balish A, et al. Antigenic and genetic characteristics of swine-origin 2009 A (H1N1) influenza viruses circulating in humans. Science. 2009;325(5937):197-201.
52. Fitch WM, Leiter J, Li X, Palese PJPotNAoS. Positive Darwinian evolution in human influenza A viruses. Proceedings of the National Academy of Sciences. 1991;88(10):4270-4.
53. Webby R, Webster RJPTotRSoLSBBS. Emergence of influenza A viruses. The Royal Society. 2001;356(1416):1817-28.
54. Carrat F, Flahault AJV. Influenza vaccine: the challenge of antigenic drift. Vaccine. 2007;25(39-40):6852-62.
55. Treanor JJNEJoM. Influenza vaccine—outmaneuvering antigenic shift and drift. The New England Journal of Medicine. 2004;350(3):218-20.
56. Ferguson NM, Galvani AP, Bush RMJN. Ecological and immunological determinants of influenza evolution. Nature. 2003;422(6930):428-33.
57. Long JS, Mistry B, Haslam SM, Barclay WSJNRM. Host and viral determinants of influenza A virus species specificity. Nature Reviews Microbiology. 2019;17(2):67-81.
58. Scholtissek CJMP, Practice. Pigs as ‘mixing vessels’ for the creation of new pandemic influenza A viruses. 1990;2(2):65-71.
59. Beare A, Webster RJAov. Replication of avian influenza viruses in humans. Archives of Virology. 1991;119(1):37-42.
60. Ito T, Couceiro JNS, Kelm S, Baum LG, Krauss S, Castrucci MR, et al. Molecular basis for the generation in pigs of influenza A viruses with pandemic potential. Journal of Virology. 1998;72(9):7367- 73.

61. (WHO) WHO. Avian influenza A(H5N8) infects humans in Russian Federation 2021 [Available from: https://www.euro.who.int/en/countries/poland/news/news/2021/3/avian-influenza-ah5n8-infects-humans-in-russian-federation.
62. (WHO) WHO. Human infection with avian influenza A(H10N3) – China: WHO; 2021 [Available from: https://www.who.int/emergencies/disease-outbreak-news/item/human-infection-with-avian-influenza-a(h10n3)-china.
63. Scholtissek C, Naylor EJN. Fish farming and influenza pandemics. Nature. 1988;331(6153):215-.
64. Smith GJ, Vijaykrishna D, Bahl J, Lycett SJ, Worobey M, Pybus OG, et al. Origins and evolutionary genomics of the 2009 swine-origin H1N1 influenza A epidemic. Nature 2009;459(7250):1122-5.
65. Trifonov V, Khiabanian H, Rabadan RJNEjom. Geographic dependence, surveillance, and origins of the 2009 influenza A (H1N1) virus. The New England Journal of Medicine. 2009;361(2):115-9.
66. Weitnauer M, Mijošek V, Dalpke AJMi. Control of local immunity by airway epithelial cells. Mucosal Immunology. 2016;9(2):287-98.
67. Whitsett JA, Alenghat TJNi. Respiratory epithelial cells orchestrate pulmonary innate immunity. Nature Immunology. 2015;16(1):27.
68. Bustamante-Marin XM, Ostrowski LEJCSHpib. Cilia and mucociliary clearance. Cold Spring Harbor Perspectives in Biology. 2017;9(4):a028241.
69. Numata M, Mitchell JR, Tipper JL, Brand JD, Trombley JE, Nagashima Y, et al. Pulmonary surfactant lipids inhibit infections with the pandemic H1N1 influenza virus in several animal models. The Journal of Biological Chemistry. 2020;295(6):1704-15.
70. Li G, Siddiqui J, Hendry M, Akiyama J, Edmondson J, Brown C, et al. Surfactant protein-A–deficient mice display an exaggerated early inflammatory response to a β-resistant strain of influenza A virus. American Journal of Respiratory Cell and Molecular Biology. 2002;26(3):277-82.
71. LeVine AM, Whitsett JA, Hartshorn KL, Crouch EC, Korfhagen TRJTJoI. Surfactant protein D enhances clearance of influenza A virus from the lung in vivo. Journal of Immunology. 2001;167(10):5868- 73.
72. Hartshorn KL, Crouch EC, White MR, Eggleton P, Tauber AI, Chang D, et al. Evidence for a protective role of pulmonary surfactant protein D (SP-D) against influenza A viruses. The Journal of clinical investigation. 1994;94(1):311-9.
73. Hsieh I-N, De Luna X, White MR, Hartshorn KLJFii. The role and molecular mechanism of action of surfactant protein D in innate host defense against influenza A virus. Frontiers in Immunology. 2018;9:1368.
74. Hartshorn KL, Webby R, White MR, Tecle T, Pan C, Boucher S, et al. Role of viral hemagglutinin glycosylation in anti-influenza activities of recombinant surfactant protein D. Respiratory Research. 2008;9(1):1-12.
75. Hawgood S, Brown C, Edmondson J, Stumbaugh A, Allen L, Goerke J, et al. Pulmonary collectins modulate strain-specific influenza a virus infection and host responses. Journal of Virology. 2004;78(16):8565-72.
76. Vénéreau E, Ceriotti C, Bianchi MEJFii. DAMPs from cell death to new life. 2015;6:422.
77. Allen IC, Moore CB, Schneider M, Lei Y, Davis BK, Scull MA, et al. NLRX1 protein attenuates inflammatory responses to infection by interfering with the RIG-I-MAVS and TRAF6-NF-κB signaling pathways. Immunity. 2011;34(6):854-65.
78. Barton GM, Medzhitov RJS. Toll-like receptor signaling pathways. Science. 2003;300(5625):1524-5.
79. Alexopoulou L, Holt AC, Medzhitov R, Flavell RAJN. Recognition of double-stranded RNA and activation of NF-κB by Toll-like receptor. Nature. 2001;413(6857):732-8.

80. Le Goffic R, Pothlichet J, Vitour D, Fujita T, Meurs E, Chignard M, et al. Cutting Edge: Influenza A virus activates TLR3-dependent inflammatory and RIG-I-dependent antiviral responses in human lung epithelial cells. The Journal of Immunology. 2007;178(6):3368-72.
81. Lund JM, Alexopoulou L, Sato A, Karow M, Adams NC, Gale NW, et al. Recognition of single-stranded RNA viruses by Toll-like receptor. PNAS. 7. 2004;101(15):5598-603.
82. Heil F, Hemmi H, Hochrein H, Ampenberger F, Kirschning C, Akira S, et al. Species-specific recognition of single-stranded RNA via toll-like receptor 7 and 8. Science. 2004;303(5663):1526-9.
83. Diebold SS, Kaisho T, Hemmi H, Akira S, e Sousa CR. Innate antiviral responses by means of TLR7-mediated recognition of single-stranded RNA. Science. 2004;303(5663):1529-31.
84. Allen IC, Scull MA, Moore CB, Holl EK, McElvania-TeKippe E, Taxman DJ, et al. The NLRP3 inflammasome mediates in vivo innate immunity to influenza A virus through recognition of viral RNA. Immunity. 2009;30(4):556-65.
85. Loo Y-M, Gale Jr MJI. Immune signaling by RIG-I-like receptors. Immunity. 2011;34(5):680-92.
86. Killip MJ, Fodor E, Randall RE. Influenza virus activation of the interferon system. Virus research. 2015;209:11-22.
87. Kato H, Takeuchi O, Sato S, Yoneyama M, Yamamoto M, Matsui K, et al. Differential roles of MDA5 and RIG-I helicases in the recognition of RNA viruses. Nature. 2006;441(7089):101.
88. Hüsser L, Alves MP, Ruggli N, Summerfield A. Identification of the role of RIG-I, MDA-5 and TLR3 in sensing RNA viruses in porcine epithelial cells using lentivirus-driven RNA interference. Virus research. 2011;159(1):9-16.
89. Mibayashi M, Martínez-Sobrido L, Loo Y-M, Cárdenas WB, Gale M, García-Sastre AJJov. Inhibition of retinoic acid-inducible gene I-mediated induction of beta interferon by the NS1 protein of influenza A virus. Journal of Virology. 2007;81(2):514-24.
90. Gack MU, Albrecht RA, Urano T, Inn K-S, Huang I-C, Carnero E, et al. Influenza A virus NS1 targets the ubiquitin ligase TRIM25 to evade recognition by the host viral RNA sensor RIG-I. Cell Host Microbe. 2009;5(5):439-49.
91. Anastasina M, Le May N, Bugai A, Fu Y, Söderholm S, Gaelings L, et al. Influenza virus NS1 protein binds cellular DNA to block transcription of antiviral genes. Biochimica et Biophysica Acta (BBA)-Gene Regulatory Mechanisms. 2016;1859(11):1440-8.
92. Chen S, Short J, Young D, Killip M, Schneider M, Goodbourn S, et al. Heterocellular induction of interferon by negative-sense RNA viruses. Virology. 2010;407(2):247-55.
93. Ank N, West H, Bartholdy C, Eriksson K, Thomsen AR, Paludan SRJJov. Lambda interferon (IFN-λ), a type III IFN, is induced by viruses and IFNs and displays potent antiviral activity against select virus infections in vivo. Journal of Virology. 2006;80(9):4501-9.
94. Siegal FP, Kadowaki N, Shodell M, Fitzgerald-Bocarsly PA, Shah K, Ho S, et al. The nature of the principal type 1 interferon-producing cells in human blood. Science. 1999;284(5421):1835-7.
95. Ioannidis I, Ye F, McNally B, Willette M, Flaño E. Toll-like receptor expression and induction of type I and type III interferons in primary airway epithelial cells. Journal of virology. 2013;87(6):3261-70.
96. Zhou Z, Hamming OJ, Ank N, Paludan SR, Nielsen AL, Hartmann RJJov. Type III interferon (IFN) induces a type I IFN-like response in a restricted subset of cells through signaling pathways involving both the Jak-STAT pathway and the mitogen-activated protein kinases. Journal of Virology. 2007;81(14):7749-58.
97. Klinkhammer J, Schnepf D, Ye L, Schwaderlapp M, Gad HH, Hartmann R, et al. IFN-λ prevents influenza virus spread from the upper airways to the lungs and limits virus transmission. Elife. 2018;7:e33354.
98. Chawla-Sarkar M, Lindner DJ, Liu Y-F, Williams B, Sen GC, Silverman RH, et al. Apoptosis and interferons: role of interferon-stimulated genes as mediators of apoptosis.

Apoptosis. 2003;8(3):237-49.
99. Villalón-Letelier F, Brooks AG, Saunders PM, Londrigan SL, Reading PCJV. Host cell restriction factors that limit influenza A infection. Viruses. 2017;9(12):376.
100. Goodman AG, Smith JA, Balachandran S, Perwitasari O, Proll SC, Thomas MJ, et al. The cellular protein P58IPK regulates influenza virus mRNA translation and replication through a PKR-mediated mechanism. Journal of virology. 2007;81(5):2221-30.
101. Bergmann M, Garcia-Sastre A, Carnero E, Pehamberger H, Wolff K, Palese P, et al. Influenza virus NS1 protein counteracts PKR-mediated inhibition of replication. Journal of Virology. 2000;74(13):6203-6.
102. Li S, Min J-Y, Krug RM, Sen GCJV. Binding of the influenza A virus NS1 protein to PKR mediates the inhibition of its activation by either PACT or double-stranded RNA. Virology. 2006;349(1):13-21.
103. Chesarino NM, Compton AA, McMichael TM, Kenney AD, Zhang L, Soewarna V, et al. IFITM 3 requires an amphipathic helix for antiviral activity. EMBO reports. 2017;18(10):1740-51.
104. Brass AL, Huang I-C, Benita Y, John SP, Krishnan MN, Feeley EM, et al. The IFITM proteins mediate cellular resistance to influenza A H1N1 virus, West Nile virus, and dengue virus. Cell. 2009;139(7):1243-54.
105. Desai TM, Marin M, Chin CR, Savidis G, Brass AL, Melikyan GB. IFITM3 restricts influenza A virus entry by blocking the formation of fusion pores following virus-endosome hemifusion. PLoS Pathog. 2014;10(4):e1004048.
106. Bailey CC, Huang I-C, Kam C, Farzan M. Ifitm3 limits the severity of acute influenza in mice. PLoS Pathog. 2012;8(9):e1002909.
107. Zhang J, Huang F, Tan L, Bai C, Chen B, Liu J, et al. Host protein Moloney leukemia virus 10 (MOV10) acts as a restriction factor of influenza A virus by inhibiting the nuclear import of the viral nucleoprotein. Journal of virology. 2016;90(8):3966-80.
108. Chen G, Liu C-H, Zhou L, Krug RM. Cellular DDX21 RNA helicase inhibits influenza A virus replication but is counteracted by the viral NS1 protein. Cell host & microbe. 2014;15(4):484-93.
109. Tang Q, Wang X, Gao G. The short form of the zinc finger antiviral protein inhibits influenza A virus protein expression and is antagonized by the virus-encoded NS1. Journal of virology. 2017;91(2).
110. Li Y, Banerjee S, Wang Y, Goldstein SA, Dong B, Gaughan C, et al. Activation of RNase L is dependent on OAS3 expression during infection with diverse human viruses. Proceedings of the National Academy of Sciences. 2016;113(8):2241-6.
111. Fu B, Wang L, Ding H, Schwamborn JC, Li S, Dorf ME. TRIM32 senses and restricts influenza A virus by ubiquitination of PB1 polymerase. PLoS Pathog. 2015;11(6):e1004960.
112. Di Pietro A, Kajaste-Rudnitski A, Oteiza A, Nicora L, Towers GJ, Mechti N, et al. TRIM22 inhibits influenza A virus infection by targeting the viral nucleoprotein for degradation. 2013;87(8):4523-33.
113. Liu C-H, Zhou L, Chen G, Krug RM. Battle between influenza A virus and a newly identified antiviral activity of the PARP-containing ZAPL protein. Proceedings of the National Academy of Sciences. 2015;112(45):14048-53.
114. Xiao H, Killip MJ, Staeheli P, Randall RE, Jackson D. The human interferon-induced MxA protein inhibits early stages of influenza A virus infection by retaining the incoming viral genome in the cytoplasm. Journal of virology. 2013;87(23):13053-8.
115. Arimori Y, Nakamura R, Yamada H, Shibata K, Maeda N, Kase T, et al. Type I interferon plays opposing roles in cytotoxicity and interferon-γ production by natural killer and CD8+ T cells after influenza a virus infection in mice. Journal of Innate Immunity. 2014;6(4):456-66.
116. Högner K, Wolff T, Pleschka S, Plog S, Gruber AD, Kalinke U, et al. Macrophage-expressed IFN-β contributes to apoptotic alveolar epithelial cell injury in severe influenza

virus pneumonia. PLoS Pathogens. 2013;9(2).
117. Hemann EA, Green R, Turnbull JB, Langlois RA, Savan R, Gale MJNi. Interferon-λ modulates dendritic cells to facilitate T cell immunity during infection with influenza A virus. Nature Immunology. 2019;20(8):1035-45.
118. Newton AH, Cardani A, Braciale TJ, editors. The host immune response in respiratory virus infection: balancing virus clearance and immunopathology. Seminars in immunopathology; 2016: Springer.
119. Yang S, Adaway M, Du J, Huang S, Sun J, Bidwell JP, et al. NMP4 regulates the innate immune response to influenza A virus infection. Mucosal Immunology. 2020:1-10.
120. Teijaro JR, Walsh KB, Cahalan S, Fremgen DM, Roberts E, Scott F, et al. Endothelial cells are central orchestrators of cytokine amplification during influenza virus infection. Cell. 2011;146(6):980-91.
121. Kochs G, Martínez-Sobrido L, Lienenklaus S, Weiss S, García-Sastre A, Staeheli PJTJogv. Strong interferon-inducing capacity of a highly virulent variant of influenza A virus strain PR8 with deletions in the NS1 gene. The Journal of General Virology. 2009;90(Pt 12):2990.
122. Varga ZT, Ramos I, Hai R, Schmolke M, García-Sastre A, Fernandez-Sesma A, et al. The influenza virus protein PB1-F2 inhibits the induction of type I interferon at the level of the MAVS adaptor protein. PLoS Pathogens. 2011;7(6):e1002067.
123. Graef KM, Vreede FT, Lau Y-F, McCall AW, Carr SM, Subbarao K, et al. The PB2 subunit of the influenza virus RNA polymerase affects virulence by interacting with the mitochondrial antiviral signaling protein and inhibiting expression of beta interferon. Journal of Virology. 2010;84(17):8433-45.
124. Kolaczkowska E, Kubes PJNri. Neutrophil recruitment and function in health and inflammation. Nature Reviews Immunology. 2013;13(3):159-75.
125. Hunter CA, Gabriel KE, Radzanowski T, Neyer LE, Remington JS. Type I interferons enhance production of IFN-γ by NK cells. Immunology Letters. 1997;59(1):1-5.
126. Jegerlehner A, Schmitz N, Storni T, Bachmann MFJTJoI. Influenza A vaccine based on the extracellular domain of M2: weak protection mediated via antibody-dependent NK cell activity. Journal of Immunology. 2004;172(9):5598-605.
127. Biron CA, Nguyen KB, Pien GC, Cousens LP, Salazar-Mather TPJAroi. Natural killer cells in antiviral defense: function and regulation by innate cytokines. 1999;17(1):189-220.
128. Monteiro JM, Harvey C, Trinchieri GJJov. Role of interleukin-12 in primary influenza virus infection. Journal of Virology. 1998;72(6):4825-31.
129. Weiss ID, Wald O, Wald H, Beider K, Abraham M, Galun E, et al. IFN-γ treatment at early stages of influenza virus infection protects mice from death in a NK cell-dependent manner. JOURNAL OF INTERFERON & CYTOKINE RESEARCH. 2010;30(6):439-49.
130. Stein-Streilein J, Guffee JJTJoI. In vivo treatment of mice and hamsters with antibodies to asialo GM1 increases morbidity and mortality to pulmonary influenza infection. Journal of Immunology. 1986;136(4):1435-41.
131. Stein-Streilein J, Guffee J, Fan WJ. Locally and systemically derived natural killer cells participate in defense against intranasally inoculated influenza virus. Regional Immunology. 1988;1(2):100-5.
132. Zhou G, Juang SWW, Kane KP. NK cells exacerbate the pathology of influenza virus infection in mice. European Journal of Immunology. 2013;43(4):929-38.
133. Kay AW, Fukuyama J, Aziz N, Dekker CL, Mackey S, Swan GE, et al. Enhanced natural killer-cell and T-cell responses to influenza A virus during pregnancy. PNAS. 2014;111(40):14506- 11.
134. Carlin LE, Hemann EA, Zacharias ZR, Heusel JW, Legge KLJFii. Natural killer cell recruitment to the lung during influenza A virus infection is dependent on CXCR3, CCR5, and virus exposure dose. Frontiers in Immunology. 2018;9:781.
135. Waithman J, Mintern JD. Dendritic cells and influenza A virus infection. Virulence.

2012;3(7):603-8.
136. Kim TS, Braciale TJ. Respiratory dendritic cell subsets differ in their capacity to support the induction of virus-specific cytotoxic CD8+ T cell responses. PLoS ONE. 2009;4(1):e4204.
137. Flaherty DK. Immunology for pharmacy: Elsevier/Mosby; 2012.
138. Hufford MM, Richardson G, Zhou H, Manicassamy B, García-Sastre A, Enelow RI, et al. Influenza-infected neutrophils within the infected lungs act as antigen presenting cells for anti-viral CD8+ T cells. PLoS ONE. 2012;7(10):e46581.
139. Tate MD, Brooks AG, Reading PC, Mintern JD. Neutrophils sustain effective CD8+ T-cell responses in the respiratory tract following influenza infection. Immunology and Cell Biology. 2012;90(2):197-205.
140. Smed-sörensen A, Chalouni C, Chatterjee B, Cohn L, Blattmann P, Nakamura N, et al. Influenza A Virus Infection of Human Primary Dendritic Cells Impairs Their Ability to Cross-Present Antigen to. PLoS Patogens. 2011.
141. Corthay AJS. A three-cell model for activation of naive T helper cells. Scandinavian Journal of Immunology, 2006;64(2):93-6.
142. Gizinski AM, Fox DA, Sarkar SJ. Co-stimulation and T cells as therapeutic targets. Best Pract Res Clin Rheumatology. 2010;24(4):463-77.
143. Bhat P, Leggatt G, Waterhouse N, Frazer IH. Interferon-γ derived from cytotoxic lymphocytes directly enhances their motility and cytotoxicity. Cell death & Disease. 2017;8(6):e2836-e.
144. Luckheeram RV, Zhou R, Verma AD, Xia B. CD4+ T cells: differentiation and functions. Clinical and Developmental Immunology. 2012;2012.
145. Bender BS, Croghan T, Zhang L, Small Jr P. Transgenic mice lacking class I major histocompatibility complex-restricted T cells have delayed viral clearance and increased mortality after influenza virus challenge. The Journal of experimental medicine. 1992;175(4):1143-5.
146. Dong W, Bhide Y, Sicca F, Meijerhof T, Guilfoyle K, Engelhardt OG, et al. Cross-protective immune responses induced by sequential influenza virus infection and by sequential vaccination with inactivated influenza vaccines. Frontiers in Immunology. 2018;9:2312.
147. Riberdy JM, Christensen JP, Branum K, Doherty PCJJov. Diminished primary and secondary influenza virus-specific CD8+ T-cell responses in CD4-depleted Ig−/− mice. Journal of Virology. 2000;74(20):9762-5.
148. Belz GT, Wodarz D, Diaz G, Nowak MA, Doherty PCJJov. Compromised influenza virus-specific CD8+-T-cell memory in CD4+-T-cell-deficient mice. Journal of Virology. 2002;76(23):12388-93.
149. Duan S, Thomas PG. Balancing immune protection and immune pathology by CD8+ T-cell responses to influenza infection. Frontiers in Immunology. 2016;7:25.
150. Wells MA, Albrecht P, Ennis FA. Recovery from a viral respiratory infection. I. Influenza pneumonia in normal and T-deficient mice. Journal of Immunology. 1981;126(3):1036-41.
151. Lim K, Hyun Y-M, Lambert-Emo K, Capece T, Bae S, Miller R, et al. Neutrophil trails guide influenza-specific CD8+ T cells in the airways. Science. 2015;349(6252):aaa4352.
152. Sun J, Madan R, Karp CL, Braciale TJ. Effector T cells control lung inflammation during acute influenza virus infection by producing IL-10. Nature medicine. 2009;15(3):277-84.
153. Brincks EL, Katewa A, Kucaba TA, Griffith TS, Legge KL. CD8 T cells utilize TRAIL to control influenza virus infection. Journal of Immunology. 2008;181(7):4918-25.
154. Brincks EL, Gurung P, Langlois RA, Hemann EA, Legge KL, Griffith TS. The magnitude of the T cell response to a clinically significant dose of influenza virus is regulated by TRAIL. Journal of Immunology. 2011;187(9):4581-8.

155. Chaplin, DD. Overview of the immune response. The Journal of Allergy and Clinical Immunology. 2010;125(2):S3- S23.
156. Graham MB, Braciale TJ. Resistance to and recovery from lethal influenza virus infection in B lymphocyte–deficient mice. Journal of Experimental Medicine. 1997;186(12):2063-8.
157. Mozdzanowska K, Furchner M, Maiese K, Gerhard WJV. CD4+ T cells are ineffective in clearing a pulmonary infection with influenza type A virus in the absence of B cells. Virology. 1997;239(1):217-25.
158. Gerhard W, Mozdzanowska K, Furchner M, Washko G, Maiese K. Role of the B-cell response in recovery of mice from primary influenza virus infection. Journal of Immunology. 1997;159(1):95- 103.
159. Topham DJ, Doherty PCJ. Clearance of an influenza A virus by CD4+ T cells is inefficient in the absence of B cells. JOURNAL OF VIROLOGY. 1998;72(1):882-5.
160. Seder RA, Ahmed R. Similarities and differences in CD4+ and CD8+ effector and memory T cell generation. Nature Immunology. 2003;4(9):835-42.
161. Weston WM, LeClair EE, Trzyna W, McHugh KM, Nugent P, Lafferty CM, et al. Differential display identification of plunc, a novel gene expressed in embryonic palate, nasal epithelium, and adult lung. Journal of Biological Chemistry. 1999;274(19):13698-703.
162. Bingle CD, Bingle LJBeBA-GS, Expression. Characterisation of the human plunc gene, a gene product with an upper airways and nasopharyngeal restricted expression pattern. Biochimica et Biophysica Acta. 2000;1493(3):363-7.
163. Sung YK, Moon C, Yoo J-Y, Moon C, Pearse D, Pevsner J, et al. Plunc, a member of the secretory gland protein family, is up-regulated in nasal respiratory epithelium after olfactory bulbectomy. Journal of Biological Chemistry. 2002;277(15):12762-9.
164. Wheeler TT, Haigh BJ, McCracken JY, Wilkins RJ, Morris CA, Grigor MRJBeBA-GS, et al. The BSP30 salivary proteins from cattle, LUNX/PLUNC and von Ebner's minor salivary gland protein are members of the PSP/LBP superfamily of proteins. Biochimica et Biophysica Acta. 2002;1579(2-3):92-100.
165. Larsen K, Madsen LB, Bendixen CJBeBA-GS, Expression. Porcine SPLUNC1: molecular cloning, characterization and expression analysis. Biochimica et Biophysica Acta. 2005;1727(3):220-6.
166. McGillivary G, Bakaletz LO. The multifunctional host defense peptide SPLUNC1 is critical for homeostasis of the mammalian upper airway. PLoS One. 2010;5(10):e13224.
167. Shen W, Chen K, Sun Y, Guo H, Chen D, Cao YJA-Ajoas. Cloning and sequence analysis of Wild Argali short palate, lung and nasal epithelium clone 1 cDNA. Asian-Australasian Journal of Animal Sciences. 2017;30(5):736.
168. 2020 [Available from: https://www.ncbi.nlm.nih.gov/gene/?term=splunc1.
169. Garland AL, Walton WG, Coakley RD, Tan CD, Gilmore RC, Hobbs CA, et al. Molecular basis for pH-dependent mucosal dehydration in cystic fibrosis airways. PNAS. 2013;110(40):15973-8.
170. Ghafouri B, Kihlström E, Tagesson C, Lindahl MJBeBA-P, Proteomics. PLUNC in human nasal lavage fluid: multiple isoforms that bind to lipopolysaccharide. Biochimica et Biophysica Acta. 2004;1699(1- 2):57-63.
171. LeClair E, Nguyen L, Bingle L, MacGowan A, Singleton V, Ward S, et al. Genomic organization of the mouse plunc gene and expression in the developing airways and thymus. Biochemical and Biophysical Research Communications. 2001;284(3):792-7.
172. Little MS, Redinbo MRJACSFSBC. Crystal structure of the mouse innate immunity factor bacterial permeability-increasing family member A1. Acta Crystallogr F Struct Biol Commun. 2018;74(5):268-76.
173. Vitorino R, Lobo MJC, Ferrer-Correira AJ, Dubin JR, Tomer KB, Domingues PM, et al. Identification of human whole saliva protein components using proteomics. Proteomics.

2004;4(4):1109-15.
174. Kohlgraf KG, Ackermann AR, Burnell KK, Srikantha RN, Joly SA, Bartlett JA, et al. Quantitation of SPLUNC1 in saliva with an xMAP particle-based antibody capture and detection immunoassay. Archives of Oral Biology. 2012;57(2):197-204.
175. Zhou H-D, Fan S-Q, Zhao J, Huang D-H, Zhou M, Liu H-Y, et al. Tissue distribution of the secretory protein, SPLUNC1, in the human fetus. Histochemistry and Cell Biology. 2006;125(3):315-24.
176. Ghafouri B, Kihlström E, Ståhlbom B, Tagesson C, Lindahl M. PLUNC (palate, lung and nasal epithelial clone) proteins in human nasal lavage fluid. Portland Press Ltd.; 2003.
177. Kim C-H, Kim K, Jik Kim H, Kook Kim J, Lee J-G, Yoon J-H. Expression and regulation of PLUNC in human nasal epithelium. Acta Otolaryngol. 2006;126(10):1073-8.
178. Bingle L, Cross SS, High AS, Wallace WA, Devine DA, Havard S, et al. SPLUNC1 (PLUNC) is expressed in glandular tissues of the respiratory tract and in lung tumours with a glandular phenotype. Journal of Pathology. 2005;205(4):491-7.
179. Britto CJ, Liu Q, Curran DR, Patham B, Dela Cruz CS, Cohn LJAjorc, et al. Short Palate, Lung, and Nasal Epithelial Clone–1 Is a Tightly Regulated Airway Sensor in Innate and Adaptive Immunity. American Journal of Respiratory Cell and Molecular Biology. 2013;48(6):717-24.
180. Campos MA, Abreu AR, Nlend MC, Cobas MA, Conner GE, Whitney PL, et al. Purification and characterization of PLUNC from human tracheobronchial secretions. American Journal of Respiratory Cell and Molecular Biology. 2004;30(2):184-92.
181. Seshadri S, Lin DC, Rosati M, Carter RG, Norton JE, Suh L, et al. Reduced expression of antimicrobial PLUNC proteins in nasal polyp tissues of patients with chronic rhinosinusitis. Allergy. 2012;67(7):920-8.
182. Musa M, Wilson K, Sun L, Mulay A, Bingle L, Marriott HM, et al. Differential localisation of BPIFA1 (SPLUNC1) and BPIFB1 (LPLUNC1) in the nasal and oral cavities of mice. Cell and Tissue Research. 2012;350(3):455-64.
183. Britto CJ, Liu Q, Curran DR, Patham B, Dela Cruz CS, Cohn L. Short Palate, Lung, and Nasal Epithelial Clone–1 Is a Tightly Regulated Airway Sensor in Innate and Adaptive Immunity. American journal of respiratory cell and molecular biology. American Journal of Respiratory Cell and Molecular Biology. 2013;48(6):717-24.
184. González-Arriagada WA, Santos-Silva AR, Ito FA, Vargas PA, Speight PM, Bingle L, et al. Expression pattern of PLUNC proteins as an auxiliary tool for the diagnosis of high-grade mucoepidermoid carcinoma of the salivary gland. Journal of Oral Pathology & Medicine. 2012;41(8):589-97.
185. Yeh T-H, Lee S-Y, Hsu W-CJ. Expression of SPLUNC1 protein in nasal polyp epithelial cells in air–liquid interface culture treated with IL-13. American Journal of Rhinology and Allergy. 2010;24(1):17-20.
186. Arba M, Iavarone F, Vincenzoni F, Manconi B, Vento G, Tirone C, et al. Proteomic characterization of the acid-insoluble fraction of whole saliva from preterm human newborns. Journal of Proteomics. 2016;146:48-57.
187. Bingle CD, Craven CJ. PLUNC: a novel family of candidate host defence proteins expressed in the upper airways and nasopharynx. Human Molecular Genetics. 2002;11(8):937-43.
188. LeClair EJ. Four reasons to consider a novel class of innate immune molecules in the oral epithelium. Journal of Dental Research. 2003;82(12):944-50.
189. Zhou H-D, Li X-L, Li G-Y, Zhou M, Liu H-Y, Yang Y-X, et al. Effect of SPLUNC1 protein on the Pseudomonas aeruginosa and Epstein-Barr virus. Molecular and Cell Biochemistry. 2008;309(1-2):191-7.
190. Sayeed S, Nistico L, St Croix C, Di YP. Multifunctional role of human SPLUNC1 in Pseudomonas aeruginosa infection. Infection and Immunity. 2013;81(1):285-91.

191. Gakhar L, Bartlett JA, Penterman J, Mizrachi D, Singh PK, Mallampalli RK, et al. PLUNC is a novel airway surfactant protein with anti-biofilm activity. PLoS One. 2010;5(2).
192. Lukinskiene L, Liu Y, Reynolds SD, Steele C, Stripp BR, Leikauf GD, et al. Antimicrobial activity of PLUNC protects against Pseudomonas aeruginosa infection. The Journal of Immunology. 2011;187(1):382-90.
193. Liu Y, Di ME, Chu HW, Liu X, Wang L, Wenzel S, et al. Increased susceptibility to pulmonary Pseudomonas infection in Splunc1 knockout mice. Immunology. 2013;191(8):4259-68.
194. Liu Y, Bartlett JA, Di ME, Bomberger JM, Chan YR, Gakhar L, et al. SPLUNC1/BPIFA1 contributes to pulmonary host defense against Klebsiella pneumoniae respiratory infection. American Journal of Pathology. 2013;182(5):1519-31.
195. Ahmad S, Tyrrell J, Walton WG, Tripathy A, Redinbo MR, Tarran R, et al. Short palate, lung, and nasal epithelial clone 1 has antimicrobial and antibiofilm activities against the Burkholderia cepacia complex. Antimicrobial agents and Chemotherapy. 2016;60(10):6003-12.
196. Gally F, Di YP, Smith SK, Minor MN, Liu Y, Bratton DL, et al. SPLUNC1 promotes lung innate defense against Mycoplasma pneumoniae infection in mice. American Journal of Pathology. 2011;178(5):2159-67.
197. Chu HW, Thaikoottathil J, Rino JG, Zhang G, Wu Q, Moss T, et al. Function and regulation of SPLUNC1 protein in Mycoplasma infection and allergic inflammation. Immunology. 2007;179(6):3995-4002.
198. Chu HW, Gally F, Thaikoottathil J, Janssen-Heininger YM, Wu Q, Zhang G, et al. SPLUNC1 regulation in airway epithelial cells: role of Toll-like receptor 2 signaling. Respiratory Research. 2010;11(1):155.
199. Walton WG, Ahmad S, Little MS, Kim CS, Tyrrell J, Lin Q, et al. Structural features essential to the antimicrobial functions of human SPLUNC1. Biochemistry. 2016;55(21):2979-91.
200. Yu Z, Deslouches B, Walton WG, Redinbo MR, Di YPJPo. Enhanced biofilm prevention activity of a SPLUNC1-derived antimicrobial peptide against Staphylococcus aureus. PLoS One. 2018;13(9).
201. Di YP, Tkach AV, Yanamala N, Stanley S, Gao S, Shurin MR, et al. Dual acute proinflammatory and antifibrotic pulmonary effects of short palate, lung, and nasal epithelium clone–1 after exposure to carbon nanotubes. American Journal of Respiratory Cell and Molecular Biology. 2013;49(5):759-67.
202. Liu Y, Bartlett JA, Di ME, Bomberger JM, Chan YR, Gakhar L, et al. SPLUNC1/BPIFA1 contributes to pulmonary host defense against Klebsiella pneumoniae respiratory infection. The American journal of pathology. 2013;182(5):1519-31.
203. Britto CJ, Niu N, Khanal S, Huleihel L, Herazo-Maya JD, Thompson A, et al. BPIFA1 regulates lung neutrophil recruitment and interferon signaling during acute inflammation. American Journal of Lung Cell and Molecular Physiology. 2019;316(2):L321-L33.
204. Bartlett JA, Hicks BJ, Schlomann JM, Ramachandran S, Nauseef WM, McCray Jr PB. PLUNC is a secreted product of neutrophil granules. Journal of Leukocyte Biology. 2008;83(5):1201-6.
205. Di Jiang SEW, Wu Q, Bowler RP, Schnell C, Chu HWJPO. Human neutrophil elastase degrades SPLUNC1 and impairs airway epithelial defense against bacteria. PLoS One. 2013;8(5).
206. Jiang D, Persinger R, Wu Q, Gross A, Chu HWJRr. α1-antitrypsin promotes SPLUNC1-mediated lung defense against Pseudomonas aeruginosa infection in mice. Respiratory Research. 2013;14(1):122.
207. Thaikoottathil JV, Martin RJ, Di PY, Minor M, Case S, Zhang B, et al. SPLUNC1 deficiency enhances airway eosinophilic inflammation in mice. American Journal of

Respiratory Cell and Molecular Biology. 2012;47(2):253-60.
208. Yang L-L, Liu X-Q, Liu W, Cheng B, Li M-TJIr. Comparative analysis of whole saliva proteomes for the screening of biomarkers for oral lichen planus. Inflammatory Research. 2006;55(10):405-7.
209. Guo Y, Guo L-N, Zhu J-F, Tang C-Y, Feng Y-Z, Zhou H-DJ. Associations of salivary BPIFA1 protein in chronic periodontitis patients with type 2 diabetes mellitus. International Journal of Endocrinology. 2017;2017.
210. Chu HW, Thaikoottathil J, Rino JG, Zhang G, Wu Q, Moss T, et al. Function and regulation of SPLUNC1 protein in Mycoplasma infection and allergic inflammation. The Journal of Immunology. 2007;179(6):3995-4002.
211. Wei Y, Xia W, Ye X, Fan Y, Shi J, Wen W, et al. The antimicrobial protein short palate, lung, and nasal epithelium clone 1 (SPLUNC1) is differentially modulated in eosinophilic and noneosinophilic chronic rhinosinusitis with nasal polyps. The Journal of Allergy and Clinical Immunology. 2014;133(2):420- 8. e12.
212. Tsou Y-A, Lin C-D, Chen H-C, Hsu H-Y, Wu L-T, Chiang-Ni C, et al. Interleukin-13 inhibits lipopolysaccharide-induced BPIFA1 expression in nasal epithelial cells. PLoS One. 2015;10(12).
213. Erickson NA, Dietert K, Enders J, Glauben R, Nouailles G, Gruber AD, et al. Soluble mucus component CLCA1 modulates expression of leukotactic cytokines and BPIFA1 in murine alveolar macrophages but not in bone marrow-derived macrophages. Histochemistry and Cell Biology. 2018;149(6):619-33.
214. Wright PL, Yu J, Di YP, Homer RJ, Chupp G, Elias JA, et al. Epithelial reticulon 4B (Nogo-B) is an endogenous regulator of Th2-driven lung inflammation. Journal of Experimental Medicine. 2010;207(12):2595-607.
215. Thaikoottathil J, Chu HW. MAPK/AP-1 activation mediates TLR2 agonist-induced SPLUNC1 expression in human lung epithelial cells. Molecular Immunology. 2011;49(3):415-22.
216. Schaefer N, Li X, Seibold MA, Jarjour NN, Denlinger LC, Castro M, et al. The effect of BPIFA1/SPLUNC1 genetic variation on its expression and function in asthmatic airway epithelium. JCI Insight. 2019;4(8).
217. Chen P, Guo X, Zhou H, Zhang W, Zeng Z, Liao Q, et al. SPLUNC1 regulates cell progression and apoptosis through the miR-141-PTEN/p27 pathway, but is hindered by LMP1. PLoS One. 2013;8(3).
218. Ou C, Sun Z, Zhang H, Xiong W, Ma J, Zhou M, et al. SPLUNC1 reduces the inflammatory response of nasopharyngeal carcinoma cells infected with the EB virus by inhibiting the TLR9/NF-κB pathway. Oncology Reports. 2015;33(6):2779-88.
219. Wu Q, Di Jiang MM, Chu HWJPo. Electronic cigarette liquid increases inflammation and virus infection in primary human airway epithelial cells. PLoS One. 2014;9(9).
220. Leeming GH, Kipar A, Hughes DJ, Bingle L, Bennett E, Moyo NA, et al. Gammaherpesvirus infection modulates the temporal and spatial expression of SCGB1A1 (CCSP) and BPIFA1 (SPLUNC1) in the respiratory tract. Angiogenesis, Cardiovascular and Pulmonary Systems. 2015;95(6):610-24.
221. Da Silva A, Bingle L, Speight P, Bingle C, Mauad T, da Silva L, et al. PLUNC protein expression in major salivary glands of HIV-infected patients. Oral Diseases. 2011;17(3):258-64.
222. Akram KM, Moyo NA, Leeming GH, Bingle L, Jasim S, Hussain S, et al. An innate defense peptide BPIFA1/SPLUNC1 restricts influenza A virus infection. Mucosal immunology. 2018;11(1):71.
223. LeMessurier KS, Lin Y, McCullers JA, Samarasinghe AEJAr. Antimicrobial peptides alter early immune response to influenza A virus infection in C57BL/6 mice. Antiviral Research. 2016;133:208- 17.
224. Rollins BM, Garcia-Caballero A, Stutts MJ, Tarran RJC. SPLUNC1 expression reduces surface levels of the epithelial sodium channel (ENaC) in Xenopus laevis oocytes. Channels.

2010;4(4):255-9.
225. Webster MJ, Reidel B, Tan CD, Ghosh A, Alexis NE, Donaldson SH, et al. SPLUNC1 degradation by the cystic fibrosis mucosal environment drives airway surface liquid dehydration. European Respiratory Journal. 2018;52(4):1800668.
226. Garcia-Caballero A, Rasmussen JE, Gaillard E, Watson MJ, Olsen JC, Donaldson SH, et al. SPLUNC1 regulates airway surface liquid volume by protecting ENaC from proteolytic cleavage. PNAS. 2009;106(27):11412-7.
227. Bingle L, Barnes FA, Cross SS, Rassl D, Wallace WA, Campos MA, et al. Differential epithelial expression of the putative innate immune molecule SPLUNC1 in cystic fibrosis. Respiratory research. 2007;8(1):79.
228. Ning F, Wang C, Berry KZ, Kandasamy P, Liu H, Murphy RC, et al. Structural characterization of the pulmonary innate immune protein SPLUNC1 and identification of lipid ligands. The FASEB Journal. 2014;28(12):5349-60.
229. Sesma JI, Wu B, Stuhlmiller TJ, Scott DWJJoCF. SPX-101 is stable in and retains function after exposure to cystic fibrosis sputum. Journal of Cystic Fibrosis. 2019;18(2):244-50.
230. Hobbs CA, Blanchard MG, Alijevic O, Tan CD, Kellenberger S, Bencharit S, et al. Identification of the SPLUNC1 ENaC-inhibitory domain yields novel strategies to treat sodium hyperabsorption in cystic fibrosis airway epithelial cultures. American Journal of Physiology - Lung Cellular and Molecular Physiology. 2013;305(12):L990- L1001.
231. Terryah ST, Fellner RC, Ahmad S, Moore PJ, Reidel B, Sesma JI, et al. Evaluation of a SPLUNC1-derived peptide for the treatment of cystic fibrosis lung disease. Evaluation of a SPLUNC1-derived peptide for the treatment of cystic fibrosis lung disease. 2018;314(1):L192-L205.
232. Scott DW, Walker MP, Sesma J, Wu B, Stuhlmiller TJ, Sabater JR, et al. SPX-101 is a novel epithelial sodium channel–targeted therapeutic for cystic fibrosis that restores mucus transport. American Journal of Respiratory and Critical Care Medicine. 2017;196(6):734-44.
233. Garland AL, Walton WG, Coakley RD, Tan CD, Gilmore RC, Hobbs CA, et al. Molecular basis for pH-dependent mucosal dehydration in cystic fibrosis airways. Proceedings of the National Academy of Sciences. 2013;110(40):15973-8.
234. Ahmad S, Gilmore RC, Alexis NE, Tarran RJAjor, medicine cc. SPLUNC1 Loses Its Antimicrobial Activity in Acidic Cystic Fibrosis Airway Secretions. American Journal of Respiratory and Critical Care Medicine. 2019;200(5):633-6.
235. De Smet EG, Seys LJ, Verhamme FM, Vanaudenaerde BM, Brusselle GG, Bingle CD, et al. Association of innate defense proteins BPIFA1 and BPIFB1 with disease severity in COPD. International Journal of Chronic Obstructive Pulmonary Disease. 2018;13:11.
236. Boon K, Bailey NW, Yang J, Steel MP, Groshong S, Kervitsky D, et al. Molecular phenotypes distinguish patients with relatively stable from progressive idiopathic pulmonary fibrosis (IPF). PLoS One. 2009;4(4).
237. Wu T, Huang J, Moore PJ, Little MS, Walton WG, Fellner RC, et al. Identification of BPIFA1/SPLUNC1 as an epithelium-derived smooth muscle relaxing factor. Nature Communications. 2017;8(1):1-10.
238. Fang F, Pan J, Li Y, Li Y, Feng X, Wang JJMi. Identification of potential transcriptomic markers in developing asthma: An integrative analysis of gene expression profiles. Molecular Immunology. 2017;92:38-44.
239. Irander K, Borres MP, Ghafouri BJIjopo. The effects of physical exercise and smoking habits on the expression of SPLUNC1 in nasal lavage fluids from allergic rhinitis subjects. International Journal of Pediatric Otorhinolaryngology. 2014;78(4):618-22.
240. Steiling K, Kadar AY, Bergerat A, Flanigon J, Sridhar S, Shah V, et al. Comparison of proteomic and transcriptomic profiles in the bronchial airway epithelium of current and never smokers. PLoS One. 2009;4(4).
241. Moore PJ, Reidel B, Ghosh A, Sesma J, Kesimer M, Tarran RJTFJ. Cigarette smoke modifies and inactivates SPLUNC1, leading to airway dehydration. The FASEB Journal.

2018;32(12):6559-74.
242. Moore PJ, Sesma J, Alexis NE, Tarran RJRr. Tobacco exposure inhibits SPLUNC1-dependent antimicrobial activity. Respiratory Research. 2019;20(1):94.
243. Ghafouri B, Ståhlbom B, Tagesson C, Lindahl M. Newly identified proteins in human nasal lavage fluid from non-smokers and smokers using two-dimensional gel electrophoresis and peptide mass fingerprinting. PROTEOMICS: International Edition. 2002;2(1):112-20.
244. Fornander L, Graff P, Wåhlén K, Ydreborg K, Flodin U, Leanderson P, et al. Airway symptoms and biological markers in nasal lavage fluid in subjects exposed to metalworking fluids. PLoS One. 2013;8(12).
245. Ghafouri B, Irander K, Lindbom J, Tagesson C, Lindahl MJ. Comparative proteomics of nasal fluid in seasonal allergic rhinitis. Journal of Proteome Research. 2006;5(2):330-8.
246. Lv M, WU MZ, ZHAO YJ, Yang D, WANG EH, WU GPJR. Expression and clinical significance of lung-specific X protein mRNA in bronchial brushing specimens from patients with or without lung cancer. Respirology. 2011;16(7):1076-80.
247. Kim B, Lee HJ, Choi HY, Shin Y, Nam S, Seo G, et al. Clinical validity of the lung cancer biomarkers identified by bioinformatics analysis of public expression data. Cancer Research. 2007;67(15):7431-8.
248. Wang H, Jiang D, Li W, Wang S. Increased expression of BPI fold-containing family A member 1 is associated with metastasis and poor prognosis in human colorectal carcinoma. Oncology Letters. 2017;14(4):4231-6.
249. Sentani K, Oue N, Sakamoto N, Arihiro K, Aoyagi K, Sasaki H, et al. Gene expression profiling with microarray and SAGE identifies PLUNC as a marker for hepatoid adenocarcinoma of the stomach. Modern Pathology. 2008;21(4):464-75.
250. Cheng M, Chen Y, Yu X, Tian Z, Wei HJBc. Diagnostic utility of LunXmRNA in peripheral blood and pleural fluid in patients with primary non-small cell lung cancer. BMC Cancer. 2008;8(1):156.
251. Iwao K, Watanabe T, Fujiwara Y, Takami K, Kodama K, Higashiyama M, et al. Isolation of a novel human lung-specific gene, LUNX, a potential molecular marker for detection of micrometastasis in non-small-cell lung cancer. International Journal of Cancer. 2001;91(4):433-7.
252. Wu M, Li X, Li X, Li GJCg. Signaling transduction network mediated by tumor suppressor/susceptibility genes in NPC. Current Genomics. 2009;10(4):216-22.
253. Mitas M, Hoover L, Silvestri G, Reed C, Green M, Turrisi AT, et al. Lunx is a superior molecular marker for detection of non-small lung cell cancer in peripheral blood. Journal of Molecular Diagnostics. 2003;5(4):237-42.
254. Sun Y, Huo C, Qiao Z, Shang Z, Uzzaman A, Liu S, et al. Comparative proteomic analysis of exosomes and microvesicles in human saliva for lung cancer. Journal of Proteome Research. 2018;17(3):1101-7.
255. Benlloch S, Galbis-Caravajal J, Alenda C, Peiro F, Sanchez-Ronco M, Rodriguez-Paniagua J, et al. Expression of molecular markers in mediastinal nodes from resected stage I non-small-cell lung cancer (NSCLC): prognostic impact and potential role as markers of occult micrometastases. Annals of Oncology. 2009;20(1):91-7.
256. Lafuente-Sanchis A, Estors-Guerrero M, Zúñiga Á, Martínez-Hernández NJ, Cremades A, Aparisi-Aparisi F, et al. Clinical Significance of Molecular Micrometastasis in the Sentinel Lymph Node of Early-stage Non–Small Cell Lung Cancer Patients. American Journal of Clinical Oncology. 2018;41(11):1106-12.
257. Zhang B, Nie X, Xiao B, Xiang J, Shen S, Gong J, et al. Identification of tissue-specific genes in nasopharyngeal epithelial tissue and differentially expressed genes in nasopharyngeal carcinoma by suppression subtractive hybridization and cDNA microarray. Genes, Chromosomes & Cancer. 2003;38(1):80-90.

258. Zhang W, Zeng Z, Wei F, Chen P, Schmitt DC, Fan S, et al. SPLUNC 1 is associated with nasopharyngeal carcinoma prognosis and plays an important role in all-trans-retinoic acid-induced growth inhibition and differentiation in nasopharyngeal cancer cells. The FEBS Journal. 2014;281(21):4815-29.
259. Bian S, Wang Z, Chen Y, Li RJJoBOojotBUoO. SPLUNC1 and MLL3 regulate cancer stem cells in nasopharyngeal carcinoma. Journal of the Balkan Union of Oncology. 2019;24(4):1700-5.
260. Norman JA, Hobart P, Manthorpe M, Felgner P, Wheeler CJV. Development of improved vectors for DNA-based immunization and other gene therapy applications. Vaccine. 1997;15(8):801-3.
261. van Eijk M, Rynkiewicz MJ, Khatri K, Leymarie N, Zaia J, White MR, et al. Lectin-mediated binding and sialoglycans of porcine surfactant protein D synergistically neutralize influenza A virus. Journal of Biological Chemistry. 2018;293(27):10646-62.
262. Al Katy S. Role of BPIFA1/SPLUNC1 in the pathogensis and immune resonse against influenza A virus in mice In: Liverpool Uo, editor. Doctor of Philosophy thesis University of Liverpool Library 2019.
263. The Hirst Group UoN. Glycosylation Predictor 2022 [Available from: https://comp.chem.nottingham.ac.uk/glyco/.
264. Ning F, Wang C, Berry KZ, Kandasamy P, Liu H, Murphy RC, et al. Structural characterization of the pulmonary innate immune protein SPLUNC1 and identification of lipid ligands. The FASEB Journal. 2014;28(12):5349-60.
265. Ran FA, Hsu PD, Wright J, Agarwala V, Scott DA, Zhang FJNp. Genome engineering using the CRISPR-Cas9 system. Nature Protocols. 2013;8(11):2281-308.
266. Song Y, Huang H, Hu Y, Zhang J, Li F, Yin X, et al. A genome-wide CRISPR/Cas9 gene knockout screen identifies immunoglobulin superfamily DCC subclass member 4 as a key host factor that promotes influenza virus endocytosis. PLoS Pathogens. 2021;17(12):e1010141.
267. Couroux P, Farias P, Rizvi L, Griffin K, Hudson C, Crowder T, et al. First clinical trials of novel ENaC targeting therapy, SPX-101, in healthy volunteers and adults with cystic fibrosis. Pulmonary pharmacology & therapeutics. 2019:101819.
268. Djurisic S, Jakobsen JC, Petersen SB, Kenfelt M, Klingenberg SL, Gluud CJTCDoSR. Aluminium adjuvants used in vaccines. Cochrane Database of Systematic Reviews. 2018;2018(7).
269. Davis SDJAa, chemotherapy. Dissociation between results of in vitro and in vivo antibiotic susceptibility tests for some strains of Pseudomonas aeruginosa. Antimicrobial Agents & Chemotherapy. 1974;5(3):281-8.
270. Lin Y-T, Chiweshe S, McCormick D, Raper A, Wickenhagen A, DeFillipis V, et al. Human cytomegalovirus evades ZAP detection by suppressing CpG dinucleotides in the major immediate early 1 gene. PLoS Pathogens. 2020;16(9):e1008844.
271. Di Francia M, Barbier D, Mege JL, Orehek JJ. Tumor necrosis factor-alpha levels and weight loss in chronic obstructive pulmonary disease. American Journal of Respiratory and Critical Care Medicine. 1994;150(5):1453-5.
272. Perrone LA, Szretter KJ, Katz JM, Mizgerd JP, Tumpey TMJTJoid. Mice lacking both TNF and IL-1 receptors exhibit reduced lung inflammation and delay in onset of death following infection with a highly virulent H5N1 virus. Journal of Infectious Diseases.2010;202(8):1161-70.
273. AlphaFold [https://alphafold.ebi.ac.uk] Accessed 30th June 2022.